Alma Mater Studiorum – Università di Bologna

DOTTORATO DI RICERCA IN
Data Science and Computation

Ciclo XXXIII

Settore Concorsuale: 02/C1

Settore Scientifico Disciplinare: FIS06

Urban air quality: new high-resolution modeling approaches and forecasting tools for citizens

Presentata da: Francesca Di Nicola

Coordinatore Dottorato
Prof. Andrea Cavalli

Supervisore
Prof.ssa Silvana Di Sabatino

Correlatore
Dott.ssa Erika Brattich

Esame finale anno 2022

PREFACE

This Thesis work, originates as a response to the challenge concerning the integration of multiple disciplines aiming to the creation of more efficient and resilient smart cities. The idea has evolved along the way into an articulated project that has touched various aspects of air quality mitigation in urban areas and in general of the urban environment. The experience within the EU H2020-iSCAPE project was crucial, to identify a concrete and tangible product useful for the community but above all for citizens. During the iSCAPE project, different activities were carried out, for example, the thermographic campaign that made it possible to study and analyze the thermal behavior within a street canyon, a very important aspect for the thermal comfort and health of citizens. The use of low cost sensors and citizen science laboratories, useful for understanding the potential of low cost sensors and their future use in more capillary monitoring networks in the area, perhaps managed by each individual citizen. The specific use of a dispersion model to evaluate, test, study and predict policies and interventions has led to the introduction of new modeling methodologies, new approaches and the improvement of scientific knowledge on everything related to urban air quality.

All these activities always had the citizen as the final target, in fact the one who is most affected by pollution and all phenomena related to climate change is always the citizen. These considerations, together with the desire to transform the research project into something tangible, led me to conceive the final product of this thesis: a forecasting tool that can be used by citizens.

ABSTRACT

Air pollution is one of the greatest health risks in the world. At the same time, the strong correlation with climate change, as well as with Urban Heat Island and Heat Waves, make more intense the effects of all these phenomena. A good air quality and high levels of thermal comfort are the big goals to be reached in urban areas in coming years.

Air quality forecast help decision makers to improve air quality and public health strategies, mitigating the occurrence of acute air pollution episodes. Air quality forecasting approaches combine an ensemble of models to provide forecasts from global to regional air pollution and downscaling for selected countries and regions. The development of models dedicated to urban air quality issues requires a good set of data regarding the urban morphology and building material characteristics. Only few examples of air quality forecast system at urban scale exist in the literature and often they are limited to selected cities.

Following the motivation, this Thesis addresses the topic of filling the knowledge gap and to design the practical tool that can be used for practical applications. This thesis develops by setting up a methodology for the development of a forecasting tool. The forecasting tool can be adapted to all cities and uses a new parametrization for vegetated areas. The parametrization method, based on aerodynamic parameters, produce the urban spatially varying roughness. At the core of the forecasting tool there is a dispersion model (urban scale) used in forecasting mode, and the meteorological and background concentration forecasts provided by two regional numerical weather forecasting models. The tool produces the 1-day spatial forecast of NO_2, PM_{10}, O_3 concentration, the air temperature, the air humidity and BLQ-Air index values. The tool is developed in python programming language, and it is automatized to run every day, the maps produced are displayed on the e-Globus platform, updated every day. The results obtained indicate that the forecasting output were in good agreement with the observed measurements.

INDEX

LIST OF ACRONYMS

2017BC - Base Case; 66
2017P1EC - Policy 1 Electric Centre; 62
2017P2EB - Policy 2 Electric Buses; 62
AADT - Annual Average Daily Traffic; 59
ADMS - Atmospheric Dispersion Modelling System; 53
ADMS-TH - ADMS-Temperature and Humidity; 53
API - Application Programming Interface; 46
AQ - Air quality; 30
ARPAE - Agenzia Regionale per la Protezione Ambientale ed Energetica; 38
As - Asinelli; 55
BLQ - Bologna urban scale simulation; 89
BU - Bologna Urbana; 55
CERC- Cambridge Environmental Research Consultants; 53
CFD - Computational Fluid Dynamics; 86
CSV - Comma-Separated Values; 138
ECMWF - European Centre for Medium-Range Weather Forecasts; 125
EEA - European Environment Agency; 24
EMEP - European Monitoring and Evaluation Programme; 59
EMIT - Atmospheric Emissions Inventory Toolkit; 58
EU - European Union; 20
Fac2 - Factor of two; 60
Fb - Fractional bias; 60
GI - Green Infrastructure; 37
GIS - Geographic Information System; 54
GM - Giardini Margherita; 57
GRIB - GRIdded Binary; 125
HW - Heat Waves; 34
Im - Imola; 55
IR - Infra-Red; 39
iSCAPE - Improving the Smart Control of Air Pollution in Europe; 20
JSON - Java Script Object Notation; 145
LAI - Leaf Area Index; 87
LB - Laura Bassi St.; 39
LCS - Low-Cost Sensor; 39
LCZ - Local Climate Zone; 75
LLS - Living Lab Station; 46
LOD - Limit of detection; 45

MA - Marconi St.; 39
Mz - Mezzolara; 55
NAEI - National Atmospheric Emissions Inventory; 58
NBV - Normalized Building Volume; 76
netCDF - Network Common Data Form; 127
NINFA - Northern Italy Network for Photochemical Smog and Aerosol; 127
NMSE - Normalized Mean Square Error; 59
PBL - Planetary Boundary Layer; 29
PCS - Passive Control System; 37
PNG - Portable Network Graphic; 143
PSB - Padulle-Sala Bolognese; 55
SCK - Smart Citizen Kit; 46
SF - Porta San Felice; 57
SM - Sasso Marconi; 55
SNPA - National Environmental Protection System; 127
SPC - San Pietro Capofiume; 55
TSV - Tab-Separated Values; 138
UCAR - University Corporation for Atmospheric Research; 139
UHI - Urban Heat Island; 34
USVR - Urban Spatially Varying Roughness; 87
VC - Via Chiarini; 57
WHO - World Health Organization; 20
WMO - World Meteorological Organization; 55
WRF - Weather Research and Forecasting; 110
WS - Weather Stations; 55

LIST OF TABLES

LIST OF FIGURES

1 INTRODUCTION

Air pollution is one of the greatest risks to environmental health in Europe and in general overall the world. It can be considered a sneaky enemy because it is difficult to escape (Kampa and Castanas, 2008; Robertson and Miller, 2018). Although much progress has been made in recent years, it is still not enough. Various challenges remain on air pollution, which can be summarized as follows: how to reduce pollutant emissions, how to reduce pollutant concentrations, how to reduce the effects of air pollution on human health. This Thesis project is placed exactly in this context and ranges from the improvement of modeling techniques for the simulation of the dispersion of pollutants in an urban environment to the creation of a practical tool that allows the end user to predict which part of the city is to be avoided because it is affected by high levels of pollution or because it is affected by too high temperatures.

This chapter introduces the problem, provides an overview of the challenges related to air quality in the cities and in general of the Thesis work, starting from its motivation and following with its main limitations. Lastly, the outline of this Thesis is presented.

1.1 Background

Projections of population growth suggest that in 2050 the world population will reach 9.7 billion (ONU, 2019) and the percentage of the world's population residing in urban areas will increase from 55% in 2018 to 68% in 2050 (ONU, 2018). Urban population growth poses many serious negative consequences, one of which is poor air quality. In fact, urban areas are more susceptible to the accumulation of air pollutants owing both to the large quantity and diversity of emissions in a concentrated area and to the limited dispersion caused by the physical constraints of the urban environment (Goodsite et al., 2021). To protect citizens from high levels of pollution, many countries have developed air quality forecasting tools capable to predict the concentrations of major air pollutants. This information is used to issue early warnings that allow the government and people to take precautionary measures such as temporarily blocking major sources of emissions in some areas of the city (typically, urban city centers) or suggesting the adoption of alternative cleaner means of transport (e.g. public transport, cycling and walking).

At local level, several different emergency response systems are adopted to mitigate the problem in case of exceedances and air pollution events occurring in the short term (e.g., traffic restrictions, traffic stops). However, most often nowadays, city and regional management plans consider longer term solutions, generally consisting of land planning strategies and adoption of policies of emission reductions. Among urban planning and management plans, urban greening has become increasingly important thanks to the ability of green infrastructure to provide benefits for environmental, social and economic ecosystem services (European Commission, 2012; Tzoulas et al., 2007). It has become evident that urban greening can counteract different urban problems, among which urban heat island, air quality, biodiversity and citizen health (Ahern, 2007; Hamada and Ohta, 2010; Kong et al., 2014, 2010; Wolf, 2003). All the measures at the local level, together with the new green technologies adopted in transport and industries have allowed an improvement in pollution levels. In fact, in Europe, air pollution levels are decreasing and in many cases comply with European Union (EU) and World Health Organization (WHO) guidelines on air quality. However, many studies have reported associations between air pollution and mortality at concentrations below these guidelines, with no evidence of a safe exposure threshold (Brauer et al., 2019; Cesaroni et al., 2013; Fischer et al., 2015).

In this context, a tool on urban scale is required to provide high spatial resolution information on air pollution, useful to all citizen to limit their exposure at high air pollutant concentrations. However, nowadays this approach is limited by the low density of air quality monitoring stations and the resolution of mesoscale air quality modeling systems (of the order of 1 km of grid resolution) which cannot represent adequately represent the concentration gradients occurring typically near busy roads (Duyzer et al., 2015). Urban dispersion models can estimate these gradients but their use is often limited to a posteriori use, i.e. to evaluate and understand pollution phenomena that have already occurred, partly because background concentrations and necessary meteorological inputs are often represented by observed data.

1.1.1 Framework and research scope

This Thesis aims to make a concrete contribution in the advancement and improvement of the methodologies in the field of urban air quality. In particular, a high resolution forecasting tool was developed for citizen use. This Thesis is composed of two parts: one part is devoted to the development of the modelling framework and the second part is devoted to the development of the forecasting tool. Specifically, we focus on the development of an automated forecasting tool based on a dispersion model capable to predict the high spatial resolution distribution of hourly pollutant concentrations and other environmental variables (air temperature and air humidity), which are visualized as web maps.

1.2 Overview of the Thesis

This Thesis work is the result of several interconnected research activities that have the citizen's well-being as a common thread. As mentioned above, two main sections can be identified: modeling and forecasting tool development. The whole first part includes the research work carried out within the iSCAPE (Improving the Smart Control of Air Pollution in Europe, https://www.iscapeproject.eu/) H2020 project, mainly concerning all the simulations conducted in the city of Bologna. Furthermore, in the modeling part, minor research activities were also included, concerning an intensive thermographic campaign and the evaluation of a set of air quality low cost sensors, also carried out as part of the iSCAPE project. All these activities enabled a better understanding of the functioning of the dispersion model and of its potential as well as the testing of innovative methodologies and modeling approaches.

The second part concerns the design, development and testing of an automated forecasting tool to predict the spatial distribution of hourly variables. It is a high resolution tool that produces forecast 3D maps for the main urban pollutants, air temperature and humidity. The 3D maps have hourly time resolution and a spatial resolution of 200x200 meters, on eight levels of height from the ground. In addition, 2D maps of a newly developed air quality index are produced; these maps, again with an hourly time resolution, have a spatial resolution of 200x200 meters, on a single level of height from the ground.

All the research activities reported in this Thesis were in support of and preparatory to the realization of the Thesis objective. The whole Thesis work aims to address the following main research questions:

I. Can a simple urban dispersion model simulate detailed, high-resolution scenarios?
II. How can the performance of a dispersion model be improved in high resolution simulations?
III. What is the performance of a dispersion model used in forecasting mode?

1.2.1 Significance and limitations of the Study

Air pollution forecast on urban level is beneficial for the citizens. This study contributing to inform citizens about the concentration of air pollutants in their cities, to increase their awareness and care, together with the adoption of alternative pathways to reduce their exposure to air pollution or urban heat.

The project has been completed according with its requirements, however, there were some unavoidable limitations. The forecasting tool will in any case be updated on the basis of new and more recent research developments in the field, but above all an annual update of the emissions inventory must be provided. In fact, since the emissions inventory is not automated, it will have to be updated manually, or it will be possible to think about its future automation.

1.3 Outline of Thesis

Following this introduction chapter, the Thesis is structured as follows:

Chapter 2 contains an introduction on air pollution, describes the monitoring methodologies and the air quality models, finally includes an overview on the relationship between air quality and climate.

Chapter 3 presents the iSCAPE project, describing the field campaigns and some preliminary results. The study area, the data sets and the methodology of the dispersion simulations carried out during the project are also described.

Chapter 4 illustrates in detail all iSCAPE simulations, discusses the new methodologies developed for improving the simulations, and presents the results of all case studies.

Chapter 5 presents the forecasting tool, the design of the tool and the methodology for its development, including the coding part. The input dataset is validated with observed data and the forecast over the test period is evaluated. Finally, the web version for user end is illustrated.

Chapter 6 contains the conclusion on overall research project and in particular on the forecasting tool.

2 AIR POLLUTION IN THE URBAN ENVIRONMENT

This chapter is a brief introduction to air pollution, with brief insights into the topics necessary for reading and understanding the remaining of the Thesis. In particular, main pollutants, their relative classification and the reactions that pollutants undergo once emitted into the atmosphere are illustrated. A few notions will be introduced on monitoring methods, and the various approaches for modeling air pollution. This information is helpful in understanding the dispersion model setup. Finally, the interactions between air pollution and the effects of climate change will be reported, which is why the thermal aspects of the urban environment are included in this Thesis. In this Thesis, the urban environment refers to the urban physical environment (i.e. the built environment, pollution, and the geological and climate conditions of the area the city occupies (Ompad et al., 2007).

2.1 Introduction to air pollution

Air pollution is one of the well-studied aspects of the urban physical environment. The WHO defines air pollution as the presence chemical, physical or biological agents in the air that modify the natural characteristics of the atmosphere. According to the WHO (https://www.who.int/health-topics/air-pollution#tab=tab_1), air pollution kills around seven million people around the world each year. The deaths associated with air pollution, however, are not only related to developing countries, in fact, as the map (Figure 1) clearly shows, mortality rates attributable to air pollution are high even in industrialized countries.

The sources of atmospheric pollutants can be classified into three broad groups: primary, secondary and re-emission sources. A source can be defined as primary when it emits directly into the atmosphere. A secondary source is the formation of a pollutant in the atmosphere because of chemical or microphysical reactions. Finally, a source of re-emission results from the primary or secondary pollutants depositing on the terrestrial or aquatic surfaces of the Earth, followed by re-emission into the atmosphere. Secondary and re-emission sources tend to have lower temporal and spatial concentration gradients than primary sources. The primary sources can be further divided into point sources, mobile sources and area sources. The emission chimneys are point sources. Mobile sources are associated with transport. Area sources are sources with relatively dispersed emissions over large areas (IARC, 2016).

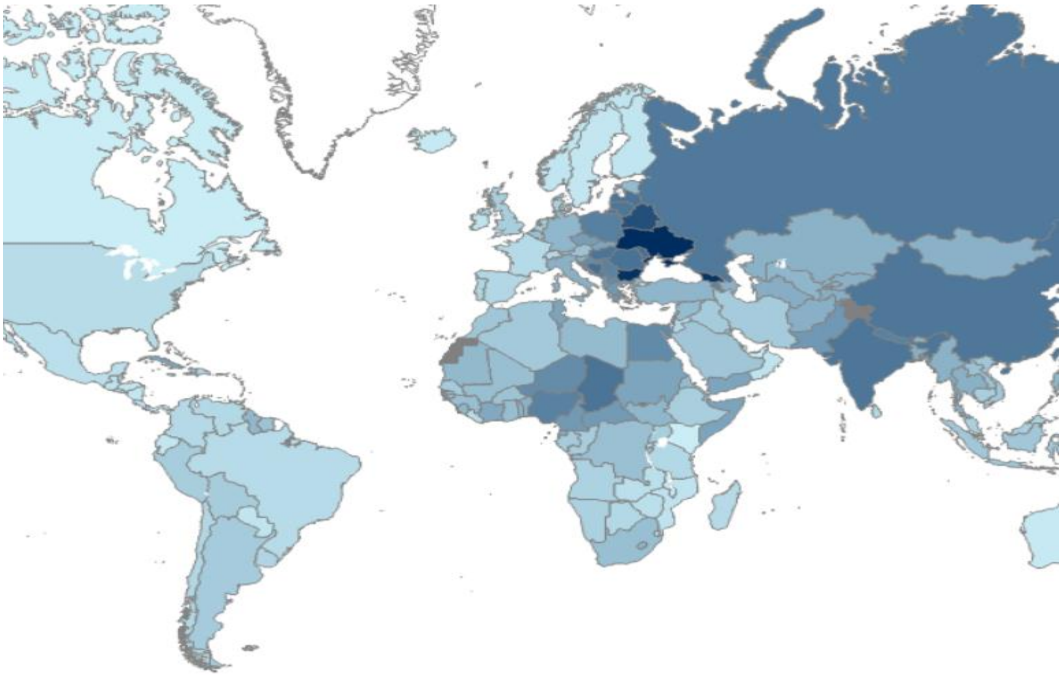

Figure 1. World map of ambient air pollution attributable death rate (per 100 000 population). (Source: The Global Health Observatory (WHO), available on https://www.who.int/data/gho/data/indicators/indicator-details/GHO/ambient-air-pollution-attributable-death-rate-(per-100-000-population)).

According to the European Environment Agency (EEA), the main emission sources of the main pollutants are represented by: road transport, commercial, institutional and households, energy production and distribution and industrial processes and product use (Figure 2).

Over the years, many researchers have studied and analyzed the health effects of air pollution (e.g. Brunekreef and Holgate, 2002; Pope et al., 1995; Pope and Dockery, 2006) and it is still a hot topic (Dominski et al., 2021; Gignac et al., 2022; Kurt et al., 2016). Even the various local and national governments consider the issue as crucial and are committed in various ways to reducing the concentrations of pollutants in urban areas in particular, especially in developed countries (e.g., Europe, USA). In fact, numerous laws, regulations and suggestions on air quality standards have been prepared (EPA, 1970; EU, 2016).

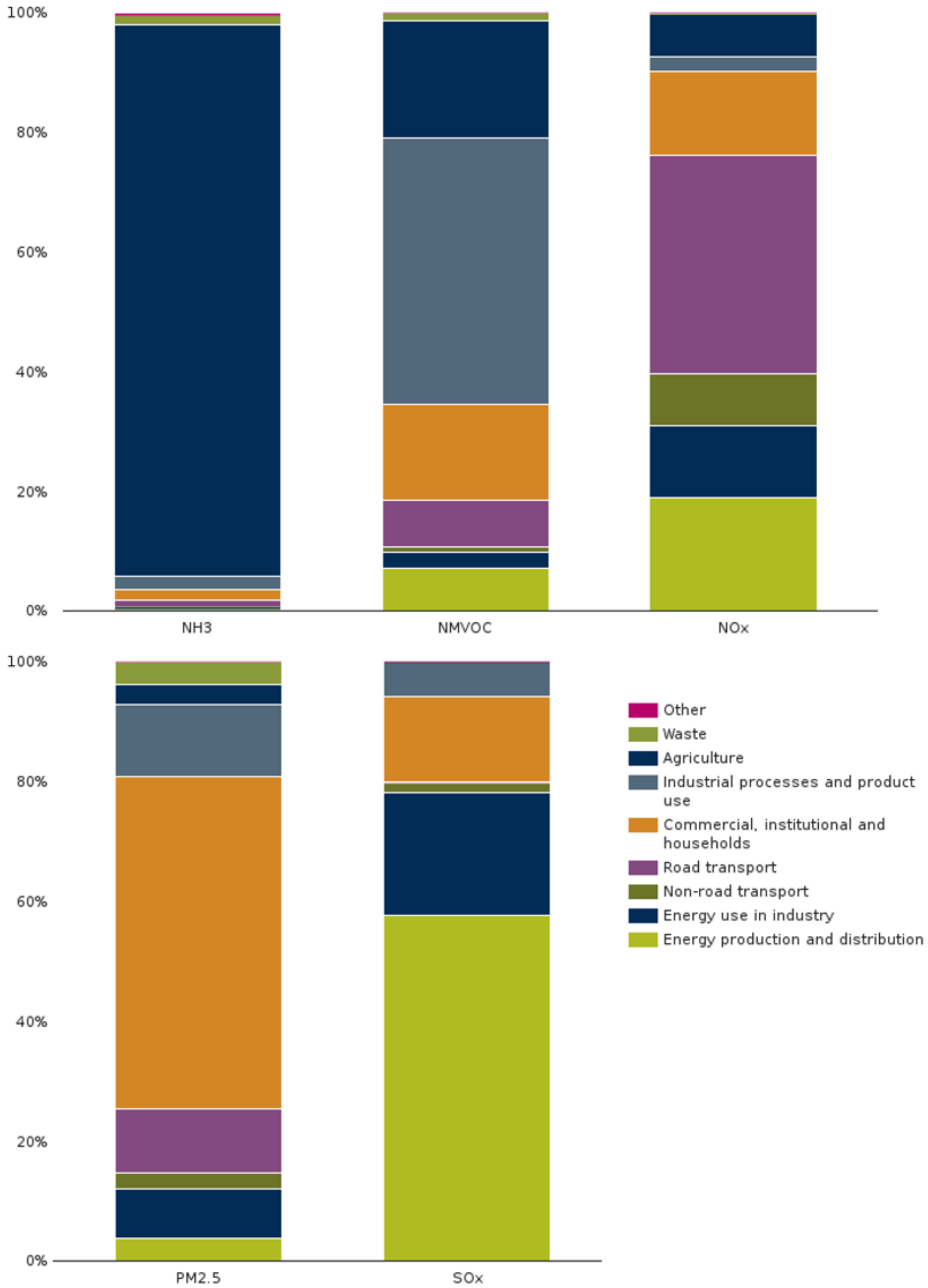

Figure 2. Percentage of emissions of the main atmospheric pollutants by sector group. Note: NMVOCs: non-methane volatile organic compounds, such as benzene, ethanol, etc. Figure source: EEA, available on https://www.eea.europa.eu/data-and-maps/daviz/share-of-eea-33-emissions-5#tab-chart_1; Data sources: Emissions of main air pollutants provided by European Environment Agency (EEA).

Air pollutants can be classified into primary or secondary. Primary pollutants are those emitted directly from a source into the atmosphere, such as carbon monoxide (CO) emitted by a motor vehicle. Secondary pollutants are those that are formed in the atmosphere, i.e. which originate when the primary pollutants react or interact with other substances or physical variables present in the atmosphere. An example of a secondary pollutant is tropospheric ozone (O_3), which is the result of chemical reactions between primary pollutants in the presence of sunlight. Some pollutants can be both primary and secondary. The main primary pollutants are:

- sulfur dioxide (SO_2) is part of the sulfur oxides (SO_x) that are formed during the combustion of substances containing sulfur, the production of gasoline from petroleum and the extraction of metals from the raw mineral;
- Volatile organic compounds (VOCs) comprise a wide range of carbon-based molecules, including aldehydes, ketones and other light hydrocarbons. VOCs play a fundamental role in the formation of secondary pollutants, such as ozone and particulate matter;
- ammonia (NH_3) is emitted from agricultural processes and is a by-product of animal origin;
- carbon monoxide (CO) is a colorless, odorless and tasteless toxic gas produced by the incomplete combustion of fuels such as wood, gasoline, coal, natural gas, etc..

To the list are added the following pollutants which are both primary and secondary:

- nitrogen oxides (NO_x) are a group of highly reactive gases (including nitrogen dioxide (NO_2) and nitrogen oxide (NO)). NO_x is the result of combustion at high temperatures, such as those used for heating, transport and energy production. NO_2 is an important precursor to ozone;
- Particulate matter (PM) is a complex mixture of particles (sulfate, nitrates, ammonia, sodium chloride, black carbon, mineral powder or water) and extremely small droplets. PM is typically classified on the basis of its size in: PM_{10}, the fraction of suspended particles with a diameter equal to or less than 10 µm; and $PM_{2.5}$, formed by particles with a maximum diameter of 2.5 µm. PM can be a primary or secondary pollutant. Black carbon is an important component of $PM_{2.5}$, a powerful climate-altering agent due to its efficient absorption of solar radiation and consequent heating capacity of the surrounding area.

The main secondary pollutants are PM and tropospheric ozone. Due to its photochemical nature, the highest ozone levels are observed during periods of sunny weather (Künkli et al., 2010).

According to the WHO and the EEA, particulate matter (Figure 3), nitrogen dioxide and ground-level ozone (Figure 4) are currently considered the three pollutants with a most significant effect on human health. Some pollutants often record concentrations higher than the limit values for the protection of human health (tropospheric ozone in the summer months, PM_{10} and NO_2 in the winter months).

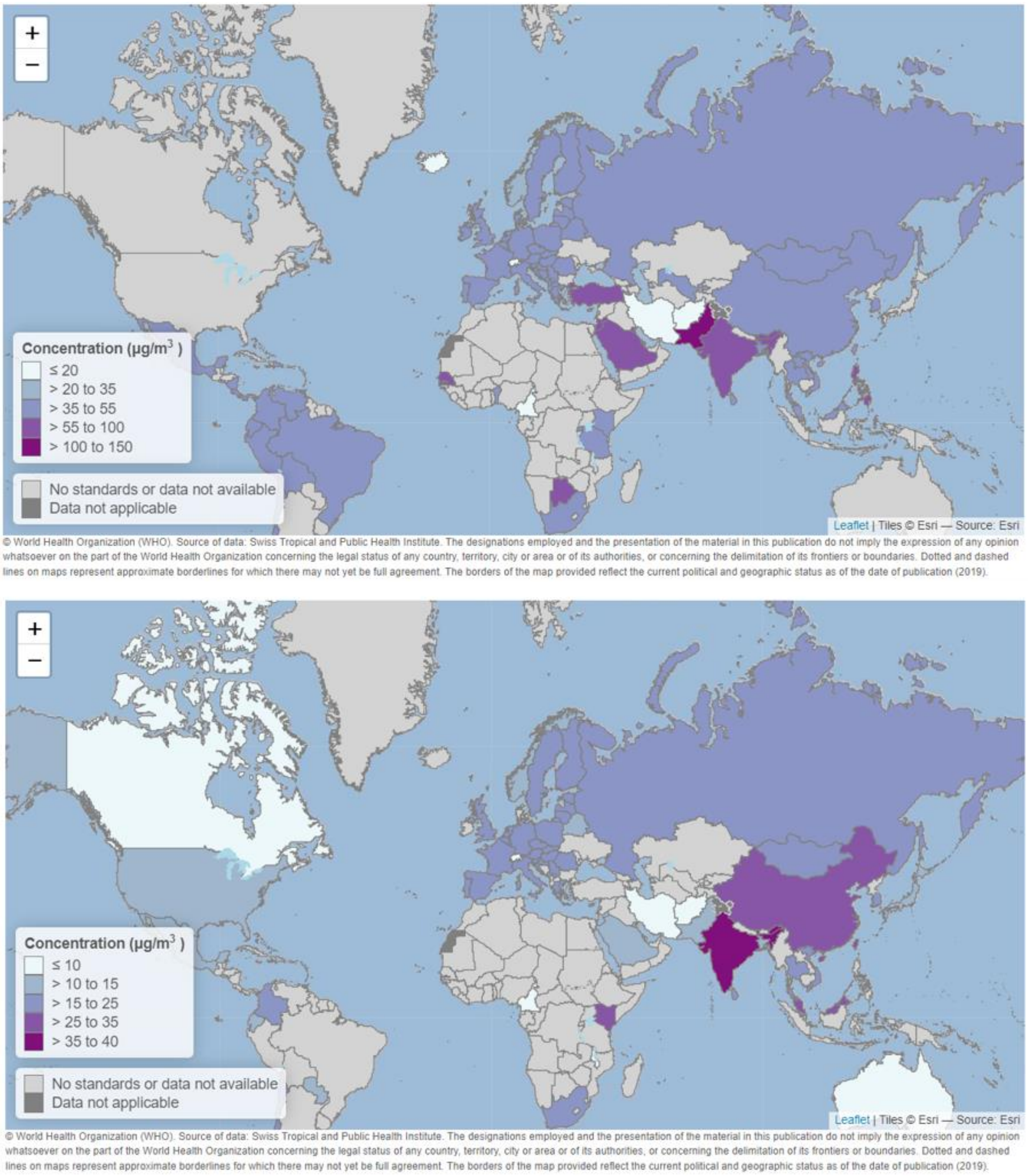

Figure 3. World maps of mean concentration of PM_{10} (top) and $PM_{2.5}$ (bottom). Averaging period: 1 year. reference year: 2019. Source: National Air Quality Standards (WHO) https://whoairquality.shinyapps.io/AirQualityStandards/.

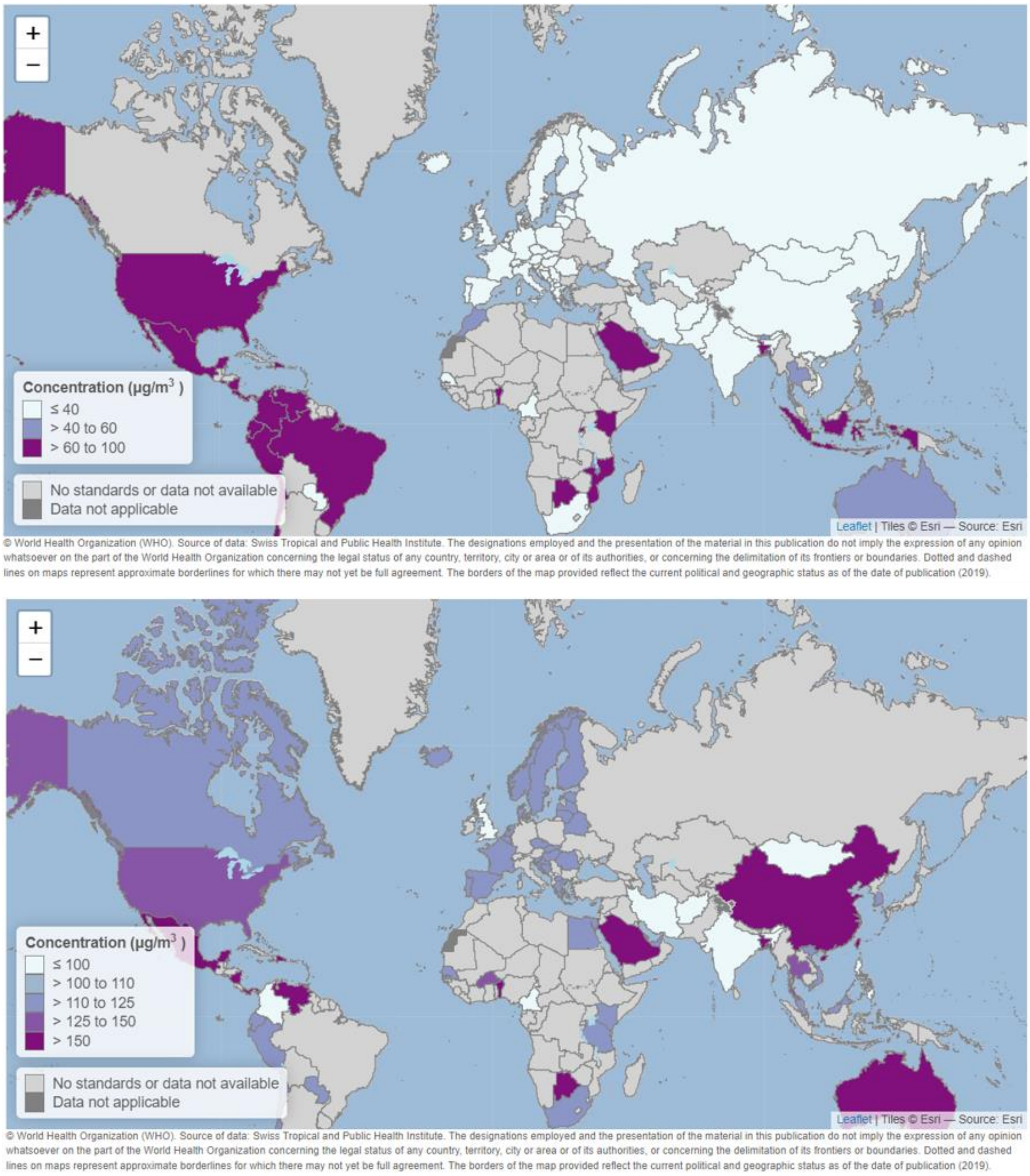

Figure 4. World maps of mean concentration of NO_2 (top) and O_3 (bottom). Averaging period: 1 year for NO_2 and 8 hours (daily max) for O_3. reference year: 2019. Source: National Air Quality Standards (WHO) https://whoairquality.shinyapps.io/AirQualityStandards/.

The EEA defines photochemical smog as: "a combination of fog and chemicals that come from automobile and factory emissions and is acted upon by the action of the sun". The formation of photochemical smog consists of a series of reactions that can give rise to hundreds of different compounds. Generally, the conditions that lead to the formation of photochemical smog occur during the hours of intense traffic in the morning, when the emissions increase the presence in the atmosphere of hydrocarbons and nitrogen oxides (monoxide (NO) and dioxide (NO_2)).

The action of sunlight causes at the same time the photolysis of NO_2 into NO and an oxygen radical (O) (EPA, 2004):

$$NO_2 + sunlight \rightarrow NO + O$$

This reaction increases in speed with increasing solar radiation. The oxygen atoms that are formed during this reaction react with the oxygen molecules present in the air to produce ozone, thus increasing the levels of ozone at ground level:

$$O + O_2 \rightarrow O_3$$

Ozone in turn can react with nitric oxide to produce NO_2 and oxygen:

$$O_3 + NO \rightarrow NO_2 + O_2$$

These three reactions make up the photo stationary ozone cycle and keep the ozone concentration at a stable level through a dynamic equilibrium. At night, ozone is consumed in the course of other processes. However, the dynamic balance of O_3 consumption/formation can be altered by the following conditions:

- the presence of sunlight (which acts as a catalyst);
- an air temperature of at least 18 °C, necessary because many of the reactions of the photochemical smog formation process require specific activation energies (guaranteed by the relatively high environmental temperature);
- the presence of volatile organic compounds (VOCs);
- the presence of nitrogen oxides.

If these requirements persist, then a series of chemical reactions take place, in which nitric oxide and NO_2 are consumed by VOCs, allowing for the accumulation of ozone at ground level. The most of the air pollution models includes modules for the calculation of chemical transformation. The complexity of these modules ranges from those simple to those describing complex photochemical reactions.

The fate of a pollutant emitted by human activities or natural sources depends on the meteorological conditions of the atmosphere in which it is released. The main phenomena that caused the movement of pollutants in the atmosphere are transport, dispersion, and deposition. Transport is primarily caused by mean wind flow. Deposition processes (such as precipitation, scavenging, and sedimentation) remove the pollutants from the air and move it to the ground surface. Dispersion results from local turbulence (Watson et al., 1988). Turbulence is generated in the Planetary Boundary Layer (PBL): the portion of the troposphere that is directly influenced by the Earth's surface, the PBL responds to combined action of mechanical and thermal forcing, in the order of 1-h timescale (Stull, 1988). In atmospheric dispersion models, turbulence parameterization is a key parameter. Within this layer, wind speed and wind direction are influenced by the roughness of the surface and the vertical height of flows (Seinfeld and Pandis, 1998). Furthermore, the urban surface morphology (presence of buildings), urban materials, vegetation differences and human activities profoundly modify the PBL structure over urban areas (Roth, 2000). This has important implications for the transport and dispersion of pollutants (Martilli, 2002).

2.2 Air pollutants monitoring

The adverse effects caused by air pollution on the state of the environment and on human health causes extreme attention of the wide public and of different authorities. In order to reduce the negative impact of air pollution on health and the environment, it is of great importance to "measure pollution" to obtain information on (Michulec et al., 2005):

- qualitative and quantitative composition of pollutants;
- spatial and temporal fluctuations;
- sources and intensity of polluting emissions;
- impact range of the emitters;
- processes of transport and transformation of pollutants in the atmosphere;
- level of emission and intensity of deposition of pollutants;
- effectiveness of the actions undertaken.

In particular, quantitative information on pollutants makes it possible to evaluate air quality. Air quality (AQ) refers to the degree to which air is suitable or clean enough for humans or the environment, and government agencies have set standards for this. Air quality standards refer to the levels of air pollutants prescribed by regulations that cannot be exceeded during a specified period of time in a defined area.

In Europe, the Directive 2008/50/EC, as well as its daughter directives, require the assessment of the ambient air quality existing in the Member States on the basis of common methods and criteria. The minimum requirements, described in the directives, are linked to the specific concentration thresholds and the population present in each zone or agglomeration. Although continuous monitoring is mandatory in specific cases, modeling is always encouraged in order to provide better information on the spatial distribution of concentrations.

The methods of measuring air quality vary significantly and range from occasional campaigns conducted with passive sampling to automatic remote monitoring systems based on optical absorption spectroscopy. In particular, methods for air quality sampling can be classified into three main groups (Marć et al., 2015; WHO, 1999):

- Passive Monitoring - Passive sampling technology is any device that monitors gas concentrations simply by allowing air to pass over it rather than being pumped. They have relatively low sampling rates, and require long sampling times in environments with low concentrations of pollutants;
- Active sampling - the gas is pumped into the absorbent medium, the sample is analyzed in the laboratory sampling devices are bulky and complex, however the

measured gas concentrations are less sensitive to environmental influences such as changes in wind speed or humidity;

- Automatic Monitoring - Automatic analyzers draw in ambient (outside) air and measure the pollutant concentration in the sampled air. They provide high resolution data and can collect data online.

In Europe, in the last 10 years, a lot of work has been done in order to standardize the monitoring techniques used in the various countries and to be able to create platforms for exchanging data. The EEA air quality database consists of a multiannual time series of AQ measurement data and statistics calculated for a range of air pollutants. It also contains meta-information about the monitoring networks involved, their stations and measurements, AQ modeling techniques, as well as air quality zones, assessment schemes, compliance results, and plans and programs for air quality reported by EU Member States (https://www.eea.europa.eu/data-and-maps/data/aqereporting-9).

Monitoring stations are generally classified as rural, suburban or urban, but the definitions of these categories may vary between the various bodies and between the various countries. Monitoring stations provide important information on pollutant concentrations, such data are also used as inputs in dispersion models.

2.2.1 Air quality models

Dispersion models take into account chemical and physical processes and assumptions of the dispersion for explaining the transformation of pollutant considering the emission sources to predict the concentrations, as well as pollutants spatiotemporal variability (Vardoulakis et al., 2003). The dispersion modelling approach requires a different kind of data to estimate pollutants concentration, such as emission inventory, meteorological data, topography data, and other environmental information.

Air pollution models can be categorized into three generic classes (Figure 5): statistical models, physical models and deterministic approach (Weber, 1982). The statistical models calculate ambient air concentrations using an empirical established statistical relationship. The statistical model is very useful for short-term forecast of concentrations and for drawn semi quantitative conclusions on some particular air quality issues. They require small computational effort and no emission inventory is needed (Srivastava and Sinha, 2004). In physical models, a real process is simulated on a smaller scale in the laboratory by a physical experiment. In the case of complex air pollution situation, laboratory simulation using scaled-down models in wind tunnels is used. In this approach, the scale-model geometry, flow speed and other essential variables can be changed and controlled (Srivastava and Sinha, 2004). Deterministic models basically deal with different types of numerical approximations in the solution of the partial equations representing the relevant physical process of atmospheric dispersion. For these models an emission inventory has to be available and meteorological data. The deterministic model is most suitable for long-term planning decisions (Srivastava and Sinha, 2004).

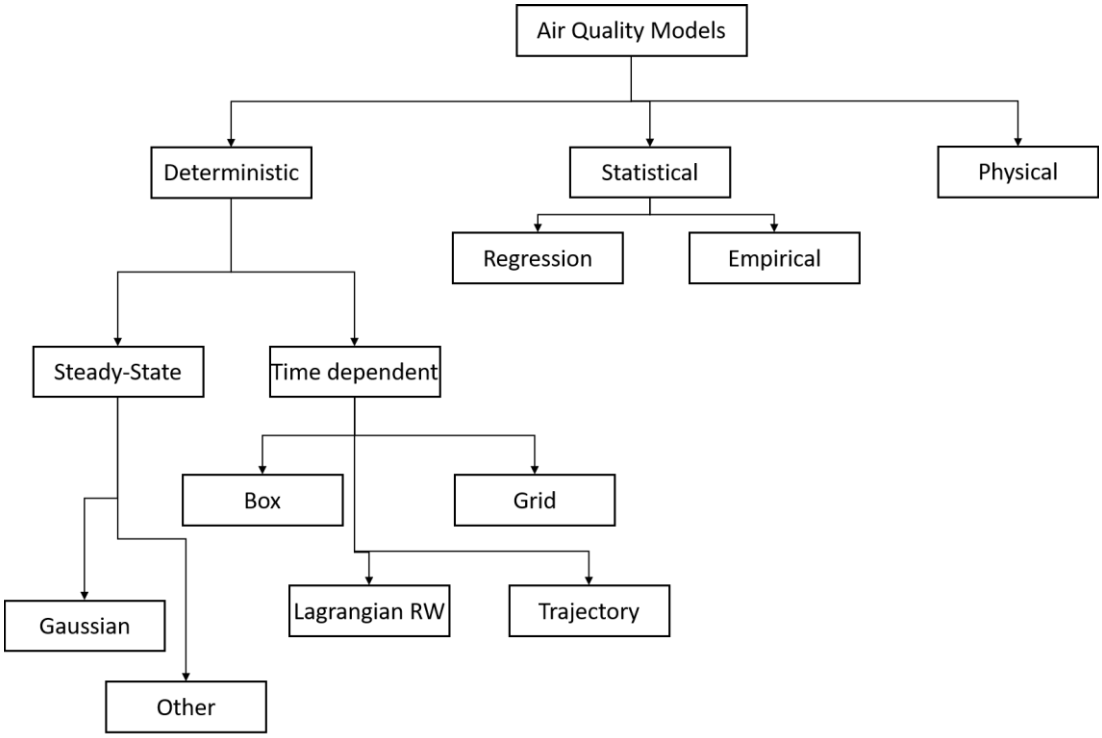

Figure 5. Classification of Air Quality Models (adapted from Weber, 1982)*)*

The deterministic models in turn are divided into (Srivastava and Sinha, 2004):

- Time-Dependent Model: In this kind of model all variables are functions of time. Examples of Time-Dependent Models are: the box models, the grid models, Lagrangian and Random Walk Models and Trajectory Models.
- Steady State Models: the steady state condition implies that all variables and parameters are constant in time, including the concentration. Steady-state models calculate concentrations for each hour from an emission rate and meteorological conditions that are uniform across the modelling domain. Thus they simulate hourly-average concentrations (NIWAR, 2002). The most common of this kind of models is the Gaussian Model, it is based on the assumption that the plume concentration, at each leeward distance, has independent Gaussian distributions both horizontally and vertically. Some Gaussian models have been modified to incorporate special dispersion cases (Zannetti, 1993).

Dispersion modelling in the atmosphere is generally a difficult task due to the complex effects of meteorology on advection and diffusion, and the wide range of different scales involved. Therefore, the spatial scale at which the models work is closely related to the spatial scale of atmospheric processes (Figure 6, Moussiopoulos et al., 1996; Silveira et al., 2019). Britter and Hanna (2003) used the following spatial scales to describe the major urban flow features: regional scale (up to 100 or 200 km), city scale (up to 10 or 20 km), neighborhood scale (up to 1 or 2 km), and street scale (less than 100 to 200 m).

	1 m	10 m	200 m	1 km	10 km	100 km	2000 km	>2000 km
Atmospheric process scale	**Microscale**			**Mesoscale**				**Macroscale**
Modelling scale	**Street scale**			**Neighborhood scale**	**City scale**	**Regional scale**		

Figure 6. Scheme of spatial scales and atmospheric processes and spatial scales of air quality models (adapted from (Britter and Hanna, 2003; Moussiopoulos et al., 1996; Silveira et al., 2019).

In particular, urban-scale modeling systems should consider variations in local-scale effects, such as the influence of buildings and obstacles, downwash and plume rise phenomena, along with chemical transformation and deposition. Urban features affect atmospheric flow and microclimate, increasing atmospheric turbulence and modifying turbulent transport, dispersion and deposition of atmospheric pollutants (Srivastava and Rao, 2011).

2.3 Climate change and Air Pollution

Historically, air pollution and climate change have been handled as separate problems. Today it has been realized that climate change and air pollution are closely intertwined. Indeed, the two problems share the same origins and sources: for example, the use of fossil fuels in energy and industrial production and transport is simultaneously the main source of carbon dioxide (CO_2) (one of the most important greenhouse gases) as well as of air pollutants (Künzli et al., 2000). The same source can emit pollutants and climate-altering substances at the same time, and in turn some pollutants (e.g., particulate matter) can have an impact on the climate system or be precursors of climate-altering species (Mangia et al., 2020).

In the past, scientific analyzes of the causes, dynamics and impacts of climate change have mainly focused on the role of CO_2 and the other five long-lived trace gases recognized as powerful greenhouse gases and subject to international climate negotiations (CH_4, N_2O, HFC, PFC, SF_6). Less prominence has been given to some of the short-lived "conventional" air pollutants, in particular ozone, methane and particulate matter. Particulate matter plays a very important role in global warming because it contributes to cloud formation and influences the transfer of radiant energy and the spatial distribution of latent heating through the atmosphere, thereby influencing the weather and climate. Particulate matter interacts with solar radiation through absorption and scattering and, to a lesser extent with terrestrial radiation through absorption, scattering and emission. Generally, aerosols influence the climate directly by scattering and absorbing incoming solar radiation, and indirectly by acting as cloud condensation nuclei and/or ice nuclei (Boucher et al., 2013; Huang et al., 2007). For this reason, the reduction of PM emissions will have the effect of protecting both human health and climate. Ground-level ozone is a greenhouse gas because it inhibits the process of plants absorbing atmospheric carbon, which significantly contributes to global warming. Methane, in addition to being one of the greenhouse gases included in the Kyoto Protocol, also contributes to the formation of ground-level ozone. The reduction of methane emissions contributes to the reduction of both ozone levels that are harmful to health and ecosystems and climate change (Swart et al., 2004).

Conversely, climatic variations (e.g., variations in temperature, pressure, mixing layer height, wind speed and direction, precipitation patterns) can impact on air quality by increasing or reducing the concentration of air pollutants. The intensity of precipitation determines the atmospheric concentration and deposition of compounds. By acting on atmospheric circulation and hydrogeological regimes, climate changes can alter the weather and emission conditions that affect air quality (Mangia et al., 2020).

2.3.1 Heat wave and Urban Heat Island

The Urban Heat Island (UHI) is defined when an urban area is significantly warmer than the surrounding (rural) environment. This temperature difference is usually greater at night than during the day, and is more noticeable when the winds are low. It is mainly caused by the retention of solar heat in the urban fabric (buildings and ground surfaces) and by the obstruction and reabsorption of the outgoing long-wave nocturnal radiation by buildings obstructing the view of the sky. Furthermore, changes in the earth's surface due to urban development together with the heat released into the environment generated by energy use generate a corresponding increase in average temperature. In particular, paved surfaces store heat during the day and release it during the night. Reduced ventilation can hinder the dispersion of urban heat islands (Parker, 2010).

The high temperatures caused by the UHI have the effect of increasing the demand for cooling energy in commercial and residential buildings to maintain thermal comfort levels. The increase in energy demand results in increased electricity production and related higher emissions of SO_2, CO, NO_x and suspended particles, as well as carbon dioxide, which contribute to the increase in atmospheric pollution and global warming and climate change (Gorsevski et al., 1998). Furthermore, temperature increases resulting from climate change are expected to impact cities, exacerbating the UHI effect.

At the same time, global warming has led to more frequent, severe and longer-lasting excessive heat events (Heat Waves (HW)) around the world. In addition to environmental and economic impacts, heat waves have a fairly devastating impact on human health with deaths in many parts of the world (Changnon, 2003; McMichael et al., 2006). The frequency and severity of such extreme events will further increase in the near future (Coumou and Robinson, 2013; Perkins et al., 2012; Schär et al., 2004). HW can be increase in frequency and duration due to UHI effects (Li et al., 2020), and the UHI impacts can be intensified during HW events (O'Neill and Ebi, 2009; Whitman et al., 1997). Negative HW effects are more pronounced in urban areas due to higher population density and the potential additive effect of UHI (Gabriel and Endlicher, 2011; McCarthy et al., 2010). However, the interaction between UHI and HW is complex and remains a hot topic: many researchers (An et al., 2020; Li et al., 2016) showed synergies, other researchers (Chew et al., 2021; Oliveira et al., 2021) did not find synergies.

There is a synergistic association between elevated temperature, and air pollutants: the photochemical reactions happen in the presence of sunlight, so there is likely to be increased production of secondary pollutants during warm seasons (Elminir, 2005; Tressol et al., 2008). For example, during HW events, stagnant phenomena happen that trap emitted pollutants, increasing level tropospheric O_3 (Monks et al., 2015; Solberg et al., 2008).

2.4 Summary

Air pollution kills around seven million people around the world each year. The main emission sources of the main pollutants are represented by: road transport, commercial, institutional and households, energy production and distribution. The local and national governments are committed to reducing the concentrations of pollutants in urban areas. In order to reduce the negative impact of air pollution on health and the environment, it is of great importance to monitoring the concentration of the pollutant. Beyond continuous monitoring, modeling provides better information on the spatial distribution of concentrations. The fate of a pollutant emitted depends on the meteorological conditions of the atmosphere. In the PBL, wind speed and wind direction are influenced by the roughness of the surface. The structure of the PBL and the roughness are very important parameters in the dispersion of pollutants, for this reason their parameterization should always be included in the modeling of the dispersion.

Climate change and air pollution are closely intertwined: the same source can emit pollutants and climate-altering substances at the same time, and some pollutants can have an impact on the climate system or be precursors of climate-altering species. On the other hand, climatic variations can impact on air quality by increasing or reducing the concentration of air pollutants. UHI and air pollution are also closely related, UHI increasing the demand of energy for cooling, that increases electricity production and related higher emissions of pollutant. The related higher emissions of pollutant contribute to the increase in atmospheric pollution and global warming and climate change. The global warming has led to more frequent HW. UHI and HW are also closely related, HW can be increase in frequency and duration due to UHI effects and the UHI impacts can be intensified during HW events. Moreover, a synergistic association between elevated temperature and air pollutants exists: during warm season, the high presence of sunlight increases production of secondary pollutants. All of these connections have an effect on the health levels of the urban environment. Therefore, in the evaluation of urban quality, in addition to atmospheric pollution, the thermal aspects of a city must also be taken into consideration.

3 CASE STUDY: BOLOGNA IN THE ISCAPE PROJECT

This chapter contains an overview of the experimental campaigns and the dispersion models application in Bologna case study within the H2020 iSCAPE project (Improving the Smart Control of Air Pollution in Europe, https://www.iscapeproject.eu/). Briefly, iSCAPE was a project funded by the European Union's H2020 Research and Innovation programme (H2020-SC5-04-2015) under the Grant agreement No. 689954. The project focus was the integration and advancement of the control of air quality in European cities in the context of climate change. Therefore, the main objectives were the efficiency evaluation of air pollution control strategies, policy interventions and behavioral change initiatives. The different strategies were being assessed using seven pilot sites in different cities across the EU (Dublin, Bottrop, Guilford, Lazzaretto, Vantaa, Hasselt and Bologna), which were being used as Living Labs. During the iSCAPE project (started on September 2016 and ended on December 2019), experimental field campaigns were carried out in different target cities, aimed monitoring air pollution and meteorological variables. At the same time, in order to evaluate the efficacy of the solutions, air quality and meteorological simulations were run at different scales. The experimental data collected during the field campaigns were used to provide the scientific basis to establish the efficacy of different pollution control strategies (such as Passive Control System (PCS)) in each city and as input and feedback for the simulations.

3.1 The Bologna experimental campaigns

The experimental campaigns carried out in Bologna (Figure 7) aimed at creating a baseline on which to evaluate the efficiency of the Green Infrastructure (GI)[1] in urban road canyons, as well as using the measurements as inputs for the simulations and validations of the models used.

Bologna is located at the foot of the Apennines in the vast flat area of the Po Plain in the north of Italy (44°29' N, 11°20' E, with a mean altitude about of 54 m a.s.l.). It is the capital city of Emilia-Romagna with about 400,000 inhabitants on an area of 140 km^2; and the center of the homonymous metropolitan city populated by more than 1 million people (Città Metropolitana di Bologna). The climate in Bologna is strongly dependent on its location: a warm and humid summer and long, cold winter, with scarce rainfall that concentrates in spring and autumn periods. During autumn and winter, there are often strong thermal inversions that favor fog. Bologna is characterized by a regime of breezes favored by the presence of the Adriatic Sea on the eastern side and mostly all by the presence of the mountains south of the city, that prevent the development of intense winds. However, Bologna appears to be the windiest city in the Po Valley and

[1] Green infrastructure (GI) is a term that can mean different things. Here, we use the term to refer to trees and vegetation that provide ecological benefits in urban areas.

consequently records better air quality than the nearby cities affected by the same emission sources, thanks to the dilution of pollutants by ventilation (Di Sabatino et al., 2019).

The campaigns were carried out in two different periods: (1) the summer campaign from 10/08/2017 to 24/09/2017; (2) the winter campaign from 16/01/2018 to 14/02/2018. The area interested by the experimental campaigns comprehends both the historical city center as well as the residential part of Bologna. Two urban street canyons inside the city were identified (Figure 7), sharing similar traffic conditions and emitting sources, but characterized by different presence of vegetation (Di Sabatino et al., 2019). Laura Bassi St. is a typical street on the outskirts of Bologna, 700 m long in which there are low buildings with 2-3 floors and taller buildings with 4-5 floors, the average height of the buildings is about 17 m. The road is surrounded by deciduous trees present regularly on both sides of the street. Marconi St. is a representative street of the historical territory, about 600 m long, it is surrounded by buildings with 4-5 floors up to buildings with 9-10 floors and an average height of 33 m. Along the roadway there are arcades, but there is no vegetative element, except for the 50 m near one end of the road, here there are deciduous trees placed on one side of the road. In both campaigns, high-resolution instrumentation was used to monitor meteorological and air quality variables. The equipment consisted of two mobile laboratories of local environmental protection agency ARPAE (Agenzia Regionale per la Protezione Ambientale ed Energetica), i.e., vans equipped for continuous measurements of the main air pollution pollutants (NO_x, PM_{10}, $PM_{2.5}$, CO, O_3 and SO_2). ARPAE mobile laboratories are also equipped with instruments for measuring meteorological variables (wind speed and direction, pressure, air temperature and air relative humidity): GILL Windmaster sonic anemometers (Gill Instruments Limited, Hampshire, UK), HCS2S3 Rotronic thermos-hygrometers (Rotronic Instruments Ltd., Crawley, UK) and Vaisala PTB110 barometers (Vaisala, Helsinki, Finland) and CNR4 radiometers (Kipp & Zonen B.V., Delft, The Netherlands).

A further experimental campaign was conducted in the summer 2018, to evaluate the efficacy of TiO_2 photocatalytic coatings for NO_x abatement during weak synoptic conditions. The experimental site comprised two real street canyons within the Lazzaretto, area in the outskirts of Bologna (44°29′ N, 11°20′ E, Italy).

Figure 7. Locations of Bologna, Marconi and Laura Bassi Sts.. The left map indicates the positions of Bologna (red dot) in Italy and its municipal boundaries with the cyan line (map with red box). The right map at bottom shows the location of the two streets in Bologna where the iSCAPE experimental campaigns were conducted: Marconi St. (red line) and Laura Bassi St. (green line). Source: Open Street Map.

Furthermore, two intensive thermographic campaigns lasting 24 hours were also carried out, one for each experimental campaign (Di Sabatino et al., 2018), the high-performance thermal imaging cameras were used to quantify thermal characteristics of various physical elements on urban streets (building façades and asphalt) (Di Sabatino et al., 2018). During the intensive thermographic campaign carried out in the winter, I took care of the acquisition methodology. In addition, I dealt with the analysis of the data collected during both campaigns, as described below. In the winter campaign Low-Cost Sensors (LCSs) for the measurement of pollutants were collocated with ARPAE reference AQ sensor in order to collect sensor data and evaluate their usability, through feedback about operation and installation. I took care of the sensor setup, installation, data collection and related data analysis.

3.1.1 Intensive thermographic campaigns

Here, the theoretical and operating notions of an Infra-Red (IR) camera are illustrated, followed by the description of the methodology I used for the acquisition of the thermal images (or frames) and for the analysis of the same.

During both the winter and summer experimental field campaigns, two intensive thermographic campaigns in the two streets (Marconi (MA) and Laura Bassi (LB) Sts.) were carried out. The main goal of the intensive thermographic campaigns was to collect and analyze temperature data at street scale levels and to evaluate the UHI effect, defined as the phenomenon of enhanced temperatures in urban areas compared to the surrounding countryside. For this reason, two thermal cameras were used, one for each site. Specifically, two high performance FLIR T620 Thermal Imaging IR Camera (Figure 8) were used, with uncooled micro-bolometer, 640x480 pixels resolution and an image acquisition frequency of 30 Hz (https://www.flir.it/products/t620/). The main parameters of the cameras that must be set are:

- reflected temperature can be changed in post-processing;
- atmospheric attenuation correction is automatic and is based on input distance, ambient temperature and relative humidity: (1) Distance below 50 m, the missed/incorrect entry of the distance leads to a maximum measurement error of 0.3° C; (2) air temperature and (3) air humidity were entered via the Extech device (digital USB Thermo-Hygrometer, FLIR).
- Emissivity, the maximum measurement error associated with the failure/incorrect setting of the emissivity will be less than one degree if the error on the emissivity estimate will be included within 0.1. Since the value of common materials used in construction is between 0.85 and 0.95 (in agreement with FLIR documentation); a constant emissivity value equal to 0.9 was set on the thermal imager.

Figure 8. The high performance FLIR T620 Thermal Imaging IR Camera (a) rear section (b) front section.

In post-processing this value is adjusted according to the specific values of the prevailing material using values reported in the literature. Images were simultaneously collected in both sites, while the days of the campaigns were selected according to the weather forecast in order to have meteorological conditions characterized by the absence of precipitation and intense wind, and with clear skies. On the basis of these criteria, 22-23/08/2017 during the summer campaign, and 08-09/02/2018 during the winter campaign were selected. Each thermographic campaign covered a 24-hour period, and acquisitions with the thermal cameras were carried out at regular 2-hour intervals. The buildings analyzed were selected (Figure 9) on the basis of the homogeneity of the construction material and the absence of obstacles in order to set a unique emissivity value. Furthermore, to obtain excellent quality thermal images, it is necessary to avoid the sky and any unwanted materials (people, cars, metal objects, glass, vegetation, etc.).

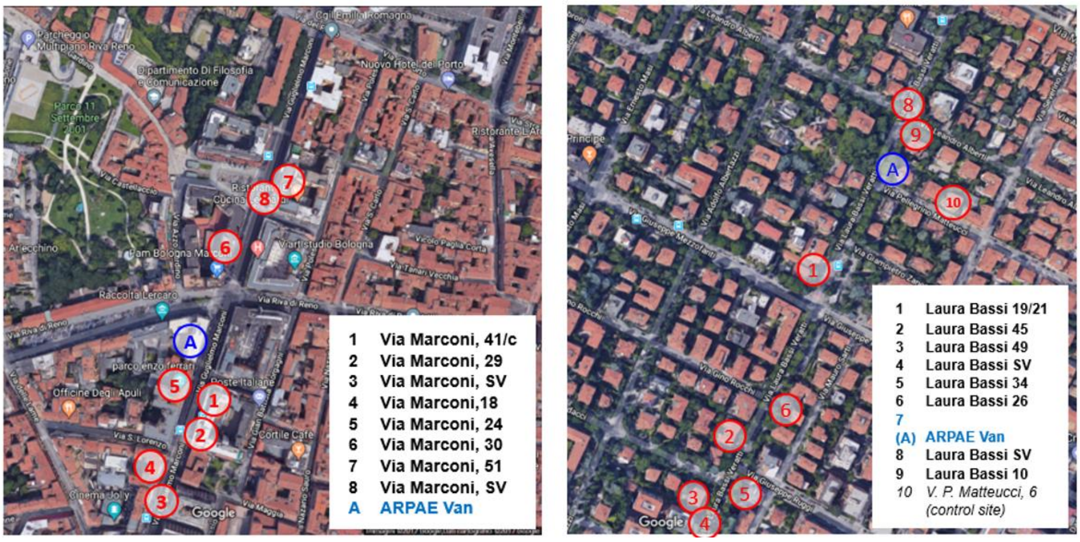

Figure 9. Location of the buildings selected for winter intensive thermographic campaigns. Right) Marconi St. building location and Left) Laura Bassi St. building location. Source: Google Maps.

For each site and each building, the scene target was established. For the larger buildings, more shots were planned with different portions of the same façade. In each site, the thermal information of the road surface was also collected. Each shot taken is a matrix that contains the thermal information of each pixel: we will refer to this type of data as a frame, in which each shot corresponds to a frame (Figure 10).

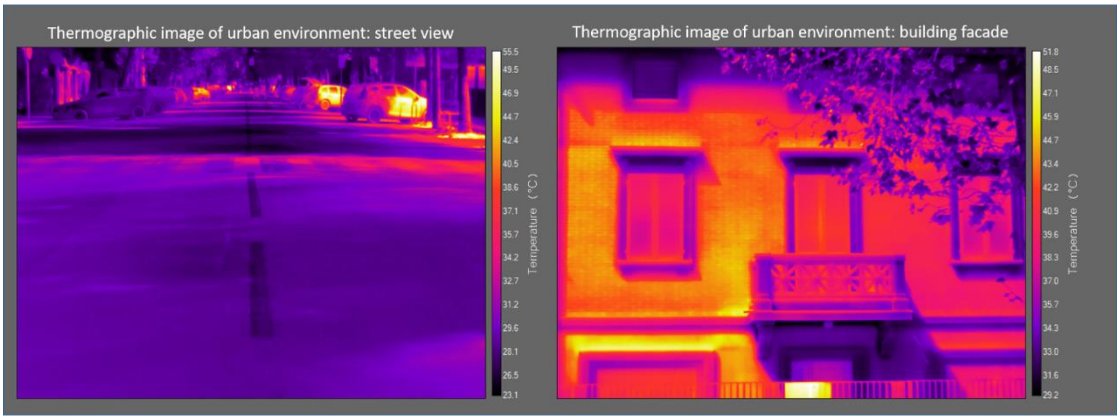

Figure 10. Examples frame of summer intensive thermographic campaigns in Laura Bassi St.. Left) Street canyon view: road surface and Right) building façade.

The data collected as part of the experimental campaigns were subjected to post-processing aimed at eliminating the pixels containing obstacles that could have altered the temperature value of the facade. The dataset was then subjected to an in-depth statistical analysis and comparison with the measurements collected in the two canyons and at other fixed ARPAE stations.

3.1.1.1 Post-processing methodology

In the post-processing, a series of elaborations were carried out aimed at identifying the exact temperature of each facade in the 24 hours of the campaigns carried out. As a first step the FLIR software is used to check the air temperature and air humidity data with the data recorded manually during the campaigns, and the effective distance between the thermal imaging camera and the target object (road 2m, buildings 8m) was entered. As regards the emissivity, the data recommended by FLIR (FLIR Systems, 2019) and consistent with values proposed by several authors (e.g. Carnielo and Zinzi, 2013; Danov et al., 2007; Di Sabatino et al., 2015) were used: 0.96 for asphalt and 0.94 for brick-limestone (building façade). For road surface, the correct data was extracted for each frame only for homogeneous areas, avoiding any types of other objects present in the scene. For the buildings, the methodology was more complex as there were many areas occupied by windows on all the facades (Figure 11).

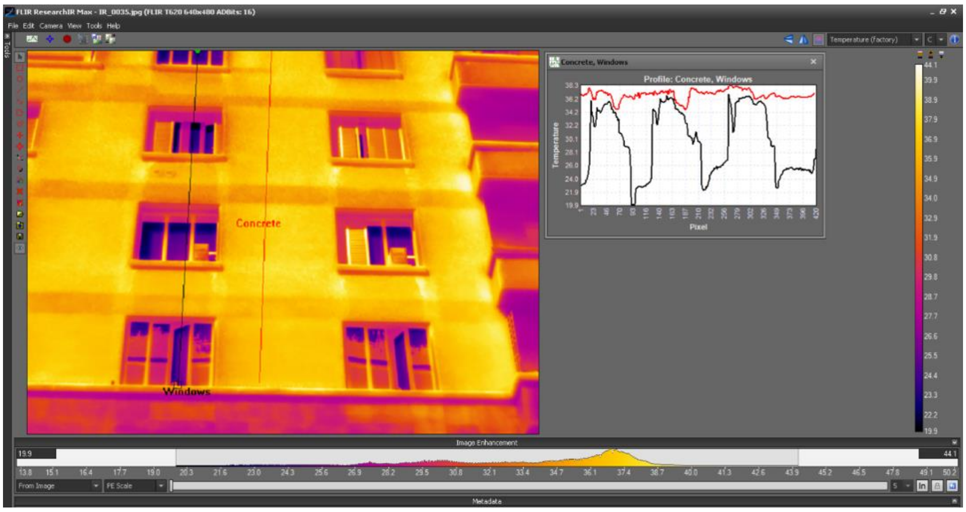

Figure 11. Building façade with windows that alter the thermal profile: red line) thermal profile with no windows; black line) thermal profile with the presence of windows. FLIR ResearchIR Max® software elaboration.

Therefore, the windowed areas and portions of the sky were identified manually using the tools of the FLIR ResearchIR Max® software. Using the " box " tool (Figure 12) for each frame, the areas were delimited and a file was saved containing information on the number of pixels for each identified area. The temperature information for each pixel of the detected area was then exported as a MAT file (MATLAB® file format).

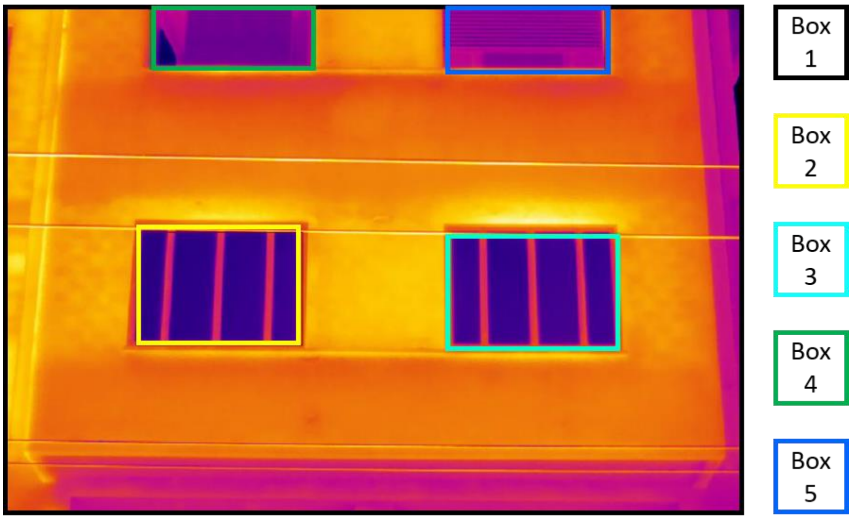

Figure 12. Example of frame with selection of areas containing windows. Box 1 (black) indicates the entire frame, the other boxes bound the different windows present; for each box, basic statistical information and the number of pixels contained are exported. FLIR ResearchIR Max® software elaboration.

The second post-processing step concerns the cleaning of the frame from the presence of windowed areas and portions of the sky. The scripts for reading the temperature data and information on the number of pixels of the windowed areas have been created in MATLAB®, in the same script a command has been included to cut the portions of the sky. The weighted average for each building was then calculated as follows:

$$\bar{T} = \frac{\sum_{i=1}^{n} x_i \cdot p_i}{\sum_{i=1}^{n} p_i} \qquad [1]$$

where x_i is the average temperature value of the i-th frame and p_i is the weight of the i-th frame:

$$p_i = \frac{A_{tot} - A_f}{A_{tot}} \qquad [2]$$

where A_{tot} is the total area of the frame expressed in pixels (the entire original frame (*box₁*) contains 307200 pixels); A_f is the total area of the windows in the frame:

$$\sum_{j=1}^{n} A_f = A_f(box_2) + A_f(box_3) + \ldots + A_f(box_j) \qquad [3]$$

3.1.1.2 *Results of intensive thermographic campaigns*

In order to evaluate the UHI effect at neighborhood and city scale, firstly the temperature distribution of building façades and ground surfaces in the two streets was retrieved from the thermal images collected during the campaigns; after that the thermal measurements in the two canyons were compared with those collected by the thermo-hygrometers by the ARPAE at nearby fixed weather stations (Bologna Urbana (urban station) and Mezzolara (rural station)). The results highlight the overheating of the urban area compared to the rural area (~5-7 °C, Figure 13).

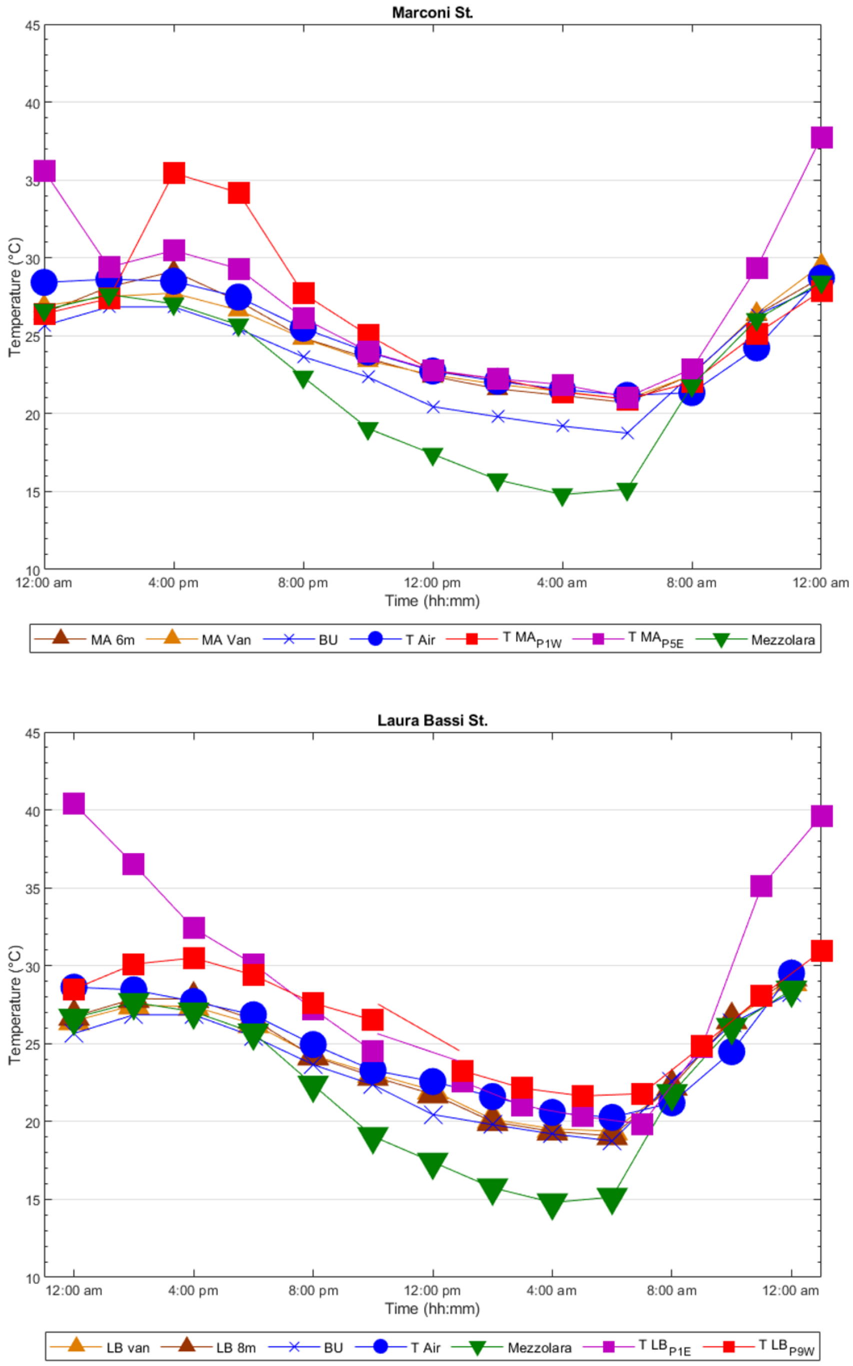

Figure 13. Daily temperature evolution in the summer thermographic campaign. The data are collected by: the thermo-hygrometers located at several heights in the streets: MA 6m and LB 6m: temperature measured 6 meters above the ground in Marconi St. and Laura Bassi St.; MA van and LB van: temperature measured on the roof of the van ARPAE in Marconi St. and Laura Bassi St.; the ARPAE weather stations located in the urban area (Bologna Urbana (BU)) and in the rural one (Mezzolara (Mz)), thermal Imaging IR Camera for the building façade temperatures refer to West (T MA$_{P1W}$ in Marconi St. and T LB$_{P9W}$ in Laura Bassi St.) and East (T MA$_{P5E}$ in Marconi St. and T LB$_{P1E}$) side of the 2 street canyons (Marconi St. upper and Laura Bassi St. lower). .

The UHI effect is different in the two city neighborhoods, and specifically is reduced in Laura Bassi St. with respect to Marconi St.. This result is due to different factors, including the presence of vegetation and the position of the street in residential area far apart from the city center. Conversely the higher UHI effect at Marconi is due to its position in the historic center of Bologna and the presence of high-density buildings. The same analysis carried out for the winter campaign highlights similar UHI effects in both neighborhoods, with differences between the urban and the surrounding rural area of about 6° C. The lack of difference between the two urban neighborhoods is likely a result of the absence of vegetation leaves in Laura Bassi.

3.1.2 Low cost sensors

Low Cost Sensor (LCS) assessment was carried out during the iSCAPE project. I took care of all the phases of the evaluation, from their setup to the analysis of the collected data, all the activities I carried out in this regard will be illustrated below. The LCSs provide high-density spatio-temporal pollution data offering a valid solution to make AQ monitoring devices available for large-scale use via a monitoring network. However, to implement a large-scale sensor network and to use all data generated in a meaningful way, it is necessary to formulate standard guidelines to evaluate its performance in the short and long terms (Rai et al., 2017). The main problems of this kind of sensors are related to: calibration, stability, measurements in the field, interferences between gas and influence of temperature and relative humidity (Rai et al., 2017; Spinelle et al., 2017). The assessment of sensors requires the knowledge of Repeatability, Reproducibility, Stability and Limit of detection of each sensor and for each pollutant:

- Repeatability: is defined as the closeness between successive measurements carried out under identical conditions of measurement, it denotes the dispersion between consecutive measurements obtained from a given sensor.
- Reproducibility: is defined as the closeness between successive measurements carried out under non-identical conditions of measurement it is used for designating dispersion between measurements obtained by using different sensors of the same model.
- Stability: is defined as a sensor's capability to maintain its performance characteristics over a sufficiently long duration (at least a few months).
- Limit of detection (LOD): is defined as the lowest concentration of a gas that can be significantly differentiated from zero concentration.

While the performance assessment under real-world conditions must take into account environmental conditions, especially temperature and humidity, and other parameters that can affect the measure. Finally, the stability of the sensor in long-term measure should be evaluated. Thus, based on the literature, the evaluation of LCSs followed a logical scheme consisting of three steps (Figure 14):

- determine Repeatability, Reproducibility, Stability and Limit of detection;
- consider environmental conditions, such as temperature and humidity, and calibrate the sensors in the field;
- consider a long term valuation.

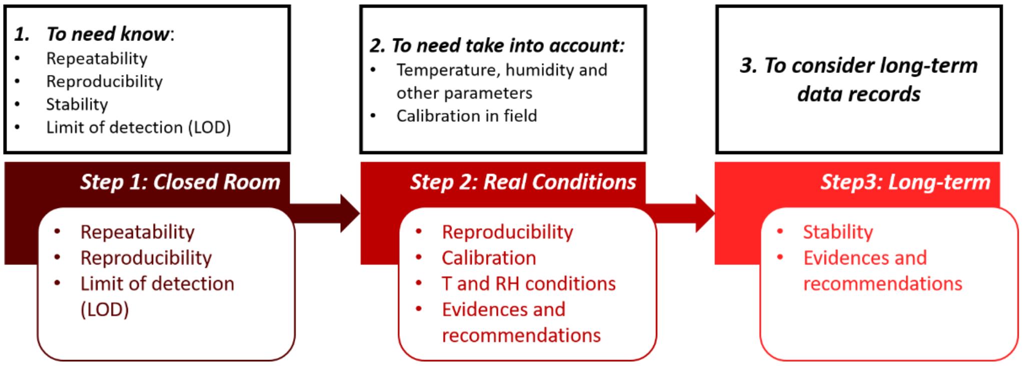

Figure 14. Logical scheme for the LCSs evaluation.

The steps coincide with three tests carried out:

- in a closed room;
- in real conditions, short term co-located with reference instruments;
- in real conditions, long term.

3.1.2.1 LCSs evaluation methodology

The sensor technology developed during the iSCAPE project bases its core design on the Smart Citizen project (Fablab Barcelona - IAAC) with his Smart Citizen Kit (SCK): a modular stack of self-designed electronics with a set of low-cost environmental sensors and data logging capabilities. The original sensors in the SCK supported qualitative measurements of air pollutants (CO and NO_x) via Metal Oxide sensors (MOs), light, temperature, humidity and noise readings. Data was logged via WiFi connectivity and sent to a dedicated API (Application Programming Interface, API indicates a set of procedures (generally grouped by specific tools) suitable for carrying out a given task; often this term designates the software libraries of a programming language), or locally in a sd-card.

Two solutions have been developed and used in sensor monitoring experiences: low-cost sensors, i.e. the SCK for Citizen Science and awareness activities, and High-end sensors, i.e. the Living Lab Station (LLS) designed as a more complex and accurate set of air pollution sensors. The updated version of the Smart Citizen Kits (SCK1.5) was tested in

Bologna, in real world conditions during the iSCAPE winter field campaign (15/01/2018-15/02/2018). The SCKs were available in three different configurations: i) Data Board (air Temperature (T), air Relative Humidity (RH), Light and Noise) with two sensors named MA02 and LB02; ii) Urban sensor Board (T, RH, Light, Noise, CO and NO_2) with two sensors named MA03 and LB03 iii) Gas Pro Board (T, RH, Light, Noise, CO, NO_2, plus three Alphasense Electrochemical gas sensors) with two sensors MA04 and LB04. Following the logical scheme (Figure 14), the sensors were tested in closed room (Figure 15A) for one day (23-24/01/2018); in real conditions on the roof of the ARPAE van equipped with air quality and meteorological instrumentations, located in Marconi St. (Figure 15B) for one day (30-31/01/2018); and in real conditions as long-term measurements in Marconi and Laura Bassi Sts. (Figure 15C and Figure 16) for 13 days (1-14/02/2018). This test should include consideration of stability issues, which, however, would require a longer test time, typically 2-6 months.

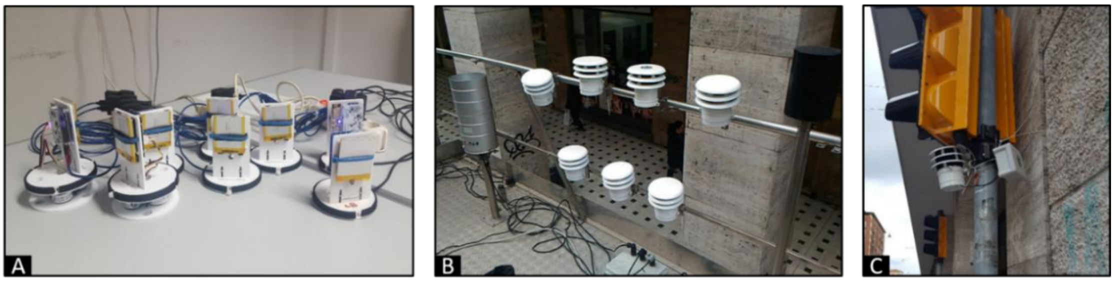

Figure 15. SCKs tests locations: A) in a closed room; B) on the roof of the ARPAE van; C) detail of a sensor during long-term measurements, located near one street intersection.

The LLSs were tested in Bologna, in real world conditions in the Lazzaretto site (6 - 29 /08/2018). The two LLS were installed in different locations (Figure 16), LLS2 was located in a street canyon treated with photocatalytic coating, and LLS3 in a canyon without this treatment.

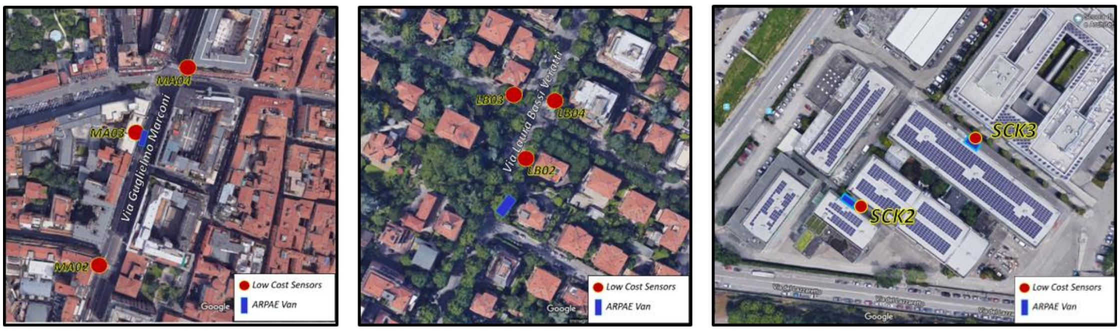

Figure 16. Maps of sensor locations 1) in Marconi St.; 2) in Laura Bassi St.; 3) in Lazzaretto site.

This version measures T, RH, CO, NO_2, O_3, PM_1, $PM_{2.5}$ and PM_{10}. In both Lazzaretto sites, instrumentation for the monitoring of air quality (ARPAE Van: mobile station) and meteorological variables was installed.

3.1.2.2 LCSs evaluation results

During the winter campaign, three tests were performed for SCKs: in a closed environment, and real conditions co-located with a reference measurement instrumentation for short-term and long term measurements.

Closed environment: Repeatability is satisfactory, as the low Standard Deviation (SD) values indicate. The reproducibility is good, in fact the values of the coefficient of determination (R^2) obtained by comparing sensors of the same type with themselves are close to 1. The LOD sensor was supplied by the manufacturer, since in our working conditions the concentrations of gaseous pollutants were always lower than the LOD, it was not possible to evaluate it (Table 1).

Short-term measurements in real conditions: The R^2 values of the same variable from different sensors show a good performance for T, RH and CO, while for NO_2 there are cases where its value is low. R^2 results of a variable against the same variable from a reference instrument (e.g. high-end) indicate a good agreement for T and RH while for gaseous pollutants the agreement is considerably poor. The latter may depend on the low concentrations in the real conditions, well under the sensor's LOD (Table 1).

	Closed Room			**Short-term**					
	R^2	**SD**	**Mean**	**R^2**	**R^2_{Ref}**	**SD**	**SD_{Ref}**	**Mean**	**Mean $_{Ref}$**
T (°C)	0.7 - 1.0	0.3 - 0.5	26.1	0.7 - 1.0	0.7 - 1.0	0.6 - 0.8	0.6	6.5	5.6
RH (%)	0.8 - 1.0	0.5 - 0.9	34.9	0.8 - 1.0	0.7 - 0.9	3.6 - 4.4	7.8	88.5	92.2
CO (mg/m^3)	0.8 - 1.0	0.1	0.9	0.9	0.3 - 0.4	0.1	0.2	0.7	0.8
NO_2 (ug/m^3)	0.9 - 1.0	1.5 - 4.4	44.9	0.3 - 0.9	-0.3 - -0.4	0.7 - 1.2	12.1	19.4	58.3

Long Term	**MARCONI**					**LAURA BASSI**				
	R^2	**SD**	**SD_{Ref}**	**Mean**	**Mean $_{Ref}$**	**R^2**	**SD**	**SD_{Ref}**	**Mean**	**Mean $_{Ref}$**
T (°C)	0.9 - 1	2.1 - 2.9	2.2	9.3	7.7	0.9 - 1	2.6 - 3.0	3.1	7.7	6.3
RH (%)	0.8 - 1	8.7 - 10.8	13.8	70	65.6		10.5 - 13.3	NA	77.6	NA
CO (mg/m^3)	0.3	0.3 - 0.4	0.3	0.9	0.9	0.3 - 0.6	0.2 - 0.8	0.4	1.8	0.8
NO_2 (ug/m^3)	0.2	32.3 - 37.6	26	128	69.6	-0.4	12.3 - 20.3	13.8	125.8	58.1

Table 1. Coefficient of determination (R^2), Standard deviation (SD) and mean of LCSs data collected Closed environment, Short-term measurements in real conditions and Long-term measurements in real conditions. ($_{Ref}$)= refers to the reference instruments.

Long-term measurements in real conditions: The T and RH sensors responded very well as shown by the values of the standard deviation of both LCSs and of the reference instrument. In fact, they are very close to each other with R^2 values close to 1. Results are worse for gas sensors with R^2 rather variable (Table 1).

Figure 17 shows an example of diurnal temporal evolution measured during this campaign: in this case, the higher NO_2 levels measured by SCKs are due to their location (near street intersection). In particular, the SCK MA04 follows the trend of the traffic profile obtained by ARPAE data elaborations, while the SCK MA03 shows peaks around 17:30, which could result from NO_2 accumulation inside the arches (where MA03 is located) during rush hours.

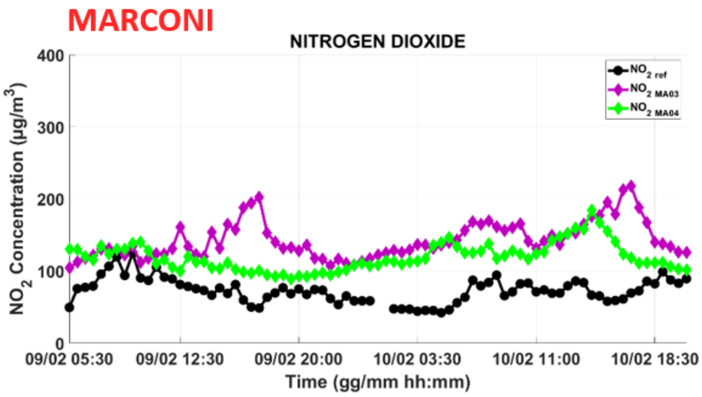

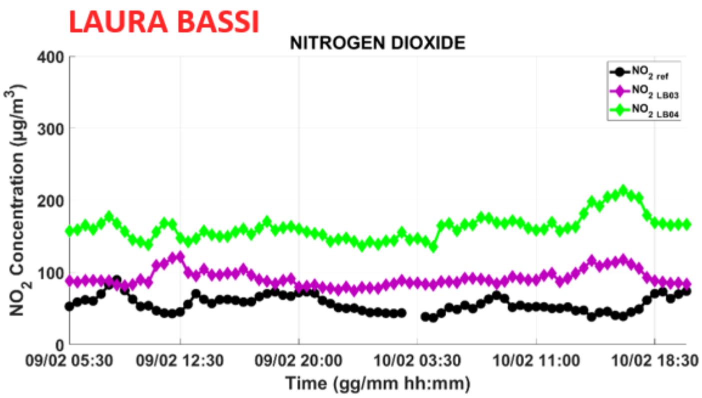

Figure 17. Example of diurnal temporal evolution of NO_2 concentration. 1) SCKs located in Marconi street. ARPAE data (BLACK), MA03 data (VIOLET), MA04(GREEN); 2) SCKs located in Laura Bassi street. ARPAE data (BLACK), LB03 data (VIOLET), LB04 (GREEN).

The LLSs were then tested in real world conditions in the Lazzaretto site, where each LLS was co-located with an ARPAE van equipped with air quality and meteorological instrumentations. The R^2 results of a variable against the same variable from a reference instrument indicate again good agreement only for T and RH, while the agreement is poor for CO and NO_2 gaseous pollutants. The latter results in this case may depend on the temperature dependence of the pollutants measurements. Figure 18 shows an example of diurnal temporal evolution observed during the campaign: in this case, the higher NO_2 levels measured by LLSs correspond to the sunny hours of the day.

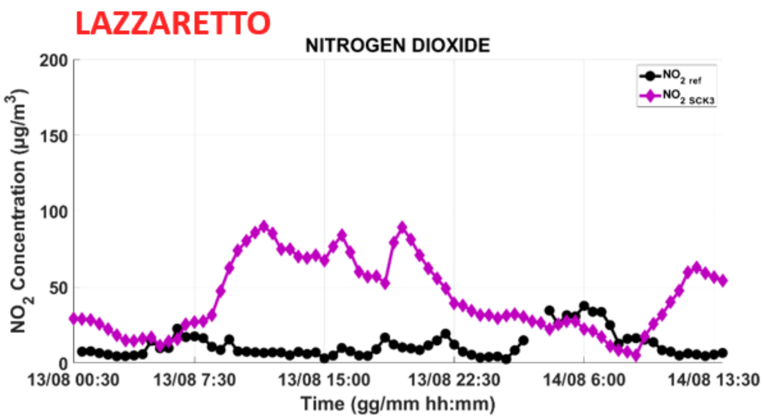

Figure 18. Example of diurnal temporal evolution of NO_2 concentration of the LLSs located in the Lazzaretto site. ARPAE data (BLACK), SCK data (VIOLET).

Figure 19 shows the result of curve fitting with a linear polynomial 1st order model (poly1); although the parameters indicate a bad fit, the figure clearly shows two distinct patterns, as highlighted also in Figure 20. To understand whether air temperature actually influenced the functioning of LLSs, Multi Linear Regression analysis was used (Figure 19). The level of significance obtained ($p<0.001$) shows that indeed T impacted on the concentration measured by the LLSs.

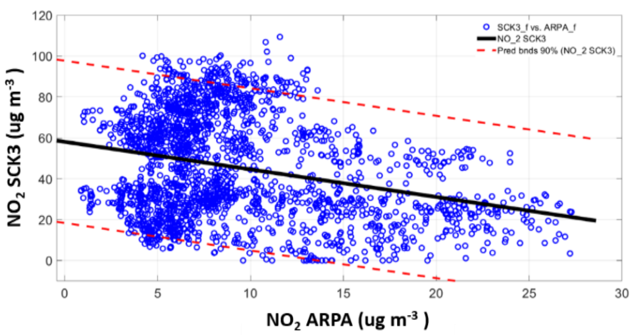

Coefficients (95% confidence bounds):
p1 = -7.188 (-8.237, -6.139)
p2 = 45.49 (44.44, 46.53)

Goodness of fit:
SSE: 1.176e+06
R-square: 0.08181
Adjusted R-square: 0.08136
RMSE: 24.09

	b*	Std.Err.	b	Std.Err.	t	p-value
Intercept			-32.706	3.179	-10.288	0.000
ARPA	-0.202	0.018	-0.947	0.084	-11.212	0.000
T	0.536	0.018	2.937	0.099	29.702	0.000

	Value
Multiple R	0.599
Adjusted R²	0.358
F(2)	563.1
p	0.000
Std.Err. of Estimate	20.0

Figure 19. Curve fitting and table of Linear Regression analysis (MLRA). Top) Curve fitting with linear model poly1: ***f(x) = p1*x + p2*** *where x is normalized with mean value of 9.309 and SD of 5.32. X data=ARPAE data; Y data=LLS data. Bottom) R^2, Multi Linear Regression analysis (MLRA). The Fisher (F) test is used to evaluate the statistical significance of the predictors within the model. With observed p-value<theoretical p-value (0.001), the predictors explain the 36% of the variance of LLS, improving the adaptation.*

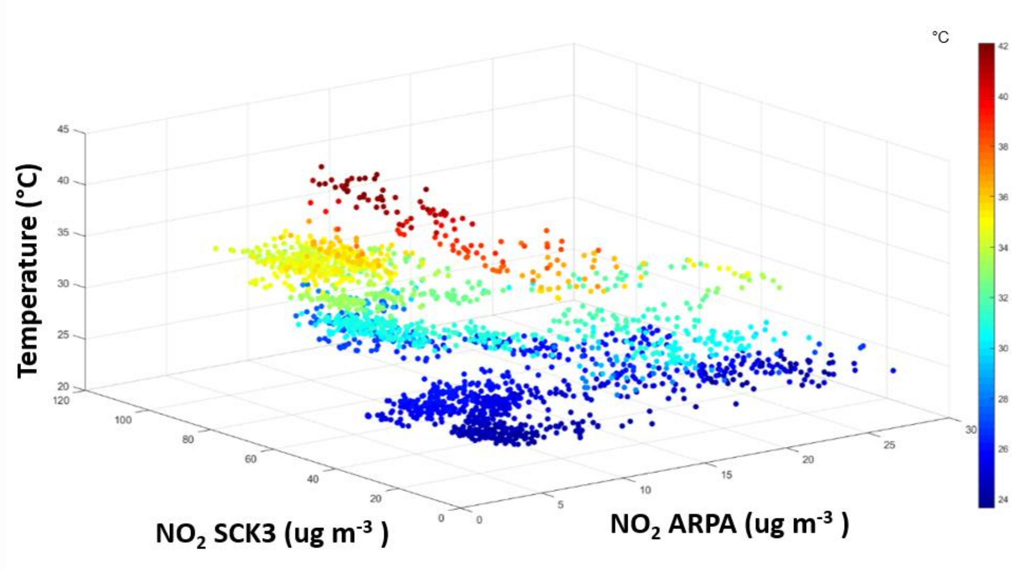

Figure 20. 3D Scatterplot: X data=ARPAE data; Y data=LLS data; colorbar=Temperature.

The results of LLSs tests highlighted that the T and RH sensors have excellent repeatability and reproducibility; in addiction, the comparison with the reference instrumentation indicated that the sensors are reliable in field measurements. Conversely, the R^2 values for CO and NO_2 gaseous pollutants indicated poor agreement, but in the range of those observed by Borrego et al. (2016) and Spinelle et al. (2015), who reported $R^2 < 0.1$ and low (0.20–0.21) R^2 values for NO_2 and CO, respectively.

The LLSs turned out to be better than the SCKs due to different technical aspects (such as humidity resistance and monitoring PM pollution). The LLS were assessed to be reliable for spatial and temporal collection of detailed data of T and RH. Regarding the NO_2 and CO sensors, the teste conducted were still not conclusive, and further investigations on the interaction with the surrounding physical environment are required. However, the preliminary results presented above, show a possible alteration of the measurement due to high air temperatures.

Subsequent evaluations of the performance of the sensors provided indications and advice on the use of LCS for measuring particulate matter, as detailed described in Brattich et al. (2020). Specifically, in this work, the performance of the low-cost sensors was evaluated through a comprehensive and robust approach by considering long-term measurements with a reference instruments. The results indicated that low-cost sensors are affected by significant bias and low correlations when working at high time resolution, while the performance improves when time resolution is reduced to hourly or daily averages. Other biases that impact on the performance of the sensors are mainly related to the prevailing meteorological conditions, suggesting particular caution in their use under high relative humidity, such as rainy and foggy days.

3.2 The iSCAPE simulations

An important part of the iSCAPE project concerned the simulations on the dispersion of pollutants, which were carried out in various cities with different purposes. In particular, in Bologna, the simulations were conducted with the following objectives:

- evaluation of the efficacy of policy options to improve AQ;
- evaluation of the efficacy of PCSs in improving AQ and urban thermal comfort;
- evaluation of the efficacy of greening policies in improving AQ and urban thermal comfort in present and future climate projections.

To these aims, various simulations at different spatial and temporal scales were carried out with different numerical approaches. I took care of the simulations conducted in the city of Bologna, in particular, I focused on the urban scale and used an advanced dispersion model called ADMS (Atmospheric Dispersion Modelling System; CERC, 2017) developed by the Cambridge Environmental Research Consultants (CERC, http://www.cerc.co.uk/). The model is a quasi-Gaussian plume air dispersion model capable of simulating a wide range of passive and buoyant releases to the atmosphere. This model has been already extensively verified within numerous studies and its performance has been compared with other EU and US EPA models, such as CALPUFF and AERMOD for instance (e.g., Carruthers et al., 2000; Di Sabatino et al., 2008; Stocker et al., 2012). Furthermore, the ADMS model includes different modules depending on the scope of the investigation.

Here, the dispersion of pollutants has been simulated with the ADMS-Urban, in which the dispersion calculations are driven by hourly meteorological. The complex terrain module applies a three-dimensional flow and turbulence field to the dispersion modelling calculations. In addition, the ADMS-Temperature and Humidity (ADMS-TH) Module was used to derive the resulting distributions as a perturbation of an existing field and reports the spatial distribution of the temperature and humidity field generated by spatial variations in land use, city morphology and anthropogenic heat emissions with respect to the unperturbed upwind input values (CERC, 2018).

In order to accurately use the models over the study area, a set of input parameters are required: the parameters of the emission sources and their variability over time, the meteorology, the background concentrations and the topography. The following sections will detail the necessary input parameters and how they were obtained.

3.2.1 Domain

The study area includes all sources of urban air pollutants, meteorological stations and the AQ monitoring network, over a domain of 12x19 km. Several cartography data used were downloaded from the geo-portal of the Emilia Romagna Region (http://geoportale.regione.emilia-romagna.it/it), while road network and buildings data were provided by the municipality of Bologna. For road emission sources, the municipality of Bologna provided traffic flows divided into light, heavy vehicles and buses, in a geo-referenced format and displayed as roads. Each road consists of several arcs (links), i.e. road segments in which the traffic flow was counted. Given the presence of many links (about 9000) that constitute the road network of Bologna, roads were divided into major and minor ones. Major roads are a source type, for which traffic emissions are represented explicitly as a line source. Minor road is instead a source type, in which emissions from traffic are not represented explicitly but are combined (aggregated) over one or more grid squares. In order to split the whole graph into major and minor roads, it was assumed that all the arches inside the internal ring road are major roads, while the arches outside the ring road are considered major roads in case the traffic flow was more than 500 vehicles. The remaining arches are treated as minor roads. The main roads are extrapolated from the spatial analysis carried out in the Geographic Information System (GIS) using QGis Desktop 3.2.3 with Grass 7.4.1 (Qgis Project, 2017). The final number of major roads considered in the emission inventory turns out to be 1593 (Figure 21).

The roads outside the ring road, with a traffic flow less than 500 vehicles, were considered as minor roads, i.e. emissions are combined (aggregated) over one or more grid squares. This typology of source is modelled as an area: from the Shapefile of roads (a vector data storage format developed by Esri which stores the location, shape, and attribute of geographic features as a set of related files), the lines are converted in square areas of 1000x1000 meters, so that the road sources become grid sources.

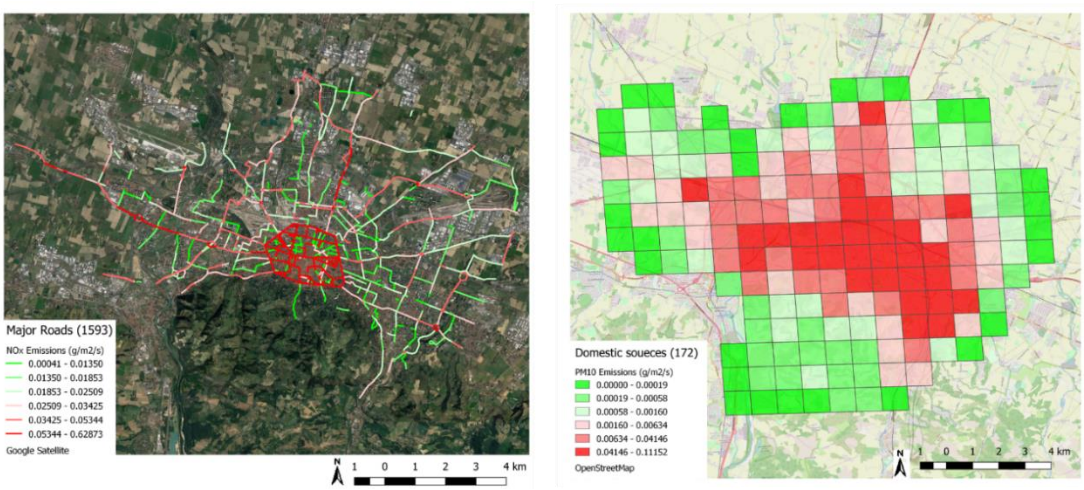

Figure 21. Maps of Bologna emissions. Left) Map of NO_x emissions from road sources ("Major Roads") in Bologna; right) Map of PM_{10} emissions from "Domestic" sources in Bologna. (Google satellite and OpenStreetMap base map provided by QGis).

The emissions from residential heating sources were modelled as grid sources, since it is very difficult to obtain the emission data of each household.

3.2.2 Meteorological data

The IdroMeteoClima Service of ARPAE Emilia-Romagna (Arpae-Simc) carries out operational observational and forecasting activities, supporting planning and research and development, in meteorology, climatology, hydrology, agro-meteorology, radar-meteorology and environmental meteorology (https://www.arpae.it/sim/). The network includes almost a thousand sensors of various types located in over three hundred regional survey sites. The instruments are connected in real time and feed different databases, data are stored in a computerized archive and can be consulted in various ways on the website (https://www.arpae.it/dettaglio_generale.asp?id=2897&idlivello=1625). For instance, observational meteorological network data are available for free through the Dexter system (https://simc.arpae.it/dext3r).

Here, I used the measurements collected at the following Weather Stations (WS, Figure 22) taken into account in the simulations are: 1) Bologna Urbana (BU) and Asinelli (As) stations as urban WSs; 2) Mezzolara (Mz) stations as rural reference WS; 3) San Pietro Capofiume (SPC), Imola (Im), Sasso Marconi (SM) and Padulle-Sala Bolognese (PSB) stations as WSs for boundary condition of Bologna.

In addition, measurements from the synoptic Bologna airport weather station (LIPE, WMO (World Meteorological Organization) number: 16140; Latitude: 44.5308 and Longitude: 11.2969) were also included. In particular, since the Bologna airport weather station is not influenced by the presence of buildings in the city itself, this station was considered the reference meteorological station for the city of Bologna.

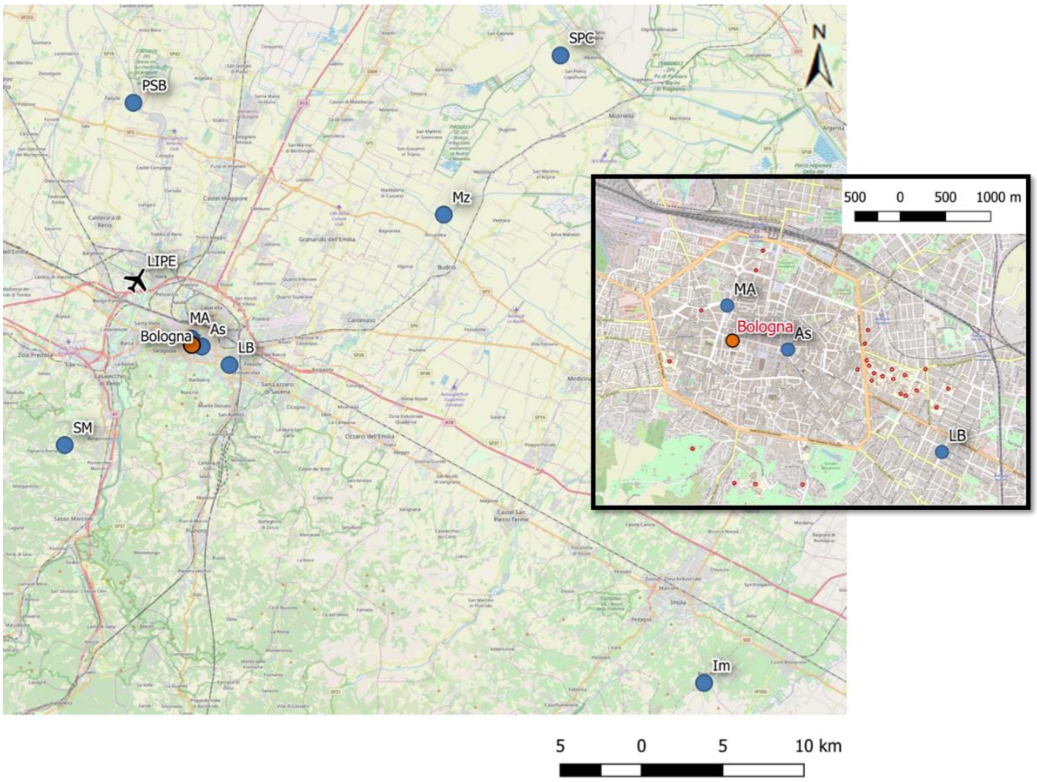

Figure 22. Weather stations (WS) for boundary condition of Bologna: San Pietro Capofiume (SPC), Imola (Im), Sasso Marconi (SM), Padulle-Sala Bolognese (PSB), Reference meteorological WS: Marconi airport (LIPE); rural reference WS: Mezzolara (Mz); urban WSs: Asinelli (As), Marconi mobile station (MA), Laura Bassi mobile station (LB) (source: Own account and OpenStreetMap).

In addition, during the two intensive field campaigns in Bologna (one summer campaign in August-September 2017, one winter campaign in January-February 2018, thoroughly described in 3.1), additional measurements of the main meteorological variables (wind speed and direction, pressure, temperature and relative humidity) collected in Marconi (MA) and Laura Bassi (LB) Sts. by instruments located on the roof of the two ARPAE mobile laboratories were used.

3.2.3 Air quality data

The regional AQ monitoring network of Emilia Romagna region (ARPAE) consists of 47 monitoring stations, with a total of 171 automatic analyzers for the main atmospheric pollutants: particulate matter (in form of PM_{10} and $PM_{2.5}$), nitrogen oxides (NO_x, NO_2 and NO), carbon monoxide (CO), benzene (C_6H_6), sulfur dioxide (SO_2), and ozone (O_3). The network is completed by other sensors of micro pollutants, as well as by 10 mobile laboratories and numerous mobile units for the implementation of evaluation campaigns. Out of the 47 stations belonging to the regional network, 4 are in the agglomeration of Bologna, 18 are in the West Plain area, 20 in the Eastern Plain area, while the remaining 5 are located in the Apennines area. Among the automatic air quality monitoring stations located in the agglomeration of Bologna, 3 are located within its urban agglomeration: Porta San Felice (SF), Via Chiarini (VC) and Giardini Margherita (GM). Table 2 provides information on the position (Figure 23), the type of station and the pollutants measured at the three AQ stations.

Station	Type	Lat	Lon	NO_x	NO_2	CO	O_3	PM_{10}	$PM_{2.5}$
Porta San Felice (SF)	Traffic	44.5000	11.3285	Hourly data	Hourly data	Hourly data		Daily data	Daily data
Via Chiarini (VC)	Suburban background	44.5001	11.2861	Hourly data	Hourly data		Hourly data	Daily data	
Giardini Margherita (GM)	Urban background	44.4836	11.3550		Hourly data		Hourly data	Daily data	Daily data

Table 2. Information on reference monitoring stations in Bologna: type, location (latitude and longitude), measured pollutants with associated time resolution. Empty cell indicates pollutants that are not measured at that station or unavailable data.

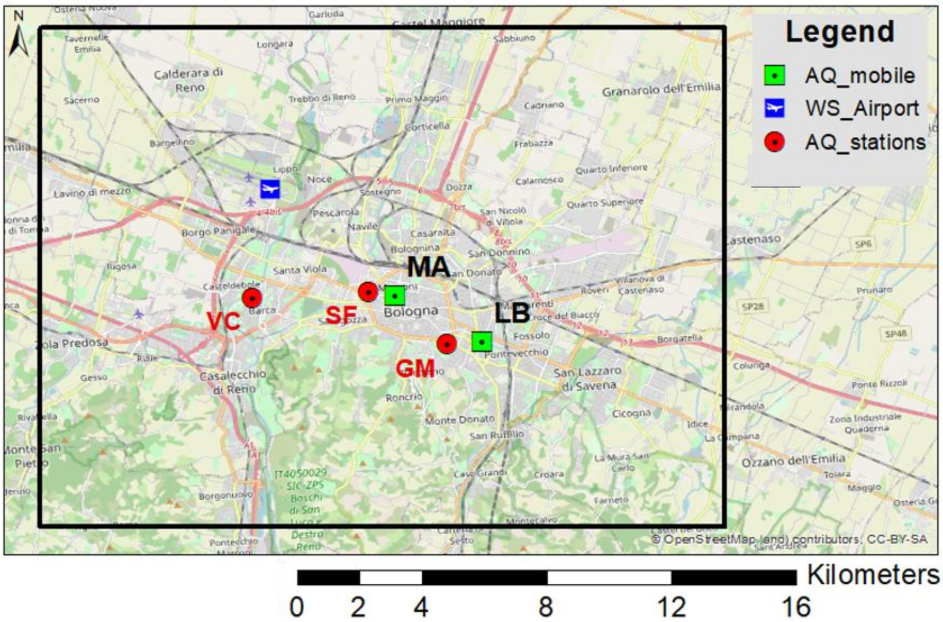

Figure 23. Location of Air Quality (AQ) stations and Weather Stations (WS): AQ stations in red: Porta San Felice (SF), Via Chiarini (VC), Giardini Margherita (GM), AQ mobile laboratories in green: Marconi (MA) and Laura Bassi (LB); and Weather station in blue: LIPE; (map source: OpenStreetMap and contributors).

In addition, during the intensive field campaigns in Bologna (thoroughly described in Section 3.1) hourly (NO_x, PM_{10}, $PM_{2.5}$, CO, O_3 and SO_2) pollutant concentrations were collected in Marconi and Laura Bassi Sts. by the two ARPAE mobile laboratories.

3.2.4 Bologna emission database

An atmospheric emission inventory is a collection of data presenting an emission of a pollutant and related parameters including:

- chemical identity: the chemical properties of the pollutant;
- activity or technology: the cause of the emission;
- location: describes both the location on the map and the height of the emission;
- time dependence: in general, as annual totals.

Bologna is one of the main crossroads between North and South Italy, heavily interested by large-scale transportation infrastructure, and mobility in general, represents the main considerable environmental pressure on the entire metropolitan area. As, the territory is not directly influenced by large-scale industrial facilities, the most important sources of emissions are traffic and domestic heating (Tositti et al., 2014). The compilation and build-up of the emission inventory of Bologna was built through the EMIT (Atmospheric Emissions Inventory Toolkit) tool available from CERC (CERC, 2015), a database tool for storing, manipulating and assessing emissions data from several sources (major roads, rail and industrial sources, minor road, commercial and domestic sources). EMIT allows storing emissions data that have been directly imported, or to calculate emissions from source activity data using emission factors. Alternately, EMIT can calculate emissions using a scaling of national or regional emissions by a local statistic, such as population. The EMIT tool was also developed to estimate the consequences of traffic management schemes such as clean air zones and local emission zones regarding emissions.

EMIT calculates the emissions of local pollutants starting from traffic flows in the roads, considering the emission factors, the fleet components and the route type. The emission factors are a set of data obtained from experimental results that relate emission rates for different pollutants to vehicle subcategories. There are numerous sets of emission factors available for road and rail traffic sources in the EMIT database. EMIT calculates the emissions using its own database containing UK emission factors. Comparing Italian and English fleet composition (fuel type and technology), it was estimated that the fleet for UK are quite likely the Italian one. In the case of Bologna, emission factor data was derived from NAEI (National Atmospheric Emissions Inventory) 2014 datasets. In this dataset the emission factor data are taken from the COPERT 4 model version 10.0 (Karsis et al., 2012) compiled as part of the UK NAEI 2014. Among the emission factors, the non-exhaust emissions, i.e. road traffic particulate emissions emitted due to mechanical abrasion and corrosion, and the re-suspension of material deposited on the road surface by tire shear, vehicle-induced turbulence and wind are very important. In fact, while the improvements in vehicle technologies are constantly decreasing the exhaust emissions, non-exhaust emissions are less controlled and increase with the increase in traffic volumes. Here, non-exhaust emission factors derived using the Tier 2 methodology in the 2009 EMEP[2]/EEA emission inventory guidebook (EEA, 2009) were considered. EMIT calculates the emission rate (the mass flux of a particular pollutant from a specified source, g/s or kg/year) for all sources and allows to directly create the input files for ADMS-Urban.

In the case of road traffic, source specific data needed are as follows:

- Annual Average Daily Traffic count (AADT)
- Fleet components, the breakdown of the AADT into the different fleet components (e.g. heavy vehicles, light vehicles and motorcycles). EMIT supports 3 or 11 fleet components for road traffic;
- Length of road;
- Drive cycle (driving behavior in 'urban', 'rural', and 'motorway' environment leads to differing rates of engine deterioration and thus of emissions).

For road emission sources, the municipality of Bologna provided traffic flows divided into light, heavy vehicles and buses, in a georeferenced format and displayed as roads. EMIT calculates the emission rates using its own database for both minor roads and major roads. The count of vehicles in the roads is used to calculate the emissions and to create the input files for the ADMS-Urban dispersion model.

The emissions from residential heating sources instead are modelled as area sources, in which an emission rate was is assigned to each grid cell scaling groups of sources using the population as a local statistic. The population at the municipal level is spread over the territory based on the resident population spread over cells of 1 km (Figure 21).

3.2.5 Model evaluation

In order to evaluate the performance of the ADMS-Urban dispersion model, predicted pollutant concentrations were compared with hourly data measured at ARPAE AQ stations. Data analysis and comparison of modelling results with observations were carried out using the Model Evaluation Toolkit (CERC, 2015). In particular, the performance of the ADMS-Urban model was evaluated by calculating some basic statistical parameters, (mean and standard deviation), and other indicators with a methodology developed by Hanna (1993) and summarized by Chang and Hanna (2004). Specifically, the following set of indicators, proposed by Carruthers et al. (2000) was considered for the evaluation of the performance of the dispersion model:

- the Normalized Mean Square Error (NMSE), a measure of the mean difference between matched pairs of modelled and observed concentrations

[2] European Monitoring and Evaluation Programme (EMEP)

$$NMSE = \frac{\overline{(C_m - C_o)^2}}{\overline{C_m C_o}}$$

- the Pearson's correlation coefficient (r), a measure of the extent of a linear relationship between the modelled and observed concentrations

$$r = \frac{\sum_{i=1}^{n}(C_{o.i} - \overline{C_o})(C_{m.i} - \overline{C_m})}{\sqrt{\sum_{i=1}^{n}\left(C_{o,i} - \overline{C_o}\right)^2 \sum_{i=1}^{n}\left(C_{m,i} - \overline{C_m}\right)^2}}$$

- the coefficient of determination (R^2), the proportion of the variance in the dependent variable that is predictable from the independent variable(s)

$$R^2 = \frac{\left[\sum_{i=1}^{n}(C_{o.i} - \overline{C_o})(C_{m.i} - \overline{C_m})\right]^2}{\sum_{i=1}^{n}\left(C_{o,i} - \overline{C_o}\right)^2 \sum_{i=1}^{n}\left(C_{m,i} - \overline{C_m}\right)^2}$$

- the Fractional bias (Fb), a measure of the mean difference between the modelled and observed concentrations

$$Fb = \frac{(\overline{C_o} - \overline{C_m})}{0.5(\overline{C_o} + \overline{C_m})}$$

- the Factor of two (Fac2), i.e. the fraction of modelled concentrations within a factor of 2 of observations
  Fac2 = the fraction of data for which $0.5 < C_m/C_o < 2$
- the Mean Bias (MB), the mean difference between the modelled and observed concentrations

$$MB = \overline{(C_m - C_o)}$$

where C_m is modelled concentration and C_o in observed concentration.

The recommended statistical criteria for the NMSE, Fac2 and Fb parameters of an acceptable model, are: NMSE ≤ 1.5, Fac2 ≥ 0.5 and –0.3 ≤ Fb ≤ 0.3 (Di Sabatino et al., 2011) while r and R^2 must tend to 1.

3.3 Summary

iSCAPE (H2020 Research and Innovation programme) focus was the integration and advancement of the control of air quality in European cities in the context of climate change. During the iSCAPE project experimental field campaigns were carried out in different target cities. The Bologna experimental campaigns aimed at creating a baseline on which to evaluate the efficiency of the GI in urban area and using the measurements as inputs for the simulations. Two urban street canyons were identified, sharing similar traffic conditions and emitting sources, but characterized by different presence of vegetation. Within the iSCAPE project, I took care of the acquisition of thermal images and their analysis, the performance evaluation of LCS (SCKs and LLSs) and the urban-scale Bologna simulations.

I processed an acquisition protocol, as well as a post processing methodology for thermal images. The results highlight a UHI effect around 5-7 °C. The UHI effect was different in the two city neighborhoods due to the different presence of trees, the position in the city center and the different building density. This step of my work provided information on the state of the UHI of the city of Bologna, identifying the thermal aspect of the city as a critical one. The problem of citizens' thermal comfort is very much felt during the summer, which is why it has been included in the forecasting tool design.

The LCS performance were assessed in a closed room and in real conditions, in both short term and long term measurements. The test results, for both for SCKs and LLSs, highlighted that the T and RH sensors are reliable in field measurements, while gas sensors indicated poor agreement with reference instrumentation (due to the interaction with the surrounding physical environment). This step of my work aimed to evaluate whether LCS could be used to improve pollutant dispersion simulations, but the results obtained discouraged their inclusion in the forecasting tool.

For the Bologna simulations at the urban scale an advanced dispersion model called ADMS was used. All simulations conducted are detailed in the next chapter.

4 CASES AND SIMULATED SCENARIOS ON BOLOGNA

In this chapter, the simulations conducted on the city of Bologna are presented. In particular, the simulations conducted to test traffic policies and to test greening interventions will be presented, also considering the effect of future climate change. In the case of greening interventions, simulations are also carried out to evaluate the effects of greening on the variation in air temperature. Furthermore, a new methodology is presented to consider the effects of trees on the dispersion of pollutants within the dispersion model. For each case and scenario, the methodology used and the results obtained are described.

4.1 Traffic management policies

This section focuses on the efficacy of policy options to improve air quality at urban scale, considering also possible behavioral changes. One of the main results is the evaluation of the model's performance, obtained from an ad-hoc setting of the model on Bologna. In addition, the efficacy evaluation of policy options was conducted by reconstructing detailed air quality maps using ADMS-Urban dispersion model. The evaluation of the policies implemented was carried out considering the current scenario, i.e., implementing only the policies but with no change in the rest of the setup of the dispersion model (as for meteorology, background concentrations, and emission sources other than traffic). The estimation of the effectiveness of the policies is then evaluated, comparing the results obtained for long-term averages with those obtained in the reference current case (baseline scenario).

The main traffic area in Bologna is the city center (inside the inner ring road) which also corresponds to the main commercial area. In order to improve the air quality, the policies chosen to be implemented and simulated in Bologna act specifically on the composition of the fleet and on certain traffic limitations, and as such also indirectly affect the behavior of citizens. In particular, the policies investigated are:

- Policy 1 "Electric Centre" (2017P1EC): light and heavy vehicles are banned from the internal ring road, and only electric vehicles are allowed in this area.
- Policy 2 "Electric Buses" (2017P2EB): conversion of the bus fleet in Bologna to electric with increase in bus frequency in the center, and all non-electric vehicles are banned from the internal ring road.

4.1.1 The ADMS-Urban model setup

The dispersion of pollutants on Bologna was modeled considering the year 2017 as a base case. The Bologna Emissions inventory created based on traffic flow counts provided by municipality (as described in section 3.2.4). The input meteorological dataset contained hourly sequential data measured by the Bologna airport weather station, considered the reference meteorological station for the city of Bologna not influenced by the presence of buildings in the city itself. The MET file (input file for ADMS-Urban) must contain hourly data of the meteorological variables (temperature (T0C), relative humidity (RHUM), wind speed (U), wind direction (PHI), cloud cover (CL) and solar radiation (SOLAR RAD)) observed at the coordinates that identify the LIPE meteorological station (Bologna airport).

Background pollutant concentrations were obtained from observations at measured at the ARPAE monitoring stations located in the outskirts of Bologna: Via Chiarini (VC), in the western part of Bologna, measuring hourly data for NO_x, NO_2, O_3 and daily data for PM_{10} and Giardini Margherita (GM) in the southern part of Bologna, measuring hourly data for NO_2. Since the legal limit for CO is 0.6 mg/m^3 and the annual average CO is lower than this limit, this pollutant is no longer included in the AQ monitoring for background stations (GM and VC). According to the work of Righi et al. (2009), to model well also the CO emissions, it is necessary to insert its background value, in particular considering that it is affected by a "memory effect" that can be corrected taking into account the concentrations of CO present in the hours immediately preceding the specific time considered in the model. For these reasons, here the concentration referred to the previous hour from the urban traffic Porta San Felice (SF) station, was used as background concentration.

The emissions from air pollution sources are time dependent, so time varying emission factors for road and grid sources need to be considered. The ADMS-Urban model is capable of considering hourly factors for weekdays, Saturdays, and Sundays and monthly factors. In this study, detailed data of hourly factors for weekdays (24 hours), Saturdays (24 hours) and Sundays (24 hours) (i.e. diurnal profiles) and monthly profiles are defined.

4.1.2 The evaluation of ADMS-Urban model performance

The validation of dispersion modeling simulations carried out for Bologna was performed comparing hourly concentrations of pollutants (NO_x, NO_2, O_3, CO, and PM_{10}) observed at the fixed AQ measuring stations (SF, GM and VC stations) with those simulated with the ADMS-Urban model during the 2017 year. In particular, the assessment was made considering pollutant measurements over the whole 2017 year. Figure 24 represent the comparison of daily simulated and observed NO_x and PM_{10} concentrations related to SF station. The modeled data are comparable with those observed, even though the model tends to overestimate simulated concentrations, as highlighted in Figure 25, which shows the NO_x weekly time concentration cycle in San Felice.

However, as from Table 3, statistical parameters for the ADMS simulations are reasonably good. The NMSE, Fac2 and Fb parameters fulfill the recommended statistical criteria (i.e. NMSE ≤ 1.5, Fac2 ≥ 0.5 and –0.3 ≤ Fb ≤ 0.3 (Di Sabatino et al., 2011)).

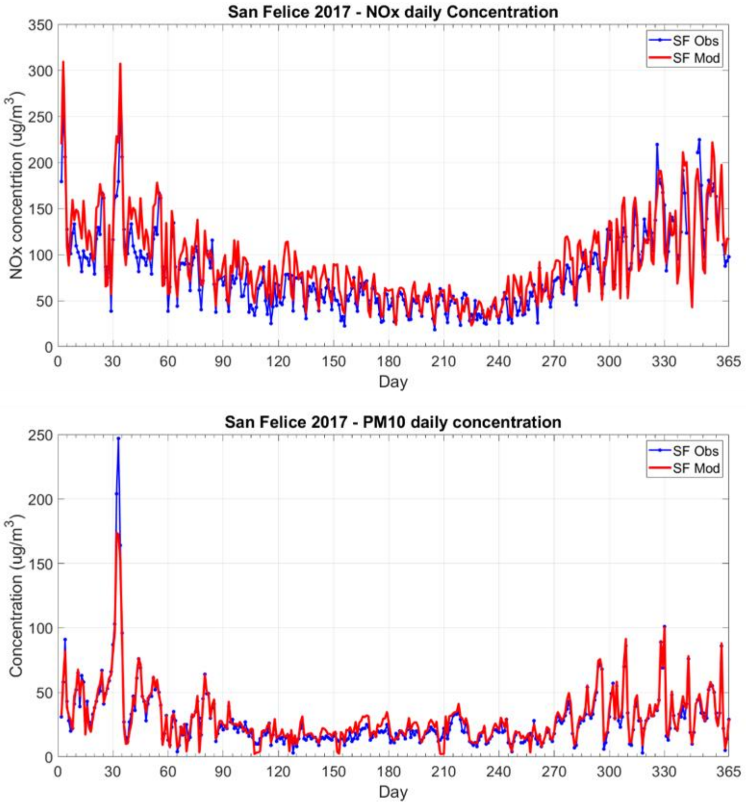

Figure 24. Time series of daily average pollutant concentrations for 2017 at the AQ ARPAE Porta San Felice (SF) station. Top) NO_x concentration and Bottom) PM_{10} concentration. Modeled data (Mod) in red and observed data (Obs) in blue.

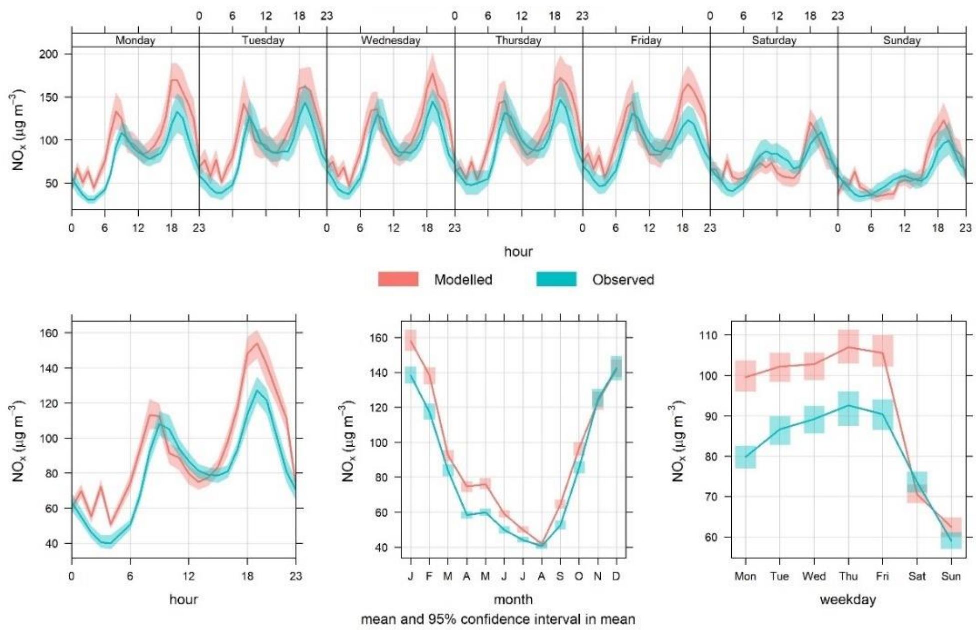

Figure 25. Diurnal, weekly and monthly pattern for NO_x, period:1/01/2017 – 1/01/2018 for the base case simulation as compared to the measured values at Porta San Felice (SF) station.

Station	Pollutant	$Mean_{Obs}$ ± SD	$Mean_{Mod}$ ± SD	MB	NMSE	Fb	R	R^2	Fac2
SF	NO_x	81.8 ± 43.7	91.9 ± 47.4	10.18	0.07	0.12	0.91	0.82	1.00
SF	NO_2	46.1 ± 14.9	43.9 ± 16.7	-2.17	0.05	-0.05	0.82	0.68	0.97
SF	CO	0.7 ± 0.2	0.7 ± 0.2	-0.01	0.00	-0.01	1.00	0.47	1.00
SF	PM_{10}	28.9 ± 24.2	30.3 ± 21.7	1.37	0.05	0.05	0.97	0.94	0.96
GM	NO_2	25.0 ± 16.8	25.6 ± 15.0	0.61	0.02	0.02	0.99	0.96	0.97
GM	O_3	48.0 ± 35.4	44.2 ± 32.2	-3.81	0.02	-0.08	1.00	0.95	0.98
GM	PM_{10}	25.0 ± 23.0	26.4 ± 20.8	1.42	0.06	0.06	0.96	0.93	0.94
VC	NO_x	33.2 ± 28.6	33.3 ± 24.7	0.17	0.04	0.01	0.98	0.99	0.99
VC	NO_2	20.4 ± 10.6	24.9 ± 15.1	4.50	0.11	0.20	0.94	0.89	0.98
VC	O_3	41.2 ± 32.9	42.9 ± 32.9	1.70	0.09	0.04	0.92	0.83	0.88
VC	PM_{10}	27.7 ± 20.4	27.7 ± 20.4	0.01	0.00	0.00	1.00	1.00	1.00

Table 3. Statistical indices calculated to compare the simulated data (mod) of pollutant concentrations with the measured values (obs) in the ARPAE background AQ stations (Porta S. Felice (SF), Giardini Margherita (GM) and Via Chiarini (VC)) in Bologna for the period from 1/01/2017 – 1/01/2018. SD: Standard deviation; MB: mean bias; NMSE: normalized mean square error; R: Pearson's correlation coefficient; Fac2: factor of two; Fb: fractional bias.

Considering SF station (traffic reference station), R^2 correlation coefficients are in the range 0.47-0.94 (for CO and PM_{10}, respectively). The normalized mean square error is low for all pollutants. The values of the fractional bias are very low (0.01 for CO): specifically, the low positive values observed for fb (NO_x and PM_{10} in SF; NO_2 and PM_{10} in GM and all pollutant in VC) indicate a slight overestimation, while the low negative values (NO_2 and CO in SF and O_3 in GM) indicate a slight underestimation.

4.1.3 Base Case Vs Polices

The concentrations of pollutants present large seasonal variations, and these variations are especially consistent between the summer and winter periods. Therefore, two periods were analyzed, i.e. winter (January, February and March 2017) and summer (June July and August 2017) to present the current (baseline) scenario (base case, 2017BC) and the application of the two selected policies (Policy1 and Policy2).

In general, this simulation shows that the center of Bologna is the main pollution hot spot for all pollutants. The comparison of the average values at the receptors (point corresponding to the ARPAE control units, used in the simulations to model the dispersion at that point), highlights how winter represents a critical period (Table 4).

Season	Receptor name	NO_x (µg m^{-3})	NO_2 (µg m^{-3})	CO (mg m^{-3})	O_3 (µg m^{-3})	PM_{10} (µg m^{-3})
Winter	V. Chiarini	64.81	41.44	0.82	24.80	38.79
Winter	Porta S. Felice	166.00	60.55	0.85	18.37	43.15
Winter	Giardini Margherita	66.20	41.83	0.82	24.67	38.87
Summer	V. Chiarini	15.81	12.07	0.47	76.19	19.67
Summer	Porta S. Felice	60.77	30.21	0.48	63.25	21.60
Summer	Giardini Margherita	16.17	12.29	0.47	76.02	19.68

Table 4. Average pollutant concentration values at receptor sites in winter and summer for the 2017BC scenario in Bologna.

The concentration maps in the 2017BC scenario for Bologna are reported below (Figure 26 and Figure 27).

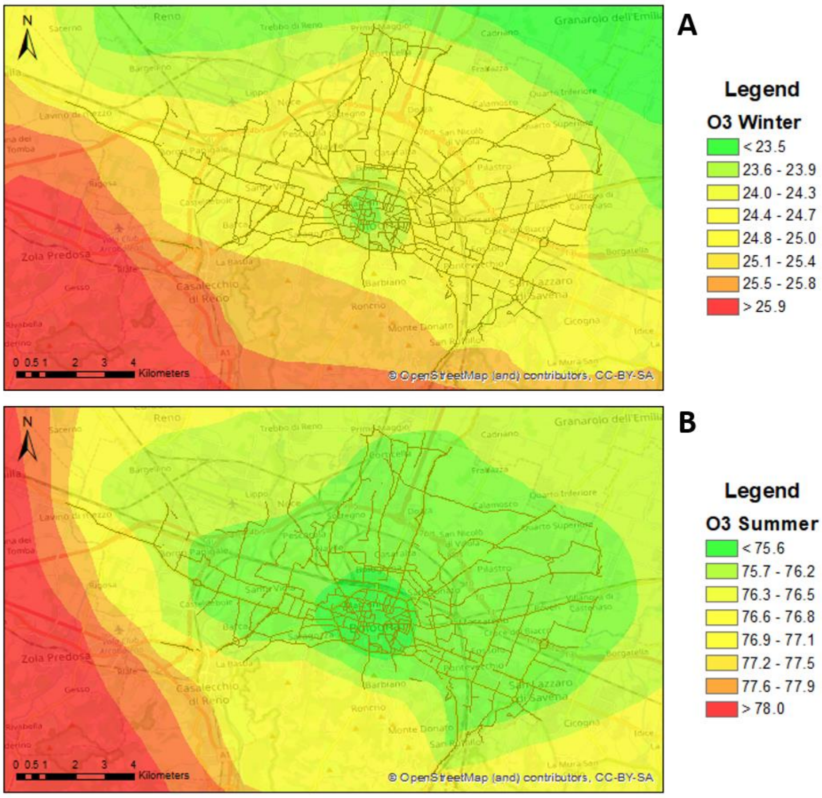

Figure 26. Concentration maps in the 2017BC scenario for Bologna, A) O_3 ($\mu g\ m^{-3}$) in winter and B) O_3 ($\mu g\ m^{-3}$) in summer).

Figure 26 shows the spatial distribution of the O_3 concentration in the 2017BC scenario in winter and summer seasons, governed by atmospheric chemistry. The spatial distribution of the concentration of O_3 shows lower concentrations in trafficked areas than in non-urban areas, as expected.

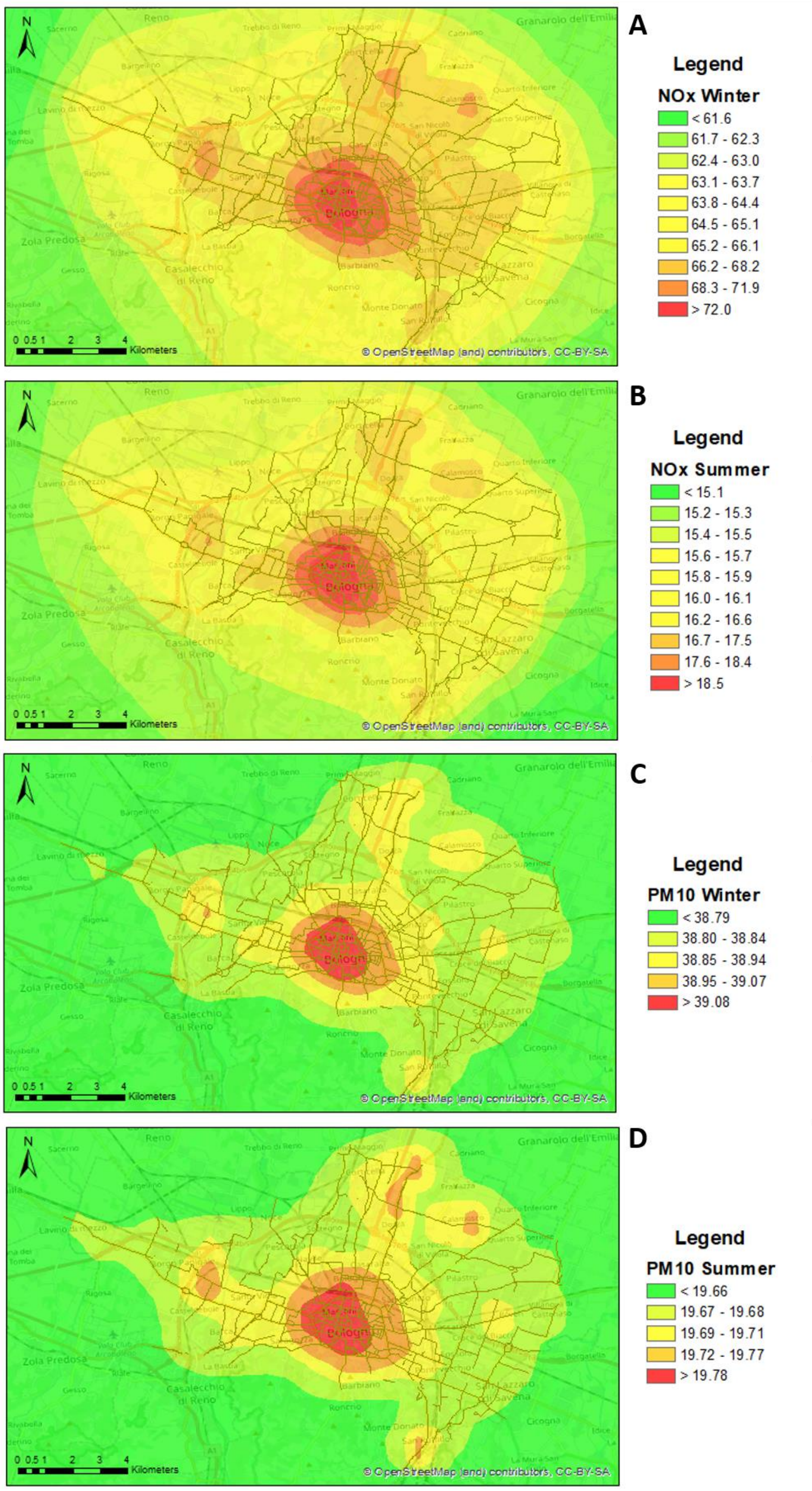

Figure 27. Concentration maps in the 2017BC scenario for Bologna, for: A) NO_x ($\mu g\ m^{-3}$) in winter; B) NO_x ($\mu g\ m^{-3}$) in summer; C) PM_{10} ($\mu g\ m^{-3}$) in winter, D) PM_{10} ($\mu g\ m^{-3}$) in summer.

The spatial distribution of the concentration of air pollutants (Figure 27) in the 2017BC scenario appears similar in the two seasons for both NO_x and PM_{10} concentration, while the simulated concentration ranges are very different in the two seasons, as expected.

4.1.3.1 Policy 1: Electric Centre

The Policy 1 tested on the territory of Bologna is a traffic limitation for the entire area inside the inner ring road: only electric vehicles are allowed to enter and circulate in this area. The comparison of the average values of receptors in Electric Centre scenario (2017P1EC scenario) for the two periods (Table 5), shows that winter is still a critical period. However, the average concentrations are lower than in the 2017BC scenario for all pollutants, except for ozone.

Season	Receptor	NO_x (µg m^{-3})	NO_2 (µg m^{-3})	CO (mg m^{-3})	O_3 (µg m^{-3})	PM_{10} (µg m^{-3})
Winter	VC	64.67	41.37	0.82	24.82	38.78
Winter	SF	65.27	41.47	0.83	24.82	39.26
Winter	GM	64.65	41.29	0.82	24.89	38.80
Summer	VC	15.71	12.01	0.47	76.23	19.66
Summer	SF	15.92	12.10	0.47	76.16	19.86
Summer	GM	15.70	11.98	0.47	76.25	19.67

Table 5. Average concentration values to receptors (Via Chiarini (VC); Porta San Felice (SF) and Giardini Margherita (GM) in winter and summer for 2017P1EC scenario in Bologna.

Considering the winter case, the concentration maps for NO_x and PM_{10} pollutants in 2017P1EC scenario for comparison with the 2017BC scenario, show that the maximum values have decreased compared to the base case, especially for NO_x. Furthermore, the spatial pattern changed (Figure 28), in fact the hot spot located over the center of Bologna is no more present, but it is possible to recognize different less intense hot spots distributed on the territory, near the busiest streets.

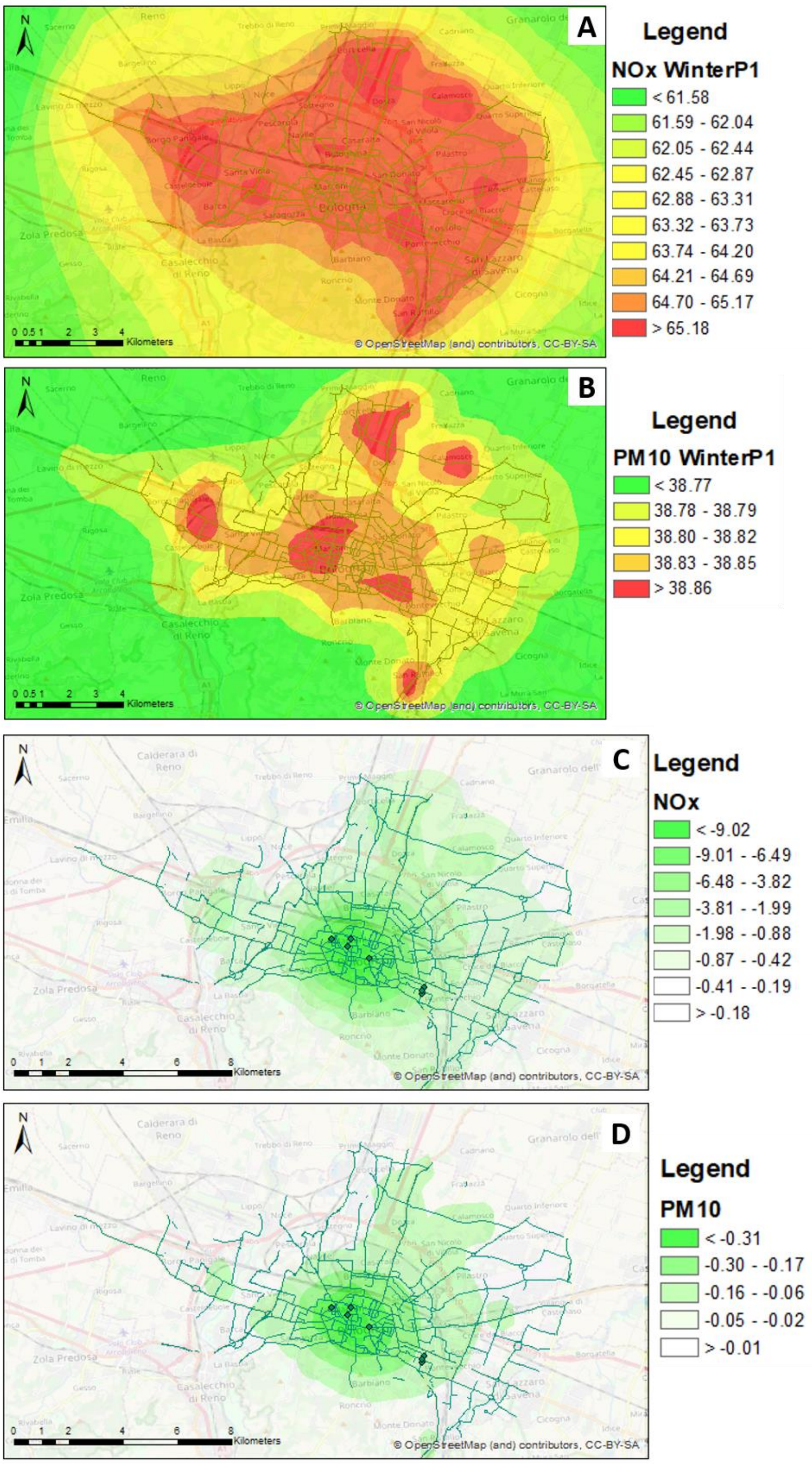

Figure 28. Concentration (μg m^{-3}) maps for the 2017P1EC scenario for winter 2017 in Bologna. The maps represent: A) concentration for NO_x and B) PM_{10}; Maps of concentration differences for C) NO_x and D) PM_{10}. The differences are calculated between 2017P1EC *scenario and 2017BC scenario.*

To highlight more clearly the effect of the policy in terms of increase and decrease in concentrations, maps of concentration differences between the two scenarios are calculated. These maps show a decrease in concentrations over the city center. Therefore, the effect of the policy can be considered satisfactory, as shown by the percentages of reduction/increase in concentration, compared to the base case (Table 7, calculated for all the receptor sites).

4.1.3.2 Policy 2: Electric Buses

The second policy implemented concerns the conversion of the entire urban buses fleet to electric. Furthermore, the city center (the area inside the internal ring road) was affected by an increase in bus frequency and a ban on all non-electric vehicles. The comparison of the average values of receptors in Electric Buses scenario (2017P2EB scenario) for the two periods shows that the winter is still a critical period (Table 6). However, average pollutant concentrations are lower than the 2017BC scenario for all pollutants, with the exception of ozone and PM_{10}.

Season	Receptor	NO_x (μg m^{-3})	NO_2 (μg m^{-3})	CO (mg m^{-3})	O_3 (μg m^{-3})	PM_{10} (μg m^{-3})
Winter	VC	64.77	41.39	0.82	24.79	38.81
Winter	SF	65.80	41.55	0.83	24.74	44.66
Winter	GM	64.74	41.31	0.82	24.87	38.92
Summer	VC	15.77	12.04	0.47	76.20	19.68
Summer	SF	16.14	12.22	0.47	76.04	22.20
Summer	GM	15.75	12.01	0.47	76.22	19.70

Table 6. Average concentration values to receptors (Via Chiarini (VC); Porta San Felice (SF) and Giardini Margherita (GM) in winter and summer for 2017P2EB scenario in Bologna.

Compared to the base case, the Policy 2 also results in a decrease in the maximum pollutant values, especially for NO_x. Regarding the spatial pattern (Figure 29), NO_x concentrations present several hot spots, less intense and distributed throughout the territory, close to the most trafficked roads, while the PM_{10} concentrations still show a hot spot in the center of Bologna. This could be caused by non-exhaust emissions due to increased frequency in electric buses. In fact, the electrification of the fleet though having potential for NO_x and CO abatement, has limited impact on PM_{10} reductions because of the high contribution of non-exhaust which is not reduced by fleet electrification.

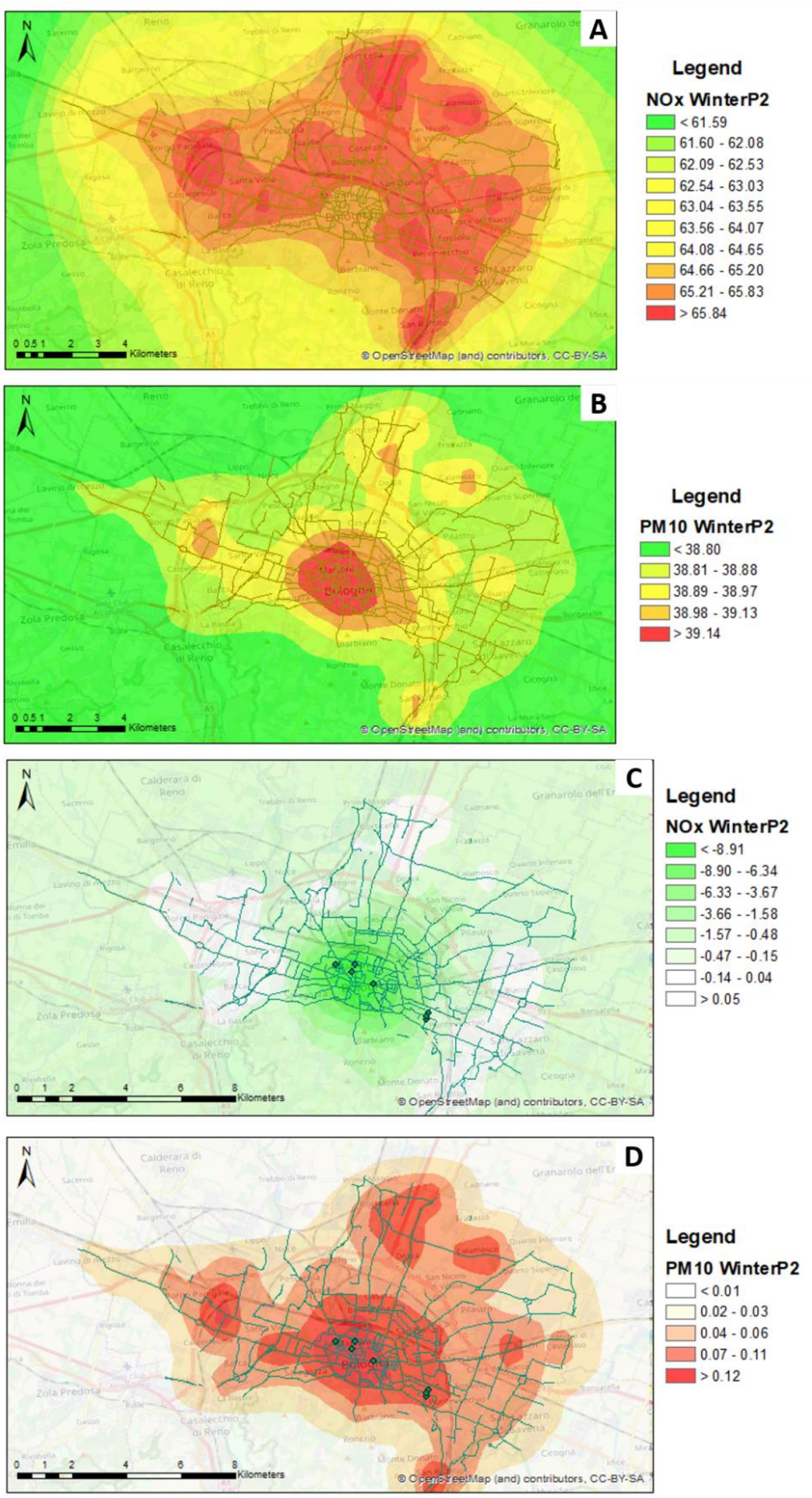

Figure 29. Concentration (µg m^{-3}) maps for the 2017P2EB scenario for winter 2017 in Bologna. The maps represent: concentration for A) NO_x and B) PM_{10}; Maps of concentration differences for C) NO_x and D) PM_{10} (bottom). The differences are calculated between 2017P2EB *scenario and 2017BC scenario.*

The maps of concentration difference between 2017P2EB scenario and 2017BC scenario (Figure 29), highlight a decrease in NO_x concentrations. Also, it can be noted that there is no decrease for PM_{10}, which can be attributed to the non-exhaust emission due to the increased frequency of electric buses. The effect of Policy 2 can thus be considered satisfactory, as shown by the percentages of reduction/increase in concentration compared to the base case (Table 7, calculated for all receptor).

Policy	**Season**	**Receptor**	**NO_x**	**NO_2**	**CO**	**O_3**	**PM_{10}**
1	Winter	VC	0.2%	-0.2%	0.0%	0.1%	0.0%
1	Summer	VC	-1%	-1%	0.0%	0.1%	0.0%
2	Winter	VC	-0.1%	-0.1%	0.0%	0.0%	0.1%
2	Summer	VC	-0.3%	-0.3%	0.0%	0.0%	0.0%
1	Winter	GM	-2%	-1%	-0.1%	1%	-0.2%
1	Summer	GM	-3%	-3%	0.0%	0.3%	-0.1%
2	Winter	GM	-2.2%	-1.2%	-0.1%	0.8%	0.1%
2	Summer	GM	-2.6%	-2.3%	0.0%	0.3%	0.1%
1	Winter	SF	-61%	-32%	-2%	35%	-9%
1	Summer	SF	-74%	-60%	-2%	20%	-8%
2	Winter	SF	-60.4%	-31.4%	-2.3%	34.7%	3.5%
2	Summer	SF	-73.4%	-59.6%	-1.8%	20.2%	2.8%

Table 7. Percentages of reduction/increase in concentration of the Policy 1 and Policy 2 compared to the base case (calculated for all receptor (Via Chiarini (VC); Porta San Felice (SF) and Giardini Margherita (GM)).

The only exception to the improvement are the increases in PM_{10} concentration already found in the map, this increase is greater for the SF station (3.5% in winter and 2.8% in summer) than for the GM and VC stations.

4.2 Passive Control System and infrastructure interventions

This section illustrates the approaches used to evaluate the effects of PCSs on AQ and UHI. The PCSs (such as low boundary walls, avenue trees) are effective passive controls in air pollution (e.g., Abhijith et al., 2017; Buccolieri et al., 2009; Gallagher et al., 2012; Gromke, 2011). In particular, trees may provide air quality benefit through a combination of the deposition and dispersion effects on air pollutants (Abhijith and Kumar, 2019; Janhäll, 2015). The effects caused by the insertion of trees on UHI and AQ were studied at the urban scale in the current scenario and with the possible introduction of PCS, through: (1) a UHI analysis with ADMS-TH model and (2) an AQ analysis with ADMS-Urban model.

In this case, the challenge was to parameterize the PCSs within the ADMS-TH and ADMS-Urban models. In the first case, the inclusion of PCSs in the model was implemented by modifying parameters referred to land use (calculated following an ad-hoc methodology), in the case of ADMS-Urban, the PCSs were considered as a factor that modifies the deposition of pollutants. In addition, the performance evaluation for the ADMS-TH model is presented.

4.2.1 The UHI analysis

To evaluate the effects of PCSs on UHI, the ADMS - Temperature and Humidity (ADMS-TH) Module is used (CERC, 2018). It belongs to the category of models that derives the resulting distributions as a perturbation of an existing field. In particular, ADMS-TH reports the spatial distribution of the temperature and humidity field generated by spatial variations in land use, city morphology and anthropogenic heat emissions with respect to the unperturbed upwind input values. The land use dataset includes the radiative characteristics of the surface, soil moisture and related exchange processes with the adjoin atmosphere, and the friction force generated by the surface asperities on the air motion. This last input is fundamental when dealing with urban environments since ADMS-TH displays the city texture as a morphologically complex obstacle, treated as a variation of the surface roughness, which perturbates the input meteorological conditions. Moreover, the urban environment is also a source of heat due to the thermal forcing of the materials by which the city structures are built, that as a general inclination to behaves as a black body to solar radiation. Last, meteorological data or mesoscale model outputs need to be provided as input to assess the atmospheric patterns which will be considered as upwind conditions with respect to the analyzed domain. The model computes a spatial variation of the temperature and humidity fields resulting in the heat fluxes distribution depending on the adopted land use, and then a distribution of such temperature and humidity fields according to the meteorological input conditions. The model carries out the computation by solving the linearized forms of the heat transfer equations together with the appropriate boundary conditions.

In order to evaluate the effect of PCSs on the UHI, three scenarios are investigated: base case scenario (Bologna without trees) and two scenarios with presence of trees: Marconi St. with trees and Centre with trees. In particular, the modeling of the current base case scenario refers to the days 22 and 23 August 2017, when the summer experimental campaign and the thermographic campaign were carried out.

4.2.1.1 Land use data

The essential parameters that define the land use which the model needs to compute the temperature and humidity fields perturbations are the spatial variation of the surface resistance to evaporation and the surface roughness. In addition, other parameters, such as the surface albedo, the thermal admittance and the normalized building volume, can be specified to enhance the reliability of the simulation (Table 8).

Parameter	Units
Surface resistance to evaporation	s/m
Surface roughness length for momentum transfer	m
Albedo	-
Thermal admittance	$J/m^2 s^{1/2} K$
Normalized building volume (NBV)	m
Perturbation to the net radiation	W/m^2
Perturbation to the ground heat flux	W/m^2

Table 8. Summary of spatially varying parameters that can be entered into the ADMS-TH model.

Land use type used for the analysis is derived from the Local Climate Zone (LCZ) classification adopted by Stewart and Oke (2012). The term LCZ describes regions of uniform surface cover, structure, material and human activity on a defined horizontal spatial scale. Each LCZ has a characteristic temperature regime associated with urban environments, natural biomes and agricultural lands. The classification consists of 17 LCZs, subdivided into built types (1-10) related to structural features of the surface, and land cover types (A-G) accounting for seasonal and ephemeral properties (Stewart and Oke, 2012). A brief description of the LCZs used in the study is reported in Table 9.

	**LCZ 2: Compact Midrise:** Dense mix of midrise buildings (3–9 stories). Few or no trees. Land cover mostly paved. Stone, brick, tile, and concrete construction materials.
	**LCZ 5: Open Midrise:** Open arrangement of midrise buildings (3–9 stories). Abundance of pervious land cover (low plants, scattered trees). Concrete, steel, stone, and glass construction materials.
	**LCZ 6: Open Lowrise:** Open arrangement of low-rise buildings (1–3 stories). Abundance of pervious land cover (low plants, scattered trees). Wood, brick, stone, tile, and concrete construction materials.
	**LCZ 8: Large Lowrise:** Open arrangement of large low-rise buildings (1–3 stories). Few or no trees. Land cover mostly paved. Steel, concrete, metal, and stone construction materials.
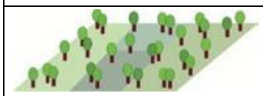	**LCZ B: Scattered Trees:** Lightly wooded landscape of deciduous and/or evergreen trees. Land cover mostly pervious (low plants). Zone function is natural forest, or urban park.
	**LCZ D: Low plants:** Featureless landscape of grass or herbaceous plants/crops. Few or no trees. Zone function is natural grassland, agriculture, or urban park.
	LCZ G: Water: Large, open water bodies such as seas and lakes, or small bodies such as rivers, reservoirs, and lagoons.

Table 9. LCZ classes used to determine the actual domain (source: Stewart and Oke, 2012).

Following this classification, the domain of the model is subdivided among the land use type (Figure 30). In th specific case of Bologna not all the classes are present in the domain. Once the surface types are defined, the first 5 parameters in Table 8 have been computed and provided as input to the model (Figure 31).

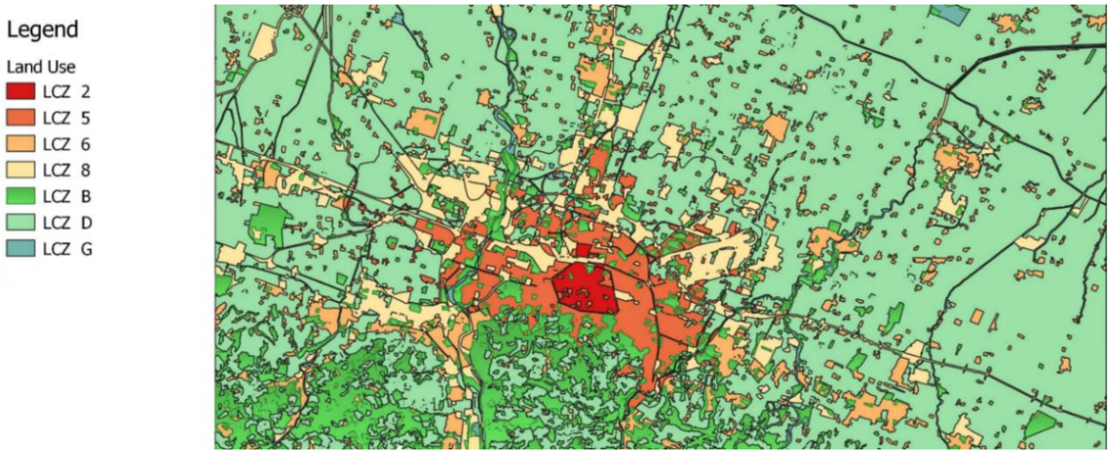

Figure 30. Land use for the simulation domain following LCZ classification.

Surface resistance to evaporation (Figure 31B) assesses the surface capacity to hold its humidity level, it is larger in urban areas, especially in the city center and for densely packaged arrays of buildings where the bare soil is covered by a complex texture of concrete and tarmac. The minimum values can be found in the plain, because bare soil, agriculture and low-risen plants offer a weak resistance to evaporation. The hill chain to the south of Bologna shows an intermediate value between urban and rural environments since the presence of forests inhibits surface evaporation due to the moist entrapment inside the canopy.

The thermal admittance (Figure 31C) determines the efficacy of the surface to absorb and emit heat from and to the atmosphere. It is strongly dependent on the material the soil is made of and it is a good indicator of the surface thermal forcing. It reaches maximum values in the city center and the most urbanized peripheral areas, while it rapidly decreases in the countryside.

Albedo and Normalized Building Volume (NBV) are directly related to the net radiation since they influence the absorbance and scattering features of the surface. Surface albedo (Figure 31D) is a measure of the reflectivity of materials to the incident solar radiation. Generally, materials like concrete and tarmac have low values for albedo, letting the solar radiation been almost all absorbed and emitted at larger wavelength enhancing the urban temperature.

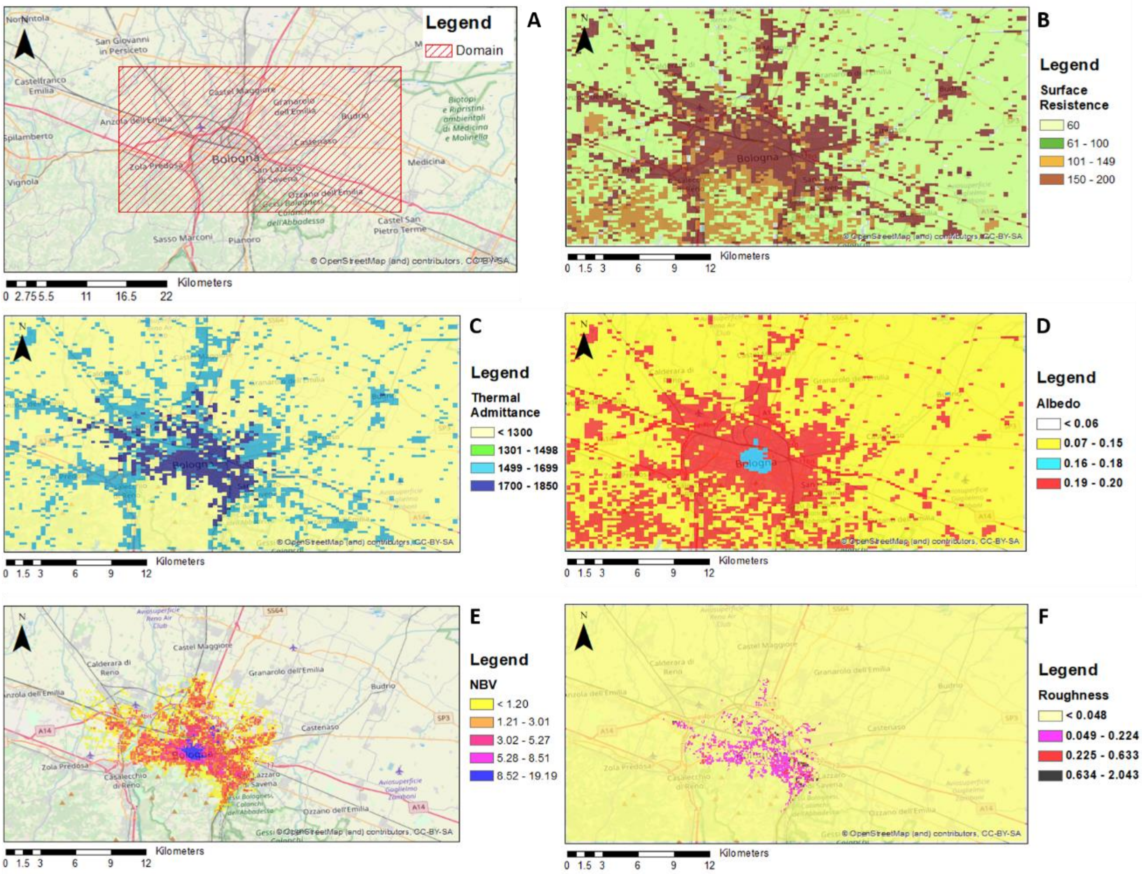

Figure 31. Domain modelling and input parameters. A) Areal view of the spatial domain and maps of the B) surface resistance to evaporation ($^{s}/_{m}$); C) thermal admittance ($^{J}/_{m^2 s^{1/2} K}$); D) surface albedo; E) normalized building volume (m); F) roughness length (m).

NBV (Figure 31E) is an exclusive parameter of the urban environment, describing the volume of built space in every grid cell of the domain. The larger values are located in the city center, the more the distance from the city center is, the less the density of the building packaging will be.

The surface roughness length (Figure 31F) is the parameter responsible for the momentum loss due to the interaction of the atmospheric flows with the obstacles on the surface. Together with the surface resistance to evaporation, it has a direct impact on the flow. The roughness length is computed following the formulation by (MacDonald et al., 1998):

$$\frac{z_0}{H} = \left(1 - \frac{d}{H}\right) exp\left(-\left(0.5\beta \frac{C_D}{k^2}\left(1 - \frac{d}{H}\right)\lambda_f\right)^{-0.5}\right)$$

The larger values are displayed inside the urban environment, together with the larger and more frequent horizontal gradients. In rural areas roughness is more homogeneous, since despite the different cultivation types, cultivated fields offer small friction to atmospheric flows.

4.2.1.2 The ADMS-TH model setup

The spatial domain (Figure 31A) used for the simulation is a 20x40 km box centered on the Metropolitan Area of Bologna. It covers a most extended area than domain used in AQ analysis, including the rural areas around Bologna in order to evaluate the temperature difference between urban and rural areas.

Meteorological data for model input must be provided as unperturbed upwind conditions with respect to the domain, i.e. undisturbed flow conditions approaching the study area retrieved outside the domain (Maggiotto et al., 2014a, 2014b). Therefore, an array of measured meteorological data must be obtained around the simulation domain in order to cover all the possible wind directions. First, observations of wind velocity and directions for whole month of August 2017, were collected from the station at Bologna Airport, located to the north-east with respect to the city but inside the domain and representative of conditions not affected by the presence of buildings in the city. The most suitable stations to describe upwind conditions with respect to the domain were identified from the analysis of wind directions. All meteorological input data were then collected from different stations surrounding the domain depending on wind directions (φ). Specifically, meteorological input data were collected from meteorological stations located in:

- San Pietro Capofiume (SPC) if $20° < \varphi < 90°$;
- Imola (Im) if $90° < \varphi < 180°$;
- Sasso Marconi (SM) if $180° < \varphi < 300°$;
- Padulle-Sala Bolognese (PSB) if $300° < \varphi < 20°$.

Model performance was evaluated by comparing hourly simulated air temperature values with measured ones. This comparison was carried out for three specific sites corresponding to the reference measurement stations of Bologna Urbana (BU), Asinelli (As) and Mezzolara (Mz) (Figure 22). The time series of simulated values and measured data for the whole month of August 2017 at the BU, As and Mz WS (Figure 32) show an overestimation of the model that tends to be larger at the Bologna Urbana site. This overestimation might be attributed to site-specific parameters that do not emerge in albedo maps, thermal admittance, and surface resistance to evaporation.

The statistical indices (Table 10, methodology in section 3.2.5) indicate an overall good agreement between the simulated and observed temperature values, with Fac2 results close to 1. Also, the values of the fractional bias are very low (0.07 in BU station and in the range of 0.06 to 0.08), where the low positive values indicate the tendency of the simulations to a slight overestimation of temperature values. Also, R values close to 1, and R^2 values higher than 0.7 and even larger at BU and Mz stations show the good performance of the model simulations. Finally, the NMSE, Fac2 and Fb parameters fulfill recommended statistical criteria (NMSE $\leq$ 1.5, Fac2 $\geq$ 0.5 and –0.3 $\leq$ Fb $\leq$ 0.3 (Di Sabatino et al., 2011)) at all stations.

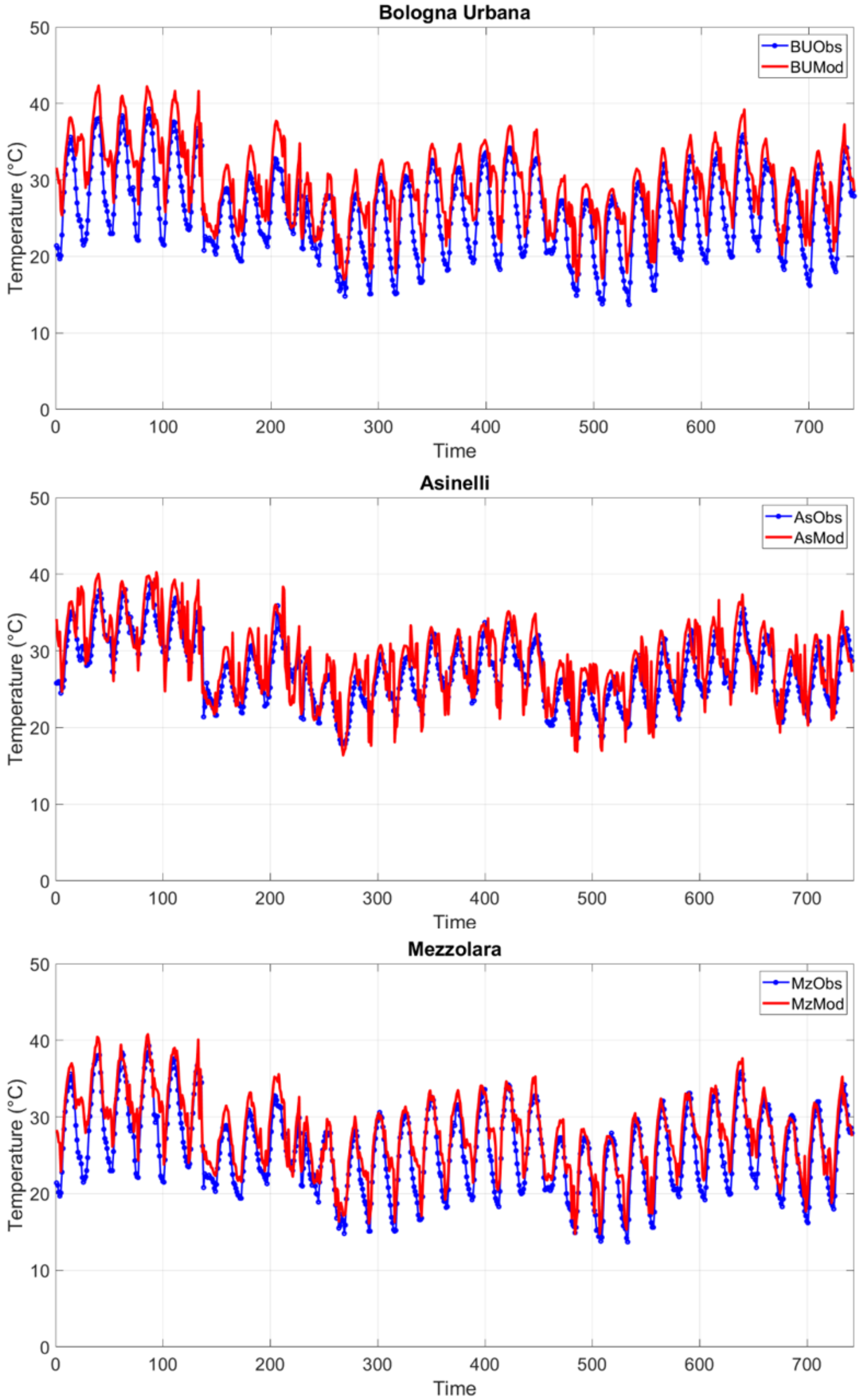

Figure 32. Time series of modelled (red line) and observed (blue dotted line) hourly temperature values for the month of August 2017 (1/08/2017 0:00 – 31/08/2017 23:00) at the Bologna Urbana (BU) (top), Asinelli (As) synoptic meteorological station (middle) and Mezzolara (Mz) rural WS (bottom).

Station	Type	$Mean_{obs}$ + SD	$Mean_{mod}$ + SD	MB	NMSE	R	R^2	Fac2	Fb
BU	Urban	27.4 ± 3.0	29.5 ± 3.2	2.11	0.01	0.99	0.77	1.00	0.07
AS	Urban	27.3 ± 3.1	28.8 ± 3.1	1.56	0.00	0.97	0.70	1.00	0.06
Mz	Rural	25.7 ± 2.6	27.9 ± 3.1	2.18	0.01	0.99	0.84	1.00	0.08

Table 10. Statistical indices calculated to compare the simulated data (mod) of pollutant concentrations with the measured values (obs) in the ARPAE weather stations (Bologna Urbana (BU), Asinelli (As) and Mezzolara (Mz)) in Bologna for the period from 1/08/2017to 31/08/2017. SD: Standard deviation; MB: mean bias; NMSE: normalized mean square error; R: Pearson's correlation coefficient; Fac2: factor of two; Fb: fractional bias.

The center of Bologna has been classified as "Compact Midrise" (from the previously presented LCZ classification: Dense mix of midrise buildings. Few or no trees. Land cover mostly paved. Stone, brick, tile, and concrete construction materials) and the effects that PCSs produce on the UHI effect at city scale were evaluated by modifying the LCZ classes (Figure 33).

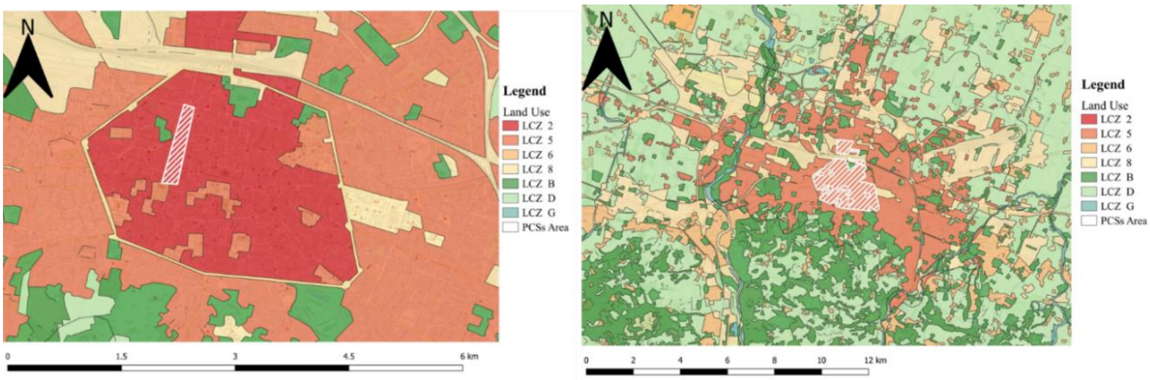

Figure 33. Map of the area affected by the modification of the surface parameter where trees were introduced: left) in Marconi St; right) over the whole Bologna city center.

In particular, two scenarios were simulated:

- Marconi St. with trees: considering Marconi St. as a typical representative street canyon in the Bologna city center (LCZ2), the presence of trees was simulated by modifying the surface parameter of the reference class with that used in the LCZ5 class.
- Centre with trees: the parameter thermal admittance was changed over the whole city center of Bologna.

4.2.1.3 Results

The temperature simulated by the ADMS-TH model provides with an indication of the UHI extension at that time. In this way, it is possible to evaluate the change in the temperature and UHI effect when introducing a variation of land use, which might be consider as an indication of the effect of the introduction of trees in that location. For the period of 22 and 23 August analyzed, the temperature in the case when trees were added in Marconi St. seems to present a similar value as that of the base case, with a reduction during some hours and especially at night and during the first hours of the day (Figure 34).

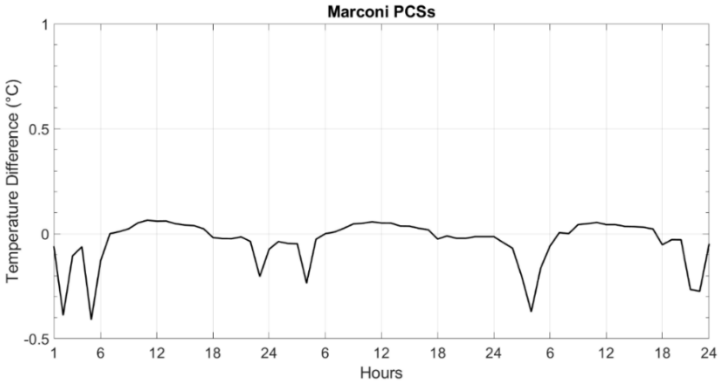

Figure 34. Difference between the temperature before and after the change in land use in Marconi St.

Considering the first hours of the day, for example the 4:00 am on 23 august, the map of differences in temperature shows the temperature reduction (in °C) and shows how the introduction of trees over a small area, i.e. Marconi St. can produce effects over the observed temperature even in the surrounding areas (Figure 35).

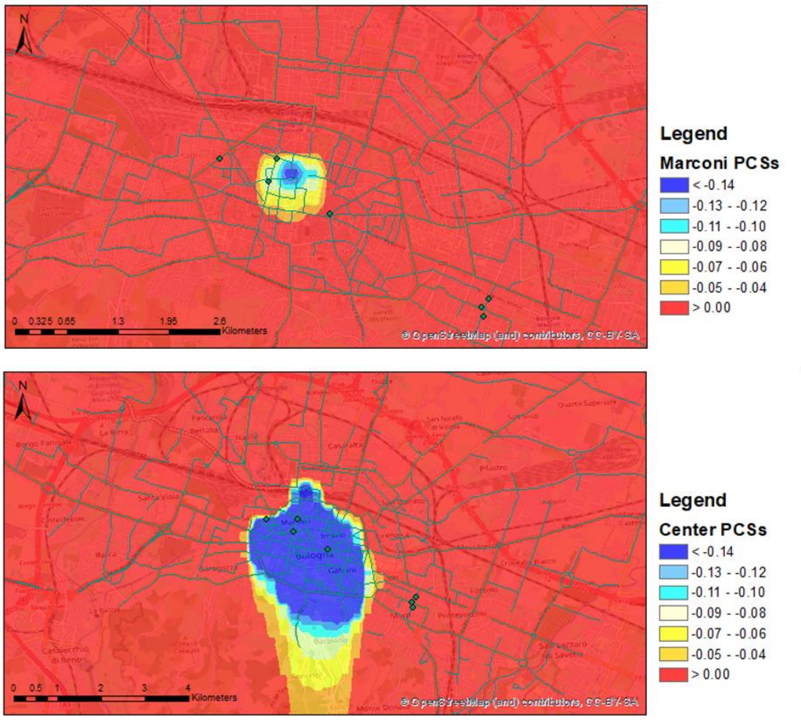

Figure 35. The difference of temperature between the NO PCSs (base case) case and: top) Marconi PCSs (adding trees in the street canyon); bottom) Center PCSs (trees added over the whole city center). The difference is expressed in °C.

In the second scenario (change in land use extended over the whole center of Bologna) the presence of trees induces a temperature reduction over a large area covering the city center and surrounding areas.

4.2.2 The Air Quality analysis

In order to evaluate the effect of PCSs on the AQ, two scenarios were investigated: Urban scenario (base case, Bologna without trees, considering as Urban surfaces the walls) and PCSs scenario (Bologna with trees) where the deposition velocity values were set to consider the presence of trees over 30% of the Bologna area. Similar to what presented in the previous section for UHI effects in Bologna, the modeling of the scenarios was carried out for August.

4.2.2.1 The ADMS-Urban model setup

For the AQ analysis, the ADMS-Urban model was used with the same setup described in section 3.2.1. Briefly, the emission inventory is covering the Bologna area and consisting of traffic sources over a domain of 12x19 km, the year 2017 was selected as a base case. The simulations used hourly measured meteorological data from Marconi airport for the whole domain and the background pollutant concentrations included in the modelling were obtained from the ARPAE monitoring stations, as described in section 4.1.1. The model simulations carried out in Bologna with the ADMS-Urban dispersion model were verified comparing simulated pollutant concentrations with measured values at ARPAE AQ stations for the whole 2017 year, as described in section 3.2.5.

In order to set up the dry deposition it is necessary to set the deposition velocity (V_{dep}) values for each pollutant. This speed varies according to the type of pollutant (gas, particle), the size, the reactivity, and the type of surface on which it is deposited. Zhang et al. (2003) provided the deposition velocity values for the gaseous pollutants deposited over a wide range of surfaces, in particular tabulating the values for urban surfaces and different types of trees. In the model, tabulated values for deciduous broad-leaved, the most widespread in Bologna, were used (Table 11). The PM_{10} deposition velocity values were istead provided in the report of the National Radiological Protection Board (National Radiological Protection Board (NRPB), 2001) was used.

	V_{dep} (m s^{-1}) - Urban	**V_{dep} (m s^{-1}) - Tree**	**Ref.**
NO_2	0.0060	0.0078	Zhang et al., 2003
NO_x	0.0060	0.0078	Zhang et al., 2003
O_3	0.0060	0.0078	Zhang et al., 2003
SO_2	0.0080	0.0101	Zhang et al., 2003
PM_{10}	0.0085	0.0099	NRPB, 2001

Table 11. Deposition velocity values used for Urban scenario and PCSs scenario in Bologna.

4.2.2.2 *Results*

The results are illustrated below with deposition maps of NO_x and PM_{10} for the Urban scenario (base case), while in order to evaluate the effect of PCSs, the scenario with PCSs was compared with the base case through differences maps. In the Urban scenario, the NO_x and PM_{10} deposition maps (Figure 36) show that the spatial deposition pattern follows the spatial concentration pattern so that the deposition is larger in the most trafficked areas. To compare the Urban and PCSs scenarios, maps of deposition difference in the two scenarios were calculated (Figure 37).

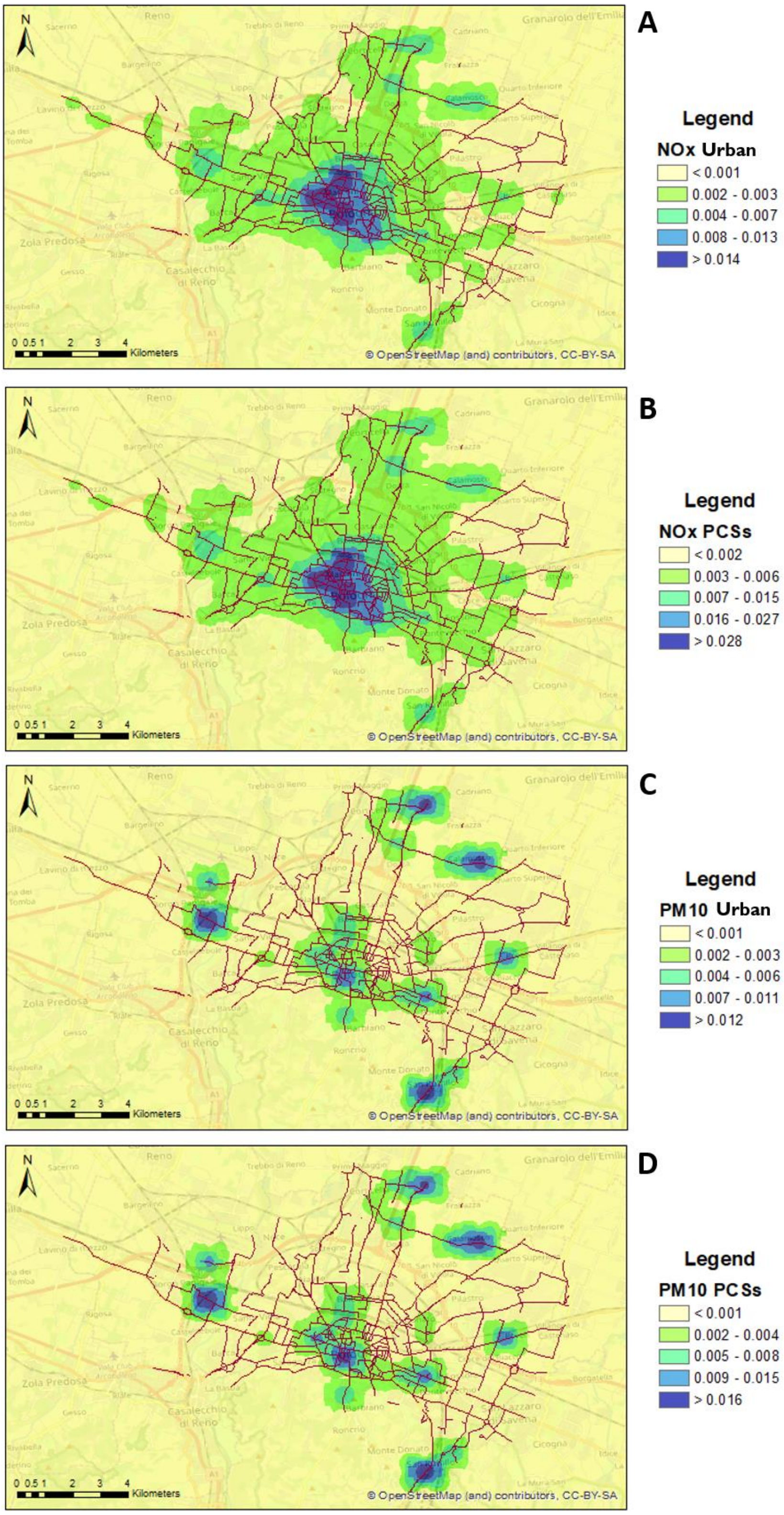

Figure 36. Deposition map (μg/m^2/s) for Bologna: NO_x A) in Urban scenario and B) in PCSs scenario; and PM_{10} D) in Urban scenario and) in PCSs scenario.

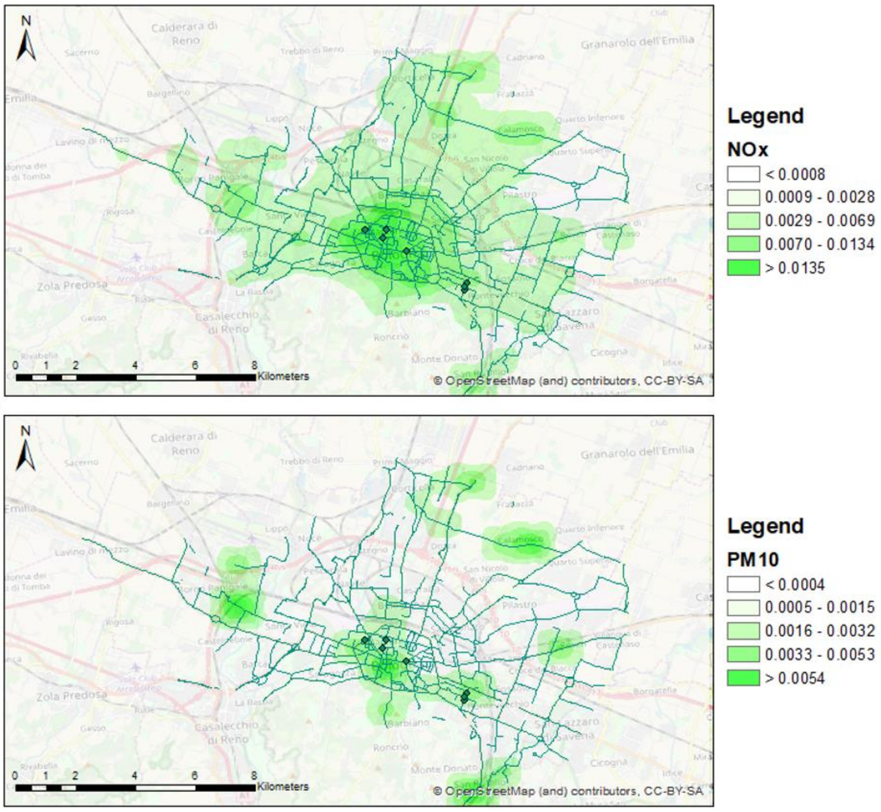

Figure 37. Maps of differences in deposition (µg/m^2/s) between the two scenarios for top) NO_x and bottom) PM_{10}. The differences are calculated between the PCSs scenario and the Base Case Scenario

The maps of difference in deposition show an increase in deposition in the same areas where the deposition is more active. In order to quantify the increase in deposition due to PCSs, a proxy of the reductions in concentrations, the percentage of increase maps (Table 12) was calculated both at the Porta San Felice (SF) receptor located at the urban traffic ARPAE AQ station in Bologna and considering the maximum value of the maps (max Grid).

	Urban (µg m^{-2} s)	**PCSs** (µg m^{-2} s)	**Difference** (µg m^{-2} s)	**Deposition increase** (%)
NO_x (max Grid)	0.014	0.028	0.014	100%
PM_{10} (max Grid)	0.012	0.016	0.004	33%
NO_x (SF)	0.071	0.140	0.966	97%
PM_{10} (SF)	0.111	0.165	0.485	49%

Table 12. Summary of deposition data calculated from the map (max Grid) and at Porta San Felice receptor (SF). NO_x and PM_{10} deposition values for the Urban scenario (Urban) and PCSs scenario (PCSs); deposition differences between PCSs scenario and the Urban scenario, percentage of increase in deposition due to PCSs.

The deposition increases in the case of the PCSs scenario, and the increment is greater for NO_x than for PM_{10}, both considering the point identified by the coordinates of the SF station, and considering the maximum value on the whole map.

4.3 New parametrization for vegetate areas

This section reports the main results of the work carried out to integrate the effects of vegetation in dispersion models, such as ADMS-Urban (Di Nicola et al., 2022, under revision). Compared to section 4.2, where the vegetation effect was considered through deposition, the challenge here was to include also the parameterization of aerodynamic effects. To simulate the effects of the presence of trees at urban scale, a reliable methodology is the Computational Fluid Dynamics (CFD) approach, that completely reconstructs urban geometry within a (generally relatively small) computational domain and solves the system of governing equations. However, CFD approaches work on very reduced spatial and temporal scales and need high calculation costs when modeling the entire city. In the urban scale dispersion models, the exact geometry of vegetation is not the possibility of making explicit, an alternative to this issue is given by the possibility of providing a suitable parameterization of the vegetation that can be included in the dispersion model (Tiwari et al., 2019). For this purpose, a parameterization for vegetation based on aerodynamic parameters (i.e. length of the aerodynamic roughness (z_0), and the displacement in the zero plane (z_d)) is developed, which consider the surface roughness of vegetation spatially-varying in the domain. Only few models include the possibility to specify a surface roughness that takes into account spatial variability (i.e. SIRANE (Soulhac et al., 2011) and ADMS-Urban (CERC, 2017). The ADMS-Urban model performance improvement due to the introduction of spatially varying roughness, calculated starting from aerial LIDAR and cartographic data, was demonstrated (Barnes et al., 2014). In a recent study (Tiwari and Kumar, 2020) have use spatially variable roughness calculated on the basis of the land use of Guildford in the United Kingdom. However, the land use data fails to capture the effect of urban vegetation that is not classified as public green, such as roadside trees or hedges.

The aerodynamic parameters can be derived from morphometric parameters such as: the average height of the building (weighted with the planar area); the maximum height of the building; standard deviation of the building height; the density of the planar area (λ_p); and the density of the frontal area, (λ_f) (Britter and Hanna, 2003). The fundamental morphometric parameters can be retrieved from cartographic data of the territory or LIDAR data, typically, detailed open databases of cartographic data are available in major cities.

In this work a detailed 3D database of buildings and vegetation, it is available from the open data of Bologna municipality. In particular, the database contains aerodynamic information in high spatial resolution, including details such as trees along a road or a hedge around a lawn. The vegetation is included in roughness parameter calculation using the morphometric method (MacDonald et al., 1998), according to the following equations:

$$z_d = \left[1 + \alpha^{-\lambda_p}\left(\lambda_p - 1\right)\right] \cdot z \qquad [4]$$

$$z_0 = \left(\left(1 - \frac{z_d}{z}\right) exp^{\left[-\left(\frac{1}{\kappa^2}0.5\beta C_D\left(1-\frac{z_d}{z}\right)\lambda_f\right)^{-0.5}\right]}\right) \cdot z \qquad [5]$$

where α is z_d correction coefficient equal to 4.43 (MacDonald et al., 1998), λ_p is the plan area index of roughness elements (the area occupied by each building and the projection of the trees crown to the surface, this one it is equal to the area of the circle with a radius equal to half the width of the crown), z is the average height of roughness-elements, κ is von Karman's constant equal to 0.4 (Hogstrom, 1996), β is the drag correction coefficient set equal to 0.55 (MacDonald et al., 1998), C_D is the drag coefficient equal to 1.2, λ_f is the frontal area index of roughness elements of both solid and porous elements. The trees are included considering them as porous bodies (Kent et al., 2017) in the calculation of λf:

$$\lambda_f = \frac{\{A_{fb} + A_{ft}\}}{A_{Tot}} \qquad [6]$$

where A_{fb} is frontal area of buildings, A_{ft} is frontal area of trees, A_{Tot} is the total area under consideration. The frontal area was instead calculated starting from the perimeter of the buildings and trees divided by 4, buildings are approximated to a square shape and then multiplying the value with the height of the building. For the trees, the same criterion using the circumference and height of the crown was used. A good estimator of the porosity of the tree can be the Leaf Area Index (LAI) (Yuan et al., 2017), a dimensionless index defined as the leaf area per unit ground area (m^2 m^{-2}). Thus, the frontal area index of trees is calculated by multiply Aft and LAI, and the equation of λ_f became:

$$\lambda_f = \frac{\{A_{fb} + (A_{ft} \cdot LAI)\}}{A_{Tot}} \qquad [7]$$

The data of the database used are stored in georeferenced files, containing the geographical coordinates, height of each building and tree; the perimeter of the buildings and the circumference of the crown of trees. All calculations are performed in a GIS environment, the affected area is divided into regular cells of 100x100m and the Urban Spatially Varying Roughness (USVR) map is obtained by Equations [4], [5] and [7]. Considering that the data on vegetation (trees and shrubs) were limited (LAI of each species present in the domain was not available, and crown and height values were approximate), I subdivided of the tree population into 4 classes: Deciduous trees, evergreen trees, deciduous shrubs and evergreen shrubs, and we used the LAI values reported in Breuer et al. (2003) (Table 13). In the calculation are included only buildings with a minimum height of 1 m, and trees with a minimum height of 3 m.

The USVR maps created are: 1) BUILD Roughness (BR): calculated using only data of buildings; 2) TREES Roughness in summer (TRS): calculated using data of both buildings and trees for the summer and 3) TREES Roughness in winter (TRW):

calculated using data of both buildings and trees for the winter (i.e. absence of trees foliage for deciduous trees and shrubs).

Tree type	LAI mean	LAI leaf-off	LAI leaf-on
Evergreen tree	6.3	6.3	6.3
Deciduous tree	5.4	3.7	7.1
Evergreen shrub	6.2	6.2	6.2
Deciduous shrub	6.2	2.4	10

Table 13. Leaf Area Index (LAI) values used for evergreen and deciduous trees and shrubs (source: Breuer et al., 2003). Leaf-off refers to the cold winter period and leaf-on refers to the warm summer period.

Numerical simulations are carried out at two different spatial scales, one at the urban scale considering the whole urban area of Bologna and one focusing on two specific neighborhoods of the city characterized by different presence of vegetation and building packing density (Figure 38): Marconi neighborhoods (MA) and Laura Bassi neighborhoods (LB) in the vicinity of two parallel urban street canyons (Marconi and Laura Bassi Sts.).

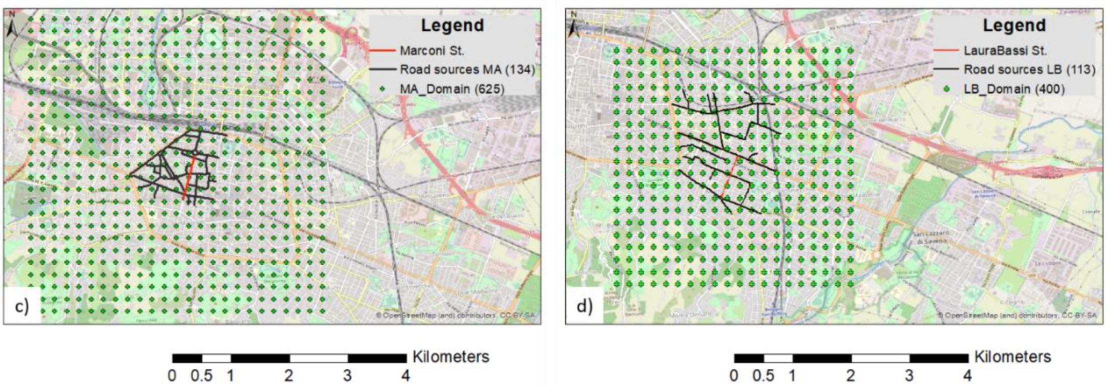

Figure 38. Domain of simulations of the neighborhoods: left) Marconi neighborhoods (MA): 134 links and 625 output points; and right) Laura Bassi neighborhoods (LB): 113 links and 400 output points (map source: OpenStreetMap and contributors).

The choice of the two neighborhoods was based on the different presence of vegetation and well different morphology of the two canyons: in particular, Marconi St. is a tree-free street canyon located in the city center, while Laura Bassi St. is a tree street canyon in a residential area close to the city center.

In the case of urban scale, the emission inventory for the whole urban area of Bologna was used (see 3.2.2). Meteorological input data was obtained from the Bologna Airport synoptic weather station. Hourly background pollutant concentrations were obtained from suburban AQ stations of the ARPAE monitoring network (GM and VC) and the same was used for model evaluation. In neighborhoods scale, the emissions of all main links around the two street canyons are represented explicitly as a line source, while the emissions of all other links are combined (aggregated) over one or more grid squares. In these two cases, the emission inventory contains 134 and 113 links represented explicitly for Marconi and Laura Bassi neighborhood respectively. Hourly background pollutant concentrations and meteorological input data were the same of those used for the simulations conducted for the urban scale case. In order to evaluate the model performance at neighborhoods scale, experimental data from iSCAPE intensive experimental field campaign during the period August-September 2017 (Barbano et al., 2020; Di Sabatino et al., 2020) were used.

Dispersion modeling simulations were performed for different cases (Figure 39), which can be summarized as follows: 1) the Base case (BASE), i.e. the base situation in which only two single roughness values at the meteorological and dispersion sites are specified; 2) Buildings case (BUILD), i.e. the case in which information of urban spatially varying roughness is added considering the presence of buildings over the simulation domain. 3) Trees case (TREES), in which information of USVR is calculated considering the presence of both buildings and trees.

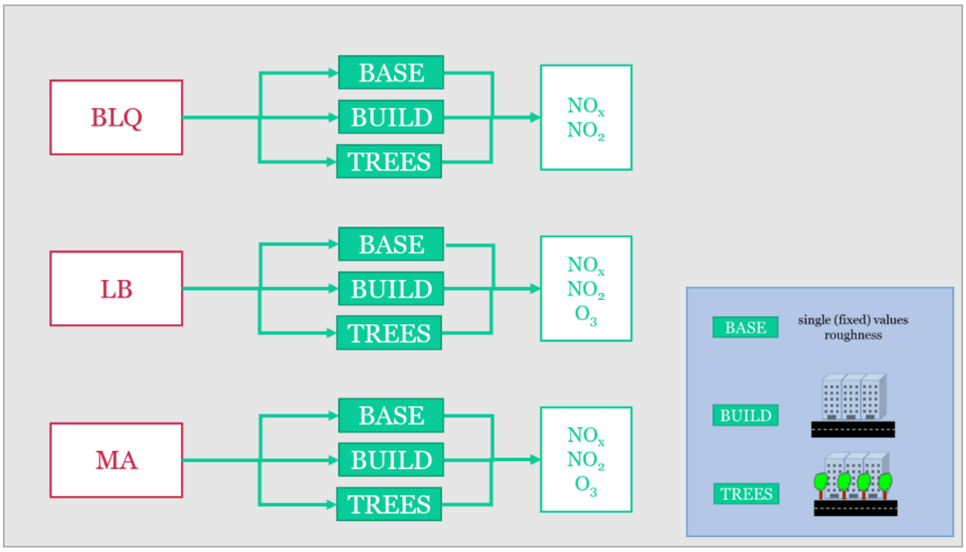

Figure 39. Summary diagram of the simulations by scale (BLQ, LB and MA), case (BASE, BUILD and TREES) and pollutants considered (NO_x, NO_2, and O_3).

The urban scale simulations (BLQ) cover the entire year 2017, while the neighborhood scale simulations cover the periods of the experimental campaigns, in particular spanning the period 10-23 August 2017 for Marconi (MA) and 10 August-23 September 2017 for Laura Bassi (LB). The performance of the ADMS-Urban model was evaluated through the method described in section 3.2.5.

Specifically, simulations conducted at city-wide scale were verified against hourly pollutant concentrations (NO_x and NO_2) observed during the year 2017 at an urban traffic

AQ station located in the city center (Porta San Felice; SF) in Bologna. Conversely, simulations conducted at neighborhood scale in the vicinity of the two urban street canyons were evaluated against data collected by mobile laboratories located along the two street canyons in Bologna (Marconi and Laura Bassi) during the previously mentioned intensive field campaign.

4.3.1 Model evaluation

The model evaluation carried out in the BASE case considering a single fixed value of roughness for dispersion site shows an overestimation of the model's output compared to the observations especially in neighborhood scale simulations (Table 14), as indicated by the fractional bias values. The high values of the Pearson coefficient (0.9 and 0.8 respectively for NO_x and NO_2) obtained for the urban scale simulation (BLQ) indicate the good agreement with the observations.

Sites	Pollutant	Case	NMSE	r	Fac2	Fb
SF	NO_x	BASE	0.1	0.9	0.9	0.3
SF	NO_2	BASE	0.1	0.8	1.0	0.1
MA	NO_x	BASE	0.8	-0.7	0.2	0.8
MA	NO_2	BASE	0.4	0.3	0.7	0.5
LB	NO_x	BASE	0.9	0.5	0.2	0.9
LB	NO_2	BASE	0.7	0.5	0.4	0.7

Table 14. Model evaluation for the simulations conducted on BASE case for urban scale (Bologna (BLQ)at Porta san Felice site (SF)) and both neighborhood scales (Marconi (MA) and Laura Bassi (LB)). Evaluation by comparison with the observations data and calculation of a set of statistical parameters (NMSE= normalized mean square error, r= Pearson correlation coefficient, Fac2=factor of two, Fb= fractional bias).

For neighborhood scale simulations (MA and LB) the statistical parameters indicate a bad performance of the model, with low correlation coefficients. Despite this result, the numerical outputs obtained for the urban scale simulation fulfill the recommended statistical criteria for the NMSE, Fac2 and Fb parameters, specifically NMSE $\leq$ 1.5, Fac2 $\geq$ 0.5 and $-0.3 \leq$ Fb $\leq$ 0.3 (Di Sabatino et al., 2011), Figure 40 clearly shows the overestimation of the model especially in the maximum values.

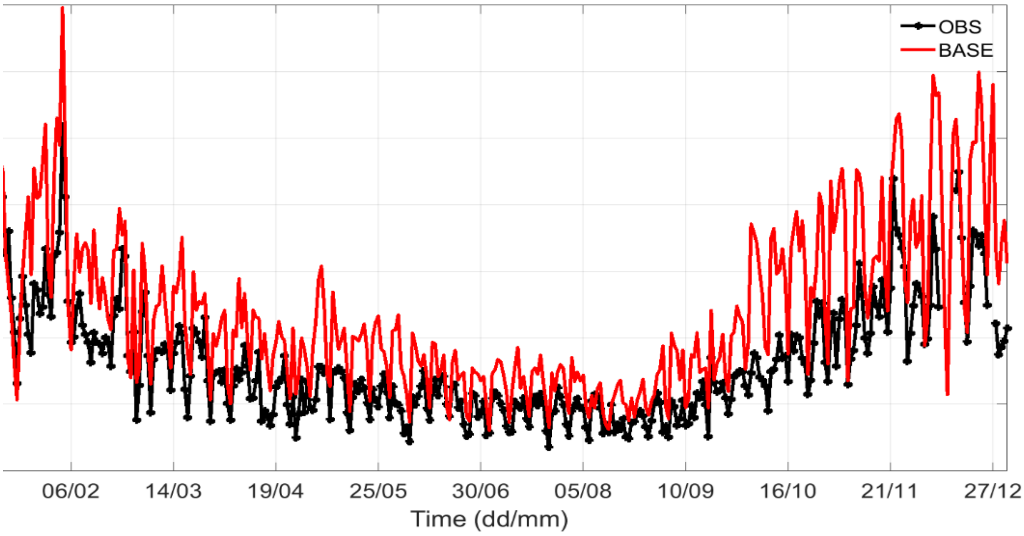

Figure 40. Time series of NO_x daily concentration at Porta San Felice site (SF) for urban scale during 2017. Observed data in black and simulated values for BASE case in red.

Figure 41 shows an example of the spatial distribution of the NO_x concentration simulated by the model, in particular the average distribution for the month of August 2017.

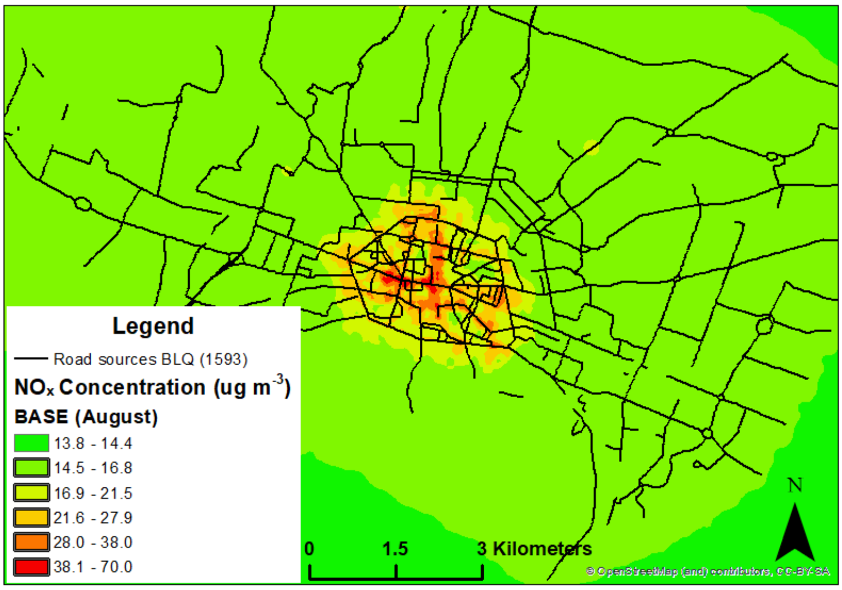

Figure 41. Example of map of NO_x concentration in BASE cases for urban scale (BLQ), reference month: August 2017 (map source: OpenStreetMap and contributors).

On the map, the area with the highest NO_x concentrations coincides with the city center, and some areas with higher concentration corresponding to the busiest streets in the center can be recognized, while lower concentrations are observed in the outskirts of Bologna. Figure 42 and Figure 43 present respectively the time series of NO_x concentrations and maps of NO_x concentrations obtained for MA and LB sites in the BASE case.

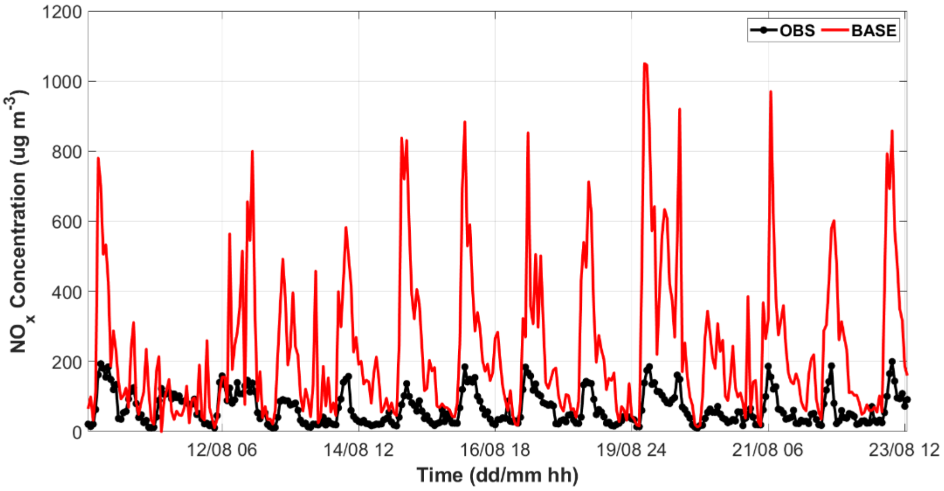

Figure 42. Time series of NO_x concentration at Marconi site (MA) for neighborhood scale. Observed data in black and simulated values for BASE case in red.

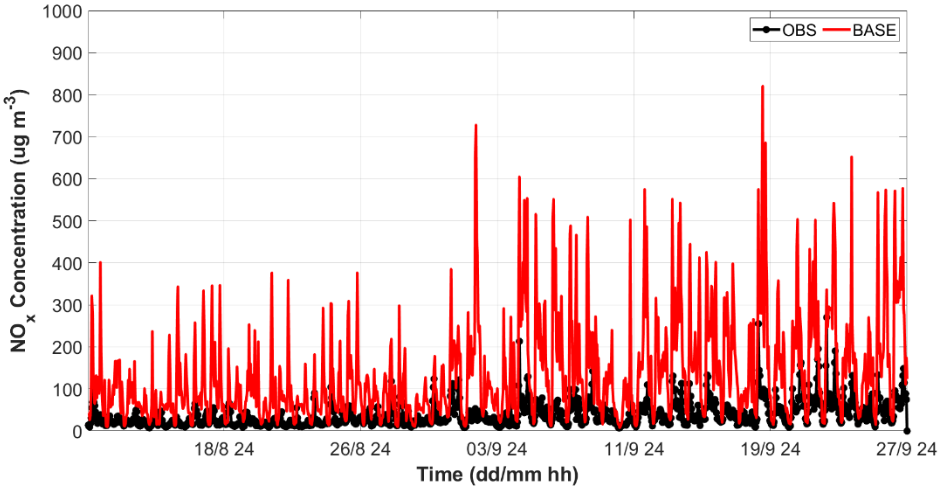

Figure 43. Time series of NO_x concentration at Laura Bassi site (LB) for neighborhood scale. Observed data in black and simulated values for BASE case in red

The results obtained for the BASE case on a neighborhood scale show a greater overestimation of NO_x concentrations compared to the urban scale, as already highlighted by the values of the statistical indices reported in Table 14. The maps in the following show the spatial distribution of the NO_x concentrations simulated by the model in BASE case for the two neighborhoods MA (Figure 44) and LB (Figure 45) sites.

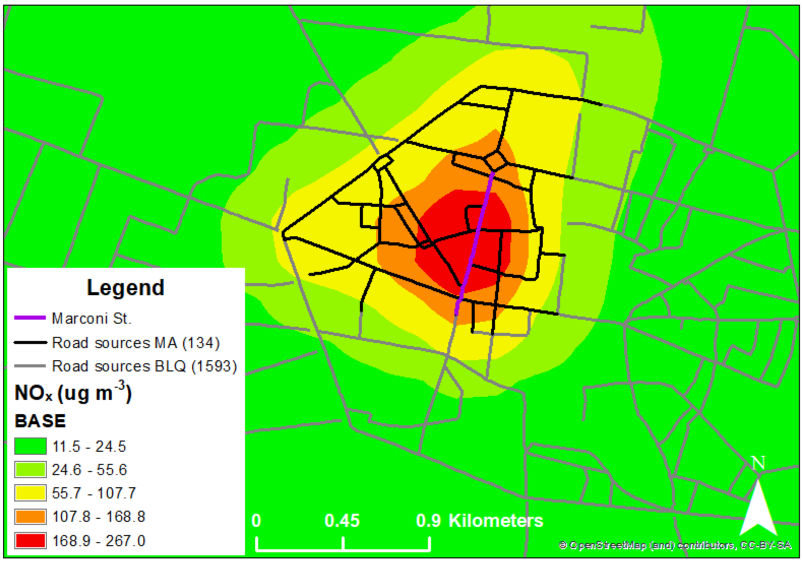

Figure 44. Map of NO_x concentration in BASE cases for neighborhood scale (MA) (map source: OpenStreetMap and contributors).

Figure 45. Map of NO_x concentration in BASE cases for neighborhood scale (LB) (map source: OpenStreetMap and contributors)

The distribution pattern of pollutant concentrations is consistent with the maximum values that coincide with the locations impacted by the highest emission (street canyons and road crossings of higher relevance).

4.3.2 Results

The USVR method proposed in this work for the parameterization of buildings and trees has been applied for the BUILD and TREES cases, respectively with spatial roughness calculated considering only the buildings and considering both buildings and trees. The inclusion of trees in the calculation of spatial roughness on average leads to a decrease in the roughness value, due to the inclusion of trees in the calculation. Indeed, the calculation of the percentage differences between the TREES and BUILD cases shows a decrease reaching 90% (Figure 46a) in summer, and a slightly lower reduction with a maximum value of 86.5% in winter (Figure 46b). The seasonal effect due to the presence of foliage on deciduous trees during summer cause a difference between the roughness value in the two seasons not exceeding 1% (Figure 46c). In particular, the percentage variations in the USVR around the AQ stations in the three sites are respectively: SF= -14% (BUILD = 5.7 m; TREES = 4.9 m); MA= -5% (BUILD = 4.2 m; TREES = 4.0 m) and LB= -39% (BUILD = 6.7 m; TREES = 4.1 m).

In computational terms, the USVR method involves an increase in the run time, a relevant aspect to take into account in the simulations planning, especially when considering the urban scale. Indeed, the time required to perform a short term run switches from 2 hours and 24 minutes in the BASE case to 61 hours and 36 minutes in the BUILD case for the BLQ simulations. At neighborhood scale, where the sources considered are much smaller and the simulated period is short, the required run time is far less than that needed to perform the simulation at urban scale. However, also in this case the insertion of the roughness information increases considerably the run time (1 minute for the BASE case vs. 22 hours and 33 minutes for the BUILD case).

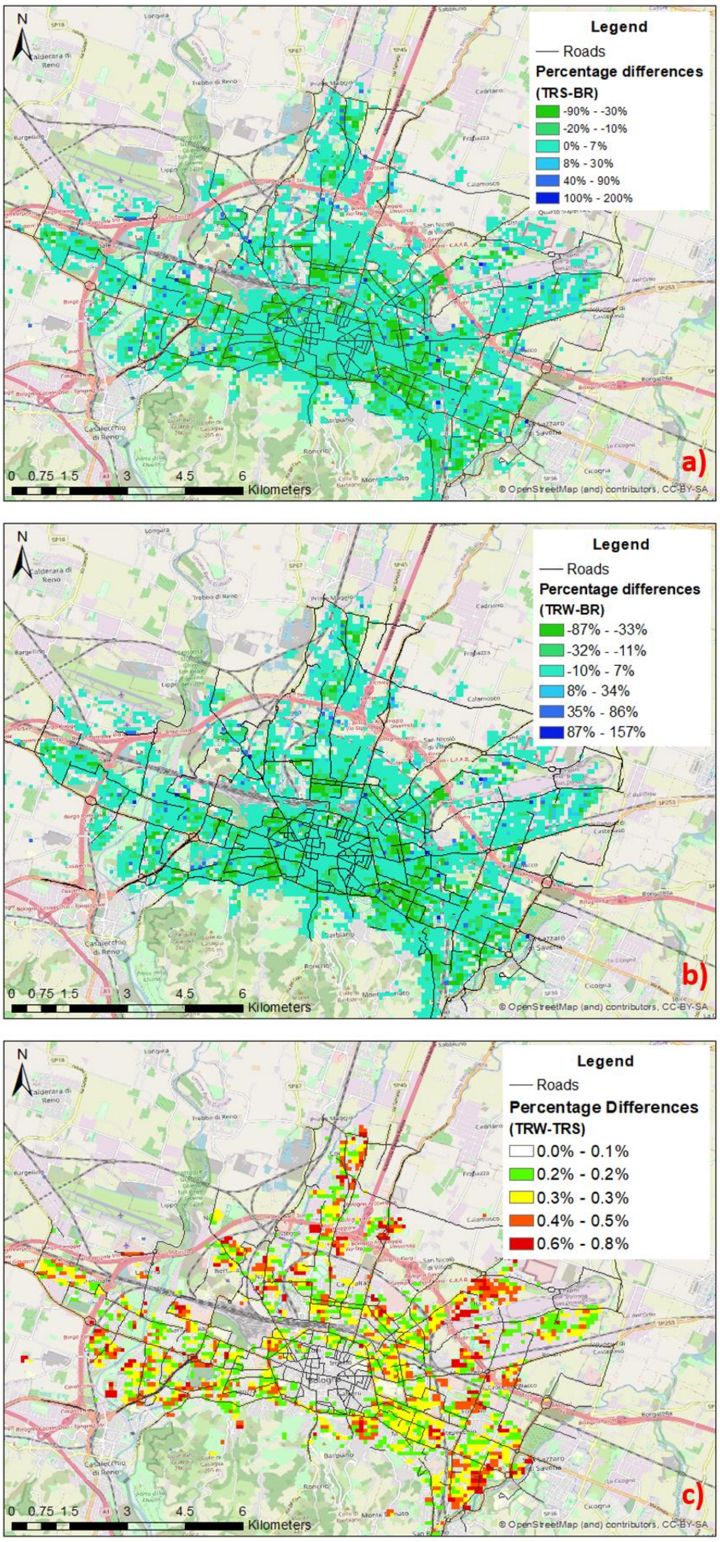

Figure 46. map of the percentage differences of roughness. a) between TREES roughness in summer (TRS) and BUILD roughness (BR); b) between TREES roughness in winter (TRW) and BUILD roughness (BR); between TREES roughness in winter (TRW) and TREES roughness in summer (TRS) (map source: OpenStreetMap and contributors).

At the urban scale, the comparison of simulated and observed time series (Figure 47a) shows the better agreement of numerical values obtained in this case with respect to the BASE case, without the tendency for the model to overestimate the maximum values. This observation is confirmed from Figure 47b which reports the diurnal cycle for the observed and simulated concentrations in the BASE and BUILD cases, which highlights that the maximum values during the day are much closer to the observations when the information on roughness from the buildings is inserted in the simulation.

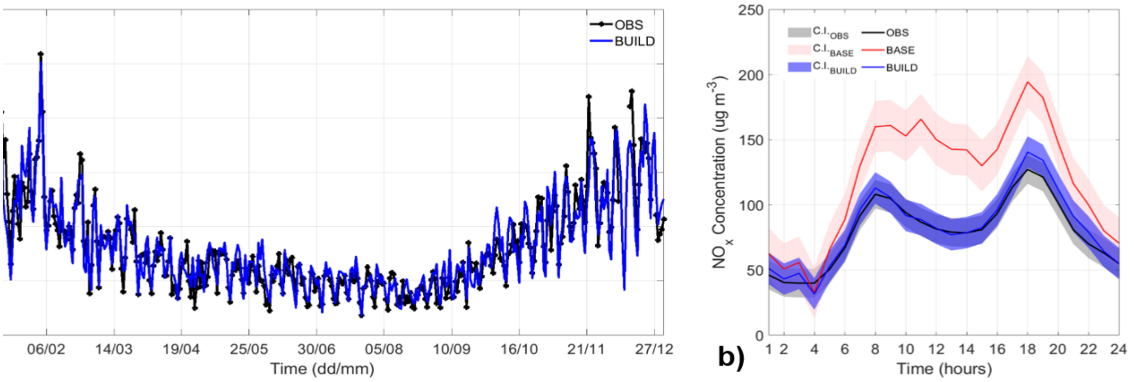

Figure 47. NO_x daily concentration in Porta San Felice (SF) site for urban scale during 2017. Observed data in black, simulated values for Base case in red and simulated values for BUILD case in blue. a) Time series and b) Mean diurnal temporal variations, the shaded area shows the 95 % confidence interval (C.I.) around the mean.

The percentage difference between the simulated concentrations in BUILD and BASE case is -24% at SF site. When considering the spatial distribution of the concentrations we observe that the percentage difference increases locally in some areas, for example it reaches -65% in the city center for the month of August (Figure 48). Considering the minimal differences between the winter and summer, I chose to examine the results in the summer period when foliage is present on trees and when observations from the intensive experimental campaign in Bologna were available. In particular, August was chosen as the representative month for the summer period of 2017 because of its meteorological characteristics and because of the availability of the observations from the intensive field campaign in the two street canyons (see 3.2.1). The percentage differences indicate a decrease in concentration due to the aerodynamic effect of the buildings included in the model through the USVR. Furthermore, the combined effect with wind direction and speed, such as ventilation paths and stagnation areas, must be considered. Some areas of the city can be identified as turbulence producing areas, with a higher dispersion capacity and therefore lower pollutant concentrations, while other areas show an increase in concentration. These differences with respect to the BASE case are attributable to the USVR use that identifies roughness heterogeneity in the domain.

Even at the neighborhood scale, the comparison of the simulated and observed time series (Figure 49) shows a better agreement between observations and the numerical values obtained in this case with respect to the BASE case at both neighborhoods. As the diurnal cycle for the observed and simulated concentrations in the BASE and BUILD cases also shows, the model no longer tends to overestimate, as indicated by the reduced bias between simulated and observed peak concentrations when information on the roughness of the buildings is inserted in the simulation.

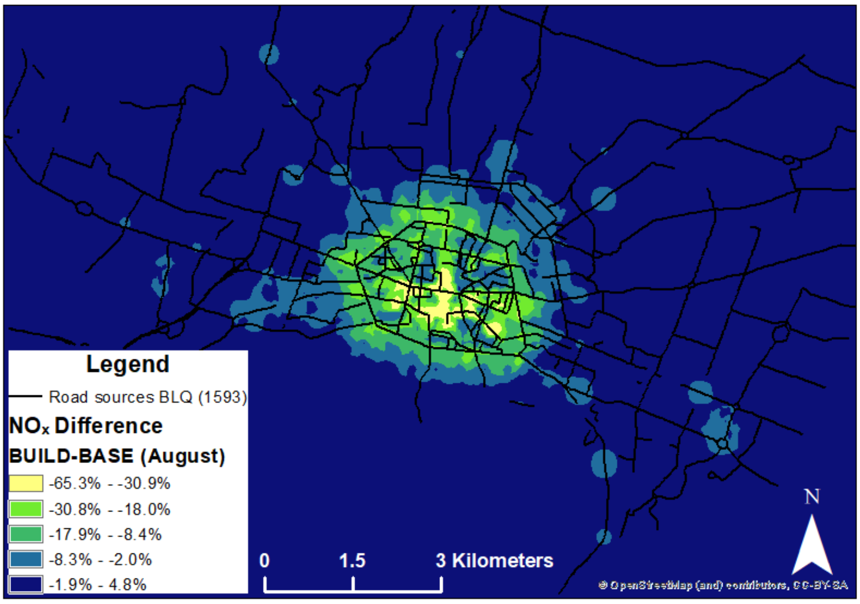

Figure 48. Example of map of NO_x concentration difference between BUILD and BASE cases for urban scale (BLQ), reference month: August (map source: OpenStreetMap and contributors).

For the Marconi site, the percentage difference between the simulated concentrations in the BUILD and BASE case is -69%, while the map of the percentage difference shows that in the neighborhood considered the percentage difference reaches a maximum of -60% (Figure 50a). The percentage resulting in the MA site does not appear in the map due to the spatial average carried out at the output resolution level. Furthermore, the distribution pattern indicates that the considered area is characterized by the presence of highly packaged buildings. In Laura Bassi site, the percentage difference between the simulated concentrations in the BUILD and BASE case also is -69%, and the map of the percentage difference shows a maximum of -82% (Figure 50b). In this case the spatial distribution pattern is clearly related with a different conformation of the district with low and distant buildings, as can be observed by the fact that the variation is visible at the street level.

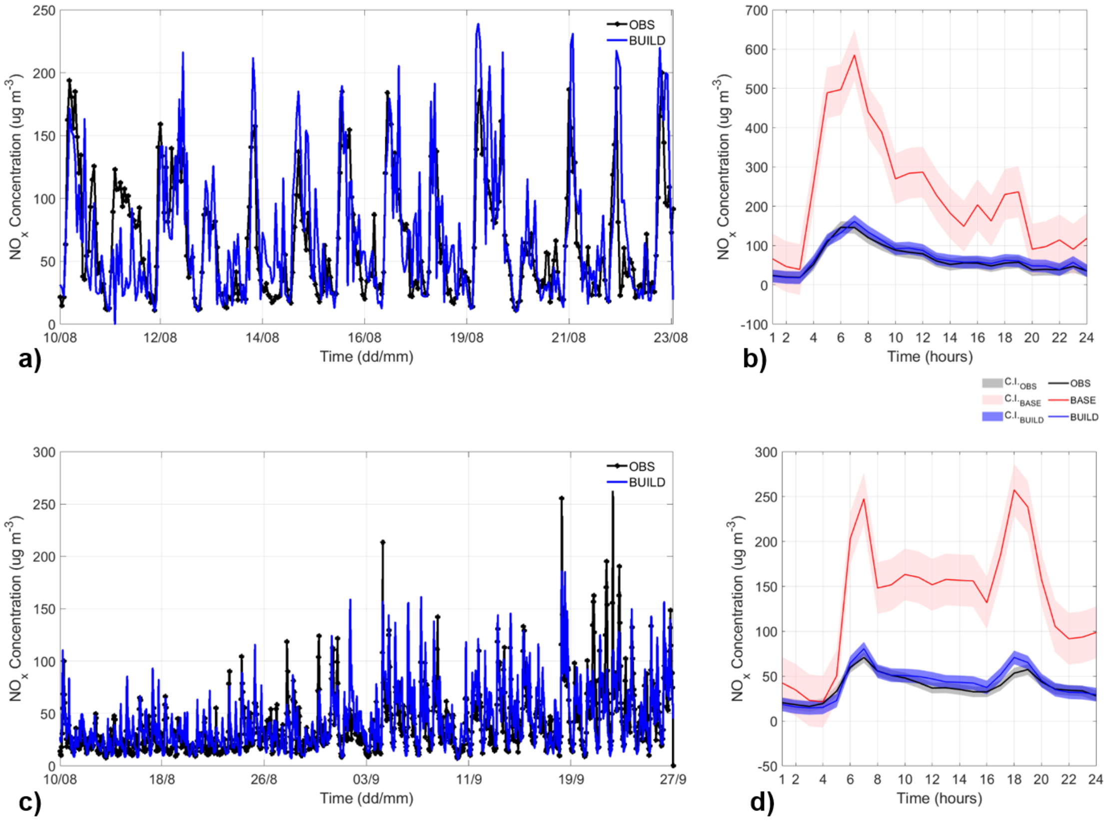

Figure 49. NOₓ daily concentration for neighborhood scale: a) Marconi site and c) Laura Bassi site. Observed data in black, simulated values for BASE case in red and simulated values for BUILD case in blue. Mean diurnal temporal variations: b) Marconi site and d) Laura Bassi site. The shaded area shows the 95 % confidence interval (C.I.) around the mean.

The statistical parameters for the BUILD and TREES cases for all simulations and spatial scales considered, relative to NO_x and NO_2 pollutants are reported in Table 15, Table 16 and Table 17. Also for the NO_2 the results of the BUILD case show the improvement of the model. In all cases and at all scales, the values of Fac2 and Fb fully satisfy the recommended criteria.

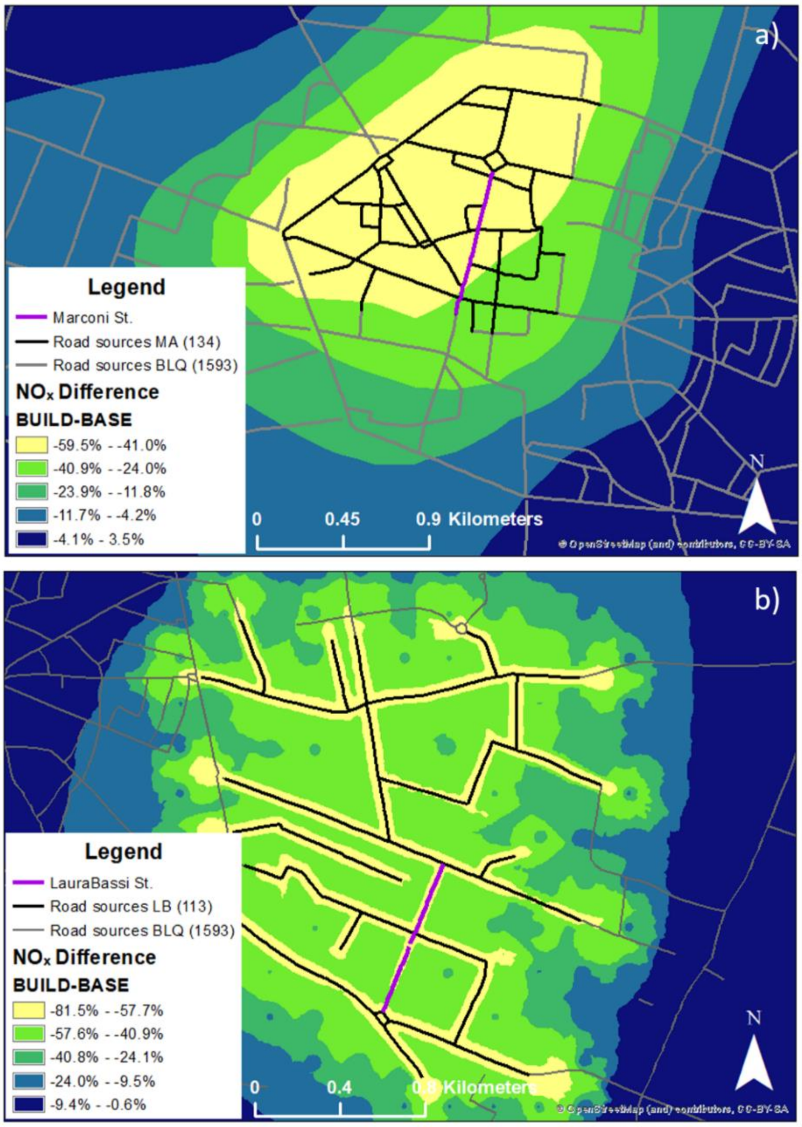

Figure 50. Map of NO_x concentration difference between BUILD and BASE cases for neighborhood scale: a) Marconi site (MA) and b) Laura Bassi site (LB) (map source: OpenStreetMap and contributors).

pollutant	case	n. valid values	r	Fac2	Fb
NO_x	BUILD	352	0.9	1.0	0.0
NO_x	TREES	352	0.9	1.0	0.0
NO_2	BUILD	352	0.8	1.0	-0.1
NO_2	TREES	352	0.8	1.0	-0.1

Table 15. Model evaluation on BASE and BUILD cases for urban scale (SF site). Evaluation by comparison with the observations data and calculation of a set of statistical parameters (r= Pearson correlation coefficient, Fac2=factor of two, Fb= fractional bias).

pollutant	case	n. valid values	r	Fac2	Fb
NO_x	BUILD	48	0.9	1.0	0.1
NO_x	TREES	48	0.9	1.0	0.0
NO_2	BUILD	48	0.9	1.0	0.1
NO_2	TREES	48	0.9	1.0	0.1

Table 16. Model evaluation on BASE and BUILD cases for neighborhood scale (LB site). Evaluation by comparison with the observations data and calculation of a set of statistical parameters (r= Pearson correlation coefficient, Fac2=factor of two, Fb= fractional bias).

pollutant	case	n. valid values	r	Fac2	Fb
NO_x	BUILD	14	0.7	0.9	0.1
NO_x	TREES	14	0.7	1.0	0.1
NO_2	BUILD	14	0.7	0.9	-0.2
NO_2	TREES	14	0.7	1.0	-0.2

Table 17. Model evaluation on BASE and BUILD cases for neighborhood scale (MA site). Evaluation by comparison with the observations data and calculation of a set of statistical parameters (r= Pearson correlation coefficient, Fac2=factor of two, Fb= fractional bias).

The comparison of the statistical parameters obtained for the two cases does not show significant differences at urban scale (BLQ), while at neighborhood scale the performance of the model greatly improves when the aerodynamic effects of the trees are included. Specifically, for LB neighborhood with an important presence of vegetation, the mean bias between modeled and observed values decreases from 3.4 to -0.7 $\mu g\ m^{-3}$. The high correlation coefficients of 0.9, 0.7 and 0.9 (respectively for the urban scale, and for the two neighborhoods MA and LB simulations) indicate the good performance of the model in reproducing the observed variability of NO_x pollutant concentrations. In this case, the statistical parameters meet the previously mentioned criteria for all sites and cases. The inclusion of the information of the urban spatially varying roughness improves the model's performance, as indicated by the increase in the correlation coefficients, and the decrease in Fb and MB.

In the TREES case, the improvement in the model's performance is much less evident, especially in the SF and MA sites. This can be explained from the fact that at the urban scale and for the MA neighborhood, the evaluation of the model was conducted considering only one monitoring site, located in an area of the city characterized by reduced variations in the USVR and reduced presence of vegetation. In fact, the percentage difference between the simulated concentrations in TREES and BUILD case is -1.4% in SF site for August, where the percentage variations in the USVR is only -14%. However, when considering the spatial distribution of the concentrations we observe that the percentage difference decreases in some areas, for example it reaches -29% in the city center for the month of August (Figure 51). In fact, in Figure 51b areas of both concentration decreases and increases can be observed in the city center compared to the BUILD case. The areas of decrease in concentration can be identified as locations where the decrease in roughness is higher than 20%, whereas the concentrations tend to increase at intersections of busy roads and at the edges of areas of decrease.

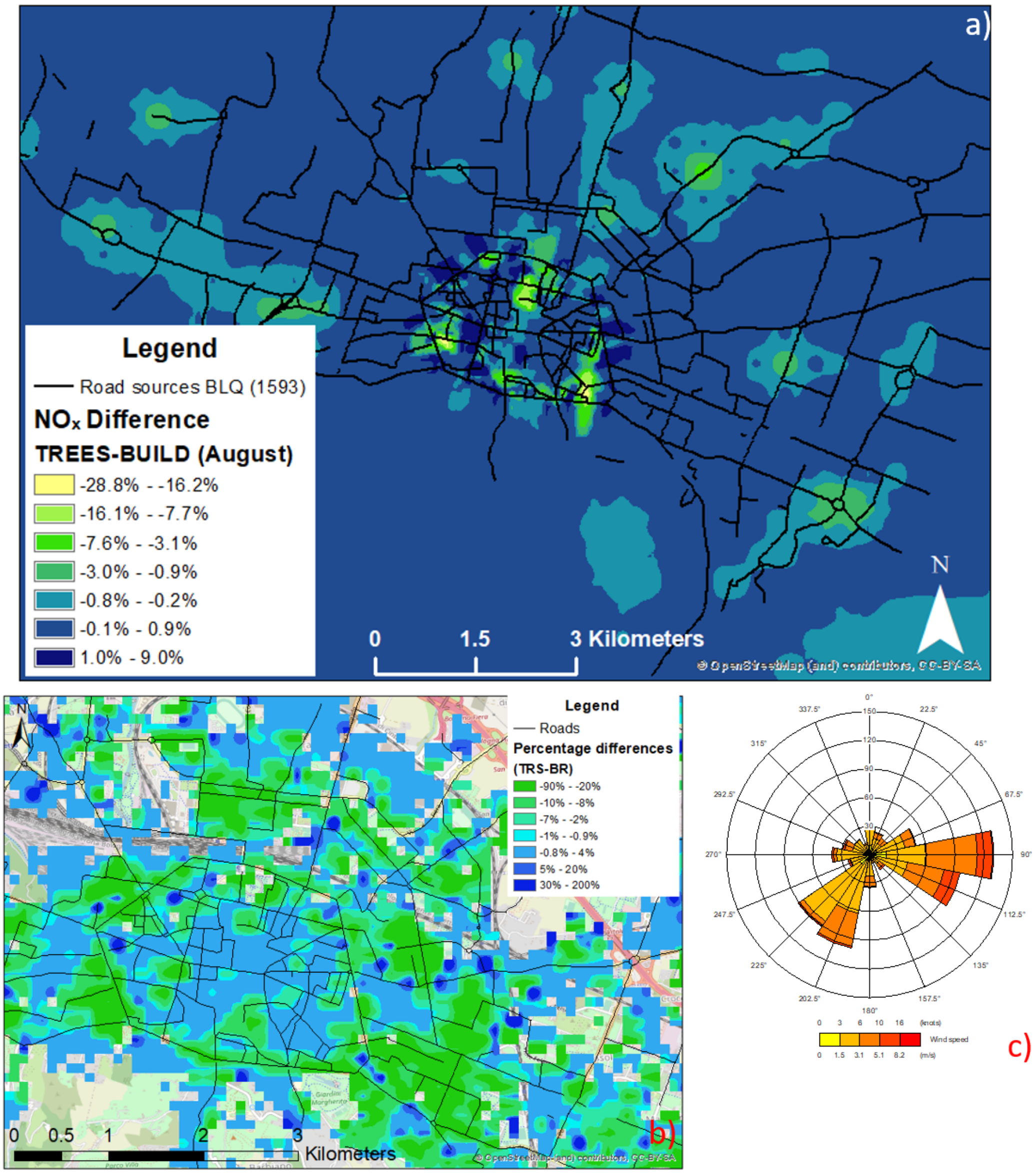

Figure 51. Difference between TREES and BUILD cases for urban scale (BLQ): a) example of map of NO_x concentration difference; b) Map of roughness difference and c) Wind rose showing occurrences of hourly average wind direction and speed for the city of Bologna in august 2017, as recorded at the Bologna Urbana (BU) WS (map source: OpenStreetMap and contributors).

The improvement evidenced for the simulation in the LB neighborhood is instead due to the high presence of vegetation in this area, reflected in the strong variation in roughness between BUILD and TREES (-39%). Therefore, the inclusion of trees in the roughness calculation further improves the simulation of pollutants in this case, as it better describes local aerodynamic characteristics. Figure 52 shows the comparison of observed and simulated hourly NO_x and O_3 concentrations at the MA and LB sites considering the different simulation setups. The regression lines confirm the previously discussed overestimation of the model and a very low agreement of simulations with the observations at all sites obtained in the BASE case. Conversely, the agreement between simulations and observations improves considerably for the BUILD and TREES cases. Further, Figure 52 shows that the simulations conducted with the USVR method agree better with both NO_x and O_3 observations, suggesting that the improvement in NO_x concentrations increases the capability of the model to correctly reproduce not only the share between NO and NO_2 but also all the photochemical reactions involved in the simplified chemical scheme adopted by ADMS.

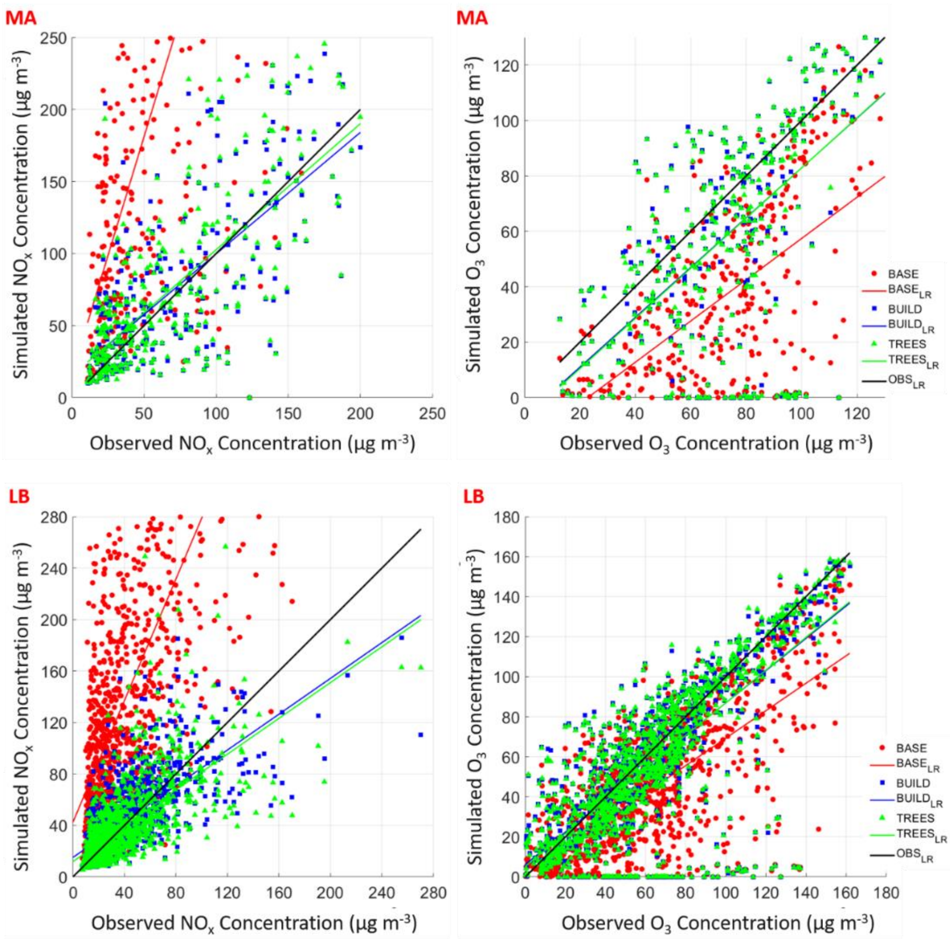

Figure 52. Scatter plot of simulated vs. observed concentrations and linear regression lines. NO_x (left) and O_3 (right) concentration, respectively for Marconi (MA) (top) and for Laura Bassi (LB) (bottom) site.

Figure 53 provides the evaluation of the mean NO_x and O_3 diurnal cycles, for the BUILD and TREES cases. As previously indicated by the increase in the correlation coefficients, the plots demonstrate how the model is capable to capture the diurnal cycle of NO_x concentration, that strongly reflects the pattern of source emissions, showing morning and afternoon traffic-related NO_x peaks and a dip around midday. Conversely, O_3 peaks are observed around midday, related to NO accumulation and intense solar radiation.

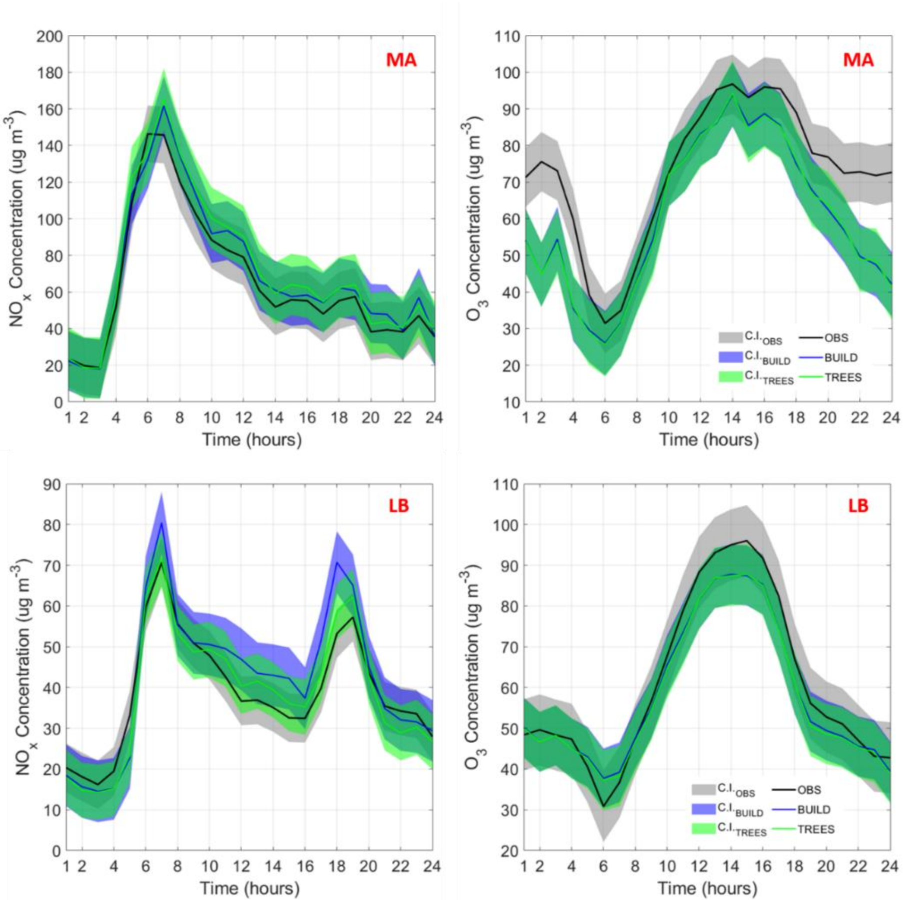

Figure 53. Mean diurnal temporal variations of NO_x (left) and O_3 (right) concentrations, respectively for Marconi (MA) (top) and Laura Bassi (LB) (bottom) sites. The shaded area shows the 95 % confidence interval around the mean.

As from Figure 53, NO_x diurnal cycles observed in the two urban street canyons are well different. Specifically, at Laura Bassi NO_x shows the typical traffic pattern with two peaks during the morning and evening rush hours, while at Marconi concentrations exhibit a single peak with very high concentrations in the morning rush hours gradually decreasing until reaching a nighttime minimum. This pattern, evident in observations and correctly reproduced in the simulations, is likely produced by the transit of buses, more frequent during the morning than in the evening rush hours. At both sites, the daytime O_3 cycles show a drop in correspondence of the NO_x peaks and a peak around midday.

More specifically, in this case we can observe that the model tends to underestimate the O_3 peak concentrations at Laura Bassi, while at Marconi the underestimation occurs for secondary maxima observed in early morning and late evening. Taking into account the good model performance in reproducing NO_x concentrations, this bias in O_3 may be connected to a range of different factors, including issues with the O_3 and VOCs background concentrations advected to the study sites and participating in the photochemical reaction cycle of ADMS, flaws in the input meteorological values of temperature and solar radiation. The results clearly suggest the presence of a relationship between the VOC/NO_x ratio and the overestimation of the model during the hours highlighted in the diurnal cycle (Figure 54), suggesting that the O_3 production tends to be more VOC-sensitive rather than NO_x sensitive (high VOC/NO_x values) late in the evening. This is clearly linked with the biases observed in the simulated O_3 pattern, and in particular with the absence of VOCs background concentrations in our simulation setup.

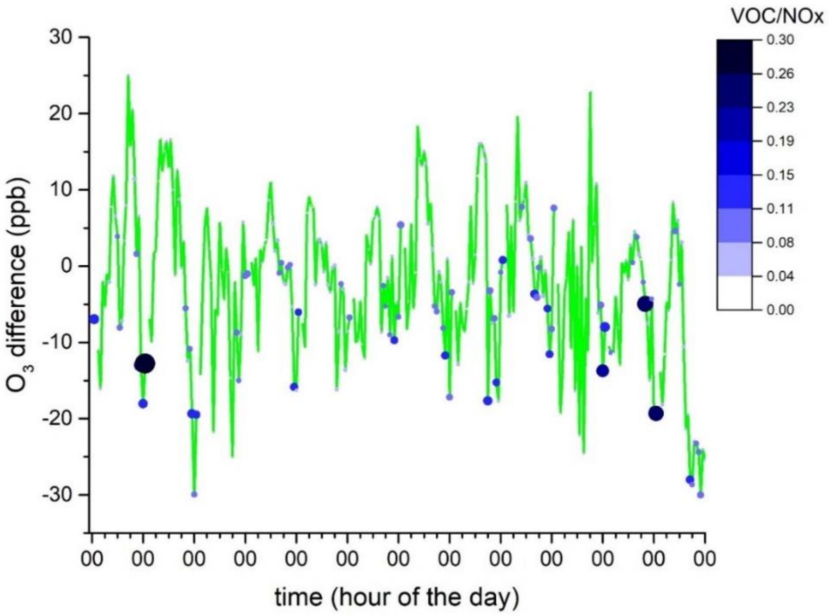

Figure 54. Time series of the difference between simulated and observed O_3 concentrations (green line) and VOC/NO_x ratio (blue marker). The marker dimension and color scale is proportional to the value of VOC/NO_x ratio.

Figure 54 shows the pattern of observed VOC/NO_x ratio at Marconi together with the difference between the simulated and observed O_3 concentrations, for O_3 secondary maxima observed in early morning and late evening we note the sensitivity to VOC and not to NO_x concentrations, suggesting a link with the absence of VOC background concentrations in our simulation setup.

The percentage difference between the simulated concentrations in TREES and BUILD case is 2.5% in MA site. Considering the spatial distribution of the concentrations we note that the percentage difference increases in some areas, reaching 9% (Figure 55), and in other areas it shows a decrease in NO_x concentration (-2%). The concentration increase can be explained from the fact that the MA neighborhood is characterized by reduced variations in the urban spatially varying roughness (-5%) and reduced presence of vegetation.

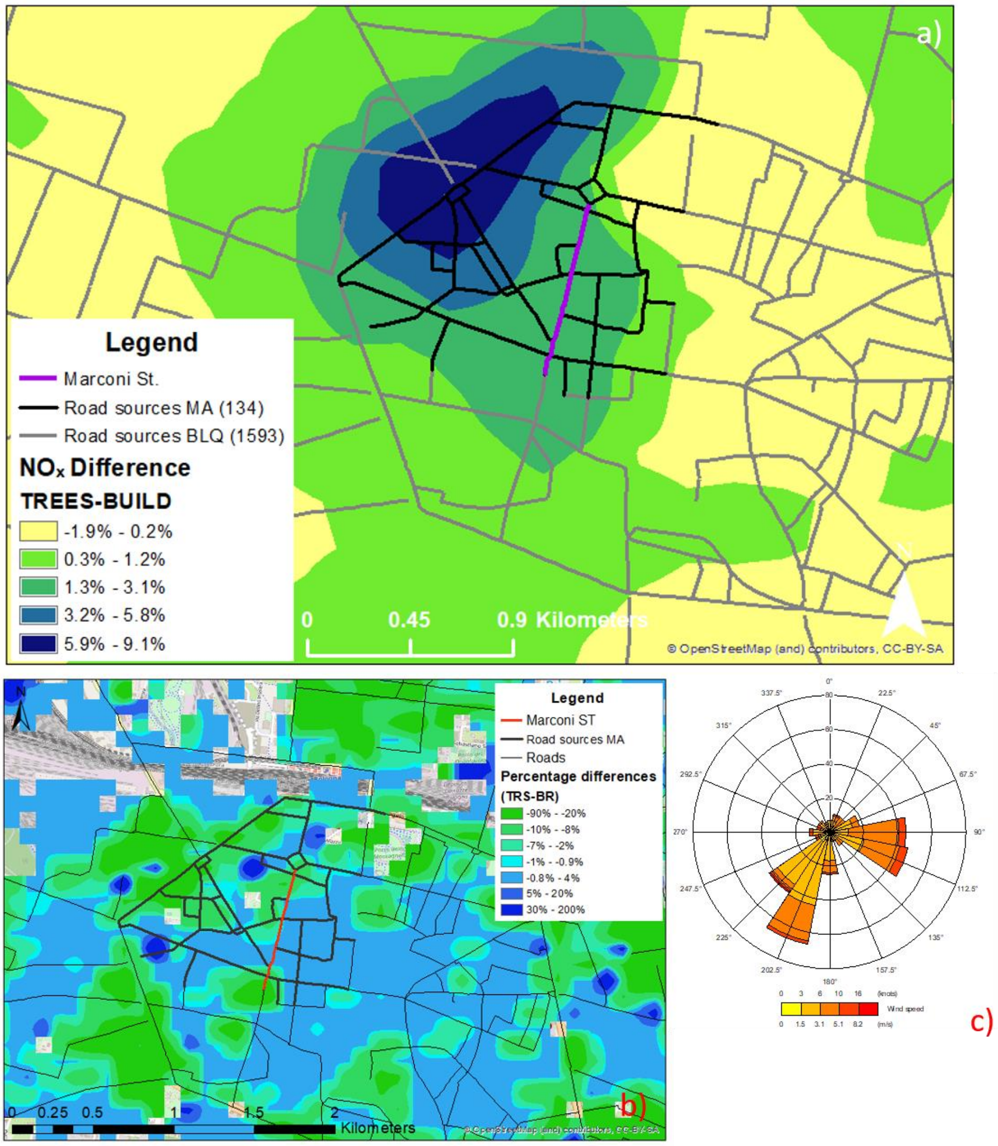

Figure 55. Difference between TREES and BUILD cases for neighborhood scale (Marconi, MA): a) map of NO_x concentration difference; b) Map of roughness difference and c) Wind rose showing occurrences of hourly average wind direction and speed for the city of Bologna from 10 to 23 august 2017, as recorded at the Bologna Urbana (BU) WS (map source: OpenStreetMap and contributors).

In LB site, the evaluation of the diurnal cycles shows that on average the NO_x concentrations tend to decrease in the TREES case compared to the BUILD case. In fact, the percentage difference between the simulated concentrations in TREES and BUILD case is -7.6%. Considering the spatial distribution of the concentrations we can observe that the percentage difference decreases in some areas, in particular reaching -19% within the canyon (Figure 56), while, in the remaining area it increases of 38%. In this site, variations in the USVR due to the presence of vegetation are around -39%.

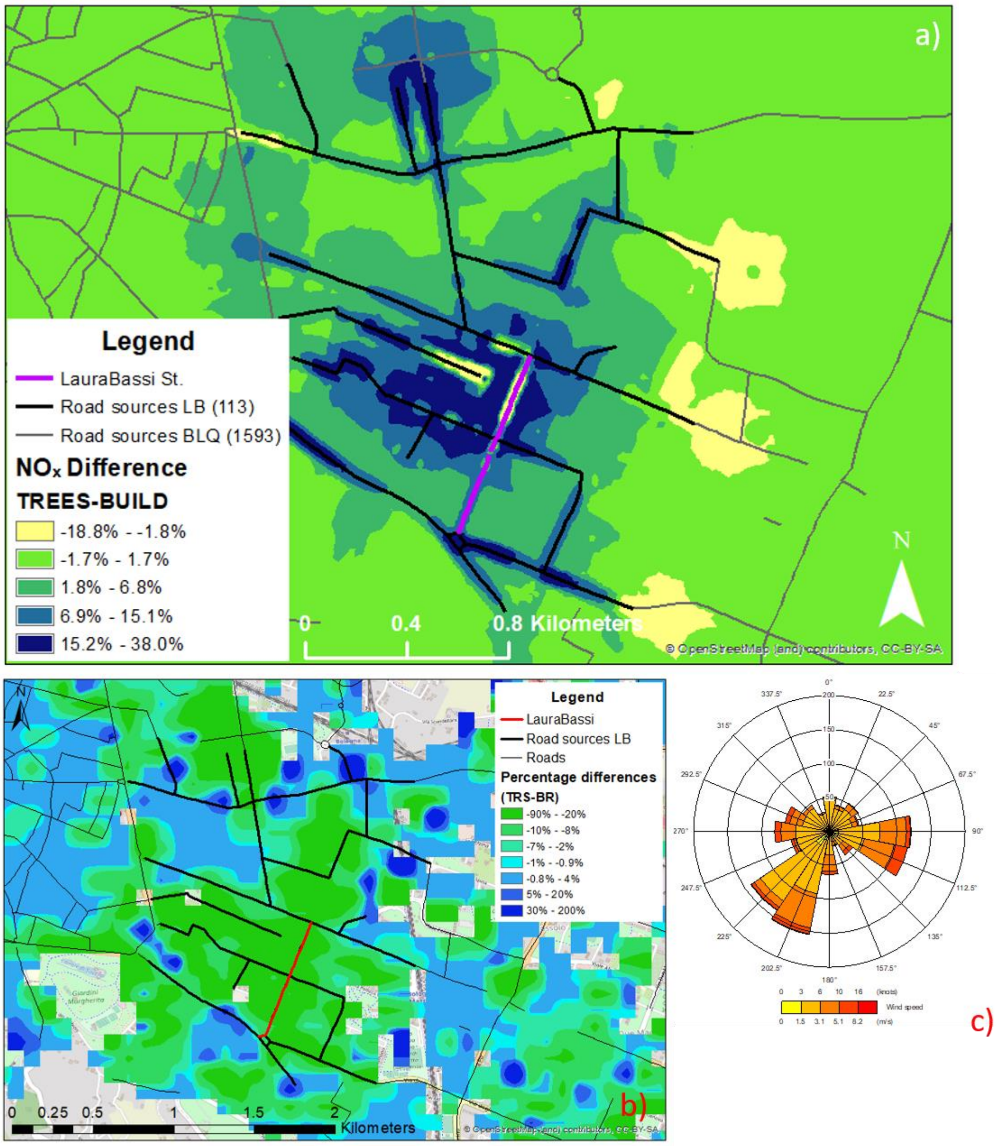

Figure 56. Difference between TREES and BUILD cases for neighborhood scale (Laura Bassi, LB): a) map of NO_x concentration difference; b) Map of roughness difference and c) Wind rose showing occurrences of hourly average wind direction and speed for the city of Bologna from 10 to 23 august 2017, as recorded at the Bologna Urbana (BU) WS (map source: OpenStreetMap and contributors).

The contribution of deposition to concentration was assessed for the neighborhood scale. Simulations were conducted at LB site for BUILD and TREES scenarios by adding the dry deposition to the pollutants investigated (NO_x). The value of the deposition velocity was chosen on the basis of the type of material over which the deposition occurred: specifically, a value for urban surfaces was used in the BUILD case (0.0006 m s^{-1}; (Environment Agency, 2008)), while in the TREES case, the deposition rate was calculated taking into account the surface occupied by buildings (urban surface) and trees (conifers (0.001 m s^{-1}) and deciduous (0.004 m s^{-1}; (Environment Agency, 2008)). Specifically, a value representative for urban surfaces was used in the BUILD case, while in the TREES case, the deposition rate was calculated taking into account the surface occupied by buildings (urban surface) and trees (conifers and deciduous) (Table 18).

Deposition material	**Deposition velocity (m s^{-1})**
BUILD	0.0006
TREES	0.0012

Table 18. NO_x deposition velocity values used in BUILD and TREES case.

The results obtained at the LB site show that the deposition has a reduced contribution on NO_x concentration, both in the BUILD and in the TREES case (Table 19). The same result is highlighted in the percentage difference maps (Figure 57) considering the two cases with and without deposition.

	NO_x Concentration (μg m^{-3})		**NO_x concentration (μg m^{-3})**		**Percentage differences (%)**	
	BUILD	*TREES*	*BUILD* (with deposition)	*TREES* (with deposition)	*BUILD*	*TREES*
Mean	50.2	38.9	50.3	38.7	0.2	-0.5
Min	6.2	5.5	6.2	5.5	0.0	0.0
Max	234.0	301.8	235.8	296.3	0.8	-1.8
SD	36.8	31.7	36.9	31.4		

Table 19. Results for BUILD and TREES cases in LB site with and without deposition.

The results indicate that deposition has a reduced impact on the concentration of gaseous pollutants such as NO_x, lowering the concentration of 0.5% at maximum in the TREES case, in agreement with previous works who suggested that the largest effects exerted by trees on pollutant concentrations are mainly related with the aerodynamic effects (Jeanjean et al., 2017; Jeanjean et al., 2016; Santiago et al., 2017).

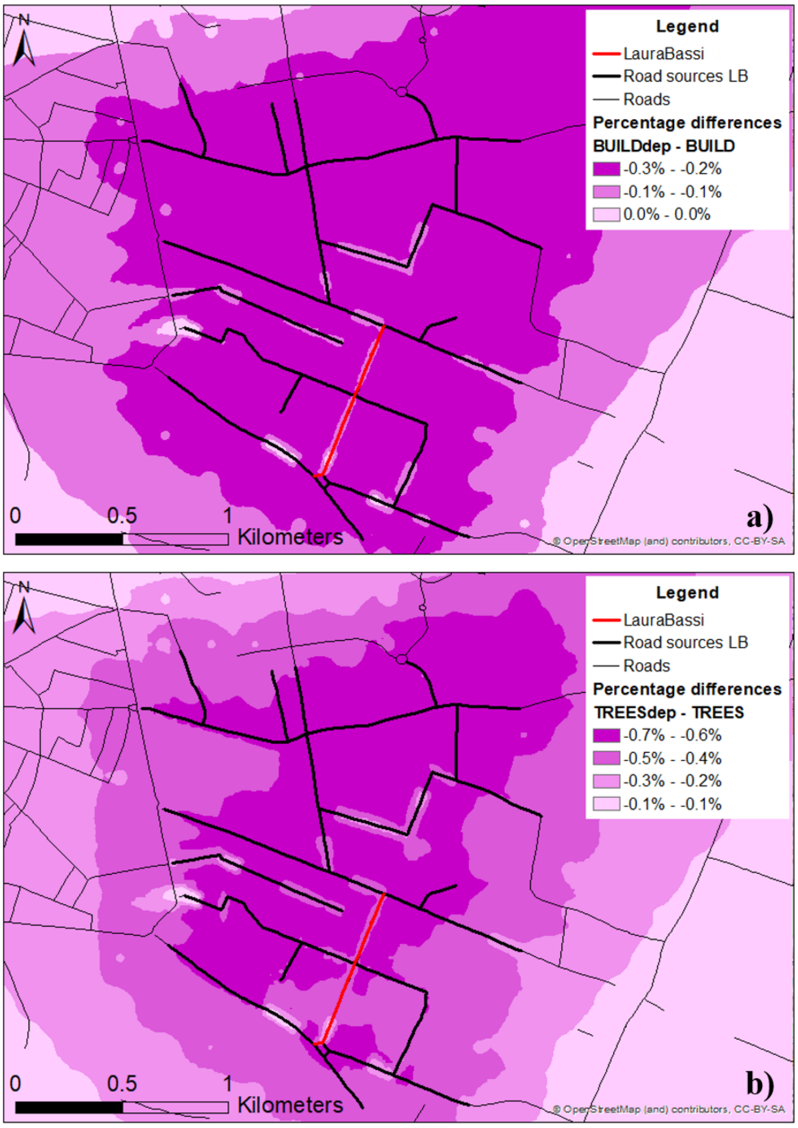

Figure 57. Map of NO_x concentration difference between simulation with and without deposition for Laura Bassi site (LB): a) BUILD case and b) TREES case (map source: OpenStreetMap and contributors).

In conclusion, despite the urban-scale model in the BASE case fulfills the recommended criteria for the NMSE, Fac2 and Fb parameters, it shows a tendency for the simulation to overestimate observed concentrations. Instead, the simulations conducted for the two neighborhoods show a poor model's performance. Significant improvements were obtained at all scales and sites introducing USVR. The introduction of the presence of buildings improves the agreement of the simulations with the observations.

The insertion of the roughness due to buildings and trees has produced different results based on the spatial scale and on the characteristics of the dispersion site. At the urban scale, the presence of trees does not seem to significantly alter the results. However, this observation may result from the fact that the observations used to evaluate the model performance were available only for a not densely vegetated site. Indeed, the spatial map highlights the presence of areas characterized by significant variations in pollutant concentrations where vegetation is present. At the neighborhood scale, the inclusion of vegetation significantly improves the agreement of the simulations with observations, especially for vegetated areas such Laura Bassi in our case. Therefore, this methodology is strongly recommended to improve the performance of dispersion simulations, and particularly to limit the overestimation of the simulated concentrations. The inclusion of vegetation is particularly necessary in high spatial resolution studies, and for densely vegetated sites. In inhomogeneous urban cases, in order to study local dispersion and the influence of vegetation, it is instead advisable to divide the area into homogeneous sub-areas.

4.4 Climate change and air quality

This section focused on greening policy, and their effects on AQ and urban thermal comfort in the present and in the future. The strategy followed was those to simulate a reference base case of a tree-free street canyon, Marconi St., which trees were added along the street using new parametrization for vegetate areas presented in section 4.3. The simulations in this street canyon were conducted in a real base case (Base Case - Actual Trees scenario) and in a scenario of tree planting (Base Case - Added Trees scenario). The two scenarios created were compared to evaluate the impact of planting trees in a neighborhood in the vicinity of the street canyon. Furthermore, the impact of the intervention under the influence of climate change is also tested, for which purpose two additional scenarios are created: Future Case - Actual Trees scenario to assess the impact of climate change only and Future Case - Added Trees scenario to evaluate the effectiveness of trees in mitigating air pollution in the future climate conditions. Unlike section 4.2, which dealt with the effects of trees on deposition, here, the effect of trees on dispersion was evaluated.

4.4.1 The greening of Marconi St.

In order to evaluate the effectiveness of PCSs in Bologna, the simulations were conducted at the neighborhood scale. In particular, Marconi St., one of the two street canyons where the two iSCAPE campaigns were carried out is considered as study site. In summary, Marconi St. is a tree-free street canyon located in the city center of Bologna. Marconi St. is a tree-free street canyon in the base current scenario, so a scenario in which trees will be planted in the center of the road (Figure 58) was take into account. In particular, the scenario was developed considering the planting of deciduous trees, to include also the seasonal effects due to the fall of foliage and of trees having all the same dimensions (crown diameter = 7 m, tree height = 10 m, distance between two crowns =

3 m, Figure 58). In the model, the trees are modeled as elements of roughness (porous bodies), which, together with the buildings, contribute to modify the wind field.

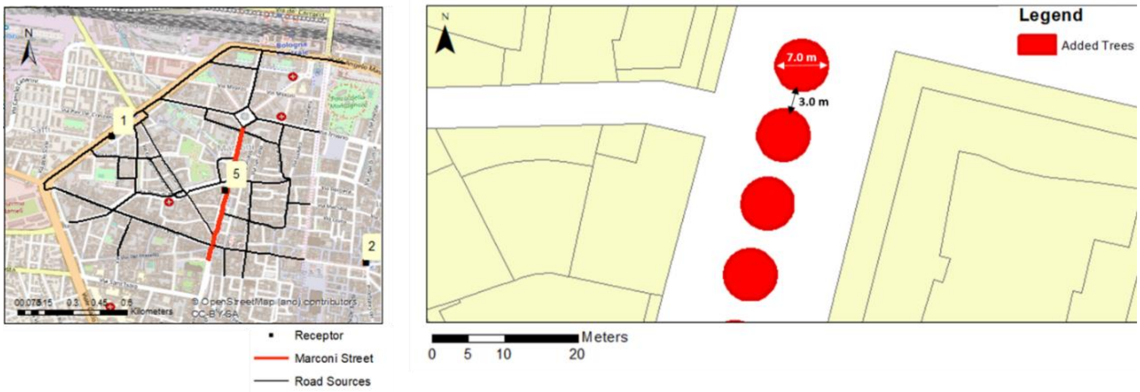

Figure 58. Site of PCSs intervention. Left) Roads inside the area around Marconi street and location of the receptor sites (points corresponding to the ARPAE AQ stations): 1) Porta S. Felice Receptor; 5) ARPAE van receptor; 2) Asinelli Receptor. Right) Detail of the location of trees added in Marconi and relative crown diameter and distance between two crowns.

In AQ analysis, emissions covering the Bologna area were considered, using the same emission inventory illustrated in section 3.2.2. In order to get down to the street canyons scale, the whole road graph is split into major and minor roads. For the purpose of this work, it has been assumed that all the main roads around Marconi street canyon are major roads (Figure 58), while all the other roads are considered minor roads. Also, the USVR is used in these dispersion simulations, the methodology to calculate the USVR is described in section 4.3, together the results of evaluation of the model.

In UHI analysis, the LCZ classification (Stewart and Oke, 2012) was used to define the land use of the domain. The PCSs effects on the UHI effect were evaluated by modifying the LCZ classes and using the USVR (like in dispersion model). In Marconi St., the presence of trees was simulated by modifying the surface parameter of the reference class (LCZ2) with that used in the LCZ5 class, as described in section 4.2.1.2. Furthermore, the trees were also modeled as elements of roughness, so the USVR was modified with trees added in Marconi St. (as described above).

4.4.2 AQ analysis results

The results of the dispersion modelling were conducted in the current and future scenarios. In the actual case, the dispersion of pollutants in the neighborhood of the street canyon was modeled considering the months of August in 2017 and February 2018 as representative of both the summer and winter seasons. The future case was derived running high resolution with the mesoscale numerical weather prediction model WRF (Weather Research and Forecasting). The WRF simulations were performed for two time periods, one in the warm period 20–26 August 2050, and one in the warm period 20-25

February 2050. For both actual case and future case, the simulations were conducted in a scenario of trees planting (added trees) and in the absence of trees (actual trees) (Table 20).

Case	Street	Year	Season	Trees	Scenario
Base Case	Marconi	2017	summer	actual trees	Base Case-Actual trees-summer (BC-AcT-sum)
Base Case	Marconi	2017	summer	added trees	Base Case-Added trees-summer (BC-AdT-sum)
Base Case	Marconi	2018	winter	actual trees	Base Case-Actual trees-winter (BC-AcT-win)
Base Case	Marconi	2018	winter	added trees	Base Case-Added trees-winter (BC-AdT-win)
Future Case	Marconi	2050	summer	actual trees	Future Case-Actual trees-summer (FC-AcT-sum)
Future Case	Marconi	2050	summer	added trees	Future Case-Added trees-summer (FC-AdT-sum)
Future Case	Marconi	2050	winter	actual trees	Future Case-Actual trees-winter (FC-AcT-win)
Future Case	Marconi	2050	winter	added trees	Future Case-Added trees-winter (FC-AdT-win)

Table 20. Scheme of the simulations carried out on Bologna for AQ analysis.

The statistical evaluation (Table 21) of the performance of the ADMS-Urban model was carried out comparing simulated and observed values at Marconi St. for August 2017 and February 2018 from the ARPAE van during the summer and winter experimental field campaign in Bologna.

Station	Season	$\text{Mean}_{\text{OBS}} \pm$ SD	$\text{Mean}_{\text{MOD}} \pm$ SD	NMSE	r	Fac2	FB
Arpae van	Summer	65. ± 18.0	58.7 ± 26.1	0.05	0.91	1	-0.10
Arpae van	Winter	165.3 ± 41.0	160.8 ± 43.7	0.07	0.48	1	-0.03

Table 21. Statistical indices calculated to compare the simulated data (mod) of for NO_x concentration with the measured values (obs) in the reference station: ARPAE van located in Marconi street in Bologna for August 2017 (summer) and February 2018 (winter). SD: Standard deviation; MB: mean bias; NMSE: normalized mean square error; R: Pearson's correlation coefficient; Fac2: factor of two; Fb: fractional bias.

In particular, the assessment was carried out considering NO_x concentrations. The results show that the model represents correctly the overall pattern of pollutants, even though it tends to underestimate NO_x concentrations. In particular, snow events occurred during the winter period, besides affecting deeply wet deposition, might have impacted on the traffic flow, determining a non-optimal correspondence between simulated and measured data. However, statistical parameters for the ADMS simulations are reasonably good and fulfill the recommended statistical criteria, specifically NMSE $\leq$ 1.5, Fac2 $\geq$ 0.5 and $-0.3 \leq$ Fb $\leq$ 0.3 (Di Sabatino et al., 2011).

4.4.2.1 Base Case Vs Future Case

The simulations for the current scenario (base case) were conducted selecting two periods, one during summer (20 - 25 August 2017) and one during winter (6 - 11 February

2018). For each period, simulations were conducted both in a scenario of trees planting (added trees) and in the absence of trees (actual trees).

In the base case for 2017, the NO_x concentration maps (Figure 59) appear similar in the two seasons as for the spatial distribution, with higher values in the study area and a lower and more homogeneous background around; however, the winter case shows higher concentrations in a larger spatial area, in agreement with the more frequent stagnation regimes typical of the winter season.

The concentration maps for NO_x in Base Case - Added Trees (Figure 60) show that the trees planting intervention does not impact neither on maximum values have not substantially changed compared to the base case, neither on the spatial pattern. The comparison between the two cases is presented in terms of maps of concentration differences (Figure 61), which highlight more clearly the presence of areas of reduced and increased NO_x concentrations.

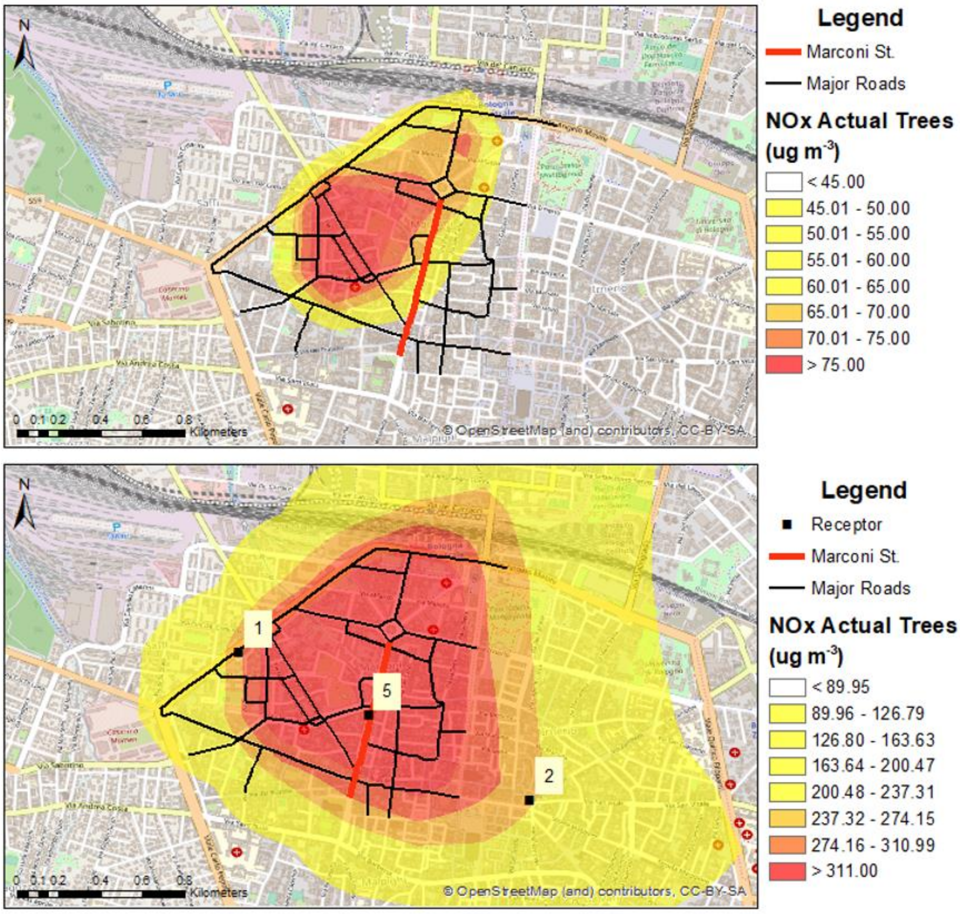

Figure 59. Concentration maps for NO_x (top: summer 2017, bottom: winter 2018) in the current reference case (Base Case - Actual trees) for a neighborhood of Marconi St. in Bologna. The location of the receptor sites is indicated with a number: 1) Porta S. Felice Receptor; 5) ARPAE van receptor; 2) Asinelli Receptor.

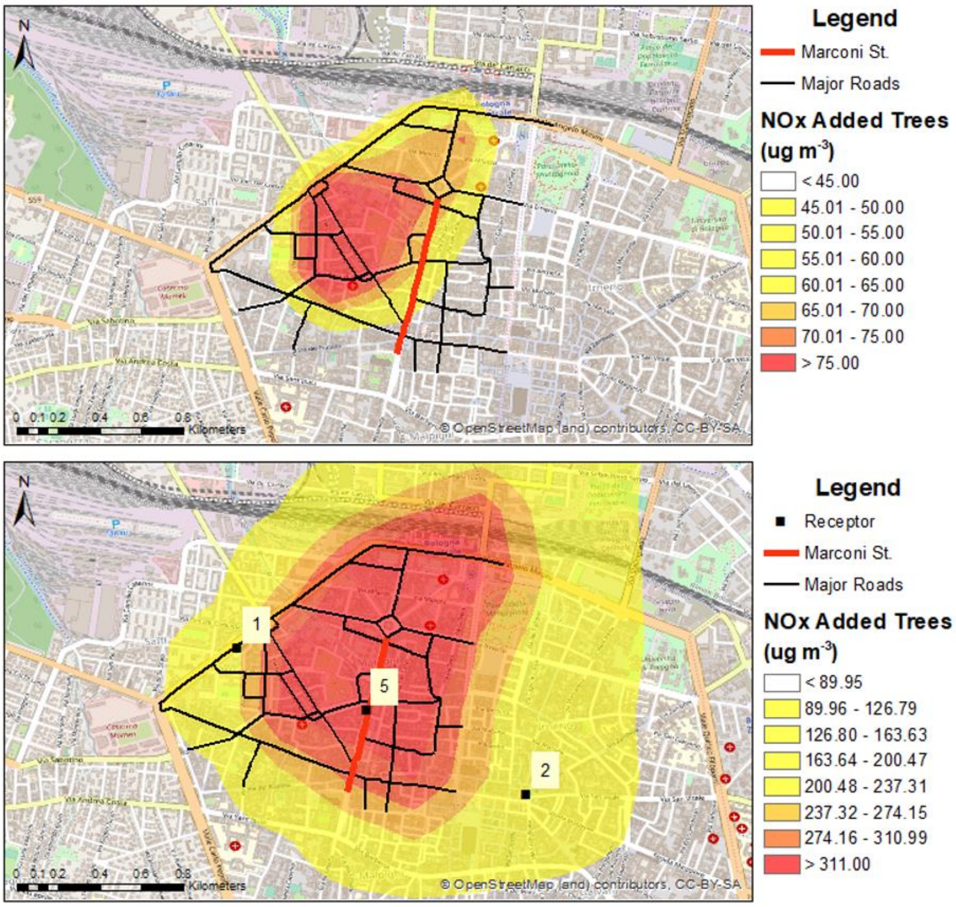

Figure 60. Concentration maps for NO_x with a trees planting scenario (Base Case - Added trees) in the current climate conditions (top: summer 2017, bottom: winter 2018) for a neighborhood of Marconi St. in Bologna. The location of the receptor sites is indicated with a number: 1) Porta S. Felice Receptor; 5) ARPAE van receptor; 2) Asinelli Receptor.

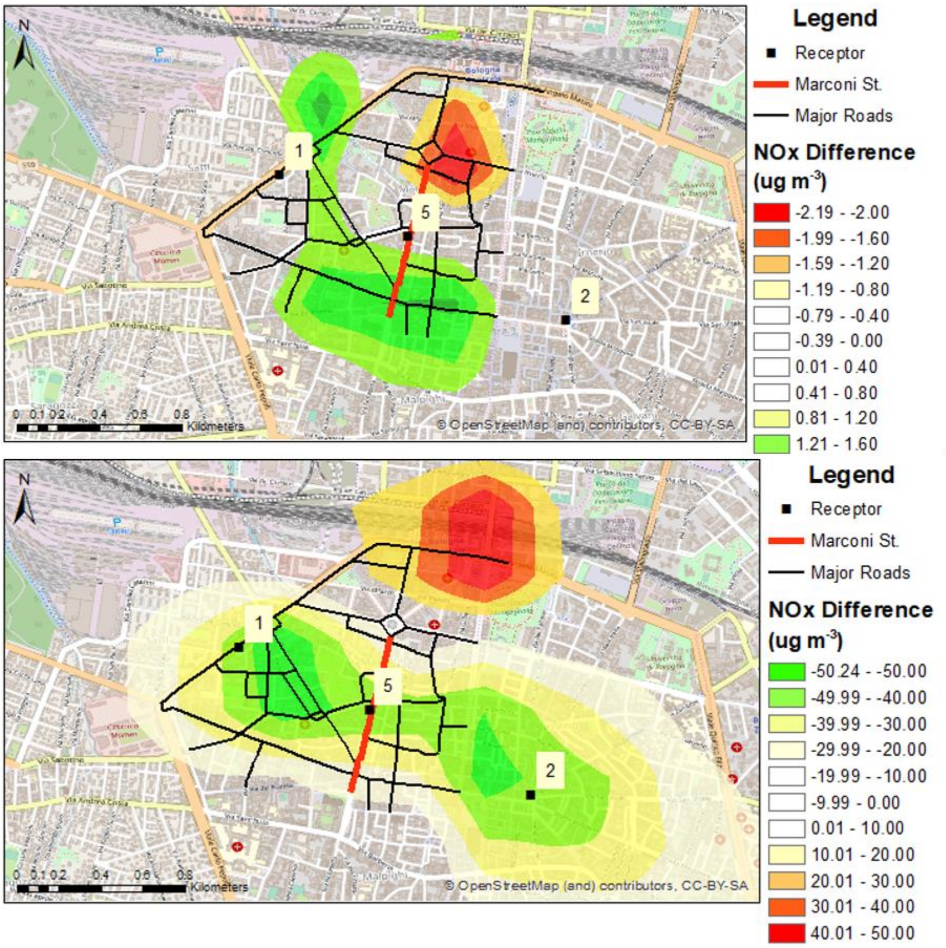

Figure 61 Maps of concentration differences for NO_x in the current climate conditions (top: summer 2017, bottom: winter 2018) for a neighborhood of Marconi St. in Bologna. The differences are calculated between the Base Case - Added Trees scenario and the Base Case - Actual Trees scenario. The location of the receptor sites is indicated with a number: 1) Porta S. Felice Receptor; 5) ARPAE van receptor; 2) Asinelli Receptor.

The results in the future case for 2050 are presented below as concentration maps (Figure 62) for reference case (Future Case - Actual trees), concentration map (Figure 63) for a trees planting scenario (Future Case - Added trees) and maps of concentration differences (Figure 64) calculated between the Future Case - Added Trees scenario and the Future Case - Actual Trees scenario.

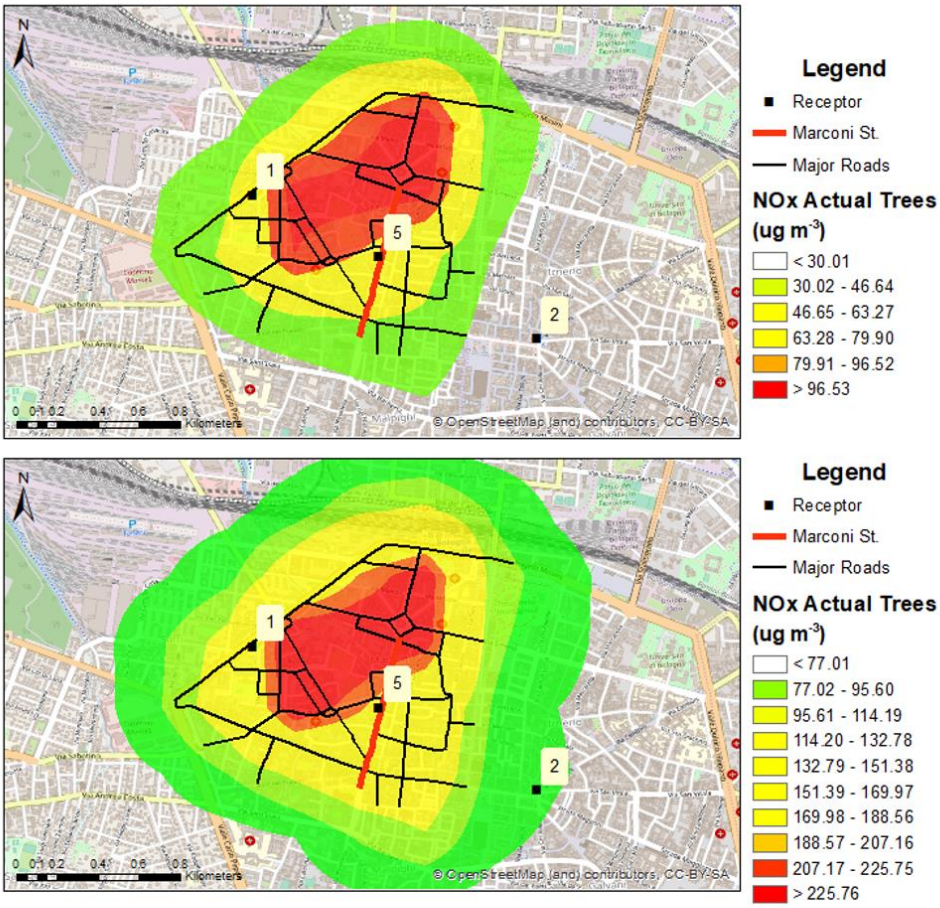

Figure 62. Concentration maps for NO_x (top: summer 2050, bottom: winter 2050) in the future reference case (Future Case - Actual trees) for a neighborhood of Marconi St. in Bologna. The location of the receptor sites is indicated with a number: 1) Porta S. Felice Receptor; 5) ARPAE van receptor; 2) Asinelli Receptor.

The spatial distribution of pollutant concentrations in the future case for 2050 (Figure 62) appears similar in the two seasons with regard to the spatial distribution, with higher values in the study area and a lower and more homogeneous background around. Even here, as in the base case, the winter period shows higher concentrations in a wider spatial area.

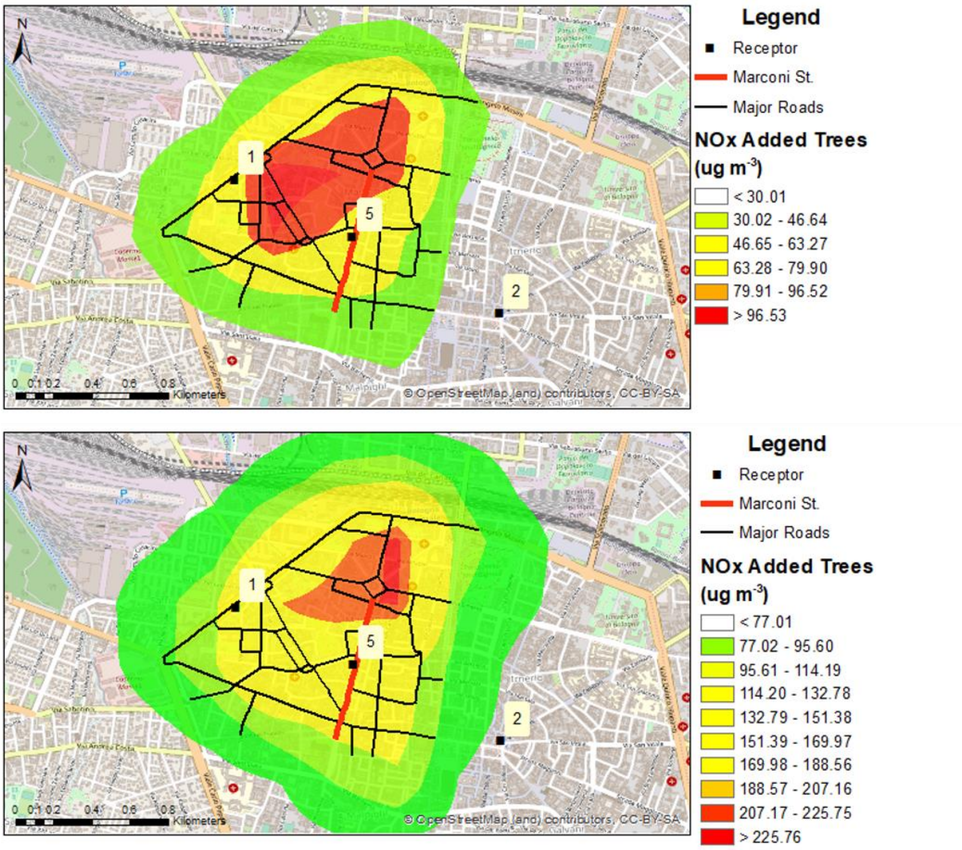

Figure 63. Concentration maps for NO_x with a trees planting scenario (Future Case - Added trees) in the future climate conditions (top: summer 2050, bottom: winter 2050) for a neighborhood of Marconi St. in Bologna. The location of the receptor sites is indicated with a number: 1) Porta S. Felice Receptor; 5) ARPAE van receptor; 2) Asinelli Receptor.

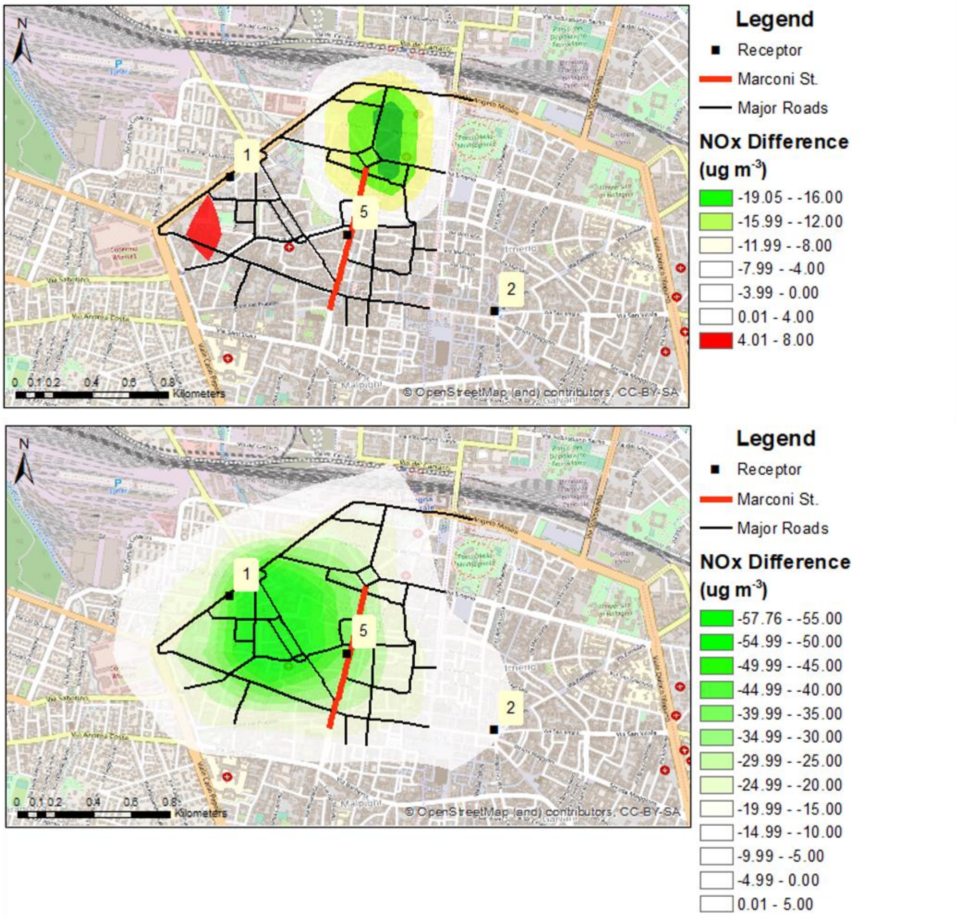

Figure 64. Maps of concentration differences for NO_x in the future climate conditions (top: summer 2050, bottom: winter 2050) for a neighborhood of Marconi St. in Bologna. The differences are calculated between the Future Case - Added Trees scenario and the Future Case - Actual Trees scenario. The location of the receptor sites is indicated with a number: 1) Porta S. Felice Receptor; 5) ARPAE van receptor; 2) Asinelli Receptor.

The NO_x concentration maps (Figure 63) in the scenario when planting trees under future climate conditions (Future Case - Added Trees scenario) compared with the results obtained under climate change only (Future Case - Actual Trees scenario) indicate a similar spatial pattern in the two scenarios, but in the summer period concentration levels are more reduced than in the scenario without trees (Future Case - Actual Trees scenario). The maps of concentration differences (Figure 64) highlight more clearly the presence of areas of reduced or increased concentrations.

4.4.3 UHI analysis results

The simulations with ADMS-TH model were conducted in the current and future scenarios considering the months of August in 2017. The future case was derived running high resolution with the mesoscale numerical weather prediction WRF model, performed in the warm period 20-26 August 2050. For both the actual and future cases, the simulations were conducted in a scenario of trees planting (added trees) and in the absence of trees (actual trees) (Table 22).

Case	Street	Year	Season	Trees	Scenario
Base Case	Marconi	2017	summer	actual trees	Base Case-Actual trees-summer (BC-AcT-sum)
Base Case	Marconi	2017	summer	added trees	Base Case-Added trees-summer (BC-AdT-sum)
Future Case	Marconi	2050	summer	actual trees	Future Case-Actual trees-summer (FC-AcT-sum)
Future Case	Marconi	2050	summer	added trees	Future Case-Added trees-summer (FC-AdT-sum)

Table 22. Scheme of the simulations carried out on Bologna for UHI analysis.

The model performance was evaluated by comparing hourly temperature modelled values with measured ones at reference measurement stations of Bologna Urbana (BU), Asinelli (As) and Mezzolara (Mz); see section 3.2.5 for more methodology details and section 4.2.1.2 for the model evaluation results.

4.4.3.1 Base Case Vs Future Case

The simulations of the ADMS-TH model in the current scenario, i.e. considering the actual land use and the hourly meteorological variables recorded by ARPAE stations during the summer 2017, have produced the map of temperature for the base case – Actual Trees, PCSs intervention and map of temperature differences (Figure 65). The same maps are produced for the future case (Figure 66).

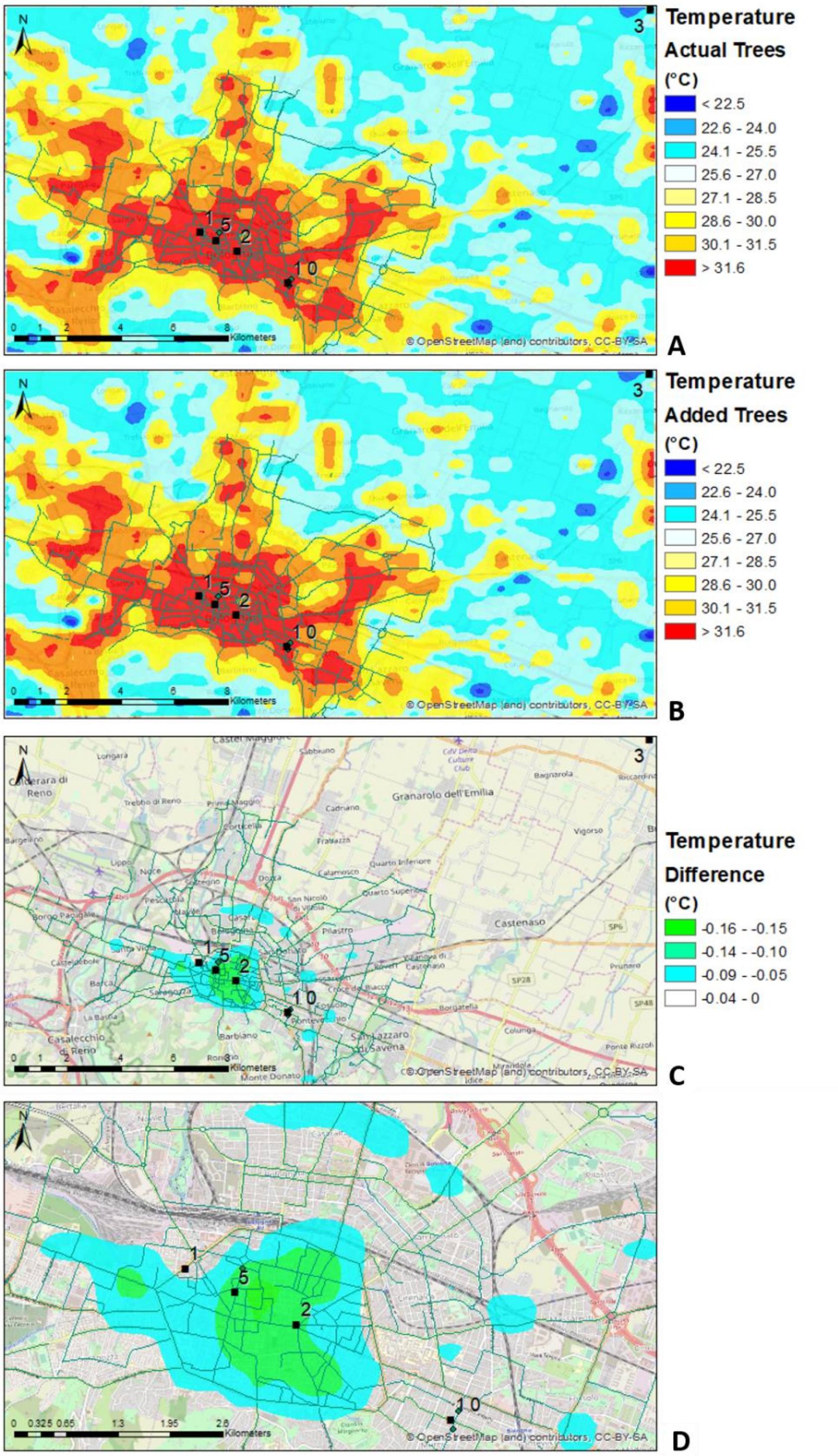

Figure 65. UHI analysis for Bologna: A) Maps of the temperature for Base Case –Actual Trees scenario; B) Maps of the temperature for Base Case –Added Trees scenario; C) Difference of temperature between the Base Case - Actual Trees scenario and Base Case - Added Trees scenario (adding trees in the street canyon); D) view of the entire domain, below: zoom on Marconi St., street canyon affected by PCSs intervention. The location of the receptor sites is indicated with a number: 1) Bologna Urbana Receptor; 5) Marconi ARPAE van receptor; 2) Asinelli Receptor; 3) Mezzolara receptor; 10) Laura Bassi ARPAE van receptor.

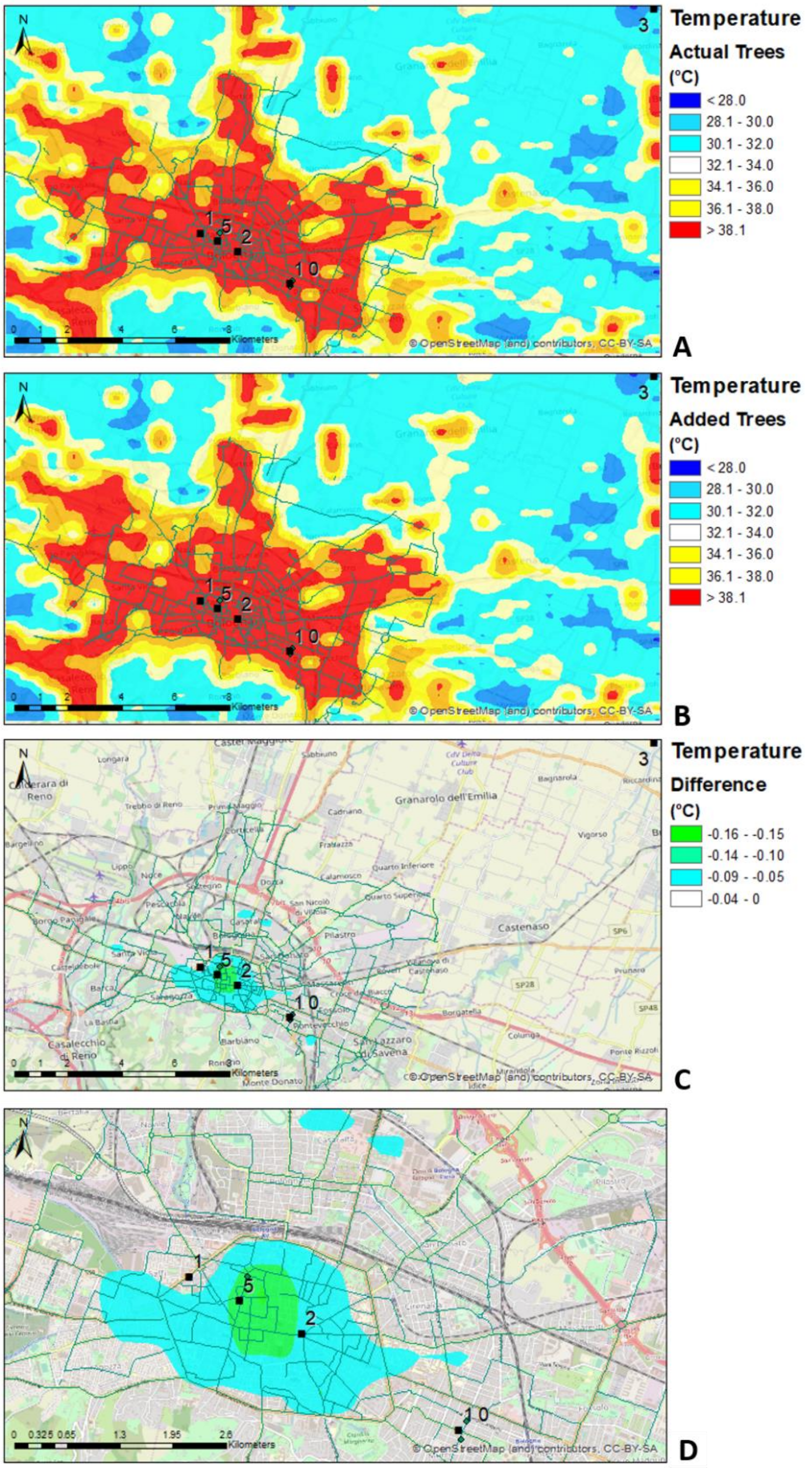

Figure 66. UHI analysis for Bologna: A) Maps of the temperature for Future Case –Actual Trees scenario; B) Maps of the temperature for Future Case –Added Trees scenario; C) Difference of temperature between the Future Case - Actual Trees scenario and Future Case - Added Trees scenario (adding trees in the street canyon); D) view of the entire domain, below: zoom on Marconi St., street canyon affected by PCSs intervention. The location of the receptor sites is indicated with a number: 1) Bologna Urbana Receptor; 5) Marconi ARPAE van receptor; 2) Asinelli Receptor; 3) Mezzolara receptor; 10) Laura Bassi ARPAE van receptor.

The map for the base case clearly shows the urban heat island of Bologna, with higher temperatures in the city center compared with the surrounding rural areas. For the Base Case considering the PCSs intervention (Figure 65B), the spatial pattern of temperature distribution is substantially the same, but the map of temperature differences (Figure 65C) indicates a variation in the difference between urban and rural temperature.

In the future case, as in the base case, the map of the temperature for Future Case - Actual Trees scenario (Figure 66A) shows the urban heat island of Bologna, which tends to increase in the future as a result of climate change. The same spatial pattern is highlighted in the temperature map in the scenario considering the implementation the intervention planting deciduous trees in Marconi St. (Figure 66B). The map of temperature differences (Figure 66C) shows the same reduction values, with a slightly different pattern than in the Base Case; however also in this case it can be observe how the introduction of trees over a small area potentially affects the temperature observed even in the surrounding areas.

4.5 Summary

The cases and simulated scenarios in Bologna aimed to evaluate:

- Effect of traffic management policies on AQ;
- Effect of PCS interventions on AQ and UHI;
- Effect of greening policy on AQ and UHI in the present and in the future.

The setup of the ADMS models (ADMS-Urban and ADMS-TH) involves the use of the chemical module, input data from the ARPAE (pollutant concentrations) and LIPE (meteorological) stations and use of the complex terrain module. For ADMS-TH, the meteorological input data were collected from different stations surrounding the domain depending on wind directions. The performance evaluation of the ADMS-Urban and ADMS-TH models highlighted slight overestimates in the urban site. However, the statistical indices indicate an overall good agreement between the simulated and observed values.

The traffic policies simulated in Bologna are two: (1) Policy 1 "electric centre" (2017P1EC) and (2) Policy 2 "electric buses" (2017P2EB). In order to evaluate the effect of the policies, base case (2017BC) was compared with both scenarios. The concentration differences calculated between 2017P1EC scenario and 2017BC scenario show a decrease in NO_x and PM_{10} concentrations over the city center. The differences calculated between 2017P2EB scenario and 2017BC scenario highlight a decrease in NO_x concentrations, but there is no decrease for PM_{10}. Therefore, the effect of the Policy 1 can be considered more satisfactory than Policy 2.

The effects caused by the insertion of trees on UHI and AQ were studied through: (1) a UHI and (2) an AQ analysis. The inclusion of PCSs in the ADMS-TH model was implemented by modifying parameters referred to land use, in the case of ADMS-Urban, the PCSs were considered as a factor that modifies the deposition of pollutants. In UHI analysis, two scenarios were simulated: (1) Marconi PCSs (adding trees in the street canyon) and (2) Center PCSs (trees added over the whole city center). NO PCSs (base case) case was compared with both scenarios. The difference of temperature between NO PCSs and Marconi PCSs scenarios shows the temperature reduction even in the surrounding areas. In the comparison between NO PCSs and Center PCSs scenarios, the presence of trees induces a temperature reduction over a large area covering the city center and surrounding areas. In AQ analysis, two scenarios were investigated: (1) Urban scenario (Bologna without trees) and (2) PCSs scenario (Bologna with trees). The deposition differences calculated between Urban and PCSs scenarios show an increase in deposition in the case of the PCSs scenario, and the increment is greater for NO_x than for PM_{10}.

The greening policy effects on AQ and urban thermal comfort in the present and in the future, were evaluated, simulating the follow scenarios: (1) real base case (Base Case - Actual Trees scenario); (2) tree planting (Base Case - Added Trees scenario) scenario; (3) Future Case - Actual Trees scenario and (4) Future Case - Added Trees scenario. The trees were added along the street using new parametrization for vegetate areas, using the urban spatially varying roughness (USVR) map in the complex terrain module. This methodology was described in detail, and its inclusion in ADMS-Urban models significantly improves the agreement of the simulations with observations. The future case was derived using as meteorological input the output of running with the mesoscale numerical weather prediction model WRF. The concentration differences were calculated between Actual Trees and Added Trees scenarios in both present and future case. The results highlight clearly the presence of areas of reduced and increased NO_x concentrations, with a slightly higher decrease in the future than in the present. About the UHI analysis, the urban heat island of Bologna tends to increase in the future as a result of climate change. The temperature differences, calculated between Actual Trees and Added Trees scenarios in both present and future case, shows the same reduction values, with a slightly different pattern with a smaller spatial area for Future case than in the Base Case.

5 FORECASTING TOOL

In a city like Bologna, affected by significant levels of traffic (as extensively discussed in previous chapters), cyclists and pedestrians can be the most exposed to pollution and extreme heat situations (i.e. heat waves, see section 2.3). In this context, the users need specific tools capable of providing forecasts on AQ and other environmental parameters to assess and choose the city areas that is better. The tools currently available are AQ indices processed on the data measured at the monitoring stations, or pollution maps with regional resolution. To date, there is no tool that can predict whether a road has a higher or lower air quality/thermal comfort in respect to another road. This chapter illustrates the path that led to the development of the high resolution air quality, temperature and humidity forecasting tool for the city of Bologna (Figure 67).

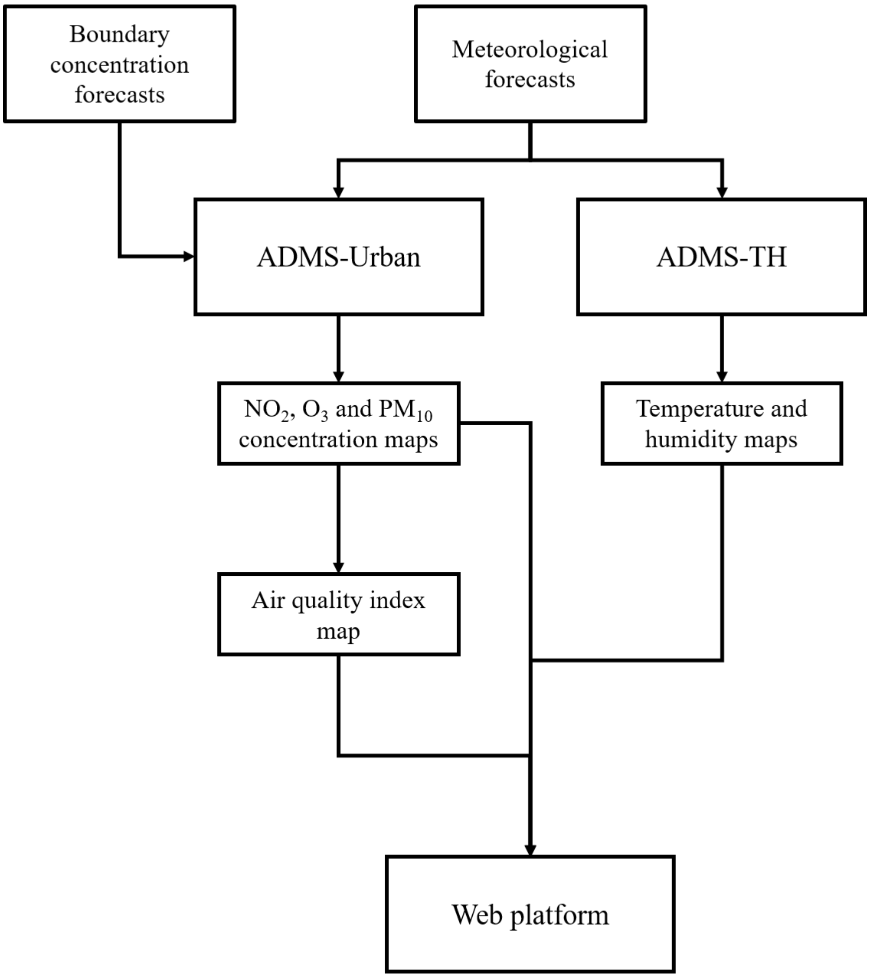

Figure 67. Summary diagram of the forecasting tool: the meteorological forecast and background concentration datasets are used as inputs in the ADMS-Urban model for pollutant forecasting and in the ADMS-TH model for temperature and humidity forecasting. The outputs of the models are processed to obtain maps of: pollutant concentration, AQ index, air temperature and air relative humidity, which are provided to the end-user through a web platform.

The implemented forecasting tool allows to obtain the necessary inputs and to create the files required by the models, to start the simulations for both ADMS-Urban model and ADMS-TH model and to process the results to obtain the maps of pollutant concentration (NO_2, O_3 and PM_{10}), AQ index, air temperature, and air relative humidity, which will be displayed to the end users through a web platform.

In the following sections, the methodology, the implementation of the code that allows to automate the various pieces that make up the forecasting tool, the results obtained and the public accessibility to the forecasts will be illustrated.

5.1 Forecasting methodology

The AQ monitoring, analysis and forecasting systems should operate at different spatial scales from the global scale to urban scales. Thanks to research advancement, high-performance computational resources, and data access, a full chain of multi-scale AQ modelling and forecasting can be build (Baklanov and Zhang, 2020). Since the complexity in the modeling unfolds, as the scale gets finer, in terms of geospatial data and its physic-chemical interactions with the atmosphere, the fine scale models need to be integrated with coarser scale models to get realistic initial and boundary conditions (Kadaverugu et al., 2019). There are some recent examples where mesoscale models of weather and chemistry are coupled with dispersion models at urban scale. CALIOPE-Urban (Benavides et al., 2019) is a coupled regional- to street-scale modelling system, comprising the mesoscale AQ forecasting system CALIOPE with the urban roadway dispersion model, R-LINE. The coupled system shows better agreement in highly trafficked areas, while, overestimates spatially close to highly trafficked areas. Hood et al. (2018) have tested a coupled regional-to-local modelling system comprising a regional chemistry–climate model with 5 km horizontal resolution (EMEP4UK) and an urban dispersion and chemistry model with explicit road source emissions (ADMS-Urban). The results of the test show that the regional model underestimates concentrations of gases at near-road sites, while the urban and coupled models both show good agreement compared to measurements.

ADMS models (ADMS-Urban and ADMS-TH) can be used in forecasting mode (Hood et al., 2017), using numerical forecasts of meteorological variables and boundary pollutant concentrations as meteorological input and background respectively. The meteorological forecasts and concentration forecasts for Bologna are provided as open data by ARPAE. The meteorological forecasts and concentration forecasts as well as the results of the two models were validated with data measured by reference monitoring stations. Following the logical flow presented in the summary scheme, detailed information on the datasets used, the validation, the processing of the variables considered and the calculation of the AQ index for Bologna are provided below.

5.1.1 Input for ADMS models

The meteorological forecast dataset provided by ARPAE contains the numerical weather forecasts for Emilia Romagna in GRIB (GRIdded Binary or General Regularly-distributed Information in Binary form[3]) format. The forecasts are produced by Arpae Emilia-Romagna and based on the COSMO numerical meteorological model. The COSMO model is developed and managed by a European Consortium among the various National Meteorological Services, called COSMO. At a national level, an agreement called Lami was stipulated between the Meteorological Service of the Air Force, the IdroMeteoClima Service (SIMC) of Arpae Emilia-Romagna and Arpa Piemonte for the development and operational management of national forecast numerical chains in Italy. Within Lami, Arpae manages the Cosmo 5M and Cosmo 2I operating chains, which respectively provide numerical forecasts on the Mediterranean area with a grid pitch of 5 km and on the national territory with a grid pitch of 2.2 km. All processing is performed on the supercomputing systems of CINECA, on the basis of a contract stipulated with the IdroMeteoClima Service and the Department of National Civil Protection. COSMO-5M data are produced twice a day (00 and 12 UTC), on a grid that covers the entire Mediterranean Sea with a step of 5 km and with a time horizon of 72 hours, and are available from 03/07/2018. The initial analysis is produced by the analysis system of the Air Force Meteorological Service, the boundary conditions come from The European Centre for Medium-Range Weather Forecasts (ECMWF) forecasts. COSMO-2I data are produced twice a day (00 and 12 UTC), on a grid covering Italy with a pitch of 2.2 km and with a time horizon of 48 hours, and are available from 06/02/2020. The initial analysis is produced by Arpae-SIMC with a continuous data assimilation system that uses measurements provided by the Meteorological Service of the Air Force, the surrounding conditions come from COSMO-5M forecasts. For the purposes of this Thesis, the COSMO-2I dataset was used (available on https://dati.arpae.it/dataset/previsioni-meteorologiche-numeriche-emilia-romagna).

Each GRIB file contains information on: geographical coordinates, date and meteorological variables. MET files, which are needed as input to ADMS models were obtained from GRIB files. For this purpose, a code in python language was developed to download the GRIB files needed and to extract the hourly values of the meteorological variables in correspondence with the LIPE station.

In order to evaluate and validate the meteorological forecasts, the forecasted values were compared with the observed data from airport weather station (LIPE) available as open data on https://www.ogimet.com/metars.phtml.en. For this analysis a period of one year (from 25/10/2020 to 20/10/2021) was considered in order to take into account the seasonal variations of the weather parameters. In general, the statistical indexes (Table

[3] This is a concise data format commonly used in meteorology to store historical and forecast weather data.

23) indicate a quite satisfactory agreement between simulated and measured data, which is confirmed also by the time series of forecasted values (mod) and measured data (obs) (Figure 68).

Variable	$Mean_{obs}$	$Mean_{mod}$	SD_{obs}	SD_{mod}	MB	NMSE	R	Fac2	Fb
Air temperature (°C)	15.5	13.8	8.0	8.1	-1.7	0.0	1.0	0.9	-0.1
Air relative Humidity (%)	69.0	68.0	16.9	15.7	-0.9	0.0	0.8	1.0	0.0

Table 23. Statistical indices calculated to compare forecasted (mod) and measured values (obs) of air temperature and air relative humidity at the LIPE meteorological station in Bologna for the period from 25/10/2020 to 20/10/2021. SD: Standard deviation; MB: mean bias; NMSE: normalized mean square error; R: Pearson's correlation coefficient; Fac2: factor of two; Fb: fractional bias.

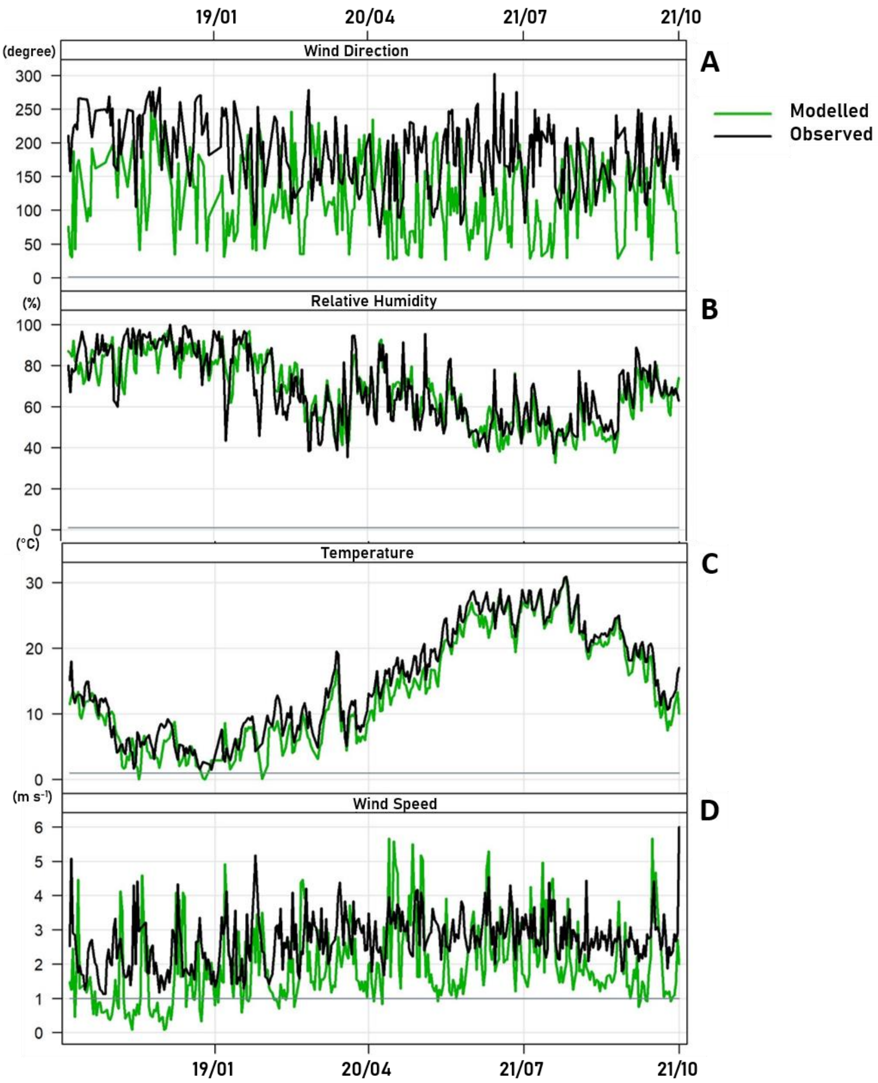

Figure 68. Time series of modelled (green line) and observed (black line) daily averages of A) wind direction, B) air temperature, C) air relative humidity and D) wind speed at the LIPE weather station for the period from 25/10/2020 to 20/10/2021.

In particular, the forecasted values of temperature and relative humidity match perfectly the observations, while the simulated values of wind direction and intensity present some discrepancies from the measurements. Indeed, the simulations of wind direction present a higher frequency of wind coming from NNE with relatively higher speeds than the measured data (Figure 69).

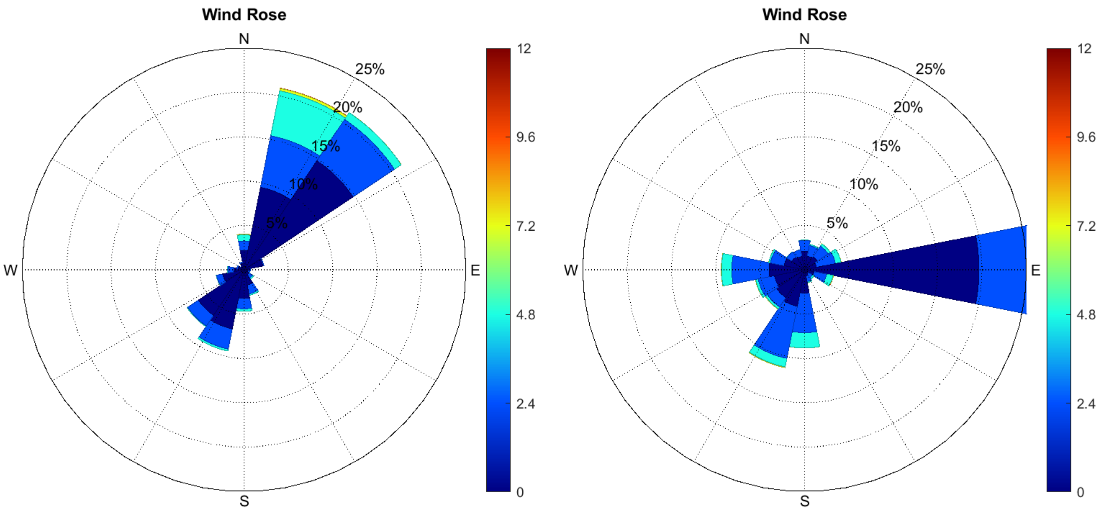

Figure 69. Wind rose obtained from wind speed and directions at the LIPE station from the COSMO model (left) and from observations (right) in the period from 25/10/2020 to 20/10/2021.

The pollutant concentration forecast dataset in netCDF (Network Common Data Form[4]) format, is provided by the ARPAE modeling chain called NINFA (Northern Italy Network for Photochemical Smog and Aerosol forecasts). The NINFA suite is based on the regional version of the CHIMERE chemical transport model, combined with the COSMO meteorological model. The pollutant concentrations at the edges of the NINFA simulation domain (boundary conditions) are provided by both the PREV'AIR air quality modeling system and the national scale model currently under development under the SNPA (National Environmental Protection System). CHIMERE is an open-access multi-scale Eulerian chemistry transport model mainly intended to produce hourly forecasts of several aerosol and gaseous pollutant concentrations. The concentrations are computed by solving the continuity equation for processes such as emissions, transport, deposition, chemical reactions, and aerosol dynamics.

For the purposes of this Thesis, the CHIMERE dataset was used (not yet available in open data mode to the public). Each netCDF file contains information on: geographical coordinates, date and pollutant concentrations. BGD files, needed as input to ADMS-urban model, were obtained from netCDF files. The BGD file must contain hourly data

[4] It is a set of software libraries and self-describing, machine-independent data formats that support the creation, access, and sharing of array-oriented scientific data

of the pollutant concentrations (NO_2, O_3, PM_{10}) foreseen at the coordinates that identify the ARPAE AQ stations (SF, VC and GM). For this purpose, a code in python language was written to download the netCDF files and to extract hourly pollutant concentration values in correspondence with the AQ stations.

In order to evaluate and validate the forecasts of pollutant concentrations, the forecasted values were compared with the observations at two ARPAE AQ stations (GM and VC) available on https://sdati-test.datamb.it/arex/. For this analysis a period of one year (from 13/10/2020 to 12/10/2021) was considered in order to take into account the seasonal variability of pollutant concentrations. The time series of simulated values (mod) and measured data (obs) indicate the tendency for the model to overestimate the observations for all pollutant species and in particular for NO_2 and O_3 at both stations (Figure 70 and Figure 71).

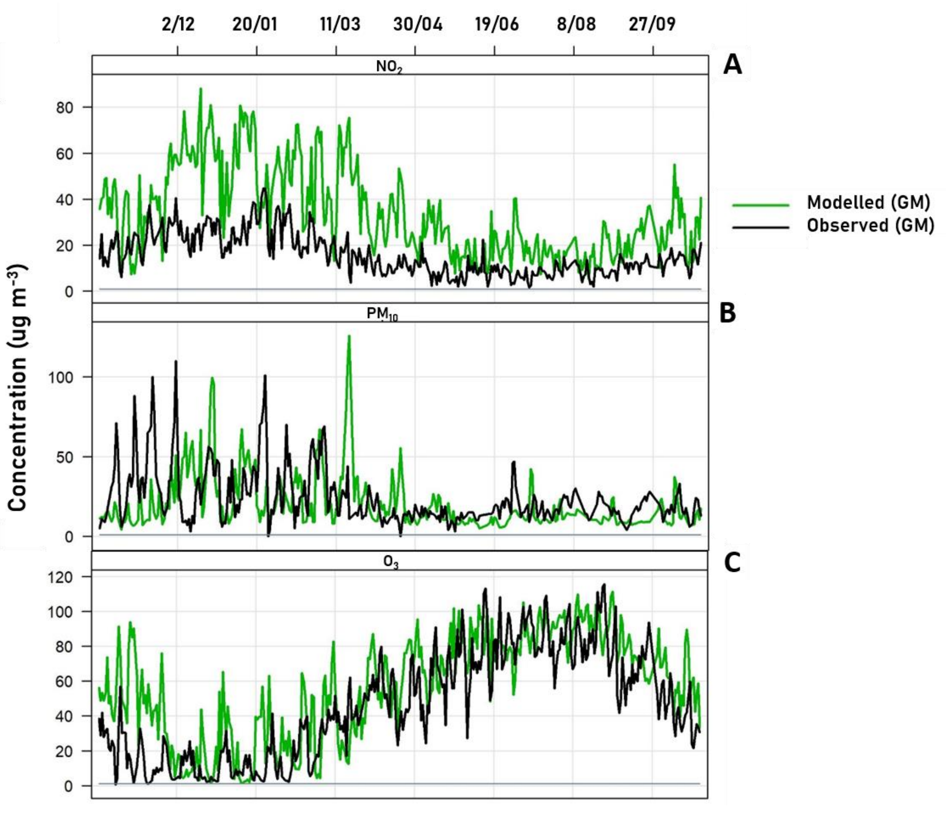

Figure 70. Time series of modelled (green line) and observed (black line) daily averages of A) NO_2, B) PM_{10}, C) O_3 concentration at the Giardini Margherita (GM) ARPAE AQ station for the period from 13/10/2020 to 12/10/2021.

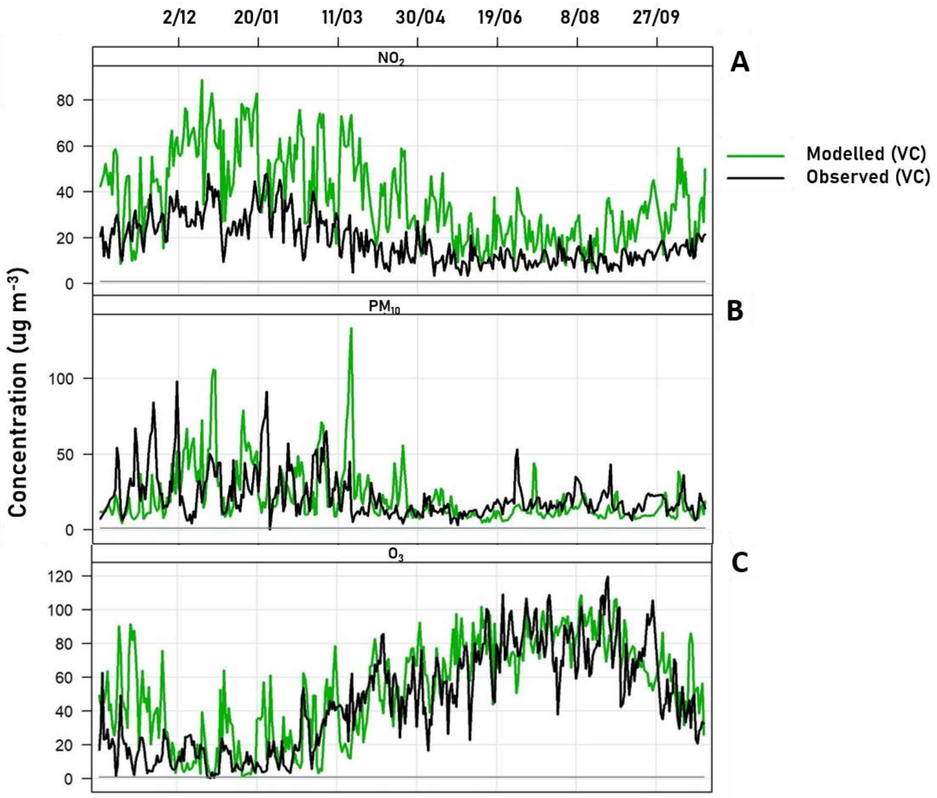

Figure 71. Time series of modelled (green line) and observed (black line) daily averages of A) NO_2, B) PM_{10}, C) O_3 concentration at the Via Chiarini (VC) ARPAE AQ station for the period from 13/10/2020 to 12/10/2021.

The overestimation is greater in the winter period for O_3 concentrations, while for NO_2 concentrations the overestimation concerns all seasons. The overestimation of the CHIMERE simulations implies that the dataset used as background concentrations in input to the ADMS model presents higher values than the observed one, resulting in a consequent overestimation of the simulations from ADMS Model. The statistical parameters (Table 24) however indicate a good agreement between simulations and observations, highlighting the overestimation already identified previously.

Station	Pollutant	$Mean_{obs}$	$Mean_{mod}$	SD_{obs}	SD_{mod}	MB	NMSE	R	Fac2	Fb
GM	**NO_2**	15.71	33.81	9.07	19.19	18.1	1.1	0.6	0.4	0.7
GM	**O_3**	45.82	56.75	30.91	29.56	10.9	0.2	0.8	0.7	0.2
GM	**PM_{10}**	24.11	20.34	17.50	17.14	-3.8	1.0	0.2	0.6	-0.2
VC	**NO_2**	18.50	36.69	9.95	18.80	18.2	0.8	0.6	0.5	0.7
VC	**O_3**	45.49	53.33	29.96	28.77	7.8	0.2	0.7	0.7	0.2
VC	**PM_{10}**	21.93	21.27	15.01	18.52	-0.7	1.0	0.2	0.6	0.0

Table 24. Statistical indices comparing the simulated (mod) and observations (obs) of NO_2, O_3, PM_{10} pollutant concentrations at the two the ARPAE background AQ stations (Giardini Margherita (GM) and Via Chiarini (VC)) in Bologna for the period from 13/10/2020 to 12/10/2021. SD: Standard deviation; MB: mean bias; NMSE: normalized mean square error; R: Pearson's correlation coefficient; Fac2: factor of two; Fb: fractional bias.

Furthermore, the numerical outputs of CHIMERE model fulfill the recommended statistical criteria for most pollutant at both stations, specifically NMSE ≤ 1.5 for all pollutant, Fac2 ≥ 0.5 for NO_2 and PM_{10} and $-0.3 \leq Fb \leq 0.3$ for O_3 and PM_{10} (Di Sabatino et al., 2011) while R value is very low for PM_{10}.

5.1.2 Setup of the ADMS models

This section illustrates the methodology followed to simulate the concentrations of the selected pollutants (NO_2, O_3, PM_{10}), the air temperature and air humidity, and to calculate the AQ index for the city of Bologna. In the forecasting tool, the two models presented previously, the ADMS-Urban and the ADMS-TH, were used. In both models, the domain considered is 10x20 km with a resolution of 200x200 m.

The ADMS-Urban dispersion model was used to simulate the concentration of NO_2, O_3, PM_{10} for the city of Bologna. The simulations provide as output the forecast of the spatial variation of pollutant concentrations with an hourly time resolution. The emission inventory previously presented in section 2.2.4 based on traffic flow counts provided by municipality was used. Following, the simulations are ingested with forecasted meteorological variables at the Bologna airport weather station (LIPE), and with forecasted background pollutant concentration at two ARPAE monitoring stations (VC and GM). Furthermore, the chemical module was set up and for complex terrain module the USVR (see section 4.3) was used.

The ADMS-TH module was used to simulate temperature and humidity for the city of Bologna. The simulations provide forecasts of the spatial variations of temperature and humidity values, with an hourly time resolution. The input datasets contained hourly forecast values on the Bologna airport weather station (LIPE). The land use data, such as the spatial variation of the surface resistance to evaporation, the surface roughness, the surface albedo, the thermal admittance and the normalized building volume are calculated as described in section 4.2.1.1.

5.1.3 Performance evaluation of the ADMS models

In order to evaluate the performance of the forecasting tool, the outputs of the two models were compared with hourly data observed at several ARPAE reference stations (SF, GM and VC for air quality and BU, Mz for meteorological variables). In particular, the performance of the models was evaluated by calculating the set of indicators described in section 3.2.5.

5.1.3.1 Air pollutants

The validation of dispersion simulations carried out in forecasting mode was performed comparing hourly concentrations of pollutants (NO_2, O_3, and PM_{10}) observed at the fixed

AQ measuring stations (SF, GM and VC stations) with the forecasts simulated with the ADMS-Urban model during the period from 13/11/2021 to 15/12/2021. In general, the statistical parameters (Table 25) indicate a poor performance of the model, with low correlation coefficients (0.4< R < 0.6).

Station	Pollutant	$Mean_{Obs} \pm SD$	$Mean_{Mod} \pm SD$	MB	NMSE	R	Fac2	Fb
SF	NO_2	70.5 ± 17.1	71.9 ± 25.2	1.4	0.1	0.4	0.9	0.0
SF	PM_{10}	27.9 ± 12.5	35.1 ± 18.9	7.2	0.3	0.5	0.8	0.2
GM	NO_2	28.9 ± 11.5	53.7 ± 20.6	24.8	0.6	0.4	0.6	0.6
GM	O_3	13.6 ± 14.8	17.2 ± 20.2	3.7	1.3	0.6	0.3	0.2
GM	PM_{10}	24.5 ± 11.8	30.8 ± 18.5	6.3	0.4	0.6	0.8	0.2
VC	NO_2	27.5 ± 10.0	54.0 ± 20.7	26.5	0.7	0.5	0.5	0.7
VC	O_3	9.9 ± 12.7	17.5 ± 20.2	7.6	1.9	0.6	0.4	0.6
VC	PM_{10}	23.1 ± 11.2	30.8 ± 18.4	7.6	0.5	0.5	0.7	0.3

Table 25. Statistical indices calculated to compare the simulated data (mod) of pollutant concentrations with the measured values (obs) in the ARPAE background AQ stations (Porta S. Felice (SF), Giardini Margherita (GM) and Via Chiarini (VC)) in Bologna for the period from 13/11/2021 to 15/12/2021. SD: Standard deviation; MB: mean bias; NMSE: normalized mean square error; R: Pearson's correlation coefficient; Fac2: factor of two; Fb: fractional bias.

Despite this result, the numerical outputs obtained for SF stations fulfill the recommended statistical criteria for the NMSE, Fac2 and Fb parameters, specifically NMSE ≤ 1.5, Fac2 ≥ 0.5 and –0.3 ≤ Fb ≤ 0.3 (Di Sabatino et al., 2011). The evaluation shows an overestimation of the model's output compared to the observations for NO_2 concentration in GM and VC stations (Table 25), as indicated by the fractional bias values, and as clearly shown in Figure 73. Figure 72 represents the comparison of hourly simulated and observed NO_2, O_3 and PM_{10} concentrations averaged over all stations. The modeled data are comparable with the observed ones, indicating a good temporal representation of the pollutant dispersion over the domain.

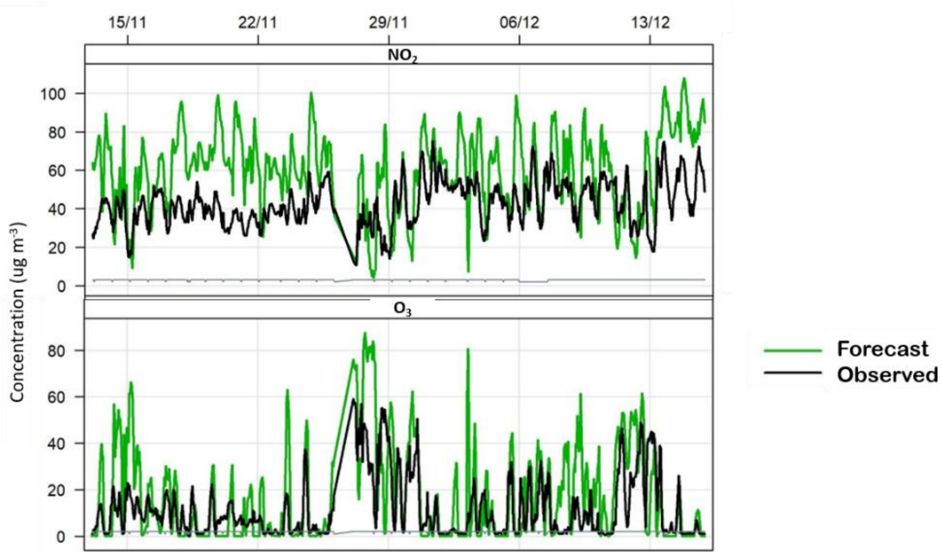

Figure 72. Time series of modelled (green line) and observed (black line) hourly averages of NO_2 (top) and O_3 (bottom) concentration averaged over all ARPAE AQ stations: Porta S. Felice, Giardini Margherita (GM) and Via Chiarini (VC) for the period from 13/11/2021 to 15/12/2021.

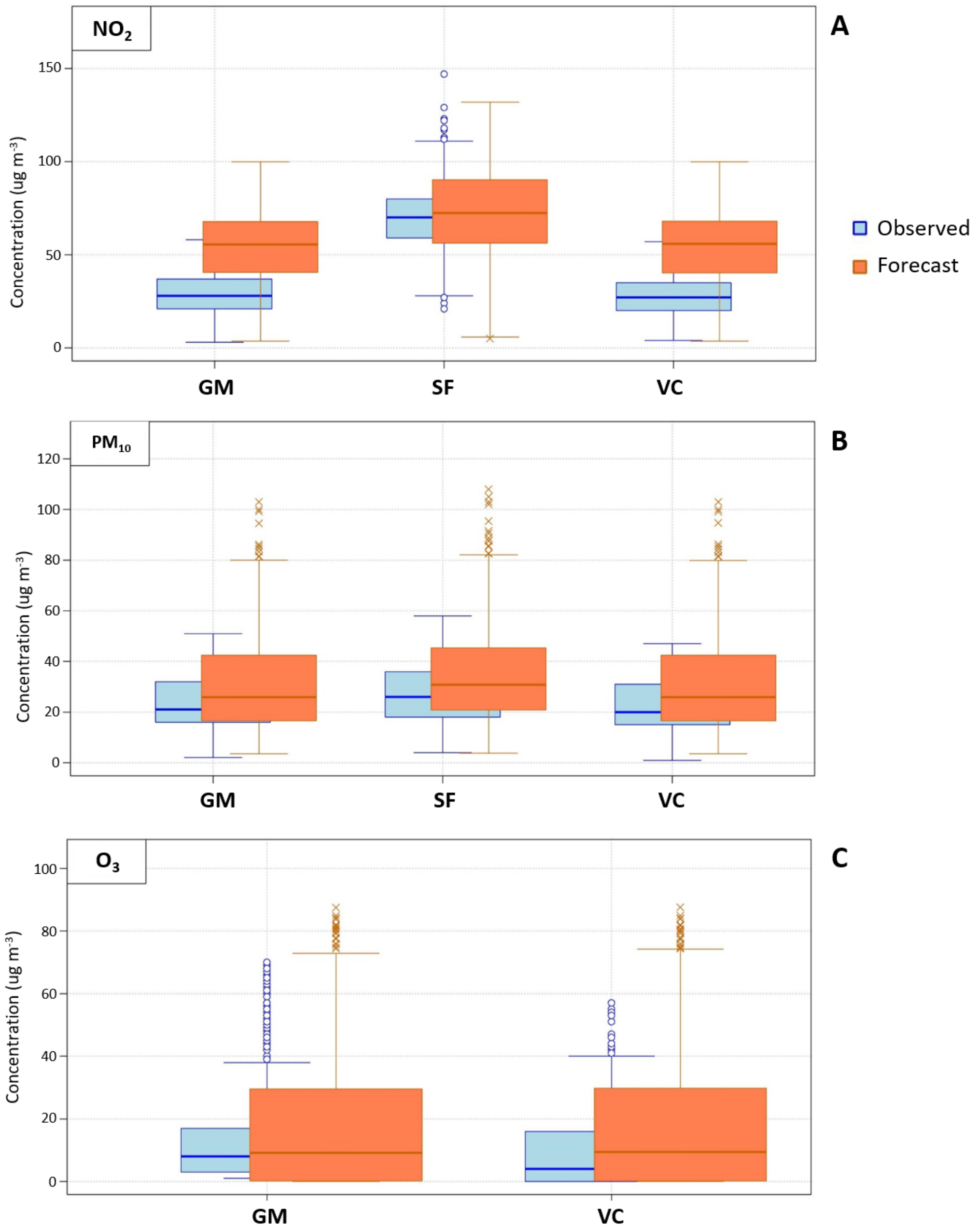

Figure 73. scatter plot of modelled (orange) and observed (blue) A) NO_2, B) O_3, C) PM_{10} concentration at ARPAE AQ stations: Porta S. Felice (SF), Giardini Margherita (GM) and Via Chiarini (VC) for the period from 13/11/2021 to 15/12/2021.

The overestimation of the model concentration, already highlighted by Fb, concerns in particular the NO_2 concentrations at the two background stations and the maximum concentrations of PM_{10} and O_3 (Figure 73). This overestimation is attributed to the overestimation of the background concentrations in the CHIMERE forecast model, as already discussed in section 5.1.1.

5.1.3.2 Temperature and humidity

The validation of temperature and humidity forecast was performed comparing hourly data observed at the fixed weather measuring stations (urban station: Bologna Urbana (BU) and rural station: Mezzolara (Mz), see section 3.2.2) with the forecasts from the ADMS-TH model during the period from 13/11/2021 to 15/12/2021. In general, the statistical parameters (Table 26) indicate a good performance of the model, with particularly elevated correlation coefficients for the urban site and for temperature at the rural site.

Station	Variable	$Mean_{Obs}$ ± SD	$Mean_{Mod}$ ± SD	MB	NMSE	R	Fac2	Fb
BU	T	7.0 ± 2.8	8.5 ± 3.3	1.5	0.1	0.8	1.0	0.2
BU	RH	75.5 ± 17.5	63.9 ± 8.4	-11.6	0.1	0.6	1.0	-0.2
Mz	T	7.0 ± 3.1	8.3 ± 3.3	1.4	0.1	0.9	1.0	0.2
Mz	RH	85.6 ± 9.7	70.0 ± 6.9	-15.6	0.1	0.2	1.0	-0.2

Table 26. Statistical indices comparing the simulations (mod) and observations of temperature and humidity at twoARPAE weather stations (Bologna Urbana (BU) and Mezzolara (MZ)) for the period from 13/11/2021 to 15/12/2021. SD: Standard deviation; MB: mean bias; NMSE: normalized mean square error; R: Pearson's correlation coefficient; Fac2: factor of two; Fb: fractional bias.

The evaluation shows an overestimation of the model's output compared to the observations for temperature as clearly shown in Figure 74 (A and B), and an underestimation of relative humidity values especially for the rural site. Figure 74 (C and D) represents the comparison of hourly simulated and observed values of temperature and relative humidity averaged over all stations. The modeled data are comparable with the observed ones, indicating a good temporal representation of the variables over the domain.

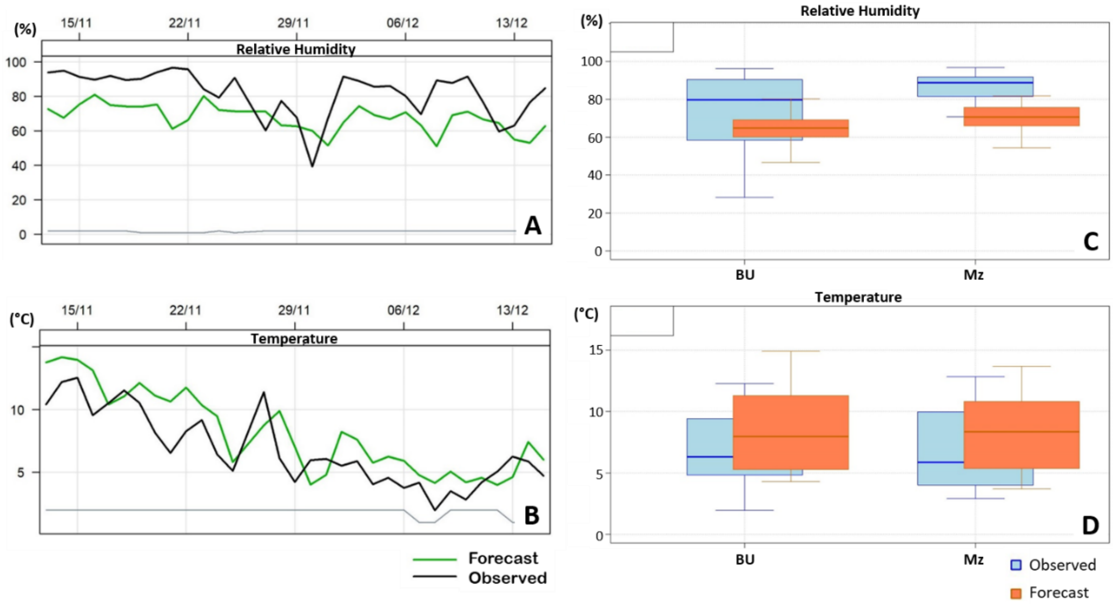

Figure 74. Time series and scatter plot of modelled and observed hourly average of temperature and humidity averaged over all ARPAE weather stations: Bologna Urbana (BU) and Mezzolara (Mz) for the period from 13/11/2021 to 15/12/2021. A and B) time series: modelled values in green line and observed data in black line; C and D) scatter plot: modelled values in orange and observed data in blue.

The underestimation of humidity is due to the period considered in simulation carried out in order to evaluate the performance of the model. In fact, the evaluation was made on the period from November to December, generally affected by rain and fog phenomena not considered in the forecasting tool. The choice of this period was dictated by the date of finalization of the tool.

5.1.4 BLQ-Air Index

Most air pollution control policies are based on the quantitative assessment of pollution levels. An AQ index is a combination of pollutants levels based on a classification scale anchored to legal limits and / or impacts on human health. Typically, these classification models consider only the worst pollutant, that is, the one with higher concentration than others. In identifying an AQ index suitable for the city of Bologna, I started from the cityAIR index (Silva and Mendes, 2011). The mathematical formulation of cityAIR follows two fundamental points: when the concentration of one of the pollutants considered exceeds the legal limits, this pollutant will be the only one relevant for the calculation of the index; when there is no violation of the limit, all pollutants are considered for the overall air quality, which is calculated by combining concentrations and considering several criteria.

$$cityAIR = \sum_i w_i c_i \prod_i v_i$$

where w_i is the relative weight of the pollutant *i*; c_i is the normalized concentration of the pollutant *i*; v_i is the dummy variable of the legal limit violation $L_i$of pollutant *i*, defined as follows:

$v_i = 1$ when $c_i \leq L_i$

$v_i = 0$ when $c_i > L_i$

The Bologna AQ index (BLQ-Air index) was designed to provide a qualitative estimate of the air quality, easy to understand and of immediate interpretation. BLQ-Air index is a spatial index, and unlike the commonly used indexes, it needs not to standardize the information to a single color. For example, in case the estimated concentration for a certain hour of a given day should be "bad", this index should be able to visually provide the " more bad" and "least bad" areas. A simple color scale to be associated with the index could be composed of three colors: green when all pollutants are below the limits, orange when a pollutant exceeding the limit, and Red when all pollutants exceed the limits. The use of the original cityAIR index formulation emphasizes the overcoming of the limits, and in particular the overcoming of the one with the highest limit:

$$BLQ - Air = \sum_i w_i c_i \prod_i v_i$$

$c_i^* = \frac{C_i - C_{min}}{C_{max} - C_{min}}$ = standardized concentration of pollutant *i* *(NO_2, O_3 and PM_{10})*,

$w_i = 1\ if\ c_i > L_i\ else\ 0$ = dummy variable of the legal limit violation Li of pollutant *i* *(NO_2, O_3 and PM_{10})*,

$v_i = 0.33$ = is the relative weight of the pollutant *i* *(NO_2, O_3 and PM_{10})*,

L_i = legal limit violation of pollutant *i* *(NO_2= 200 ug/m^3; O_3= 180 ug/m^3 and PM_{10}= 50 ug/m^3)*.

This type of formulation assigns w_i = 0 if the pollutant does not exceed the limit, therefore the index will be different from zero only in case all pollutants exceed the limit and the associated color scale will therefore indicate green until all pollutants do not exceed the limit. An index thus formulated (Figure 75A) does not provide therefore the expected information, and flattens the information to only two alternatives: exceeded limits or not exceeded limits. To avoid this, in this Thesis the assignment of the value to w_i has been changed: $w_i = 1\ if\ c_i > L_i\ else\ 0.33$ (Figure 75B).

C_i	BLQ-Air
< 50	0
50 > c_i <200	0
>200	8

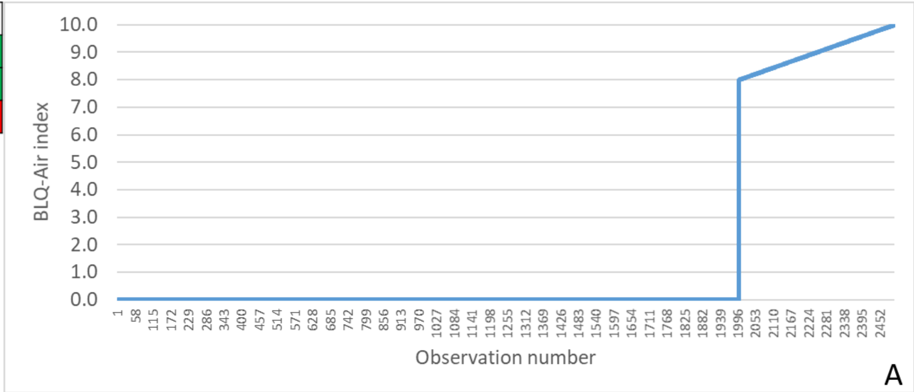

C_i	BLQ-Air
< 50	0
51-180	2-8
181-200	9-26
>200	>26

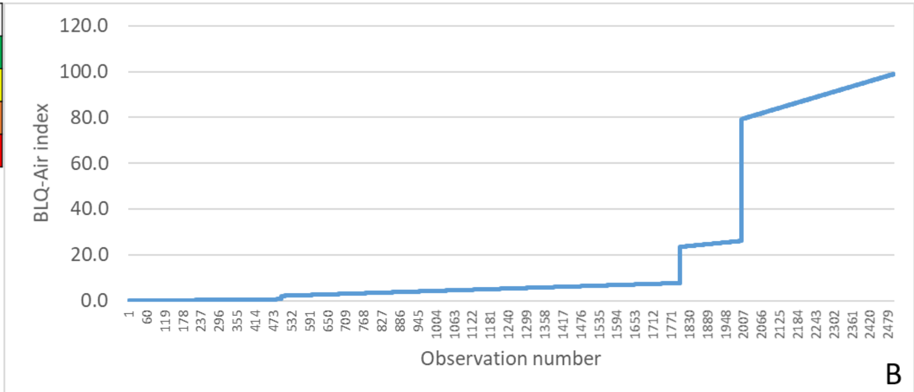

C_i	BLQ-Air
< 25	Clean air (<0.4)
26 - 50	Good (0.5-2.0)
51 - 80	Low (2.1-5.0)
81 - 100	Moderate (5.1-9.0)
101 - 180	Poor (9.1-18.0)
181 - 200	Very poor (19.0-50.0)
> 200	Severe (>50.0)

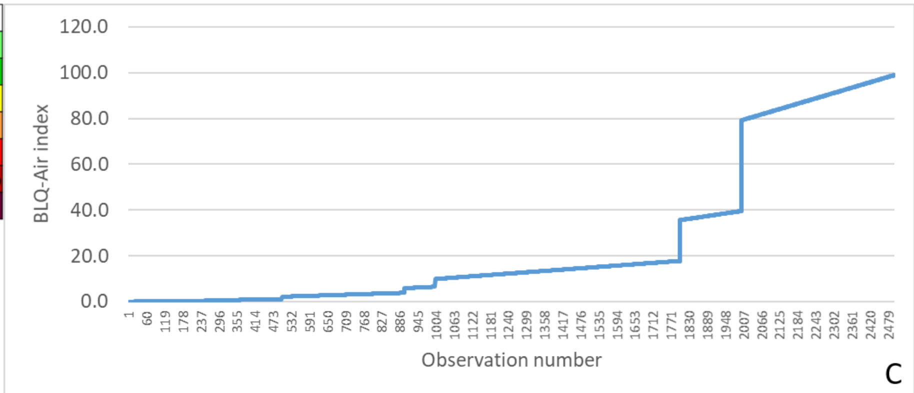

Figure 75. Formulations of the BLQ-Air index and related color scale: A) $w_i = 1\ if\ c_i > L_i\ else\ 0$; B) $w_i = 1\ if\ c_i > L_i\ else\ 0.33$ And C) $w_i = 1\ if\ C_i > L_i; 0.5\ if\ C_i > {}^1/_2\, L_i\ else\ 0.33$. In the tables with the color scale, the index value (BLQ-Air) and the relative concentration value (c_i) are indicated for each color.

With this new formulation, the index has a scale indicating green for no violation of the limits, yellow for a violation of one limit, orange for two violations and red for three violations. A further improvement concerns the cases falling in the green color: also in this case the values assigned to w_i were changed: $w_i = 1\ if\ C_i > L_i; 0.5\ if\ C_i > {}^1/_2\, L_i\ else\ 0.33$ (Figure 75C). This approach is based on the identification of a lower limit for each pollutant, for this purpose half of L_i was considered as the lower limit.

5.2 Coding

In this Thesis, Python programming language was used to develop the forecast tool because it is frequently used for data analysis and there are many libraries, such as Pandas, that can be used for data processing. Python is a Very High Level Programming Language and an Object Oriented Dynamic Language, widely used in science in the fields of numeric programming, artificial intelligence, image processing, biology and others. The definitions (functions and variables) introduced in the Python interpreter are lost every time it is terminated. Therefore, Python allows you to put the definitions in a file and use them in a script or in an interactive interpreter session. Such a file is called a module; definitions in one module can be imported into other modules. This aspect makes Python ideal as a scripting language within bigger scripts, as required in this Thesis.

5.2.1 Code setup

Several Python libraries were used in this project such as Pandas, Numpy, Matplotlib, etc. Following, the main libraries, modules and package used are described briefly.

1. Pandas (http://pandas.pydata.org/) is a library for manipulating data in sequential or tabular format, such as time series or microarray data. The main features of Pandas are:
   - Loading and saving standard formats for tabular data, such as CSV (Comma-Separated Values), TSV (Tab-Separated Values), Excel files, and database formats
   - Simplicity in performing indexing and data aggregation operations
   - Simplicity in the execution of numerical and statistical operations
   - Simplicity in viewing the results of operations
2. The NumPy (https://numpy.org/) library allows to work with vectors and matrices more efficiently and quickly than with lists and lists of lists (matrices). The basic construct is the ndarray, which can be of any size. One of the strengths of NumPy is to be able to work on vectors by exploiting the vector calculation optimizations of the machine's processor. This makes calculations particularly efficient, compared to lists.
3. Matplotlib (https://matplotlib.org/) is a 2d and 3d graphing library for the Python programming language.
4. Pygrib (https://pypi.org/project/pygrib/2.0.5/) is a Python module for reading and writing GRIB files (edition 1 and edition 2). GRIB is the WMO standard file format for the exchange of weather data.
5. Netcdf4 (https://unidata.github.io/netcdf4-python/) is a Python interface to the netCDF C library. This module can read and write files in both the new netCDF

4 and the old netCDF 3 format. NetCDF is a set of "platform independent" self-describing software and data libraries (independent of the Operating System) for the creation, access, modification and sharing of "array oriented" data ("grid data"), developed and maintained by the UNIDATA program at UCAR (University Corporation for Atmospheric Research).

6. The math module (https://docs.python.org/3/library/math.html) is a standard module in Python and is always available. This module provides access to the mathematical functions defined by the C standard.
7. The OS module (https://docs.python.org/3/library/os.html) of the Python language has several useful functions for making the program interact with the computer's operating system (Windows, Linux or Mac OS).
8. The sys module (https://docs.python.org/3/library/sys.html) is one of the basic packages included in the Python Standard Library. It contains a series of functions and parameters that will be very useful every time our program has to interact with the operating system you are working on.
9. The io module (https://docs.python.org/3/library/io.html) provides Python's main facilities for dealing with various types of I/O. There are three main types of I/O: text I/O, binary I/O and raw I/O. These are generic categories, and various backing stores can be used for each of them. A concrete object belonging to any of these categories is called a file object, so io module allows to manage file objects, such as to create files in a given directory.
10. The datetime module (https://docs.python.org/3/library/datetime.html) provides classes to manipulate dates and times, the implementation of the module focuses above all on an efficient extraction of the components, for the manipulation and formatting of the output.
11. The dateutil module (https://pypi.org/project/python-dateutil/) provides powerful extensions to the standard datetime module, available in Python.
12. The httplib2 module (https://pypi.org/project/httplib2/) is a comprehensive HTTP client library, defines the classes that implement the client side of the HTTP and HTTPS protocols.
13. MetPy (https://unidata.github.io/MetPy/latest/index.html) is a collection of tools in Python for reading, visualizing, and performing calculations with weather data.
14. Json (https://docs.python.org/3/library/json.html) is a lightweight data interchange format, it can be used to work with JSON data.
15. Zipfile (https://docs.python.org/3/library/zipfile.html) is a python module provides tools to create, read, write, append, and list a ZIP file.

In addition, a Google API was included within the forecasting tool code. Google APIs (https://github.com/googleapis) are application programming interfaces (APIs) developed by Google which allow communication with Google Services and their integration to other services. Examples of these include Search, Gmail, Translate or Google Maps. Third-party apps can use these APIs to take advantage of or extend the functionality of the existing services. The APIs provide functionality like analytics, machine learning as a service (the Prediction API) or access to user data (Drive API (V3), when permission to read the data is given).

5.2.2 Code elaboration/creation

In this project, the DRIVE API was used to allow access to Google drive services. In fact, the Drive API is required to access forecasting weather and AQ dataset stored in folders on google drive. In order to create a simple Python command-line application that makes requests to the Drive API, the following steps are needed:

1. Create a project and enable an API - This project forms the basis for creating, enabling, and using all Google Cloud services, including managing APIs, enabling billing, adding and removing collaborators, and managing permissions (for more information refers to https://developers.google.com/workspace/guides/create-project)
2. Create credentials for a desktop application - Credentials are used to obtain an access token from Google's authorization servers, so your app can call Google Workspace APIs (for more information, refers to https://developers.google.com/workspace/guides/create-credentials)
3. Install the Google client library
4. Configure the code (Figure 76 and Figure 77)

```python
#--------------------------------DATA from ARPAE
#--------- Cosmo forecast - Download
SCOPES = ['https://www.googleapis.com/auth/drive']# If modifying these scopes, delete the file token.json.
creds = None
# The file token.json stores the user's access and refresh tokens, and is
# created automatically when the authorization flow completes for the first time.
if os.path.exists('/home/PERSONALE/francesca.dinicola2/TPHD/tokenGDrive/token.json'):
    creds = Credentials.from_authorized_user_file('/home/PERSONALE/francesca.dinicola2/TPHD/tokenGDrive/token.json', SCOPES)
# If there are no (valid) credentials available, let the user log in.
if not creds or not creds.valid:
    if creds and creds.expired and creds.refresh_token:
      creds.refresh(Request())
    else:
        flow = InstalledAppFlow.from_client_secrets_file(
            '/home/PERSONALE/francesca.dinicola2/TPHD/tokenGDrive/client_secret_796322916484-qo98lnpunkc8srulqjel24qdi07b10ib.apps.googleusercontent.com.json', SCOPES)
        creds = flow.run_local_server(port=0)
    # Save the credentials for the next run
    with open('/home/PERSONALE/francesca.dinicola2/TPHD/tokenGDrive/token.json', 'w') as token:
        token.write(creds.to_json())

service = build('drive', 'v3', credentials=creds)
```

Figure 76. Python code example to authenticate and save the login credentials needed to use the Google drive API.

```python
# Call the Drive v3 API
nextpage=None
while True:
  results = service.files().list(
      pageSize=1000, fields="nextPageToken, files(id, name)",pageToken=nextpage,q="name='cosmo-2I_er'").
.execute()

  items = results.get('files', [])
  nextpage = results.get('nextPageToken', None)

  if not items:
      print('No files found.')
  else:
      #print('Files:')
      for item in items:
          print(u'{0} ({1})'.format(item['name'], item['id']))
          my_id=item['id']
  if nextpage == None:
    break

results=service.files().list(pageSize=2, fields="nextPageToken, files(id, name)",q="'"+my_id+"'"+' in
 parents',orderBy='name desc').execute()
items = results.get('files')
my_ids=[]
for item in items:
  print(u'{0} ({1})'.format(item['name'], item['id']))
  my_ids.append(item['id'])
```

Figure 77. Example of python code to call the Google drive V3 API and access the ARPAE "cosmo-2I_er" drive folder and download the weather forecast for the current day.

The purpose of these lines of code is to download the ARPAE forecasted weather data from the COSMO model: at this point the data is processed to obtain the input meteorological files (Figure 78) necessary for the ADMS-Urban and ADMS-TH models (Figure 79, see section 5.1.1).

```python
# U wind component at 10 metre (m/s) -> U
Idxs=[8,78,130,182,234,286,338,390,442,494,546,598]
Ucomp=[]
for Idx in Idxs:
  Ucomp.append(gr1[Idx].values[int(index_lat),int(index_lons)])
for Idx in Idxs:
  Ucomp.append(gr2[Idx].values[int(index_lat),int(index_lons)])

# V wind component at 10 metre (m/s)
Idxs=[9,79,131,183,235,287,339,391,443,495,547,599]
Vcomp=[]
for Idx in Idxs:
  Vcomp.append(gr1[Idx].values[int(index_lat),int(index_lons)])
for Idx in Idxs:
  Vcomp.append(gr2[Idx].values[int(index_lat),int(index_lons)])

# wind speed at 10 metre (U) --- (calm < 0.75)
U=[]
for a,b in zip(Ucomp,Vcomp):
  WS=math.sqrt(((pow(a,2))+(pow(b,2))))
  #U.append(int(WS))
  if round(WS,1)<=0.7:
    WS=0.8
  U.append(round(WS,1)) #una cifra dopo virgola

# Wind direction (degrees) -> PHI
def wind_uv_to_dir(U,V):
    WDIR= ((270-np.rad2deg(np.arctan2(V,U)))%360)-180
    cond=WDIR<0
    WDIR[cond]=WDIR[cond]+360
    return WDIR

PHI=np.around(wind_uv_to_dir(Ucomp,Vcomp),0)
```

Figure 78. Example of Python code to elaborate COSMO model forecasts and obtain the meteorological variables needed by the ADMS models.

The same procedure is used to access the ARPAE "sup" Drive folder to download the AQ forecasts of the CHIMERE model. Each variable needed in the final ADMS input file required a series of mathematical processing. As for the meteorological input data, i.e. the variables contained in the METEO.MET file, the following steps were performed:

- Coordinate identification of the LIPE station;
- Extraction of the variables in the point identified by the coordinates identified;
- Temperature conversion from kelvin to celsius;
- Calculation of wind speed from the x and y components of the wind;
- Calculation of the wind direction from the x and y components of the wind;
- Calculation of relative humidity from saturation vapor pressure and actual vapor pressure;
- Cloud cover conversion from decimal numbers to oktas;
- Creation of the final METEO.MET file with all the calculated variables.

For the background pollutant concentration input data, i.e. the variables contained in the BGD.bgd file, the following steps were performed:

- Coordinate identification of VC and GM reference stations;
- Extraction of the variables in the points identified by the coordinates identified;
- conversion of the concentration of NO_2 and O_3 from ppb to ug/m^3;
- Choice based on the hourly wind direction, from which reference station to take the hourly pollutant concentration data for the creation of the final file;
- Creation of the final BGD.bgd file with all pollutant concentrations selected.

```python
# .MET file creation
times = ['1','2','3','4','5','6','7','8','9','10','11','12','13','14','15','16','17','18','19','20','21','22','23','24']
YEAR = [str(datetime.date.today())[:4] for x in range(24)]
TDAY =['1' for x in range(24)] #modificare
THOUR = times

METDATA=pd.DataFrame.from_dict({
    'YEAR':YEAR,
    'TDAY' :TDAY,
    'THOUR' :THOUR,
    'T0C' :T0C,
    'RHUM':RHUM,
    'U' :U,
    'PHI' :PHI,
    'CL' :CL,
    'SOLAR RAD' :SOLAR_RAD
                        })
METDATA=METDATA[['YEAR','TDAY','THOUR','T0C','RHUM','U','PHI','CL','SOLAR RAD']]
METDATA.to_csv('Meteo.csv',index = False, header=False)
Meteo=open('Meteo.csv','r')
print('meteo.csv Done')

ADMS_input=open('METEO.MET','w')
ADMS_input_text='VARIABLES:'+'\n'+'9'+'\n'+'YEAR'+'\n'+'TDAY'+'\n'+'THOUR'+'\n'+'T0C'+'\n'+'RHUM'+'\n'+'U'+'\n'+'PHI'+'\n'+'CL'+'\n'+'SOLAR RAD'+'\n'+'DATA:'+'\n'
for line in Meteo:
  ADMS_input_text=ADMS_input_text+line

ADMS_input.write(ADMS_input_text)
ADMS_input.close()
```

Figure 79. Python code example to create the input MET file needed to run ADMS models.

Other important lines of code are the ones when the two ADMS models are called and run (Figure 80). The two models are executed in sequence and represent the part of the code that takes more time, in fact ADMS-Urban needs 2 hours and 15 minutes to finish a 24-hour simulation, while ADMS-TH takes 8 minutes and 34 seconds to a 24-hour simulation.

```python
#--------------------------------ADMS URBAN run
ADMScom='/home/PERSONALE/francesca.dinicola2/ADMS/ADMSUrbanModel.out /home/PERSONALE/francesca.dinicola2/TPHD/Urbanv1.UPL'
print('ADMS Urban run')
os.system(ADMScom)
print('ADMS Urban run Done')

#--------------------------------ADMS TH run
ADMScom='/home/PERSONALE/francesca.dinicola2/ADMS/ADMSUrbanModel.out /home/PERSONALE/francesca.dinicola2/TPHD/THv1.UPL'
print('ADMS T&H run')
os.system(ADMScom)
print('ADMS T&H run Done')
```

Figure 80. Python code example to call and start ADMS-Urban and ADMS-TH models.

The model outputs are then processed to produce related maps depicting the spatial variation of pollutant and meteorological variables as PNG (Figure 81) files. PNG is a file extension which stands for Portable Network Graphic, it is a raster graphic file format that supports lossless compression and is an open format with no copyright limit. Among the advantages of the PNG format, the possibility of using transparency and opacity is interesting. It also allows the use of color palettes and supports 24-bit RGB and 32-bit RGBA colors.

```
915 layer='PM10'
916 for z in range(len(zs)):
917   for hour in range(24):
918     #Change time zone
919     if hour==0:
920       filename=str(datetime.date.today()+datetime.timedelta(2))+'-'+str(hour).zfill(2)+'0000-'+
    +layer+'-'+str(zs[z]).zfill(2)
921       UTCtime=datetime.datetime.strptime(str(datetime.date.today()+datetime.timedelta(2))+' '+str(
    (hour).zfill(2)+':00', '%Y-%m-%d %H:%M').replace(tzinfo=from_zone)
922       italian_time=UTCtime.astimezone(to_zone)
923       descrizione=layer+' '+str(zs[z])+'m '+str(italian_time)[:-6]
924       date=str(datetime.date.today()+datetime.timedelta(2))+'T'+str(hour).zfill(2)+':00:00Z'
925       img=layers_PM10[z][23]
926     else:
927       filename=str(datetime.date.today()+datetime.timedelta(1))+'-'+str(hour).zfill(2)+'0000-'+
    +layer+'-'+str(zs[z]).zfill(2)
928       UTCtime=datetime.datetime.strptime(str(datetime.date.today()+datetime.timedelta(1))+' '+str(
    (hour).zfill(2)+':00', '%Y-%m-%d %H:%M').replace(tzinfo=from_zone)
929       italian_time=UTCtime.astimezone(to_zone)
930       descrizione=layer+' '+str(zs[z])+'m '+str(italian_time)[:-6]
931       date=str(datetime.date.today()+datetime.timedelta(1))+'T'+str(hour).zfill(2)+':00:00Z'
932       img=layers_PM10[z][hour-1]
933     metadata={'Id':filename,'Descr':descrizione,'Layer':layer,'Date':date,'Altitude':(zs[z]),
    'Opacity':1,'CornersLonLat': [[11.22831,44.56201],[11.45497,44.55236],[11.44221,44.46318],[11.21579
    ,44.47280]],'Source':filename+'.png'}
934     plt.imsave(filename+'.png',img,cmap=alpha_cmap,vmin=v_min,vmax=v_max)
935     zipObj.write(filename+'.png')
936     json['Datasets'].append(metadata)
937
938 FIGSIZE = (2,3)
939 mpb = plt.pcolormesh(img,cmap=alpha_cmap,vmin=v_min,vmax=v_max)
940 fig,ax = plt.subplots(figsize=FIGSIZE)
941 cb=plt.colorbar(mpb,ax=ax)
942 cb.ax.set_title('ug/m3')
943 ax.remove()
944 plt.savefig('Legend PM10.png',bbox_inches='tight',transparent=True)
945 zipObj.write('Legend PM10.png')
946 mpb.remove()
```

Figure 81. Example of python code to create PNG images, from line 917 to line 932 the code changes time zone from UTC to local so that the date of each image conforms to that used by the end user. The image metadata are created on the line 933 and will be added to the JSON archive (line 936).

For each pollutant (PM_{10}, NO_2 and O_3) 24 maps are created every day (one for each hour of the day, from 1:00 to 24:00 UTC) for 8 height levels (5, 10, 15, 20, 25, 30, 35 and 40 m above the ground). 24 maps (24 hours) for 8 levels (ground clearance) are also created every day for temperature and humidity forecasts. Only the BLQ-Air index forecasts are produced at a single level (5 m).

Diverging colormaps have been chosen for each pollutant and for temperature and humidity, to have monotonically increasing L*[5] values up to a maximum, which should be close to L* = 100, followed by monotonically decreasing L* values (for more

[5] L* is the lightness parameter used to learn more about how the matplotlib colormaps will be perceived by viewers.

information see https://matplotlib.org/stable/tutorials/colors/colormaps.html). This colormap (RdYlGn_r) assigns to maximum concentration values the red color, to minimum concentration values the green color and yellow color for intermediate concentration values.

The same kind of colormap is used for temperature and humidity, but with other colors:

- temperature - (RdYlBu_r) red color for maximum values, yellow color for intermediate values and blue color for minimum values.
- humidity - (PRGn_r) purple color for maximum values, white color for intermediate values and green color for minimum values.

Qualitative colormap personalized was used for BLQ-Air index, in this case the L^* values move all over the place throughout the colormap, and are clearly not monotonically increasing. This kind of colormap was choice because allow assigning a color to each class of index, furthermore, each color can be customized such as adding a transparency that increases as the values of that specific class decrease. The final colormap allows to identify the index class, associating the state of the air quality and within the class if the air quality is closest to the previous or next class. A legend relating to the colormap has been created, as PNG file, for each map that allows easy reading and interpretation of the maps.

Along with the PNG files, a JSON file which contains all the images metadata is also created. JSON (Java Script Object Notation) is a type of format typically used for data exchange in client-server applications. It allows the description and above all the exchange of data and is comfortable, tidy, easily readable. All PNG images created are compressed in a ZIP file which together with the JSON file are uploaded to the e-Globus drive. In addition, an additional compressed folder is created containing the model input files and all model outputs which is uploaded to a drive folder for storage.

All this series of operations (drive access, data download, data processing, file creation, model run, model output processing, map creation, saving and sending of maps, legends and metadata on the drive) are contained in the ForecastingTool.py file which must run every day in order to keep the dedicated section on the e-Globus platform updated. The automation of this part was achieved using crontab. On Linux operating systems, the crontab command allows you to schedule automatic periodic execution of tasks or scripts. Each scheduled activity is called a cron job. Cron means “command run on notice” (ie: “command run on notification”) and the command is run as a cron daemon (also known as a cron system). The cron system works in the background in an operating system and can automatically execute jobs at specific and predetermined times. The cronjob therefore arises from the union between a cron system and a predefined process (job). The information needed to program the action (time and defined action) is indicated in the crontab file. Each row of the crontab has a sequence of fields, divided by a space, as shown in the figure Figure 82.

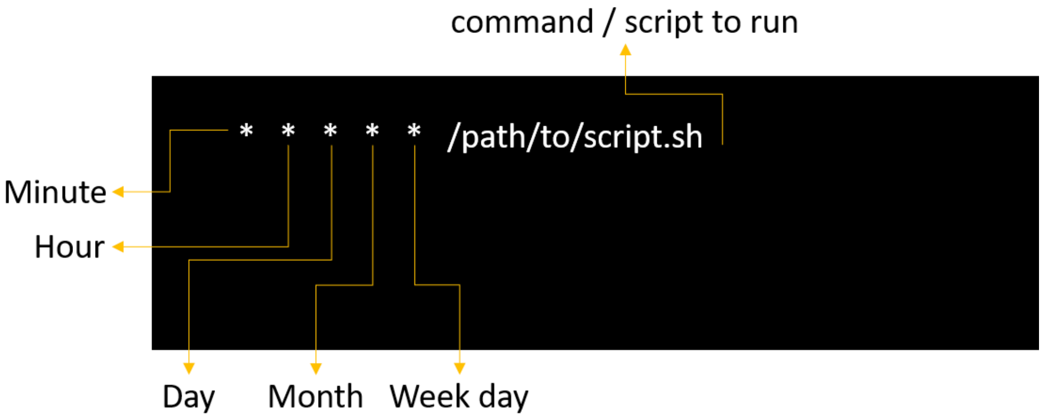

Figure 82. Crontab compilation scheme.

In the case of the forecasting tool, crontab is set up to execute a script.sh at 20:00 every day. The script.sh contains the command to run the ForecastingTool.py file.

5.3 E-Globus platform

The e-Globus (https://www.e-globus.it/) platform is an experimental project developed by e-Soft (https://www.e-soft.it/) to visualize data and statistics related to different topics and coming from various sources. Most of the information is based on free and open data and services. The information is displayed through interactive and "responsive" tables, vector graphics and cartographic maps based on geographic information systems and three-dimensional libraries (3D GIS). At the moment the platform has two sections: i) Data and Weather Forecast section which contains maps, tables and graphs on weather data and forecasts; and ii) Data section on Covid-19 where it is possible to analyze the official international and Italian data on the spread of the Covid-19 pandemic using 3D maps, interactive tables and graphs. In particular, the Data and Weather Forecast section has the following subsections:

- Emilia Romagna Weather Forecast
- Radar Map Emilia Romagna
- Hydrographic Levels Emilia Romagna
- 3D Rain Simulator Emilia Romagna

The e-Globus platform was chosen to make the forecasting tool products available to citizens and other end-users. The section added to the platform is called Environmental Forecasts at urban scale of Bologna and contains a brief description:

Forecasts relating to atmospheric pollutants (PM_{10}, NO_2, Ozone) and environmental parameters (Temperature and Humidity) estimated at various heights from the ground *by the Department of Physics and Astronomy of the University of Bologna on the basis of an advanced model of atmospheric pollution dispersion (ADMS model) developed by Cambridge Environmental Research Consultants (CERC).*

The model takes into account the meteorological forecasts made available by ARPA Emilia Romagna (ARPAE) (wind direction and intensity, rain, humidity, etc.) and numerous other territorial parameters (altimetry, land use, ...) and environmental, generating an overall AQ index (BLQ-Air Index) useful for those who intend to move to Bologna.

The screen (Figure 83) that opens by clicking on the section is occupied by the map display. The section hosts all the results of the forecasting tool, updated every day.

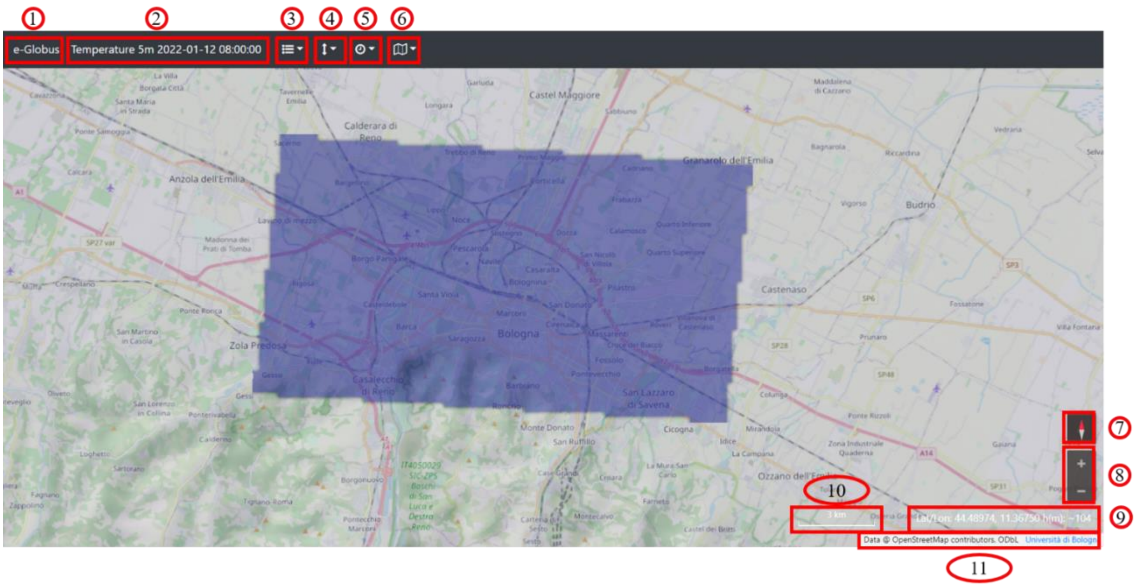

Figure 83. Visualization of the forecast maps produced by the forecast tool on the e-Globus platform. 1) Platform name and command to come back Home; 2) Information on the displayed map: variable, level, date, time; 3) variable choice menu; 4) level choice menu; 5) menu choice now; 6) base map choice menu; 7) Cardinal points indicator; 8) zoom command; 9) Latitude, longitude and altitude of the point indicated by the cursor; 10) scale of representation; 11) Sources.

There are also some commands and information, in particular, at the top, from left to right: Information on the map displayed: variable, level, date, time; variable choice menu; level choice menu; time selection menu; base map choice menu. Bottom: Cardinal points indicator; zoom command; Latitude, longitude and altitude of the point indicated by the cursor; scale of representation; Sources.

The variables (PM_{10}, NO_2 and O_3 concentration, BLQ-Air index and Temperature and humidity) are organized in hourly maps from 1:00 to 24:00 UTC on 8 levels (BLQ-Air index only one level (5 m)). Examples of maps that can be viewed on the platform are presented below (Figure 84 and Figure 85).

Figure 84. Examples of maps on the E-Globus platform: top) map of temperature (°C) at 5 m for 20/01/2022 at 19:00; bottom) map of Humidity (%) at 5 m for 20/01/2022 at 18:00.

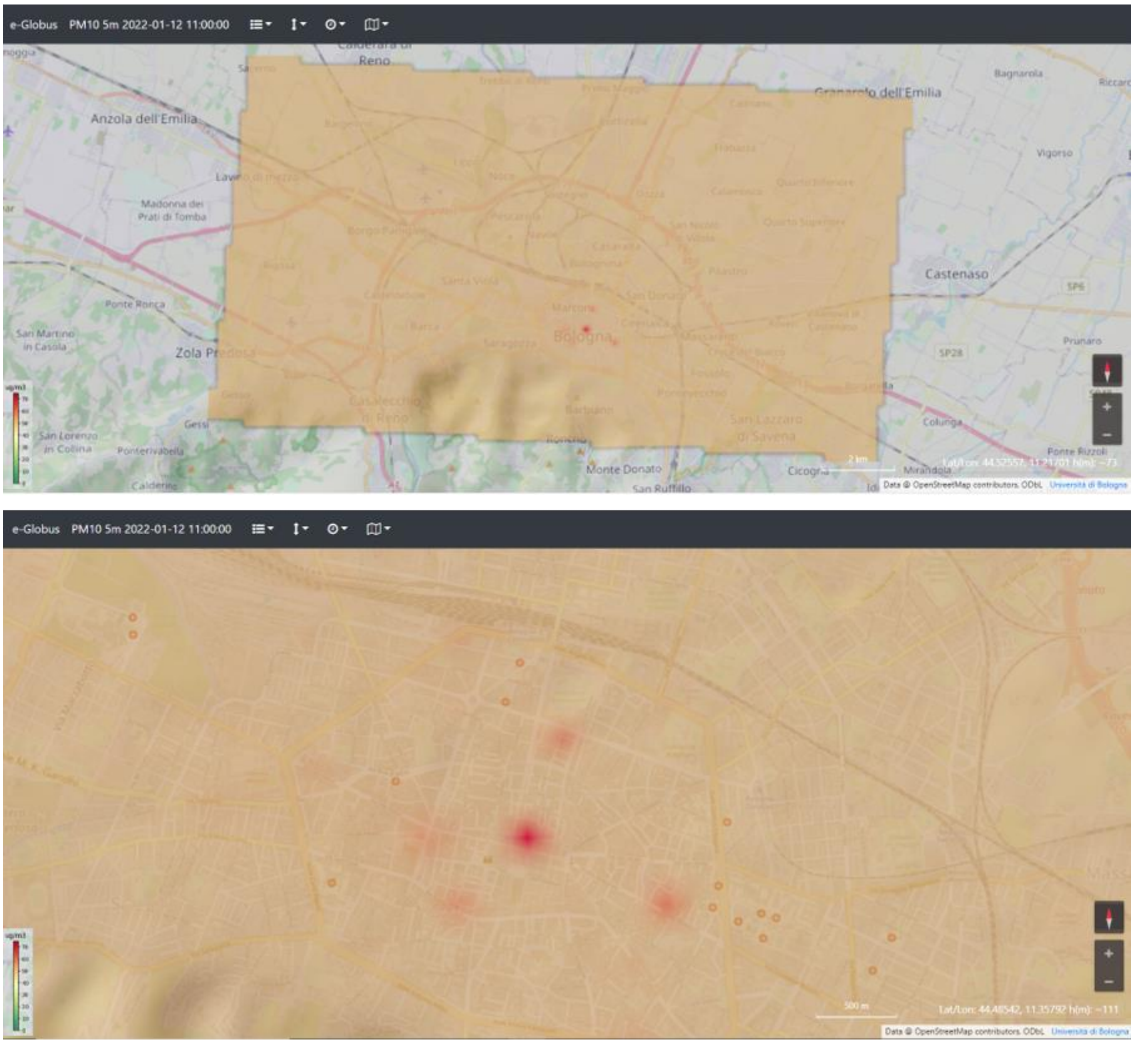

Figure 85. Examples of maps on the E-Globus platform: top) map of PM_{10} concentration (ug m^{-3}) at 5 m for 12/01/2022 at 11:00; bottom) zoom of the same map.

Figure 84 shows an example of displaying the temperature map on the e-Globus platform relating to the day 20/01/2022 at 19:00, and an example of displaying the humidity map on the relating to the day 20/01/2022 at 18:00. On the left of each map we find the legend, which allows us to understand that the temperature in Bologna at 19:00 on 20/01/2022 will be below 10 °C while the humidity on Bologna at 18:00 on 20/01/2022 will be included is approximately 80%.

Figure 85 shows an example of visualization of the map of the concentration of PM_{10} on the e-Globus platform relative to the day 12/01/2022 at 11:00. The relative legend allows us to understand that the concentration of PM_{10} in Bologna at 11:00 on 12/01/2022 will be around 50 ug/m^3, by zooming in on the center of Bologna (Figure 85), some areas are highlighted from a darker red, indicating that in those areas the concentration will be higher, around 70 ug/m^3.

5.4 Summary

In a city affected by significant levels of traffic, cyclists and pedestrians can be the most exposed to pollution and extreme heat situations. The citizens need specific tools capable of providing forecasts on AQ and other environmental parameters to assess and choose the city areas that is better. The development of the high resolution air quality, temperature and humidity forecasting tool for the city of Bologna was presented. ADMS models (ADMS-Urban and ADMS-TH) can be used in forecasting mode, using numerical forecasts of meteorological variables and boundary pollutant concentrations as meteorological input and background respectively. In both models, the domain considered is 10x20 km with a resolution of 200x200 m. The meteorological forecasts (COSMO model) and concentration (CHIMERE model) forecasts for Bologna are provided as open data by ARPAE. The meteorological forecasts and concentration forecasts as well as the results of ADMS models were validated with data measured by reference monitoring stations.

The simulated values of temperature and relative humidity match perfectly the observations, while the simulations of wind direction present a higher frequency of wind coming from NNE with relatively higher speeds than the measured data.

The results of CHIMERE performance evaluation indicate the tendency for the model to overestimate all pollutant and in particular for NO_2 and O_3. This overestimation implies that the dataset used as background concentrations in input to the ADMS model presents higher values than the observed, resulting in a consequent overestimation of the simulations from ADMS Model.

The performance evaluation of ADMS models carried out in forecasting mode was performed comparing hourly observed data with the forecasts values simulated with the ADMS-Urban models. In general, the simulated data are comparable with the observed ones, indicating a good temporal representation of the pollutant dispersion over the domain. There is an overestimation for NO_2 concentration in suburban stations, that can be attributed to the overestimation of the background concentrations in the CHIMERE forecast model; an overestimation for temperature and an underestimation for humidity, especially for the rural site.

Python programming language, with several libraries, API and modules, were used to develop the forecast tool. The ForecastingTool.py file contains all the operations necessary for the forecasting tool to work. A Google API was included within the code to allow access to Google drive services and download the ARPAE forecasted weather data from the COSMO and CHIMERE models. Each variable needed in the final ADMS input files required a series of mathematical processing.

Subsequently, the two ADMS models are called and run in sequence, taking the most of the code execution time. The model outputs are processed to produce maps, of spatial variation of pollutant and meteorological variables, saved as PNG files. For each pollutant (PM_{10}, NO_2 and O_3) 24 maps are created every day (one for each hour of the day, from 1:00 to 24:00 UTC) for 8 height levels (5, 10, 15, 20, 25, 30, 35 and 40 m above the ground). 24 maps (24 hours) for 8 levels (ground clearance) are also created every day for temperature and humidity forecasts. Only the BLQ-Air index forecasts are produced at a single level (5 m). Along with the PNG files, a JSON file which contains all the images metadata is also created. JSON. All PNG images created are compressed in a ZIP file which together with the JSON file are uploaded to the e-Globus drive. The e-Globus platform is an experimental project developed by e-Soft to visualize data and statistics related to different topics and coming from various sources. The e-Globus platform was chosen to make the forecasting tool products available to citizens and other end-users. The section added to the platform is called Environmental Forecasts at urban scale of Bologna. The ForecastingTool.py file must run every day to update the maps on the e-globus platform. The automation was achieved using crontab.

6 CONCLUSIONS

This research aimed to develop a forecasting tool for citizen use, adaptable to all cities. The tool provides high resolution forecast maps, useful for choosing the healthiest areas of the city. To achieve this, a series of steps were performed, including the simulation of different scenarios and the development of new parametrization for vegetated areas.

The simulation of each scenario had as its objective the evaluation of the effects of traffic management policies, PCSs interventions and greening policies; while the ultimate goal of all simulations was to develop methodologies that improve the performance of the dispersion model. On the basis of the results obtained with the modeling simulations of traffic policies, PCSs interventions and greening policies, it can be concluded that the models used are able to simulate very detailed and high resolution scenarios, moreover, they allow to also simulate future scenarios to include possible interactions with climate change. The results of traffic policy simulations show that the use of electric vehicles improves air quality, while increasing the frequency of buses would lead to a slight increase in PM_{10} emissions. As for PCSs interventions, they favor the deposition of pollutants, contributing to the reduction of pollutant concentrations in the air. PCSs interventions also improve thermal comfort in the areas adjacent to where they are performed. Finally, the results of simulations of greening policies show that the addition of trees in a road leads to an alteration of the dispersion, determining both areas of reduction of the NO_x concentration and areas of decrease. Furthermore, the UHI tends to increase in the future due to climate change. The differences between present and future are limited. To simulate the individual scenarios, different methodologies have been developed (such as simulating the scenario in which the vehicles were all electric, modeling the deposition due to the presence of vegetation, modeling the dispersion in the presence of trees considered as a physical obstacle). All these methodologies were useful for the development of the forecasting tool. In particular, the methodology for calculating the USVR allows very good performances, therefore the relative map produced was included in the setup of the dispersion model. Using the morphological method, detailed aerodynamic information of the city such as road trees otherwise not identifiable with other methodologies can be provided to the model. The insertion of the roughness due to buildings and trees has produced different results based on the spatial scale and on the characteristics of the dispersion site. At the urban scale, the presence of trees does not seem to significantly alter the simulation output, this result can be influenced by the not densely vegetated site used for the evaluation. At the neighborhood scale, the inclusion of vegetation significantly improves the agreement of the simulations with observations, especially for vegetated areas. Therefore, this methodology is strongly recommended to improve the performance of dispersion simulations, and particularly to limit the overestimation of the simulated concentrations. The inclusion of vegetation is particularly necessary in high spatial resolution studies, and for densely vegetated sites.

In the second part of this research, the high resolution forecasting tool was proposed. The tool developed for the city of Bologna and tested on it is presented. The tool produces the 1-day forecast NO_2, PM_{10}, O_3 concentration, the air temperature, the air humidity and BL-Air index values. The regional numerical forecasts of meteorological variables (COSMO model) and pollutant concentrations (CHIMERE model) were used as meteorological and background concentration input, respectively, into the ADMS models (ADMS-Urban and ADMS-TH), used in forecasting mode. A python code executes all operations necessary for the forecasting tool to work. The code is automatically executed every day and the maps produced are displayed on the e-Globus platform, updated every day. The output of the code are maps of pollutants concentration, temperature, Humidity, and BLQ-Air Index: 24 maps are created every day, for 8 height levels (BLQ-Air index had only one level).

During the testing phase of the tool, the two regional forecast models were evaluated by comparing the forecast values with observed data. The results of this evaluation highlight some critical issues: the COSMO simulated values of wind direction and intensity present some discrepancies from the measurements and the CHIMERE model overestimate all pollutant, in particular for NO_2 and O_3. To evaluate the final product of the tool, a performance evaluation of the ADMS models was performed. The results indicate an overestimation for NO_2 concentration in suburban stations, and an overestimation for temperature and an underestimation for humidity, especially for the rural site. The final product of the forecasting tool is available and can be consulted by everyone at the URL: https://www.e-globus.it/adms01.aspx.

6.1 Further remarks

The emissions inventory used is based on annual average traffic count data, this figure should be updated every year for the simulations to make reliable predictions.

The overestimation of the CHIMERE model amplifies the tendency of the dispersion model to overestimate the predicted concentrations, although the performance evaluation of the model gives excellent results, the input data from the CHIMERE model should be correct. The discrepancies found for wind speed and direction in the COSMO model predictions could lead to incorrect distribution patterns (both for pollutants and for temperature and humidity). Both criticalities should be studied in detail to improve the forecasting tool.

6.2 Future Perspectives

The results found so far lead to a series of recommendations, in the field of AQ, the most important is to include modeling approaches among the methodologies for evaluating urban policies. They, as has been amply documented in this thesis, allow to have space-time information, allow to evaluate multiple scenarios and to make future predictions.

As for the policies on traffic management, it is necessary to pay close attention to the effect of the policies on the different pollutants, the effect is not always the same for all. PCS interventions and greening policies are much more complex, they act on various processes that affect the dispersion of pollutants, such as the deposition and alteration of atmospheric flows due to roughness. The effects due to the change in roughness are greater than the deposition, therefore it is advisable to include detailed spatial information on roughness, such as the USVR map (methodology presented in this thesis), especially at high resolution scale.

Regarding the forecasting tool, future improvements may concern:

- Include the creation of the emission inventory based on daily traffic data.
- Correct the overestimation and the criticalities found in the forecasts provided by the COSMO and CHIMERE forecast models.
- Improve the efficiency of the code: evaluate the use of one library rather than another, replace for or if loops with more efficient Python constructs, define classes to make it reusable.

Finally, a section dedicated to product evaluation by end users would be very useful for improving the tool.

7 REFERENCES

Abhijith, K. V., Kumar, P., 2019. Field investigations for evaluating green infrastructure effects on air quality in open-road conditions. Atmos. Environ. 201, 132–147. https://doi.org/10.1016/j.atmosenv.2018.12.036

Abhijith, K. V., Kumar, P., Gallagher, J., McNabola, A., Baldauf, R., Pilla, F., Broderick, B., Di Sabatino, S., Pulvirenti, B., 2017. Air pollution abatement performances of green infrastructure in open road and built-up street canyon environments – A review. Atmos. Environ. 162, 71–86. https://doi.org/10.1016/j.atmosenv.2017.05.014

Ahern, J., 2007. Green infrastructure for cities: the spatial dimension. In, in: Cities of the Future: Towards Integrated Sustainable Water and Landscape Management. IWA Publishing.

An, N., Dou, J., González-Cruz, J.E., Bornstein, R.D., Miao, S., Li, L., 2020. An observational case study of synergies between an intense heat wave and the urban heat island in Beijing. J. Appl. Meteorol. Climatol. 59, 605–620. https://doi.org/10.1175/JAMC-D-19-0125.1

Baklanov, A., Zhang, Y., 2020. Advances in air quality modeling and forecasting. Glob. Transitions 2, 261–270. https://doi.org/10.1016/j.glt.2020.11.001

Barbano, F., Di Sabatino, S., Stoll, R., Pardyjak, E.R., 2020. A numerical study of the impact of vegetation on mean and turbulence fields in a European-city neighbourhood. Build. Environ. 186, 107293. https://doi.org/10.1016/j.buildenv.2020.107293

Barnes, M.J., Brade, T.K., Mackenzie, A.R., Whyatt, J.D., Carruthers, D.J., Stocker, J., Cai, X., Hewitt, C.N., 2014. Spatially-varying surface roughness and ground-level air quality in an operational dispersion model. Environ. Pollut. 185, 44–51. https://doi.org/10.1016/j.envpol.2013.09.039

Benavides, J., Snyder, M., Guevara, M., Soret, A., Pérez García-Pando, C., Amato, F., Querol, X., Jorba, O., 2019. CALIOPE-Urban v1.0: Coupling R-LINE with a mesoscale air quality modelling system for urban air quality forecasts over Barcelona city (Spain). Geosci. Model Dev. 12, 2811–2835. https://doi.org/10.5194/gmd-12-2811-2019

Borrego, C., Costa, A.M., Ginja, J., Amorim, M., Coutinho, M., Karatzas, K., Sioumis, T., Katsifarakis, N., Konstantinidis, K., De Vito, S., Esposito, E., Smith, P., André, N., Gérard, P., Francis, L.A., Castell, N., Schneider, P., Viana, M., Minguillón, M.C., Reimringer, W., Otjes, R.P., von Sicard, O., Pohle, R., Elen, B., Suriano, D., Pfister, V., Prato, M., Dipinto, S., Penza, M., 2016. Assessment of air quality microsensors versus reference methods: The EuNetAir joint exercise. Atmos. Environ. 147, 246–263. https://doi.org/10.1016/j.atmosenv.2016.09.050

Boucher, O., Randall, D., Artaxo, P., Bretherton, C., Feingold, G., Forster, P., Kerminen, V.-M., Kondo, Y., Liao, H., Lohmann, U., Rasch, P., Satheesh, S.K., Sherwood, S., Stevens, B., Zhang, X.Y., 2013. Clouds and aerosols, in: Cambridge University Press, Cambridge, United Kingdom and New York, NY, U. (Ed.), Climate Change 2013 the Physical Science Basis: Working Group I Contribution to the Fifth Assessment Report of the Intergovernmental Panel on Climate Change. pp. 571–658. https://doi.org/10.1017/CBO9781107415324.016

Brattich, E., Bracci, A., Zappi, A., Morozzi, P., Sabatino, S. Di, Porcù, F., Nicola, F. Di, Tositti, L., 2020. How to get the best from low-cost particulate matter sensors: Guidelines and practical recommendations. Sensors (Switzerland) 20, 1–33. https://doi.org/10.3390/s20113073

Brauer, M., Brook, J.R., Christidis, T., Chu, Y., Crouse, D.L., Erickson, A., Hystad, P., Li, C., Martin, R. V, Meng, J., Pappin, A.J., Pinault, L.L., Tjepkema, M., Donkelaar, A. Van, Weichenthal, S., Burnett, R.T., 2019. R E S E A R C H R E P O RT 5505.

Breuer, L., Eckhardt, K., Frede, H.G., 2003. Plant parameter values for models in temperate climates. Ecol. Modell. 169, 237–293. https://doi.org/10.1016/S0304-3800(03)00274-6

Britter, R.E., Hanna, S.R., 2003. Flow and dispersion in urban areas. Annu. Rev. Fluid Mech. 35, 469–496. https://doi.org/10.1146/annurev.fluid.35.101101.161147

Brunekreef, B., Holgate, S.T., 2002. Air pollution and health. Lancet 360, 1233–1242. https://doi.org/10.1016/S0140-6736(02)11274-8

Buccolieri, R., Gromke, C., Di Sabatino, S., Ruck, B., 2009. Aerodynamic effects of trees on pollutant concentration in street canyons. Sci. Total Environ. 407, 5247–5256. https://doi.org/10.1016/j.scitotenv.2009.06.016

Carnielo, E., Zinzi, M., 2013. Optical and thermal characterisation of cool asphalts to mitigate urban temperatures and building cooling demand. Build. Environ. 60, 56–65. https://doi.org/10.1016/j.buildenv.2012.11.004

Carruthers, D.J., Edmunds, H.A., Lester, A.E., McHugh, C.A., Singles, R.J., 2000. Use and validation of ADMS-Urban in contrasting urban and industrial locations. Int. J. Environ. Pollut. 14, 364–374.

CERC, 2018. ADMS-Urban Temperature and Humidity.

CERC, 2017. ADMS-Urban Urban Air Quality Management System Version 4.1 User Guide CERC 390.

CERC, 2015. EMIT Atmospheric Emissions Inventory Toolkit User Guide.

Cesaroni, G., Badaloni, C., Gariazzo, C., Stafoggia, M., Sozzi, R., Davoli, M., Forastiere, F., 2013. Long-term exposure to urban air pollution and mortality in a cohort of more than a million adults in Rome. Environ. Health Perspect. 121, 324–331. https://doi.org/10.1289/ehp.1205862

Chang, J.C., Hanna, S.R., 2004. Air quality model performance evaluation. Meteorol. Atmos. Phys. 87, 167–196. https://doi.org/10.1007/s00703-003-0070-7

Changnon, S.D., 2003. MEASURES OF ECONOMIC IMPACTS OF WEATHER EXTREMES. Am. Meteorol. Soc.

Chew, L.W., Liu, X., Li, X.X., Norford, L.K., 2021. Interaction between heat wave and urban heat island: A case study in a tropical coastal city, Singapore. Atmos. Res. 247, 105134. https://doi.org/10.1016/j.atmosres.2020.105134

Coumou, D., Robinson, A., 2013. Historic and future increase in the global land area affected by monthly heat extremes. Environ. Res. Lett. 8. https://doi.org/10.1088/1748-9326/8/3/034018

Danov, M., Tsanev, V., Petkov, D., 2007. Investigation of thermal infrared emissivity spectra of mineral and rock samples. New Dev. Challenges Remote Sens. 145–152.

Di Nicola, F., Brattich, E., Di Sabatino, S., 2022. A new approach for roughness representation within urban dispersion models.

Di Sabatino, S., Barbano, F., Brattich, E., 2020. The Multiple-Scale Nature of Urban Heat Island and Its Footprint on Air Quality in Real Urban Environment. Atmosphere (Basel). 11, 1186.

Di Sabatino, S., Brattich, E., Barbano, F., Gharbia, S., Pilla, F., Abhijith, K. V., Kumar, P., Drebs, A., Jylhä, K., Mäkelä, A., Deserti, M., Torreggiani, L., Barbieri, C., 2018. Air pollution and meteorology - D5.2.

Di Sabatino, S., Brattich, E., Di Nicola, F., Barbano, F., Adnan, M., Ahmed, S., Jylhä, K., Ruosteenoja, K., Deserti, M., Agostini, C., Poluzzi, V., 2019. Report on policy options for AQ and CC - D4.5.

Di Sabatino, S., Buccolieri, R., Olesen, H.R., Ketzel, M., Berkowicz, R., Franke, J., Schatzmann, M., Schlünzen, K.H., Leitl, B., Britter, R., Borrego, C., Costa, A.M., Castelli, S.T., Reisin, T.G., Hellsten, A., Saloranta, J., Moussiopoulos, N., Barmpas, F., Brzozowski, K., Goricsán, I., Balczò, M., Bartzis, J.G., Efthimiou, G., Santiago, J.L., Martilli, A., Piringer, M., Baumann-Stanzer, K., Hirtl, M., Baklanov, A.A., Nuterman, R.B., Starchenko, A. V., 2011. COST 732 in practice: The MUST model evaluation exercise. Int. J. Environ. Pollut. 44, 403–418. https://doi.org/10.1504/IJEP.2011.038442

Di Sabatino, S., Buccolieri, R., Pappaccogli, G., Leo, L.S., 2015. The effects of trees on micrometeorology in a real street canyon: Consequences for local air quality. Int. J. Environ. Pollut. 58, 100–111. https://doi.org/10.1504/IJEP.2015.076587

Di Sabatino, S., Buccolieri, R., Pulvirenti, B., Britter, R.E., 2008. Flow and pollutant dispersion in street canyons using FLUENT and ADMS-Urban. Environ. Model. Assess. 13, 369–381. https://doi.org/10.1007/s10666-007-9106-6

Dominski, F.H., Lorenzetti Branco, J.H., Buonanno, G., Stabile, L., Gameiro da Silva, M., Andrade, A., 2021. Effects of air pollution on health: A mapping review of systematic reviews and meta-analyses. Environ. Res. 201. https://doi.org/10.1016/j.envres.2021.111487

Duyzer, J., van den Hout, D., Zandveld, P., van Ratingen, S., 2015. Representativeness of air quality monitoring networks. Atmos. Environ. 104, 88–101.

https://doi.org/10.1016/j.atmosenv.2014.12.067

EEA, 2009. EMEP/EEA air pollutant emission inventory guidebook - 2009 — European Environment Agency.

Elminir, H.K., 2005. Dependence of urban air pollutants on meteorology. Sci. Total Environ. 350, 225–237. https://doi.org/10.1016/j.scitotenv.2005.01.043

Environment Agency, 2008. Review of modelling methods of near-field acid deposition.

EPA, 2004. Photochemical smog: what it means for us. Epa 90/04 1, 1–7.

EPA, 1970. Clean air act. Public Health. https://doi.org/10.1016/S0033-3506(31)80400-7

EU, 2016. DIRETTIVA (UE) 2016/2284 DEL PARLAMENTO EUROPEO E DEL CONSIGLIO del 14 dicembre 2016. Gazz. Uff. dell'Unione Eur.

European Commission, 2012. The Multifunctionality of Green Infrastructure. DG Environ. Brussells.

Fischer, P.H., Marra, M., Ameling, C.B., Hoek, G., Beelen, R., De Hoogh, K., Breugelmans, O., Kruize, H., Janssen, N.A.H., Houthuijs, D., 2015. Air pollution and mortality in seven million adults: The dutch environmental longitudinal study (DUELS). Environ. Health Perspect. 123, 697–704. https://doi.org/10.1289/ehp.1408254

FLIR Systems, 2019. User's manual FLIR T6 series.

Gabriel, K.M.A., Endlicher, W.R., 2011. Urban and rural mortality rates during heat waves in Berlin and Brandenburg, Germany. Environ. Pollut. 159, 2044–2050. https://doi.org/10.1016/j.envpol.2011.01.016

Gallagher, J., Gill, L.W., McNabola, A., 2012. Numerical modelling of the passive control of air pollution in asymmetrical urban street canyons using refined mesh discretization schemes. Build. Environ. 56, 232–240. https://doi.org/10.1016/j.buildenv.2012.03.013

Gignac, F., Righi, V., Toran, R., Errandonea, L.P., Ortiz, R., Nieuwenhuijsen, M., Creus, J., Basagaña, X., Balestrini, M., 2022. Co-creating a local environmental epidemiology study: the case of citizen science for investigating air pollution and related health risks in Barcelona, Spain. Environ. Heal. 21, 1–13. https://doi.org/10.1186/s12940-021-00826-8

Goodsite, M.E., Hertel, O., Johnson, M.S., Jørgensen, N.R., 2021. Urban Air Quality: Sources and Concentrations, in: Goodsite, M.E., Johnson, M.S., Hertel, O. (Eds.), Air Pollution Sources, Statistics and Health Effects. Springer US, New York, NY, pp. 193–214. https://doi.org/10.1007/978-1-0716-0596-7_321

Gorsevski, V., Taha, H., Quattrochi, D., Luvall, J., 1998. Air Pollution Prevention Through Urban Heat Island Mitigation: An Update on the Urban Heat Island Pilot Project. Proc. ACEEE Summer Study 23–32.

Gromke, C., 2011. A vegetation modeling concept for building and environmental aerodynamics wind tunnel tests and its application in pollutant dispersion studies. Environ. Pollut. 159, 2094–2099. https://doi.org/10.1016/j.envpol.2010.11.012

Hamada, S., Ohta, T., 2010. Seasonal variations in the cooling effect of urban green areas on surrounding urban areas. Urban For. Urban Green. 9, 15–24. https://doi.org/10.1016/j.ufug.2009.10.002

Hanna, S.R., 1993. Uncertainties in air quality model predictions. Boundary-Layer Meteorol. 62, 3–20. https://doi.org/10.1007/BF00705545

Hogstrom, U., 1996. Review of some basic characteristics of the atmospheric surface layer. Boundary-Layer Meteorol. 78, 215–246. https://doi.org/10.1007/BF00120937

Hood, C., MacKenzie, I., Stocker, J., Johnson, K., Carruthers, D., Vieno, M., Doherty, R., 2018. Air quality simulations for London using a coupled regional-to-local modelling system. Atmos. Chem. Phys. 18, 11221–11245. https://doi.org/10.5194/acp-18-11221-2018

Hood, C.M., Stocker, J.R., Carruthers, D.J., Grayson, W., Handley, J., Fung, J., Yueng, D., 2017. Integrating regional and local modeling to create a high-resolution air quality forecasting system for Hong Kong.

Huang, Y., Chameides, W.L., Dickinson, R.E., 2007. Direct and indirect effects of anthropogenic aerosols on regional precipitation over east Asia. J. Geophys. Res. Atmos. 112, 1–17.

https://doi.org/10.1029/2006JD007114

IARC, 2016. Outdoor Air Pollution. IARC Monograph 109.

Janhäll, S., 2015. Review on urban vegetation and particle air pollution - Deposition and dispersion. Atmos. Environ. 105, 130–137. https://doi.org/10.1016/j.atmosenv.2015.01.052

Jeanjean, A., Buccolieri, R., Eddy, J., Monks, P., Leigh, R., 2017. Air quality affected by trees in real street canyons: The case of Marylebone neighbourhood in central London. Urban For. Urban Green. 22, 41–53. https://doi.org/10.1016/j.ufug.2017.01.009

Jeanjean, A.P.R., Monks, P.S., Leigh, R.J., 2016. Modelling the effectiveness of urban trees and grass on PM2.5 reduction via dispersion and deposition at a city scale. Atmos. Environ. 147, 1–10. https://doi.org/10.1016/j.atmosenv.2016.09.033

Kadaverugu, R., Sharma, A., Matli, C., Biniwale, R., 2019. High Resolution Urban Air Quality Modeling by Coupling CFD and Mesoscale Models: a Review. Asia-Pacific J. Atmos. Sci. 55, 539–556. https://doi.org/10.1007/s13143-019-00110-3

Kampa, M., Castanas, E., 2008. Human health effects of air pollution. Environ. Pollut. 151, 362–367. https://doi.org/10.1016/j.envpol.2007.06.012

Karsis, P., Ntziachritos, L., Mellios, G., 2012. Description of new elements in COPERT 4 v10.0 1–71.

Kent, C.W., Grimmond, S., Barlow, J., Gatey, D., Kotthaus, S., Lindberg, F., Halios, C.H., 2017. Evaluation of Urban Local-Scale Aerodynamic Parameters: Implications for the Vertical Profile of Wind Speed and for Source Areas. Boundary-Layer Meteorol. 164, 1–31. https://doi.org/10.1007/s10546-017-0248-z

Kong, F., Yin, H., James, P., Hutyra, L.R., He, H.S., 2014. Effects of spatial pattern of greenspace on urban cooling in a large metropolitan area of eastern China. Landsc. Urban Plan. 128, 35–47. https://doi.org/10.1016/j.landurbplan.2014.04.018

Kong, F., Yin, H., Nakagoshi, N., Zong, Y., 2010. Urban green space network development for biodiversity conservation: Identification based on graph theory and gravity modeling. Landsc. Urban Plan. 95, 16–27. https://doi.org/10.1016/j.landurbplan.2009.11.001

Künkli, N., Perez, L., Rapp, R., 2010. Qualità dell'aria e Salute, European Respiratory Society.

Künzli, N., Kaiser, R., Medina, S., Studnicka, M., Chanel, O., Filliger, P., Herry, M., Horak Jr, F., Puybonnieux-Texier, V., Quénel, P., others, 2000. Public-health impact of outdoor and traffic-related air pollution: a European assessment. Lancet 356, 795–801.

Kurt, O.K., Zhang, J., Pinkerton, K.E., 2016. HHS Public Access. Curr. Opin. Pulm. Med. 22, 138–143. https://doi.org/10.1097/MCP.0000000000000248.Pulmonary

Li, D., Sun, T., Liu, M., Wang, L., Gao, Z., 2016. Changes in wind speed under heat waves enhance urban heat islands in the Beijing metropolitan area. J. Appl. Meteorol. Climatol. 55, 2369–2375. https://doi.org/10.1175/JAMC-D-16-0102.1

Li, Y., Schubert, S., Kropp, J.P., Rybski, D., 2020. On the influence of density and morphology on the Urban Heat Island intensity. Nat. Commun. 11, 1–9. https://doi.org/10.1038/s41467-020-16461-9

MacDonald, R.W., Griffiths, R.F., Hall, D.J., 1998. An improved method for the estimation of surface roughness of obstacle arrays. Atmos. Environ. 32, 1857–1864.

Maggiotto, G., Buccolieri, R., Santo, M.A., Di Sabatino, S., Leo, L.S., 2014a. Study of the urban heat island in Lecce (Italy) by means of ADMS and ENVI-MET. Int. J. Environ. Pollut. 55, 41–49. https://doi.org/10.1504/IJEP.2014.065903

Maggiotto, G., Buccolieri, R., Santo, M.A., Leo, L.S., Di Sabatino, S., 2014b. Validation of temperature-perturbation and CFD-based modelling for the prediction of the thermal urban environment: The Lecce (IT) case study. Environ. Model. Softw. 60, 69–83. https://doi.org/10.1016/j.envsoft.2014.06.001

Mangia, C., Ielpo, P., Cesari, R., Facchini, M., 2020. Crisi climatica e inquinamento atmosferico. Ithaca Viaggio nella Sci. 2020, 57–68.

Marć, M., Tobiszewski, M., Zabiegała, B., Guardia, M. de la, Namieśnik, J., 2015. Current air quality analytics and monitoring: A review. Anal. Chim. Acta 853, 116–126.

https://doi.org/10.1016/j.aca.2014.10.018

Martilli, A., 2002. Numerical Study of Urban Impact on Boundary Layer Structure: Sensitivity to Wind Speed, Urban Morphology, and Rural Soil Moisture. Am. Meteorol. Soc. 41.

McCarthy, M.P., Best, M.J., Betts, R.A., 2010. Climate change in cities due to global warming and urban effects. Geophys. Res. Lett. 37, 1–5. https://doi.org/10.1029/2010GL042845

McMichael, A.J., Woodruff, R.E., Hales, S., 2006. Climate change and human health: Present and future risks. Lancet 367, 859–869. https://doi.org/10.1016/S0140-6736(06)68079-3

Michulec, M., Wardencki, W., Partyka, M., Namieśnik, J., 2005. Analytical techniques used in monitoring of atmospheric air pollutants. Crit. Rev. Anal. Chem. 35, 117–133. https://doi.org/10.1080/10408340500207482

Monks, P.S., Archibald, A.T., Colette, A., Cooper, O., Coyle, M., Derwent, R., Fowler, D., Granier, C., Law, K.S., Mills, G.E., Stevenson, D.S., Tarasova, O., Thouret, V., Von Schneidemesser, E., Sommariva, R., Wild, O., Williams, M.L., 2015. Tropospheric ozone and its precursors from the urban to the global scale from air quality to short-lived climate forcer. Atmos. Chem. Phys. 15, 8889–8973. https://doi.org/10.5194/acp-15-8889-2015

Moussiopoulos, N., Berge, E., Bøhler, T., Leeuw, F. De, Grønskei, K., Mylona, S., Tombrou, M., 1996. European Topic Centre on Air Quality AMBIENT AIR QUALITY , POLLUTANT by. Policy.

National Radiological Protection Board (NRPB), 2001. Atmospheric Dispersion Modelling Liaison Committee annual report 1998/99 : including review of deposition velocity and washout coefficient and review of flow and dispersion in the vicinity of groups of buildings. 158.

NIWAR, N.I. of W. and A.R., 2002. Good practice guide for atmospheric dispersion modelling.

O'Neill, M.S., Ebi, K.L., 2009. Temperature extremes and health: Impacts of climate variability and change in the United States. J. Occup. Environ. Med. 51, 13–25. https://doi.org/10.1097/JOM.0b013e318173e122

Oliveira, A., Lopes, A., Correia, E., Niza, S., Soares, A., 2021. Heatwaves and summer urban heat islands: A daily cycle approach to unveil the urban thermal signal changes in Lisbon, Portugal. Atmosphere (Basel). 12. https://doi.org/10.3390/atmos12030292

Ompad, D.C., Galea, S., Vlahov, D., 2007. Chapter 3: Urbanicity, Urbanization, and the Urban Environment Danielle, in: Macrosocial Determinants of Population Health. pp. 1–502. https://doi.org/10.1007/978-0-387-70812-6

ONU, 2019. World population prospects 2019, Department of Economic and Social Affairs. World Population Prospects 2019.

ONU, 2018. World Urbanization Prospects 2018, Departemen of Economic and Social Affairs United Nation.

Parker, D.E., 2010. Urban heat island effects on estimates of observed climate change. Wiley Interdiscip. Rev. Clim. Chang. 1, 123–133. https://doi.org/10.1002/wcc.21

Perkins, S.E., Alexander, L. V., Nairn, J.R., 2012. Increasing frequency, intensity and duration of observed global heatwaves and warm spells. Geophys. Res. Lett. 39, 1–5. https://doi.org/10.1029/2012GL053361

Pope, C.A., Bates, D. V., Raizenne, M.E., 1995. Health Effects of Particulate Air Pollution: Time for Reassessment? Ann. Epidemiol. 103, 472–480. https://doi.org/10.1016/j.annepidem.2009.01.018

Pope, C.A., Dockery, D.W., 2006. Health effects of fine particulate air pollution: Lines that connect. J. Air Waste Manag. Assoc. 56, 709–742. https://doi.org/10.1080/10473289.2006.10464485

Qgis Project, 2017. QGIS User Guide Release 2.14.

Rai, A.C., Kumar, P., Pilla, F., Skouloudis, A.N., Di Sabatino, S., Ratti, C., Yasar, A., Rickerby, D., 2017. End-user perspective of low-cost sensors for outdoor air pollution monitoring. Sci. Total Environ. 607–608, 691–705. https://doi.org/10.1016/j.scitotenv.2017.06.266

Righi, S., Lucialli, P., Pollini, E., 2009. Statistical and diagnostic evaluation of the ADMS-Urban model compared with an urban air quality monitoring network. Atmos. Environ. 43, 3850–3857. https://doi.org/10.1016/j.atmosenv.2009.05.016

Robertson, S., Miller, M.R., 2018. Ambient air pollution and thrombosis. Part. Fibre Toxicol. 15, 1–16. https://doi.org/10.1186/s12989-017-0237-x

Roth, M., 2000. Review of atmospheric turbolence over cities. Q. J. R. Meteorol.Soc. 126, 941–990.

Santiago, J.L., Martilli, A., Martin, F., 2017. On Dry Deposition Modelling of Atmospheric Pollutants on Vegetation at the Microscale: Application to the Impact of Street Vegetation on Air Quality. Boundary-Layer Meteorol. 162, 451–474. https://doi.org/10.1007/s10546-016-0210-5

Schär, C., Vidale, P.L., Lüthi, D., Frei, C., Häberli, C., Liniger, M.A., Appenzeller, C., 2004. The role of increasing temperature variability in European summer heatwaves. Nature 427, 332–336. https://doi.org/10.1038/nature02300

Seinfeld, J.H., Pandis, S.N., 1998. Atmospheric Chemistry and Physics: From Air Pollution to Climate Change. John Wiley and Sons, New York.

Silva, L.T., Mendes, J.F.G., 2011. A New Air Quality Index for Cities. Adv. Air Pollut. 13.

Silveira, C., Ferreira, J., Miranda, A.I., 2019. The challenges of air quality modelling when crossing multiple spatial scales. Air Qual. Atmos. Heal. 12, 1003–1017. https://doi.org/10.1007/s11869-019-00733-5

Solberg, S., Hov, Søvde, A., Isaksen, I.S.A., Coddeville, P., De Backer, H., Forster, C., Orsolini, Y., Uhse, K., 2008. European surface ozone in the extreme summer 2003. J. Geophys. Res. Atmos. 113, 1–16. https://doi.org/10.1029/2007JD009098

Soulhac, L., Salizzoni, P., Cierco, F.X., Perkins, R., 2011. The model SIRANE for atmospheric urban pollutant dispersion; part I, presentation of the model. Atmos. Environ. 45, 7379–7395. https://doi.org/10.1016/j.atmosenv.2011.07.008

Spinelle, L., Gerboles, M., Villani, M.G., Aleixandre, M., Bonavitacola, F., 2017. Field calibration of a cluster of low-cost commercially available sensors for air quality monitoring. Part B: NO, CO and CO2. Sensors Actuators, B Chem. 238, 706–715. https://doi.org/10.1016/j.snb.2016.07.036

Spinelle, L., Gerboles, M., Villani, M.G., Aleixandre, M., Bonavitacola, F., 2015. Field calibration of a cluster of low-cost available sensors for air quality monitoring. Part A: Ozone and nitrogen dioxide. Sensors Actuators, B Chem. 215, 249–257. https://doi.org/http://dx.doi.org/10.1016/j.snb.2015.03.031

Srivastava, A., Rao, B.P.S., 2011. Urban Air Pollution Modeling, Air Quality-Models and Applications, InTech.

Srivastava, S., Sinha, I.N., 2004. Classification of Air Pollution CLASSIFICATION OF AIR POLLUTION DISPERSION MODELS: A CRITICAL REVIEW, in: Proceedings of the National Seminar on Environmental Engineering with Special Emphasis on Mining Environment. pp. 2004–19.

Stewart, I.D., Oke, T.R., 2012. Local climate zones for urban temperature studies. Bull. Am. Meteorol. Soc. 93, 1879–1900. https://doi.org/10.1175/BAMS-D-11-00019.1

Stocker, J., Hood, C., Carruthers, D., McHugh, C., 2012. ADMS-Urban: developments in modelling dispersion from the city scale to the local scale. Int. J. Environ. Pollut. 50, 308–316.

Stull, R.B., 1988. An introduction to boundary layer meteorology. Springer Science & Business Media.

Swart, R., Amann, M., Raes, F., Tuinstra, W., 2004. A good climate for clean air: Linkages between climate change and air pollution. An editorial essay. Clim. Change 66, 263–269. https://doi.org/10.1023/B:CLIM.0000044677.41293.39

Tiwari, A., Kumar, P., 2020. Integrated dispersion-deposition modelling for air pollutant reduction via green infrastructure at an urban scale. Sci. Total Environ. 723, 138078. https://doi.org/10.1016/j.scitotenv.2020.138078

Tiwari, A., Kumar, P., Baldauf, R., Zhang, K.M., Pilla, F., Di Sabatino, S., Brattich, E., Pulvirenti, B., 2019. Considerations for evaluating green infrastructure impacts in microscale and macroscale air pollution dispersion models. Sci. Total Environ. 672, 410–426. https://doi.org/10.1016/j.scitotenv.2019.03.350

Tositti, L., Brattich, E., Masiol, M., Baldacci, D., Ceccato, D., Parmeggiani, S., Stracquadanio, M., Zappoli, S., 2014. Source apportionment of particulate matter in a large city of southeastern Po

Valley (Bologna, Italy). Environ. Sci. Pollut. Res. 21, 872–890. https://doi.org/10.1007/s11356-013-1911-7

Tressol, M., Ordonez, C., Zbinden, R., Brioude, J., Thouret, V., Mari, C., Nedelec, P., Cammas, J.P., Smit, H., Patz, H.W., Volz-Thomas, A., 2008. Air pollution during the 2003 European heat wave as seen by MOZAIC airliners. Atmos. Chem. Phys. 8, 2133–2150. https://doi.org/10.5194/acp-8-2133-2008

Tzoulas, K., Korpela, K., Venn, S., Yli-Pelkonen, V., Kaźmierczak, A., Niemela, J., James, P., 2007. Promoting ecosystem and human health in urban areas using Green Infrastructure: A literature review. Landsc. Urban Plan. 81, 167–178. https://doi.org/10.1016/j.landurbplan.2007.02.001

Vardoulakis, S., Fisher, B.E.A., Pericleous, K., Gonzalez-Flesca, N., 2003. Modelling air quality in street canyons: A review. Atmos. Environ. 37, 155–182. https://doi.org/10.1016/S1352-2310(02)00857-9

Watson, A.Y., Bates, R.R., Kennedy, D., 1988. Assessment of Human Exposure to Air Pollution: Methods, Measurements, and Models, Air Pollution, the Automobile, and Public Health.

Weber, E., 1982. Air Pollution: Assessment Meteorology and Modelling. Plenum Press.

Whitman, S., Good, G., Donoghue, E.R., 1997. Mortality in Chicago attributed to the July 1995 heat wave Public Health Biefs Mortality in Chicago Attributed to the July 1995 Heat Wave. Am. J. Public Health 87, 1515–1518.

WHO, 1999. Monitoring ambient air quality for health impact assessment. World Heal. Organ. Reg. Publ. - Eur. Ser. 85.

Wolf, K.L., 2003. Ergonomics of the City : Green Infrastructure and Social Benefits. Eng. Green Proc. 2003 Natl. Urban For. Conf. 2003, 5.

Yuan, C., Norford, L., Ng, E., 2017. A semi-empirical model for the effect of trees on the urban wind environment. Landsc. Urban Plan. 168, 84–93. https://doi.org/10.1016/j.landurbplan.2017.09.029

Zannetti, P., 1993. Numerical simulation modeling of air pollution: an overview Paolo. Trans. Ecol. Environ. 1, 54–60.

Zhang, L., Brook, J.R., Vet, R., 2003. A revised parameterization for gaseous dry deposition in air-quality models. Atmos. Chem. Phys. 3, 2067–2082. https://doi.org/10.5194/acp-3-2067-2003

APPENDICES

A. Python codes

```
import pandas as pd
import numpy as np
import sys
import os
from matplotlib import pyplot
import matplotlib.pyplot as plt
from matplotlib import cm
from matplotlib.colors import ListedColormap,LinearSegmentedColormap
import matplotlib.gridspec as gridspec
import matplotlib as mpl
import matplotlib.pylab as pl
import matplotlib
import pygrib
import math
import netCDF4 as nc
import os.path
from google.auth import impersonated_credentials, default
from googleapiclient.discovery import build
from google_auth_oauthlib.flow import InstalledAppFlow
from google.auth.transport.requests import Request
from google.oauth2.credentials import Credentials
from apiclient.http import MediaFileUpload
from googleapiclient.http import MediaIoBaseDownload
import json as jsn
import datetime
from zipfile import ZipFile
import httplib2
import io
from dateutil import tz
import metpy.calc as mpcalc
from metpy.units import units

print('\n=== FORECASTING TOOL CODE IS RUNNING
====================================')

#----------------------------------DATA from ARPAE
#--------- Cosmo forecast - Download
```

```
SCOPES = ['https://www.googleapis.com/auth/drive']# If modifying these
scopes, delete the file token.json.
creds = None
# The file token.json stores the user's access and refresh tokens, and
is
# created automatically when the authorization flow completes for the
first time.
if
os.path.exists('/home/PERSONALE/francesca.dinicola2/TPHD/tokenGDrive/t
oken.json'):
    creds =
Credentials.from_authorized_user_file('/home/PERSONALE/francesca.dinic
ola2/TPHD/tokenGDrive/token.json', SCOPES)
# If there are no (valid) credentials available, let the user log in.
if not creds or not creds.valid:
    if creds and creds.expired and creds.refresh_token:
      creds.refresh(Request())
    else:
        flow = InstalledAppFlow.from_client_secrets_file(

'/home/PERSONALE/francesca.dinicola2/TPHD/tokenGDrive/client_secret_79
6322916484-
qo98lnpunkc8srulqjel24qdi07b10ib.apps.googleusercontent.com.json',
SCOPES)
        creds = flow.run_local_server(port=0)
    # Save the credentials for the next run
    with
open('/home/PERSONALE/francesca.dinicola2/TPHD/tokenGDrive/token.json'
, 'w') as token:
        token.write(creds.to_json())

service = build('drive', 'v3', credentials=creds)

# Call the Drive v3 API
nextpage=None
while True:
  results = service.files().list(
      pageSize=1000, fields="nextPageToken, files(id,
name)",pageToken=nextpage,q="name='cosmo-2I_er'").execute()

  items = results.get('files', [])
  nextpage = results.get('nextPageToken', None)
```

```
  if not items:
      print('No files found.')
  else:
      #print('Files:')
      for item in items:
          print(u'{0} ({1})'.format(item['name'], item['id']))
          my_id=item['id']
  if nextpage == None:
    break

results=service.files().list(pageSize=2, fields="nextPageToken,
files(id, name)",q="'"+my_id+"'"+' in parents',orderBy='name
desc').execute()
items = results.get('files')
my_ids=[]
for item in items:
  print(u'{0} ({1})'.format(item['name'], item['id']))
  my_ids.append(item['id'])


# daily files .grib (First_data = hour 00:00:00 and Second_data = hour
12:00:00)
names=['Second_data.grib','First_data.grib']
for i,my_id in enumerate(my_ids):
  file_id = my_id
  request = service.files().get_media(fileId=file_id)
  fh = io.FileIO(names[i],'wb')
  downloader = MediaIoBaseDownload(fh, request)
  done = False
  while done is False:
      status, done = downloader.next_chunk()

print('grib data Done')

gr1 = pygrib.open('First_data.grib')
gr2 = pygrib.open('Second_data.grib')
#LIPE coordinates
lat_target=44.302700
lons_target=11.21504
lat,lons=gr2[1].latlons()

difference_array = np.absolute(lat-lat_target)
```

```
index_lat =difference_array.argmin(axis=0).mean().round()
difference_array = np.absolute(lons-lons_target)
index_lons =difference_array.argmin(axis=1).mean().round()

# calculation of MET data
# Temperature (C) -> T0C
Idxs=[1,71,123,175,227,279,331,383,435,487,539,591]#,643,695,747,799,8
51,903,955,1007,1059,1111,1163,1215]##,1267,1319,1371,1423,1475,1527,1
579,1631,1683,1735,1787]
T=[]
for Idx in Idxs:
  T.append(gr1[Idx].values[int(index_lat),int(index_lons)])
for Idx in Idxs:
  T.append(gr2[Idx].values[int(index_lat),int(index_lons)])
## T0C
T0C=[]
for t in T:
  tC=t-273.15
  T0C.append(int(tC))
T0C

# Specific Humidity (H)
Idxs=[2,72,124,176,228,280,332,384,436,488,540,592]
H=[]
for Idx in Idxs:
  H.append(int(gr1[Idx].values[int(index_lat),int(index_lons)]))
for Idx in Idxs:
  H.append(int(gr2[Idx].values[int(index_lat),int(index_lons)]))

# U wind component at 10 metre (m/s) -> U
Idxs=[8,78,130,182,234,286,338,390,442,494,546,598]
Ucomp=[]
for Idx in Idxs:
  Ucomp.append(gr1[Idx].values[int(index_lat),int(index_lons)])
for Idx in Idxs:
  Ucomp.append(gr2[Idx].values[int(index_lat),int(index_lons)])

# V wind component at 10 metre (m/s)
Idxs=[9,79,131,183,235,287,339,391,443,495,547,599]
Vcomp=[]
for Idx in Idxs:
  Vcomp.append(gr1[Idx].values[int(index_lat),int(index_lons)])
```

```
for Idx in Idxs:
  Vcomp.append(gr2[Idx].values[int(index_lat),int(index_lons)])

# wind speed at 10 metre (U) --- (calm < 0.75)
U=[]
for a,b in zip(Ucomp,Vcomp):
  WS=math.sqrt(((pow(a,2))+(pow(b,2))))
  #U.append(int(WS))
  if round(WS,1)<=0.7:
    WS=0.8
  U.append(round(WS,1)) #una cifra dopo virgola

# Wind direction (degrees) -> PHI
def wind_uv_to_dir(U,V):
    WDIR= ((270-np.rad2deg(np.arctan2(V,U)))%360)-180
    cond=WDIR<0
    WDIR[cond]=WDIR[cond]+360
    return WDIR

PHI=np.around(wind_uv_to_dir(Ucomp,Vcomp),0)


## Relative Humidity (%) -> RHUM (pressione di vapore di saturazione
(Es) e la pressione di vapore reale (E) in HPa -> RHUM = (E/Es)*100)
# T2m
Idxs=[10,80,132,184,236,288,340,392,444,496,548,600]
T2m=[]
for Idx in Idxs:
  T2m.append(gr1[Idx].values[int(index_lat),int(index_lons)])
for Idx in Idxs:
  T2m.append(gr2[Idx].values[int(index_lat),int(index_lons)])
T2mC=[]
for t in T2m:
  tC=t-273.15
  T2mC.append(tC)
# T2mdewp
Idxs=[11,81,133,185,237,289,341,393,445,497,549,601]
T2mdewp=[]
for Idx in Idxs:
  T2mdewp.append(gr1[Idx].values[int(index_lat),int(index_lons)])
for Idx in Idxs:
  T2mdewp.append(gr2[Idx].values[int(index_lat),int(index_lons)])
```

```
T2mdewpC=[]
for t in T2mdewp:
  tC=t-273.15
  T2mdewpC.append(tC)
#Es
Es=[]
for t1 in T2mC:
  valueEs=6.11*10.0**(7.5*t1/(237.7+t1))
  Es.append(valueEs)
#E
E=[]
for t2 in T2mdewpC:
  valueE=6.11*10.0**(7.5*t2/(237.7+t2))
  E.append(valueE)
# RHUM
RHUM=[]
for a,b in zip(Es,E):
  RH=(b/a)*100
  RHUM.append(int(RH))


# Cloud amount (oktas) -> CL
Idxs=[15,85,137,189,241,293,345,397,449,501,553,605]
TCC=[]
for Idx in Idxs:
  TCC.append(gr1[Idx].values[int(index_lat),int(index_lons)])
for Idx in Idxs:
  TCC.append(gr2[Idx].values[int(index_lat),int(index_lons)])
#CL: Conversion between decimal numbers and oktas
CL=[]
for c in TCC:
  if c == 0:
    value=0
  elif c>0 and c<18.75:
    value=1
  elif c>18.75 and c<31.25:
    value=2
  elif c>31.25 and c<43.75:
    value=3
  elif c>43.75 and c<56.25:
    value=4
```

```
  elif c>56.25 and c<68.75:
    value=5
  elif c>68.75 and c<81.25:
    value=6
  elif c>81.25 and c<100:
    value=7
  elif c==100:
    value=8
  else:
    value=NAN
  CL.append(value)


# Incoming Solar Radiation (W/m2) -> SOLAR RAD
Idxs=[19,89,141,193,245,297,349,401,453,505,557,609]
SOLAR_RAD=[]
for Idx in Idxs:

SOLAR_RAD.append(round(gr1[Idx].values[int(index_lat),int(index_lons)]
,3))
for Idx in Idxs:

SOLAR_RAD.append(round(gr2[Idx].values[int(index_lat),int(index_lons)]
,3))

# Sensible Heat Flux (W/m2) -> FTHETA0
Idxs=[24,94,146,198,250,302,354,406,458,510,562,614]
FTHETA0=[]
for Idx in Idxs:
  FTHETA0.append(int(gr1[Idx].values[int(index_lat),int(index_lons)]))
for Idx in Idxs:
  FTHETA0.append(int(gr2[Idx].values[int(index_lat),int(index_lons)]))

#Surface pressure: Pa
Idxs=[51,121,173,225,277,329,381,433,485,537,589,641]
SP=[]
for Idx in Idxs:
  SP.append(int(gr1[Idx].values[int(index_lat),int(index_lons)]))
for Idx in Idxs:
  SP.append(int(gr2[Idx].values[int(index_lat),int(index_lons)]))
layers=np.ones((60,100))
layers_P=[]
```

```
for i in range (24):
  layers_P.append(layers*SP[i])



# .MET file creation
times =
['1','2','3','4','5','6','7','8','9','10','11','12','13','14','15','16
','17','18','19','20','21','22','23','24']
YEAR = [str(datetime.date.today())[:4] for x in range(24)]
TDAY =['1' for x in range(24)] #modificare
THOUR = times

METDATA=pd.DataFrame.from_dict({
    'YEAR':YEAR,
    'TDAY' :TDAY,
    'THOUR' :THOUR,
    'T0C' :T0C,
    'RHUM':RHUM,
    'U' :U,
    'PHI' :PHI,
    'CL' :CL,
    'SOLAR RAD' :SOLAR_RAD
                        })
METDATA=METDATA[['YEAR','TDAY','THOUR','T0C','RHUM','U','PHI','CL','SO
LAR RAD']]
METDATA.to_csv('Meteo.csv',index = False, header=False)
Meteo=open('Meteo.csv','r')
print('meteo.csv Done')

ADMS_input=open('METEO.MET','w')
ADMS_input_text='VARIABLES:'+'\n'+'9'+'\n'+'YEAR'+'\n'+'TDAY'+'\n'+'TH
OUR'+'\n'+'T0C'+'\n'+'RHUM'+'\n'+'U'+'\n'+'PHI'+'\n'+'CL'+'\n'+'SOLAR
RAD'+'\n'+'DATA:'+'\n'
for line in Meteo:
  ADMS_input_text=ADMS_input_text+line

ADMS_input.write(ADMS_input_text)
ADMS_input.close()
print('METEO.MET Done')
```

```
#--------- CHIMERE forecast - Download and read data------------------
---------------------------
SCOPES = ['https://www.googleapis.com/auth/drive']# If modifying these
scopes, delete the file token.json.
creds = None
# The file token.json stores the user's access and refresh tokens, and
is
# created automatically when the authorization flow completes for the
first time.
if
os.path.exists('/home/PERSONALE/francesca.dinicola2/TPHD/tokenGDrive/t
oken.json'):
    creds =
Credentials.from_authorized_user_file('/home/PERSONALE/francesca.dinic
ola2/TPHD/tokenGDrive/token.json', SCOPES)
# If there are no (valid) credentials available, let the user log in.
if not creds or not creds.valid:
    if creds and creds.expired and creds.refresh_token:
      creds.refresh(Request())
    else:
        flow = InstalledAppFlow.from_client_secrets_file(

'/home/PERSONALE/francesca.dinicola2/TPHD/tokenGDrive/client_secret_79
6322916484-
qo98lnpunkc8srulqjel24qdi07b10ib.apps.googleusercontent.com.json',
SCOPES)
        creds = flow.run_local_server(port=0)
    # Save the credentials for the next run
    with
open('/home/PERSONALE/francesca.dinicola2/TPHD/tokenGDrive/token.json'
, 'w') as token:
        token.write(creds.to_json())

service = build('drive', 'v3', credentials=creds)

# Call the Drive v3 API
nextpage=None
while True:
  results = service.files().list(
      pageSize=1000, fields="nextPageToken, files(id,
name)",pageToken=nextpage,q="name='sup'").execute()

  items = results.get('files', [])
```

```
  nextpage = results.get('nextPageToken', None)

  if not items:
      print('No files found.')
  else:
      #print('Files:')
      for item in items:
          print(u'{0} ({1})'.format(item['name'], item['id']))
          my_id=item['id']

  if nextpage == None:
    break

my_ids=[]


results=service.files().list(pageSize=250, fields="nextPageToken,
files(id, name)",pageToken=nextpage, q="'"+my_id+"'"+" in parents
",orderBy='name desc').execute()

nextpage=results.get('nextPageToken', None)
items = results.get('files')

for item in items:
  if 'd1' in item['name'] and 'EMR' not in item['name']:
    print(u'{0} ({1})'.format(item['name'], item['id']))
    my_ids.append(item['id'])
    break


for i,my_id in enumerate(my_ids):
  file_id = my_id
  request = service.files().get_media(fileId=file_id)
  fh = io.FileIO(str(i)+'.nc','wb')
  downloader = MediaIoBaseDownload(fh, request)
  done = False
  while done is False:
      status, done = downloader.next_chunk()


f=nc.Dataset(str(i)+'.nc')
```

```
lat = f.variables['lat'][:]
lon = f.variables['lon'][:]
times =
['1','2','3','4','5','6','7','8','9','10','11','12','13','14','15','16
','17','18','19','20','21','22','23','24']
Inqs = ['NO', 'NO2', 'O3', 'PM10', 'PM2.5']

# desired station time series location

# Giardini Margherita
lonGM = 11.355035
latGM = 44.483628
difference_array = np.absolute(lat-latGM)
index_lat_GM =difference_array.argmin(axis=0).mean().round()
difference_array = np.absolute(lon-lonGM)
index_lon_GM =difference_array.argmin(axis=1).mean().round()

# Via Chiarini
lonVC = 11.286065
latVC = 44.500093
difference_array = np.absolute(lat-latVC)
index_lat_VC =difference_array.argmin(axis=0).mean().round()
difference_array = np.absolute(lon-lonVC)
index_lon_VC =difference_array.argmin(axis=1).mean().round()

# calculation of BGD data
YEAR =
[''.join(np.asarray(f.variables['Times'][0,0:4].data).astype(str)) for
x in range(24)]
TDAY =['1' for x in range(24)]
THOUR = times


# NO
NO_GM=[]
NO_VC=[]
for time in times:

NO_GM.append(np.asarray(f.variables['NO'][int(time),0,index_lat_GM,ind
ex_lon_GM].data).reshape(-1)[0])
```

```
NO_VC.append(np.asarray(f.variables['NO'][int(time),0,index_lat_VC,ind
ex_lon_VC].data).reshape(-1)[0])
# ppb->ug/m3 conversion
NO_GM=np.asarray(NO_GM)*1.91
NO_VC=np.asarray(NO_VC)*1.91

# No2
NO2_GM=[]
NO2_VC=[]
for time in times:

NO2_GM.append(np.asarray(f.variables['NO2'][int(time),0,index_lat_GM,i
ndex_lon_GM].data).reshape(-1)[0])

NO2_VC.append(np.asarray(f.variables['NO2'][int(time),0,index_lat_VC,i
ndex_lon_VC].data).reshape(-1)[0])
# ppb->ug/m3 conversion
NO2_GM=np.asarray(NO2_GM)*1.91
NO2_VC=np.asarray(NO2_VC)*1.91

# Nox
NOx_GM=(NO2_GM+NO_GM)
NOx_VC=(NO2_VC+NO_VC)

# O3
Oz_GM=[]
Oz_VC=[]
for time in times:

Oz_GM.append(np.asarray(f.variables['O3'][int(time),0,index_lat_GM,ind
ex_lon_GM].data).reshape(-1)[0])

Oz_VC.append(np.asarray(f.variables['O3'][int(time),0,index_lat_VC,ind
ex_lon_VC].data).reshape(-1)[0])
# ppb->ug/m3 conversion
Oz_GM=np.asarray(Oz_GM)*2
Oz_VC=np.asarray(Oz_VC)*2

# PM10
PM10_GM=[]
PM10_VC=[]
for time in times:
```

```
PM10_GM.append(np.asarray(f.variables['PM10'][int(time),0,index_lat_GM
,index_lon_GM].data).reshape(-1)[0])

PM10_VC.append(np.asarray(f.variables['PM10'][int(time),0,index_lat_VC
,index_lon_VC].data).reshape(-1)[0])

# PM2.5
PM25_GM=[]
PM25_VC=[]
for time in times:

PM25_GM.append(np.asarray(f.variables['PM25'][int(time),0,index_lat_GM
,index_lon_GM].data).reshape(-1)[0])

PM25_VC.append(np.asarray(f.variables['PM25'][int(time),0,index_lat_VC
,index_lon_VC].data).reshape(-1)[0])

# SO2
SO2_GM=[]
SO2_VC=[]
for time in times:
  SO2_GM.append(0.000001)
  SO2_VC.append(0.000001)

# BGD data based on wind direction -----------------------------------
---------
wind_direction=PHI
NO=[0 for x in range(24)]
NO2=[0 for x in range(24)]
NOx=[0 for x in range(24)]
O3=[0 for x in range(24)]
PM10=[0 for x in range(24)]
PM25=[0 for x in range(24)]
SO2=[0 for x in range(24)]

for i,wd in enumerate(wind_direction):
  if wd>180:
    NO[i]=NO_GM[i]
    NO2[i]=NO2_GM[i]
    NOx[i]=NOx_GM[i]
    O3[i]=Oz_GM[i]
    PM10[i]=PM10_GM[i]
```

```
    PM25[i]=PM25_GM[i]
    SO2[i]=SO2_GM[i]
  else:
    NO[i]=NO_VC[i]
    NO2[i]=NO2_VC[i]
    NOx[i]=NOx_VC[i]
    O3[i]=Oz_VC[i]
    PM10[i]=PM10_VC[i]
    PM25[i]=PM25_VC[i]
    SO2[i]=SO2_VC[i]


# .bgd file creation
BGDDATA=pd.DataFrame.from_dict({
    'YEAR' :YEAR,
    'TDAY' :TDAY,
    'THOUR' :THOUR,
    'NO' :NO,
    'NO2' :NO2,
    'NOx':NOx,
    'O3'  :O3,
    'PM10':PM10,
    'PM2.5':PM25,
    'SO2':SO2        })

BGDDATA=BGDDATA[['YEAR','TDAY','THOUR','NO','NO2','NOx','O3','PM10','P
M2.5','SO2']]
BGDDATA.to_csv('BGD.csv',index = False, header=False)
BGD=open('BGD.csv','r')
print('BGD.csv Done')

ADMS_input_bgd=open('BGD.bgd','w')
ADMS_input_text_bgd='BackgroundVersion2'+'\n'+'7'+'\n'+'NO'+'\n'+'NO2'
+'\n'+'NOx'+'\n'+'O3'+'\n'+'PM10'+'\n'+'PM2.5'+'\n'+'SO2'+'\n\n'+'UNIT
S:'+'\n'+'ug/m3'+'\n'+'ug/m3'+'\n'+'ug/m3'+'\n'+'ug/m3'+'\n'+'ug/m3'+'
\n'+'ug/m3'+'\n'+'ug/m3'+'\n\n'+'DATA:'+'\n'
for line in BGD:
  ADMS_input_text_bgd=ADMS_input_text_bgd+line

ADMS_input_bgd.write(ADMS_input_text_bgd)
ADMS_input_bgd.close()
print('BGD.bgd Done')
```

```
#---------------------------------ADMS URBAN run
ADMScom='/home/PERSONALE/francesca.dinicola2/ADMS/ADMSUrbanModel.out
/home/PERSONALE/francesca.dinicola2/TPHD/Urbanv1.UPL'
print('ADMS Urban run')
os.system(ADMScom)
print('ADMS Urban run Done')

#---------------------------------ADMS TH run
ADMScom='/home/PERSONALE/francesca.dinicola2/ADMS/ADMSUrbanModel.out
/home/PERSONALE/francesca.dinicola2/TPHD/THv1.UPL'
print('ADMS T&H run')
os.system(ADMScom)
print('ADMS T&H run Done')

#---------Pollution
## import Concentration data (.gst file)
DF=pd.read_csv('/home/PERSONALE/francesca.dinicola2/TPHD/Urbanv1.level
s.gst',delimiter=',')
size=(60,100)
zs=[5,10,15,20,25,30,35,40]
idx=['PM10','NO2','O3']

#PM10
layers_PM10=[]
for i in range(len(zs)):
  array_listPM10=[]
  for hour in range(24):
    DF_hour=DF[DF['Hour']==hour+1]
    DF_PM10_hour=DF_hour.iloc[:,7+(i*3)]
    PM10_hour=DF_PM10_hour.values
    IMG_PM10_hour=PM10_hour.reshape(size)
    array_listPM10.append(np.flip(IMG_PM10_hour,axis=0))
  layers_PM10.append(array_listPM10)

#NO2
layers_NO2=[]
for i in range(len(zs)):
  array_listNO2=[]
  for hour in range(24):
    DF_hour=DF[DF['Hour']==hour+1]
    DF_NO2_hour=DF_hour.iloc[:,8+(i*3)]
    NO2_hour=DF_NO2_hour.values
```

```
    IMG_NO2_hour=NO2_hour.reshape(size)
    array_listNO2.append(np.flip(IMG_NO2_hour,axis=0))
  layers_NO2.append(array_listNO2)

#O3
layers_O3=[]
for i in range(len(zs)):
  array_listO3=[]
  for hour in range(24):
    DF_hour=DF[DF['Hour']==hour+1]
    DF_O3_hour=DF_hour.iloc[:,9+(i*3)]
    O3_hour=DF_O3_hour.values
    IMG_O3_hour=O3_hour.reshape(size)
    array_listO3.append(np.flip(IMG_O3_hour,axis=0))
  layers_O3.append(array_listO3)


#---------Temperature and Humidity
DF_single=[]
for i in range(24):
  try:

DF_single.append(pd.read_csv('/home/PERSONALE/francesca.dinicola2/TPHD
/THv1.E'+str(i+1).zfill(2),delimiter=','))
  except:
    try:

DF_single.append(pd.read_csv('/home/PERSONALE/francesca.dinicola2/TPHD
/THv1.E'+str(i).zfill(2),delimiter=','))
    except:
      try:

DF_single.append(pd.read_csv('/home/PERSONALE/francesca.dinicola2/TPHD
/THv1.E'+str(i+2).zfill(2),delimiter=','))
      except:
        print('An error occurred')


DF=pd.concat([DF_single[0], DF_single[1].drop('Z(m)   ',axis=1),
DF_single[2].drop('Z(m)   ',axis=1), DF_single[3].drop('Z(m)
',axis=1),
```

```
                    DF_single[4].drop('Z(m)   ',axis=1),
DF_single[5].drop('Z(m)   ',axis=1), DF_single[6].drop('Z(m)
',axis=1),
                    DF_single[7].drop('Z(m)   ',axis=1),
DF_single[8].drop('Z(m)   ',axis=1), DF_single[9].drop('Z(m)
',axis=1),
                    DF_single[10].drop('Z(m)   ',axis=1),
DF_single[11].drop('Z(m)   ',axis=1), DF_single[12].drop('Z(m)
',axis=1),
                    DF_single[13].drop('Z(m)   ',axis=1),
DF_single[14].drop('Z(m)   ',axis=1), DF_single[15].drop('Z(m)
',axis=1),
                    DF_single[16].drop('Z(m)   ',axis=1),
DF_single[17].drop('Z(m)   ',axis=1), DF_single[18].drop('Z(m)
',axis=1),
                    DF_single[19].drop('Z(m)   ',axis=1),
DF_single[20].drop('Z(m)   ',axis=1), DF_single[21].drop('Z(m)
',axis=1),
                    DF_single[22].drop('Z(m)   ',axis=1),
DF_single[23].drop('Z(m)   ',axis=1)], axis=1)


size=(60,100)
zs=[5,10,15,20,25,30,35,40]
idx=['T','H']

#T
layers_T=[]
for i in range(len(zs)):
  array_listT=[]
  for hour in range(24):
    DF_lev=DF[DF['Z(m)   ']==zs[i]]
    DF_T_lev=DF_lev.iloc[:,3+(hour*6)]
    T_lev=DF_T_lev.values
    IMG_T_Lev=T_lev.reshape(size)
    array_listT.append(np.flip(IMG_T_Lev,axis=0))
  layers_T.append(array_listT)

#H
layers_H=[]
for i in range(len(zs)):
  array_listH=[]
  for hour in range(24):
```

```
    DF_hour=DF[DF['Z(m)   ']==zs[i]]
    DF_H_hour=DF_lev.iloc[:,5+(hour*6)]
    H_lev=DF_H_hour.values
    IMG_H_lev=H_lev.reshape(size)
    array_listH.append(np.flip(IMG_H_lev,axis=0))
  layers_H.append(array_listH)

# assign units of measure
layers_H = units.Quantity(layers_H, "kg/kg")
layers_T = units.Quantity(layers_T, "degC")
layers_P = units.Quantity(layers_P, "Pa")

#RH
layers_RH=[]
for i in range(len(zs)):
  array_listRH=[]
  array_RH=[]
  for hour in range(24):

array_listRH=mpcalc.relative_humidity_from_specific_humidity(layers_P[
i],layers_T[i],layers_H[i])
    array_RH=array_listRH*100
  layers_RH.append(array_RH)

print('layers done')
#----------------------------------Calculation Bologna Air Quality
Index (BLQ-Air Index)
size=(60,100)
zs=[5]
Vi=0.33 #relative weight of the pollutant i
# legal limit violation
Li_PM10=50
Li_O3=160
Li_NO2=200
Delta=0.00001

# standardized concentration
Cistar_PM10=[]
for z in range(len(zs)):
  Norm_PM10=[]
  for hour in range(24):
    DF=layers_PM10[z][hour]
```

```
    MaxDF_PM10= DF.max()
    Max_PM10= MaxDF_PM10.max()
    MinDF_PM10= DF.min()
    Min_PM10= MinDF_PM10.min()
    Norm_PM10.append((DF-Min_PM10)/(Max_PM10-Min_PM10+Delta))
  Cistar_PM10.append(Norm_PM10)

Cistar_NO2=[]
for z in range(len(zs)):
  Norm_NO2=[]
  for hour in range(24):
    DF=layers_NO2[z][hour]
    MaxDF_NO2= DF.max()
    Max_NO2= MaxDF_NO2.max()
    MinDF_NO2= DF.min()
    Min_NO2= MinDF_NO2.min()
    Norm_NO2.append((DF-Min_NO2)/(Max_NO2-Min_NO2+Delta))
  Cistar_NO2.append(Norm_NO2)

Cistar_O3=[]
for z in range(len(zs)):
  Norm_O3=[]
  for hour in range(24):
    DF=layers_O3[z][hour]
    MaxDF_O3= DF.max()
    Max_O3= MaxDF_O3.max()
    MinDF_O3= DF.min()
    Min_O3= MinDF_O3.min()
    Norm_O3.append((DF-Min_O3)/(Max_O3-Min_O3+Delta))
  Cistar_O3.append(Norm_O3)

# dummy variable
wi_PM10=[]
for z in range(len(zs)):
  peso_PM10=[]
  for hour in range(24):
    DF=layers_PM10[z][hour]
    DF=np.where(DF>Li_PM10, 1,DF)
    peso_PM10.append(np.where(DF>(Li_PM10/2),0.5,0.33))
  wi_PM10.append(peso_PM10)
```

```
wi_NO2=[]
for z in range(len(zs)):
  peso_NO2=[]
  for hour in range(24):
    DF=layers_NO2[z][hour]
    DF=np.where(DF>Li_NO2, 1,DF)
    peso_NO2.append(np.where(DF>(Li_NO2/2),0.5,0.33))
  wi_NO2.append(peso_NO2)


wi_O3=[]
for z in range(len(zs)):
  peso_O3=[]
  for hour in range(24):
    DF=layers_O3[z][hour]
    DF=np.where(DF>Li_O3, 1,DF)
    peso_O3.append(np.where(DF>(Li_O3/2),0.5,0.33))
  wi_O3.append(peso_O3)


Prod=(np.asarray(wi_PM10)*np.asarray(wi_NO2)*np.asarray(wi_O3))

Pi_PM10=[]
for z in range(len(zs)):
  p_PM10=[]
  for hour in range(24):
    DF=Cistar_PM10[z][hour]
    p_PM10.append(DF*Prod[z,hour]*Vi)
  Pi_PM10.append(p_PM10)

Pi_NO2=[]
for z in range(len(zs)):
  p_NO2=[]
  for hour in range(24):
    DF=Cistar_NO2[z][hour]
    p_NO2.append(DF*Prod[z,hour]*Vi)
  Pi_NO2.append(p_NO2)

Pi_O3=[]
for z in range(len(zs)):
  p_O3=[]
```

```
  for hour in range(24):
    DF=Cistar_O3[z][hour]
    p_O3.append(DF*Prod[z,hour]*Vi)
  Pi_O3.append(p_O3)

BLQI=[]
for z in range(len(zs)):
  BLQindex=[]
  for hour in range(24):
    SommaInd=Pi_PM10[z][hour] +Pi_NO2[z][hour] +Pi_O3[z][hour]
    BLQindex.append(SommaInd)
  BLQI.append(BLQindex)

print('Bologna Air Quality Index done')

# create colormaps
N = 256

dark_red = np.ones((N, 4))
dark_red[:, 0] = np.linspace(159/256, 1, N)
dark_red[:, 1] = np.linspace(3/256, 1, N)
dark_red[:, 2] = np.linspace(3/256, 1, N)
dark_red_cmp = ListedColormap(dark_red)

red = np.ones((N, 4))
red[:, 0] = np.linspace(245/256, 1, N)
red[:, 1] = np.linspace(3/256, 1, N)
red[:, 2] = np.linspace(3/256, 1, N)
red_cmp = ListedColormap(red)

orange = np.ones((N, 4))
orange[:, 0] = np.linspace(230/256, 1, N)
orange[:, 1] = np.linspace(186/256, 1, N)
orange[:, 2] = np.linspace(8/256, 1, N)
orange_cmp = ListedColormap(orange)

yellow = np.ones((N, 4))
yellow[:, 0] = np.linspace(255/256, 1, N)
yellow[:, 1] = np.linspace(255/256, 1, N)
yellow[:, 2] = np.linspace(6/256, 1, N)
yellow_cmp = ListedColormap(yellow)
```

```
light_green = np.ones((N, 4))
light_green[:, 0] = np.linspace(106/256, 1, N)
light_green[:, 1] = np.linspace(255/256, 1, N)
light_green[:, 2] = np.linspace(6/256, 1, N)
light_green_cmp = ListedColormap(light_green)

green = np.ones((N, 4))
green[:, 0] = np.linspace(6/256, 1, N)
green[:, 1] = np.linspace(146/256, 1, N)
green[:, 2] = np.linspace(6/256, 1, N)
green_cmp = ListedColormap(green)

# define BLQ-Air index colormaps
BLQcmap = np.vstack((green_cmp(np.linspace(0.5, 0, 128)),
                        light_green_cmp(np.linspace(0.5, 0, 128)),
                        yellow_cmp(np.linspace(0.5, 0, 128)),
                        orange_cmp(np.linspace(0.5, 0, 128)),
                        red_cmp(np.linspace(0.5, 0, 128)),
                        dark_red_cmp(np.linspace(0.5, 0, 128)),
                        ))
Index = ListedColormap(BLQcmap, name='Index')

def multilinearize(bounds,array):
  polys=[]
  for j in range(len(bounds)-1):

polys.append(np.poly1d(np.polyfit(np.asarray([j,j+1]),np.asarray([boun
ds[j],bounds[j+1]]),1)))
  output_array=[]
  for i in array:
    for j in range(len(bounds)-1):
      if j<=i<j+1:
        output_array.append(polys[j](i))
        break

  return output_array,polys

print('Colormaps done')
#------------------------------Sending maps to Drive
nextpage=None
while True:
```

```
  results = service.files().list(
      pageSize=1000, fields="nextPageToken, files(id,
name)",pageToken=nextpage,q="name= 'ADMS-BO'").execute()

  items = results.get('files', [])
  nextpage = results.get('nextPageToken', None)

  if not items:
      print('No files found.')
  else:
      print('Files:')
      for item in items:
          print(u'{0} ({1})'.format(item['name'], item['id']))
          my_id=item['id']

  if nextpage == None:
    break

#-------------------------------Delete files in ADMS-BO drive
# all images (PNG)
response =service.files().list(q="name contains '.zip' and
'"+str(my_id)+"' in parents",pageSize=1000,
                                      spaces='drive',
                                      fields='nextPageToken, files(id,
name)').execute()
for file in response.get('files', []):
    # Process change
    print ('Found file: %s (%s)' % (file.get('name'), file.get('id')))
    service.files().delete(fileId=file.get('id')).execute()

#Cancella .json nella cartella
response =service.files().list(q="name contains '.json' and
'"+str(my_id)+"' in parents",pageSize=1000,
                                      spaces='drive',
                                      fields='nextPageToken, files(id,
name)').execute()
for file in response.get('files', []):
    # Process change
    print ('Found file: %s (%s)' % (file.get('name'), file.get('id')))
    service.files().delete(fileId=file.get('id')).execute()

# create a ZipFile object
```

```
zipObj = ZipFile('Previsioni.zip', 'w')
json={'Datasets':[]}
to_zone = tz.gettz('Europe/Rome')
from_zone = tz.gettz('UTC')

print('Delete files done')

#-------------------------------Image creation
#BLQ-Air Index
bounds = [0, 0.5, 2, 5, 9, 30, 50, 51]
cmap=Index

(fitted_bounds,polys)=multilinearize(bounds,np.linspace(0,6,Index.N).t
olist())

norm = cm.colors.BoundaryNorm(fitted_bounds,Index.N)


layer='BLQ-Air Index'
for z in range(len(zs)):
  for hour in range(24):
    plt.close()
    #Modifica fuso orario
    if hour==0:
      filename=str(datetime.date.today()+datetime.timedelta(2))+'-
'+str(hour).zfill(2)+'0000-'+layer+'-'+str(zs[z]).zfill(2)

UTCtime=datetime.datetime.strptime(str(datetime.date.today()+datetime.
timedelta(2))+' '+str(hour).zfill(2)+':00', '%Y-%m-%d
%H:%M').replace(tzinfo=from_zone)
      italian_time=UTCtime.astimezone(to_zone)
      descrizione=layer+' '+str(zs[z])+'m '+str(italian_time)[:-6]

date=str(datetime.date.today()+datetime.timedelta(2))+'T'+str(hour).zf
ill(2)+':00:00Z'
      img=BLQI[z][23]
    else:
      filename=str(datetime.date.today()+datetime.timedelta(1))+'-
'+str(hour).zfill(2)+'0000-'+layer+'-'+str(zs[z]).zfill(2)

UTCtime=datetime.datetime.strptime(str(datetime.date.today()+datetime.
timedelta(1))+' '+str(hour).zfill(2)+':00', '%Y-%m-%d
%H:%M').replace(tzinfo=from_zone)
```

```
        italian_time=UTCtime.astimezone(to_zone)
        descrizione=layer+' '+str(zs[z])+'m '+str(italian_time)[:-6]

date=str(datetime.date.today()+datetime.timedelta(1))+'T'+str(hour).zf
ill(2)+':00:00Z'
        img=BLQI[z][hour-1]

metadata={'Id':filename,'Descr':descrizione,'Layer':layer,'Date':date,
'Altitude':(zs[z]),'Opacity':0.7,'CornersLonLat':
[[11.22831,44.56201],[11.45497,44.55236],[11.44221,44.46318],[11.21579
,44.47280]],'Source':filename+'.png'}
     plt.imshow(img,  norm=norm, cmap=Index, vmin = 0, vmax =50)
     plt.axis('off')
     plt.savefig(filename+'.png',bbox_inches='tight',pad_inches=0)
     zipObj.write(filename+'.png')
     json['Datasets'].append(metadata)

FIGSIZE = (2,3)
mpb = plt.pcolormesh(img, norm=norm, cmap=Index, vmin = 0, vmax =50)
fig,ax = plt.subplots(figsize=FIGSIZE)
cb=plt.colorbar(mpb,label = 'BLQ-Air Index', extend = 'both', pad =
0.1, ticks=[0, 0.5, 2, 5, 9, 30, 50,60])
cb.ax.set_title('')
ax.remove()
plt.savefig('Legend BLQ-Air
Index.png',bbox_inches='tight',transparent=True)
zipObj.write('Legend BLQ-Air Index.png')

zs=[5,10,15,20,25,30,35,40]

#PM10
v_green=25
v_yellow=50
v_min=v_green-(v_yellow-v_green)
v_max=v_yellow+(v_yellow-v_green)
cmap = matplotlib.cm.get_cmap('RdYlGn_r')
alpha_cmap = cmap(np.arange(cmap.N)) # Get the colormap colors
alpha_cmap[:,-1] = np.linspace(0.5, 1, cmap.N) # Set alpha
alpha_cmap = ListedColormap(alpha_cmap) # Create new colormap

layer='PM10'
for z in range(len(zs)):
```

```
  for hour in range(24):
    #Change time zone
    if hour==0:
      filename=str(datetime.date.today()+datetime.timedelta(2))+'-
'+str(hour).zfill(2)+'0000-'+layer+'-'+str(zs[z]).zfill(2)

UTCtime=datetime.datetime.strptime(str(datetime.date.today()+datetime.
timedelta(2))+' '+str(hour).zfill(2)+':00', '%Y-%m-%d
%H:%M').replace(tzinfo=from_zone)
      italian_time=UTCtime.astimezone(to_zone)
      descrizione=layer+' '+str(zs[z])+'m '+str(italian_time)[:-6]

date=str(datetime.date.today()+datetime.timedelta(2))+'T'+str(hour).zf
ill(2)+':00:00Z'
      img=layers_PM10[z][23]
    else:
      filename=str(datetime.date.today()+datetime.timedelta(1))+'-
'+str(hour).zfill(2)+'0000-'+layer+'-'+str(zs[z]).zfill(2)

UTCtime=datetime.datetime.strptime(str(datetime.date.today()+datetime.
timedelta(1))+' '+str(hour).zfill(2)+':00', '%Y-%m-%d
%H:%M').replace(tzinfo=from_zone)
      italian_time=UTCtime.astimezone(to_zone)
      descrizione=layer+' '+str(zs[z])+'m '+str(italian_time)[:-6]

date=str(datetime.date.today()+datetime.timedelta(1))+'T'+str(hour).zf
ill(2)+':00:00Z'
      img=layers_PM10[z][hour-1]

metadata={'Id':filename,'Descr':descrizione,'Layer':layer,'Date':date,
'Altitude':(zs[z]),'Opacity':1,'CornersLonLat':
[[11.22831,44.56201],[11.45497,44.55236],[11.44221,44.46318],[11.21579
,44.47280]],'Source':filename+'.png'}

plt.imsave(filename+'.png',img,cmap=alpha_cmap,vmin=v_min,vmax=v_max)
    zipObj.write(filename+'.png')
    json['Datasets'].append(metadata)

FIGSIZE = (2,3)
mpb = plt.pcolormesh(img,cmap=alpha_cmap,vmin=v_min,vmax=v_max)
fig,ax = plt.subplots(figsize=FIGSIZE)
cb=plt.colorbar(mpb,ax=ax)
cb.ax.set_title('ug/m3')
ax.remove()
```

```
plt.savefig('Legend PM10.png',bbox_inches='tight',transparent=True)
zipObj.write('Legend PM10.png')
mpb.remove()


#NO2
v_green=100
v_yellow=200
v_min=v_green-(v_yellow-v_green)
v_max=v_yellow+(v_yellow-v_green)
cmap = matplotlib.cm.get_cmap('RdYlGn_r')
alpha_cmap = cmap(np.arange(cmap.N)) # Get the colormap colors
alpha_cmap[:,-1] = np.linspace(0.5, 1, cmap.N) # Set alpha
alpha_cmap = ListedColormap(alpha_cmap) # Create new colormap

layer='NO2'
for z in range(len(zs)):
  for hour in range(24):
    #Modifica fuso orario
    if hour==0:
      filename=str(datetime.date.today()+datetime.timedelta(2))+'-
'+str(hour).zfill(2)+'0000-'+layer+'-'+str(zs[z]).zfill(2)

UTCtime=datetime.datetime.strptime(str(datetime.date.today()+datetime.
timedelta(2))+' '+str(hour).zfill(2)+':00', '%Y-%m-%d
%H:%M').replace(tzinfo=from_zone)
      italian_time=UTCtime.astimezone(to_zone)
      descrizione=layer+' '+str(zs[z])+'m '+str(italian_time)[:-6]

date=str(datetime.date.today()+datetime.timedelta(2))+'T'+str(hour).zf
ill(2)+':00:00Z'
      img=layers_NO2[z][23]
    else:
      filename=str(datetime.date.today()+datetime.timedelta(1))+'-
'+str(hour).zfill(2)+'0000-'+layer+'-'+str(zs[z]).zfill(2)

UTCtime=datetime.datetime.strptime(str(datetime.date.today()+datetime.
timedelta(1))+' '+str(hour).zfill(2)+':00', '%Y-%m-%d
%H:%M').replace(tzinfo=from_zone)
      italian_time=UTCtime.astimezone(to_zone)
      descrizione=layer+' '+str(zs[z])+'m '+str(italian_time)[:-6]
```

```
date=str(datetime.date.today()+datetime.timedelta(1))+'T'+str(hour).zf
ill(2)+':00:00Z'
      img=layers_NO2[z][hour-1]

metadata={'Id':filename,'Descr':descrizione,'Layer':layer,'Date':date,
'Altitude':(zs[z]),'Opacity':1,'CornersLonLat':
[[11.22831,44.56201],[11.45497,44.55236],[11.44221,44.46318],[11.21579
,44.47280]],'Source':filename+'.png'}

plt.imsave(filename+'.png',img,cmap=alpha_cmap,vmin=v_min,vmax=v_max)
    zipObj.write(filename+'.png')
    json['Datasets'].append(metadata)

FIGSIZE = (2,3)
mpb = plt.pcolormesh(img,cmap=alpha_cmap,vmin=v_min,vmax=v_max)
fig,ax = plt.subplots(figsize=FIGSIZE)
cb=plt.colorbar(mpb,ax=ax)
cb.ax.set_title('ug/m3')
ax.remove()
plt.savefig('Legend NO2.png',bbox_inches='tight',transparent=True)
zipObj.write('Legend NO2.png')
mpb.remove()



#O3
v_green=80
v_yellow=160
v_min=v_green-(v_yellow-v_green)
v_max=v_yellow+(v_yellow-v_green)
cmap = matplotlib.cm.get_cmap('RdYlGn_r')
alpha_cmap = cmap(np.arange(cmap.N)) # Get the colormap colors
alpha_cmap[:,-1] = np.linspace(0.5, 1, cmap.N) # Set alpha
alpha_cmap = ListedColormap(alpha_cmap) # Create new colormap

layer='Ozono'
for z in range(len(zs)):
  for hour in range(24):
  #Modifica fuso orario
    if hour==0:
      filename=str(datetime.date.today()+datetime.timedelta(2))+'-
'+str(hour).zfill(2)+'0000-'+layer+'-'+str(zs[z]).zfill(2)
```

```
UTCtime=datetime.datetime.strptime(str(datetime.date.today()+datetime.
timedelta(2))+' '+str(hour).zfill(2)+':00', '%Y-%m-%d
%H:%M').replace(tzinfo=from_zone)
      italian_time=UTCtime.astimezone(to_zone)
      descrizione=layer+' '+str(zs[z])+'m '+str(italian_time)[:-6]

date=str(datetime.date.today()+datetime.timedelta(2))+'T'+str(hour).zf
ill(2)+':00:00Z'
      img=layers_O3[z][23]
    else:
      filename=str(datetime.date.today()+datetime.timedelta(1))+'-
'+str(hour).zfill(2)+'0000-'+layer+'-'+str(zs[z]).zfill(2)

UTCtime=datetime.datetime.strptime(str(datetime.date.today()+datetime.
timedelta(1))+' '+str(hour).zfill(2)+':00', '%Y-%m-%d
%H:%M').replace(tzinfo=from_zone)
      italian_time=UTCtime.astimezone(to_zone)
      descrizione=layer+' '+str(zs[z])+'m '+str(italian_time)[:-6]

date=str(datetime.date.today()+datetime.timedelta(1))+'T'+str(hour).zf
ill(2)+':00:00Z'
      img=layers_O3[z][hour-1]

metadata={'Id':filename,'Descr':descrizione,'Layer':layer,'Date':date,
'Altitude':(zs[z]),'Opacity':1,'CornersLonLat':
[[11.22831,44.56201],[11.45497,44.55236],[11.44221,44.46318],[11.21579
,44.47280]],'Source':filename+'.png'}

plt.imsave(filename+'.png',img,cmap=alpha_cmap,vmin=v_min,vmax=v_max)
    zipObj.write(filename+'.png')
    json['Datasets'].append(metadata)

FIGSIZE = (2,3)
mpb = plt.pcolormesh(img,cmap=alpha_cmap,vmin=v_min,vmax=v_max)
fig,ax = plt.subplots(figsize=FIGSIZE)
cb=plt.colorbar(mpb,ax=ax)
cb.ax.set_title('ug/m3')
ax.remove()
plt.savefig('Legend Ozono.png',bbox_inches='tight',transparent=True)
zipObj.write('Legend Ozono.png')
mpb.remove()
```

```
#Temperature
v_green=18
v_yellow=28
v_min=v_green-(v_yellow-v_green)
v_max=v_yellow+(v_yellow-v_green)
cmap = matplotlib.cm.get_cmap('RdYlBu_r')
alpha_cmap = cmap(np.arange(cmap.N)) # Get the colormap colors
alpha_cmap[:,-1] = np.linspace(0.5, 1, cmap.N) # Set alpha
alpha_cmap = cmap # Create new colormap

layer='Temperature'
for z in range(len(zs)):
  for hour in range(24):
  #Modifica fuso orario
    if hour==0:
      filename=str(datetime.date.today()+datetime.timedelta(2))+'-
'+str(hour).zfill(2)+'0000-'+layer+'-'+str(zs[z]).zfill(2)

UTCtime=datetime.datetime.strptime(str(datetime.date.today()+datetime.
timedelta(2))+' '+str(hour).zfill(2)+':00', '%Y-%m-%d
%H:%M').replace(tzinfo=from_zone)
      italian_time=UTCtime.astimezone(to_zone)
      descrizione=layer+' '+str(zs[z])+'m '+str(italian_time)[:-6]

date=str(datetime.date.today()+datetime.timedelta(2))+'T'+str(hour).zf
ill(2)+':00:00Z'
      print(len(layers_T[z]))
      img=layers_T[z][23]
    else:
      filename=str(datetime.date.today()+datetime.timedelta(1))+'-
'+str(hour).zfill(2)+'0000-'+layer+'-'+str(zs[z]).zfill(2)

UTCtime=datetime.datetime.strptime(str(datetime.date.today()+datetime.
timedelta(1))+' '+str(hour).zfill(2)+':00', '%Y-%m-%d
%H:%M').replace(tzinfo=from_zone)
      italian_time=UTCtime.astimezone(to_zone)
      descrizione=layer+' '+str(zs[z])+'m '+str(italian_time)[:-6]

date=str(datetime.date.today()+datetime.timedelta(1))+'T'+str(hour).zf
ill(2)+':00:00Z'
      img=layers_T[z][hour-1]

metadata={'Id':filename,'Descr':descrizione,'Layer':layer,'Date':date,
```

```
'Altitude':(zs[z]),'Opacity':0.7,'CornersLonLat':
[[11.22831,44.56201],[11.45497,44.55236],[11.44221,44.46318],[11.21579
,44.47280]],'Source':filename+'.png'}

plt.imsave(filename+'.png',img,cmap=alpha_cmap,vmin=v_min,vmax=v_max)
    zipObj.write(filename+'.png')
    json['Datasets'].append(metadata)

FIGSIZE = (2,3)
mpb = plt.pcolormesh(img,cmap=alpha_cmap,vmin=v_min,vmax=v_max)
fig,ax = plt.subplots(figsize=FIGSIZE)
cb=plt.colorbar(mpb,ax=ax)
cb.ax.set_title('°C')
ax.remove()
plt.savefig('Legend
Temperature.png',bbox_inches='tight',transparent=True)
zipObj.write('Legend Temperature.png')
mpb.remove()


#Humidity
v_green=50
v_yellow=75
v_min=v_green-(v_yellow-v_green)
v_max=v_yellow+(v_yellow-v_green)
cmap = matplotlib.cm.get_cmap('PRGn_r')
alpha_cmap = cmap(np.arange(cmap.N)) # Get the colormap colors
alpha_cmap[:,-1] = np.linspace(0.5, 1, cmap.N) # Set alpha
alpha_cmap = cmap # Create new colormap

layer='Humidity'
for z in range(len(zs)):
  for hour in range(24):
    #Modifica fuso orario
    if hour==0:
      filename=str(datetime.date.today()+datetime.timedelta(2))+'-
'+str(hour).zfill(2)+'0000-'+layer+'-'+str(zs[z]).zfill(2)

UTCtime=datetime.datetime.strptime(str(datetime.date.today()+datetime.
timedelta(2))+' '+str(hour).zfill(2)+':00', '%Y-%m-%d
%H:%M').replace(tzinfo=from_zone)
      italian_time=UTCtime.astimezone(to_zone)
```

```
      descrizione=layer+' '+str(zs[z])+'m '+str(italian_time)[:-6]

date=str(datetime.date.today()+datetime.timedelta(2))+'T'+str(hour).zf
ill(2)+':00:00Z'
      img=layers_RH[z][23]
    else:
      filename=str(datetime.date.today()+datetime.timedelta(1))+'-
'+str(hour).zfill(2)+'0000-'+layer+'-'+str(zs[z]).zfill(2)

UTCtime=datetime.datetime.strptime(str(datetime.date.today()+datetime.
timedelta(1))+' '+str(hour).zfill(2)+':00', '%Y-%m-%d
%H:%M').replace(tzinfo=from_zone)
      italian_time=UTCtime.astimezone(to_zone)
      descrizione=layer+' '+str(zs[z])+'m '+str(italian_time)[:-6]

date=str(datetime.date.today()+datetime.timedelta(1))+'T'+str(hour).zf
ill(2)+':00:00Z'
      img=layers_RH[z][hour-1]

metadata={'Id':filename,'Descr':descrizione,'Layer':layer,'Date':date,
'Altitude':(zs[z]),'Opacity':0.7,'CornersLonLat':
[[11.22831,44.56201],[11.45497,44.55236],[11.44221,44.46318],[11.21579
,44.47280]],'Source':filename+'.png'}

plt.imsave(filename+'.png',img,cmap=alpha_cmap,vmin=v_min,vmax=v_max)
    zipObj.write(filename+'.png')
    json['Datasets'].append(metadata)

FIGSIZE = (2,3)
mpb = plt.pcolormesh(img,cmap=alpha_cmap,vmin=v_min,vmax=v_max)
fig,ax = plt.subplots(figsize=FIGSIZE)
cb=plt.colorbar(mpb,ax=ax)
cb.ax.set_title('%')
ax.remove()
plt.savefig('Legend
Humidity.png',bbox_inches='tight',transparent=True)
zipObj.write('Legend Humidity.png')
mpb.remove()

print('.png done')

zipObj.close()
file_metadata = { 'name': 'Previsioni.zip', 'parents': [my_id] }
```

```
media = MediaFileUpload('Previsioni.zip',mimetype='application/zip',
resumable=True)
file = service.files().create(body=file_metadata,
media_body=media,fields='id').execute()

f=open('Catalogo.json','w')
jsn.dump(json,f)
f.close()

file_metadata = { 'name': 'Catalogo.json', 'parents': [my_id] }
media = MediaFileUpload('Catalogo.json',mimetype='apllication/json',
resumable=True)
file = service.files().create(body=file_metadata,
media_body=media,fields='id').execute()

print('UPload Done')

print('\n\n\n=========================================================\
n============== FORECASTING TOOL CODE COMPLETED SUCCESSFULLY
=============\n========================================================
=')
```

ACKNOWLEDGEMENTS

This Thesis reports my own work but has benefited from the experience and guidance of several people. I wish to express my sincere thanks to all people who lead me and helped me. First of all, Professor Silvana Di Sabatino (UNIBO) my supervisor, for providing me with all the necessary information for completing the study and for his great supervision. Dr. Erika Brattich (UNIBO) for her enormous contribution to all the activities carried out, her advice and always being present. Dr. Lorenzo Prandella (e-Soft) for his help in coding the forecasting tool. All the people and entities involved in the i-SCAPE project (UNIBO and ARPAE teams). The e-Soft company in the person of Dr. Mauro Lenzi for making the IT experience and the e-Globus web platform available.